Arnold Schwarzenegger
Governor

AIR QUALITY IMPACTS OF DISTRIBUTED GENERATION

PIER FINAL PROJECT REPORT

Prepared For:
California Energy Commission
Public Interest Energy Research Program

Prepared By:
University of California, Irvine

October 2005
CEC-500-2005-O69-F

Prepared By:
University of California, Irvine
Professor Scott Samuelson
Professor Donald Dabdub
Dr. Jacob Brouwer
Dr. Marc Medrano
Dr. Marco Rodriguez
Marc Carreras-Sospedra

131 Engineering Laboratory Facility
Irvine, California 92679-3550
gss@nfcrc.uci.edu
ddabdub@uci.edu

Contract No. 500-00-033

Prepared For:
California Energy Commission
Public Interest Energy Research (PIER) Program

Marla Mueller,
Contract Manager

Kelly Birkinshaw,
Program Area Team Lead

Martha Krebs, Ph.D.
Deputy Director
ENERGY RESEARCH AND DEVELOPMENT DIVISION

B. B. Blevins
Executive Director

Acknowledgements

We graciously acknowledge the financial support of the California Energy Commission, which is sponsoring this work, and the significant leadership and contributions of Marla Mueller, our Contract Manager.

We thank the California Air Resources Board and South Coast Air Quality Management District for their provision of emissions inventories and invaluable support and guidance in this effort. The regular attendance, participation, and guidance provided by Marty Kay, Ajith Kaduwela, Joseph Cassmassi, Grant Chin, Mark Rawson, Linda Kelly, and John DaMassa was invaluable to the successful completion of this effort.

We thank the Southern California Area Governments (SCAG) for their generous donation of the GIS land-use data.

Marc Medrano and Marc Carreras-Sospedra thank the Balsells-Generalitat de Catalunya Fellowship for postdoctoral and graduate research fellowships, respectively.

Marco Rodriguez thanks the University of California Institute for Mexico and the United States (UC MEXUS) for their financial support of his graduate student research efforts.

We thank William Allen and Tyler Reid for their support of this effort through research study projects.

We thank Network and Computing Services of UCI; especially Joseph Farran for his technical support of our computing infrastructure, and Tony Soeller for his assistance in processing GIS data.

Please cite this report as follows:

Samuelson, S., D. Dabdub, J. Brouwer, M. Medrano, M. Rodriguez, and M. Carreras-Sospedra. 2005. *Air Quality Impacts of Distributed Generation.* California Energy Commission, PIER Energy-Related Environmental Research. CEC-500-2005-069-F.

Preface

The Public Interest Energy Research (PIER) Program supports public interest energy research and development that will help improve the quality of life in California by bringing environmentally safe, affordable, and reliable energy services and products to the marketplace.

The PIER Program, managed by the California Energy Commission (Energy Commission), annually awards up to $62 million to conduct the most promising public interest energy research by partnering with Research, Development, and Demonstration (RD&D) organizations, including individuals, businesses, utilities, and public or private research institutions.
PIER funding efforts are focused on the following RD&D program areas:

- Buildings End-Use Energy Efficiency
- Energy-Related Environmental Research
- Energy Systems Integration
- Environmentally Preferred Advanced Generation
- Industrial/Agricultural/Water End-Use Energy Efficiency
- Renewable Energy Technologies

What follows is the final report for the Air Quality Impacts of Distributed Generation contract, contract number 500-00-033, conducted by the University of California, Irvine. The report is entitled *Air Quality Impacts of Distributed Generation.* This project contributes to the Energy-Related Environmental Research program.

For more information on the PIER Program, please visit the Energy Commission's website www.energy.ca.gov/pier/ or contract the Energy Commission at (916) 654-4628.

Table of Contents

(Note that the Appendices are available as separate documents.)

List of Figures

List of Tables

Abstract

Distributed Energy Resources (DER) have the potential to supply a significant portion of increased power demands in California and the rest of the United States. Distributed generation (DG) is characterized by a dispersion of many stationary power generators throughout an urban air basin. In contrast, central-generation sources are typically localized in remote areas, and occasionally outside the basin. As a result, distributed generation may lead to increased pollutant emissions within an urban air basin, which could adversely affect air quality.

This project develops a systematic approach based on land-use geographic information systems (GIS) data for characterizing the installation of DER in an urban air basin and simulates the potential air quality impacts using a state-of-the-art three-dimensional computer model. Model sensitivity and model uncertainty analyses are also developed in this project. The assessment of the air quality impacts associated with DER is made in the South Coast Air Basin (SoCAB) of California for the year 2010. Results suggest that DER characterization can be systematically applied to urban air basins, and that realistic DER implementation in SoCAB by the year 2010 only slightly affects concentrations of ozone and particulate matter in the basin. However, DG may increase localized exposure to pollutants, and higher levels of DG penetration in years beyond 2010 may lead to more significant air quality impacts than those presented in this study.

Keywords: Distributed generation (DG), distributed energy resources (DER), air quality, air quality impacts, scenarios, air quality model, land-use GIS data

Executive Summary

Introduction

Distributed generation of energy (DG) has the potential to meet the power demands of the near future. Deployment of DG technologies might provide additional benefits in electrical reliability and quality, besides reductions in electricity production costs. The use of Combined Heat and Power (CHP) systems could further increase energy consumption efficiency, as well as reduce emissions through reduced fuel usage. Furthermore, having power generation near the place of use minimizes electricity transmission losses.

Distributed generation is characterized by a widely dispersed distribution of emission sources within an air basin. In contrast, conventional, centralized sources of emissions from large central power plants are concentrated and localized in relatively small areas. In addition, in some areas, such as the South Coast Air Basin of California (SoCAB), central power plants are mostly in remote areas or outside the air basin. Consequently, the air quality impacts associated with a transition from centralized power generation to DG need to be estimated.

Undoubtedly, the presence of DG in urban air basins raises numerous concerns that must be examined. The results from this study provide regulatory agencies with a scientific basis to design DG implementation policies—namely, how DG will likely be implemented in the SoCAB. Will increased emissions from DG implementation affect the levels of ambient ozone, with respect to ozone standards? Could any increase in nitrogen oxides (NO_X) emissions enhance secondary particulate matter (PM) formation? What DG implementation scenarios could reduce overall environmental impacts?

Previous research has not modeled impacts on air quality from DG emissions; the results and conclusions of those studies were based purely on emissions assessments. However, because changes in emissions profiles affect the concentrations of primary and secondary atmospheric contaminants, it is important that these effects be evaluated with air quality models that include chemical and physical processes that occur in the atmosphere.

Purpose

The purpose of this work was to evaluate the effects of DG technologies in the air basin with detailed air quality models that include the chemical and physical processes that occur in the atmosphere.

Project Objectives

This project sought to develop a set of realistic scenarios for DG application in the SoCAB, and to assess their air quality impacts with a detailed three-dimensional Eulerian air quality model—the California Institute of Technology (CIT) model. This model includes atmospheric processes such as homogeneous and heterogeneous chemistry; advective and turbulent transport; and the spatial and temporal variability of the emissions and meteorology. It is under continuous revision and development at University of California, Irvine, in collaboration with researchers from other institutions.

The two primary objectives of this study were to:

1. construct a set of DG implementation scenarios for the SoCAB; and
2. determine the potential air quality impacts of DG in the SoCAB by application of these scenarios to a detailed air quality model for SoCAB.

Project Outcomes

To accomplish the first objective, the researcher team delineated a systematic and general approach, to develop realistic DG implementation scenarios in the SoCAB by the year 2010. This approach is novel in using land-use geographic information systems (GIS) data as a foundation for the DG scenarios. The team classified DG scenarios into two categories—realistic scenarios and spanning scenarios—according to the likelihood of their occurrence. Realistic scenarios reflect an expected or realistic implementation of DG in the SoCAB; whereas, spanning scenarios were developed to consider an ample range of possibilities. Spanning scenarios are developed for scientific completeness, sensitivity analyses, and to determine the potential impacts of unexpected outcomes. A total of five realistic and 20 spanning DG scenarios were developed.

The research team evaluated the sensitivity of the CIT model to input variables and to model components for baseline year 2010 simulations and identified the parameters and elements that influence the most on air quality predictions. In addition, the team compared simulation results with predictions shown in the 2003 SoCAB Air Quality Management Plan, using different air quality models. They also analyzed the sensitivity of the CIT model to emissions changes due to weekday-weekend variation and to DG implementation.

Prior to establishing any potential impacts of DG implementation in the SoCAB, a complete characterization of baseline results for year 2010 was developed. The baseline scenarios are based on emissions inventories that do not consider significant DG emissions, except for emissions from DG units already installed. All of the simulations that were developed to assess potential DG air quality impacts *add* the emissions from the DG scenario to this baseline case.

Conclusions

Results from this project lead to the following major findings and conclusions:

- CHP utilizes efficiently the electricity generated by DG, reducing the need for the existing boilers as a means of energy production. The emissions displacements due to CHP that were estimated for most of the realistic scenarios lead to significant reductions in some criteria pollutant emissions and carbon dioxide (CO_2) emissions. For NO_X, emissions from boilers are higher than NO_X emissions directly produced by DG operated in conjunction with CHP, resulting in net negative emissions of NO_X from DG. This means that the implementation of CHP offsets emissions from DG alone, resulting in net decreases in basin-wide baseline NO_X emissions.
- Increase in total basin-wide emissions due to implementation of realistic DG is no larger than 0.43%, with respect to baseline emissions. Increase in total basin-wide emissions due to implementation of spanning DG scenarios is no larger than 1.35%, with respect to baseline emissions.

- The spatial distribution of DG power based on GIS land-use data results in DG scenarios that concentrate large capacity DG technologies in industrial zones, due to the relatively high adoption rate intensity factor estimated for the industrial sector.
- The calculation of basin-wide DG power distribution among the various sectors estimated for the year 2010 show that 60% of total DG power will be implemented in the industrial sector, and nearly 32% will be implemented in the commercial-institutional sector.
- Results of the basin-wide relative contribution of each type of DG technology showed that 49% of the DG market is being met by gas turbines, whereas internal combustion engines (ICEs), microturbine generators (MTGs), photovoltaics (PV), fuel cells (FC), and gas turbine-fuel cell (GT-FC) hybrids account for 17%, 15%, 5%, 10%, and 4% of the total 2010 DG power market, respectively.
- The air quality model shows observable changes in ambient concentrations of ozone (O_3) and $PM_{2.5}$ as the result of DG installations.
- In general, increases in NO_X emissions produced by DG scenarios reduce ozone concentrations in the central area of Los Angeles—which is typically volatile organic compound (VOC)-limited—and increase ozone concentrations at downwind locations—which are typically NO_X-limited. Increases in NO_X emissions also lead to an increase in 24-hour average $PM_{2.5}$ concentrations over downwind locations near Riverside. Scenarios in which there is a net reduction of NO_X as the result of emissions displacement by CHP produce small increments in ozone over the central area of Los Angeles, and no significant changes elsewhere.
- With representative characterizations of DG use in SoCAB for the year 2010, the air quality impacts of DG scenarios are:

  Realistic DG scenarios:
  - Maximum basin-wide ozone concentrations do not change. Changes in maximum basin-wide 24-hour average $PM_{2.5}$ range from 0 to -3 micrograms per square meter ($\mu g/m^3$)
  - Maximum changes in ozone concentrations at any point throughout the basin range from +5 ppb to -9 parts per billion (ppb). Increases of up to 3 ppb in ozone concentration occur in areas where baseline values already exceed air quality standards.
  - Maximum changes in 24-hour average $PM_{2.5}$ concentrations range within $\pm$ 3 $\mu g/m^3$

  Spanning DG scenarios:
  - Changes in basin-wide maximum ozone concentration range within ±1 ppb. Maximum 24-hour average $PM_{2.5}$ changes from -2 $\mu g/m^3$ to +2 $\mu g/m^3$
  - Typically, maximum changes in ozone concentrations at any point throughout the basin are within ±10 ppb, although there are specific cases in which changes in ozone concentration range from -26 ppb to +34 ppb. Maximum changes in 24-hour average $PM_{2.5}$ concentrations range from -4 $\mu g/m^3$ to +6 $\mu g/m^3$

- Various cases with different DG spatial distributions were explored. The level of emissions introduced by these spanning DG scenarios produces similar air quality impacts. However, additional scenarios that place a considerably higher concentration of

DG show that air quality impacts from DG use are affected by the geographical location of DG units. In particular, results suggest that if DG is to be widely used in the basin, then it should not be concentrated in a small area.

- Different temporal distributions of DG emissions are explored. Results show that an amount of DG emissions concentrated during a 6-hour period (peak duty cycle) produce a larger impact in air quality than the same amount emitted during 24 hours (base load duty cycle).
- Impacts on air quality estimated by this study are small, however, DG may increase localized exposure to pollutants, and higher levels of DG penetration in years beyond 2010 may lead to more significant air quality impacts than those presented in this study.
- DG installations may impact basin-wide compliance with air quality standards only if they are adopted at significantly higher levels and/or emit more pollution than those considered in this study.

Recommendations

The current work has produced the following recommendations regarding the impacts of DG on air quality:

- The impact of DG installation on air quality should be studied through use of a detailed understanding and development of DG implementation scenarios.
- Air quality assessments should not be made without the application of DG emissions to a detailed atmospheric chemistry and transport model that includes all the major chemical and physical processes and geographic and meteorological features of the region of interest.
- Substantial DG emissions should not be released in concentrated spatial locations.
- Substantial DG emissions should not be released concentrated within a short period of time. In other words, in terms of air quality impacts, constant base-loaded DG operation is preferred over peak operation.
- If possible, DG should be installed and operated in as disperse a manner as possible in space and time, to reduce potential air quality impacts.
- Clean DG, such as fuel cells and photovoltaics, have the least air quality impact, and should be preferred to other DG that have higher emissions levels.

Benefits to California

The structure of the electricity sector in California provides a good scenario for the widespread implementation of DG. On the other hand, some areas in California, such as the South Coast Air Basin, are affected by poor air quality. This work provides a scientific basis for determining possible scenarios for DG implementation, and for assessing the air quality impacts of such scenarios. Consequently, this study will help decision makers understand what DG implementation scenarios are preferred environmentally and establishes the basis upon which air quality assessment of DG can be made.

1. INTRODUCTION

Distributed generation (DG) has the potential to meet the power demands of the near future. Deployment of DG technologies might provide benefits in electrical reliability and quality, in addition to reductions in electricity production costs. The use of Combined Heat and Power (CHP) could improve energy consumption efficiency, as well as reduce emissions from fuel usage. Furthermore, having power generation near the place of use minimizes electricity transmission losses. DG is characterized by a widely dispersed distribution of emission sources within an air basin. In contrast, conventional, centralized sources of emissions from large central power plants are concentrated and localized in relatively small areas. In some areas, such as the South Coast Air Basin of California (SoCAB), central power plants are mostly in remote areas or outside the air basin. Consequently, air quality impacts associated to changes from centralized power generation to DG still need to be estimated.

California, as one of the first regions in the United States facing the renovation of its electric power industry, will likely be one of the first locations with widespread adoption of Distributed Energy Resources (DER). DER include any technology that produces power outside of the utility grid (i.e., DG) and any technology that stores power and that can be sold back to the grid where permitted by regulation. According to the DG strategic plan developed by the California Energy Commission (Tomashefsky and Marks 2002), more than 2,000 megawatts (MW) of generating capacity can currently be classified as DG in California. From January 2001 through May 2002, 192 DG projects were proposed throughout the state, representing more than 400 MW of new generation.

The implementation of a paradigm shift from central generation to distributed generation would result in significantly different emissions profiles with increased and widely dispersed stationary source emissions increases in several air basins (compared to central generation outside of the basin). As a result, it is important to determine whether increases in pollutant emissions in the air basin would lead to ambient ozone levels that exceed the proposed new 8-hour ozone standard. Also, increases in NO_X emissions can trigger increases in secondary particulate matter (PM) formation that could impact compliance with the proposed federal 24-hour $PM_{2.5}$ standard (65 $\mu g/m^3$). The determination of these and other potential air quality impacts is of significant strategic importance to the advancement of DG technology. In addition, these impacts need to be assessed to provide a scientific basis for the design of policies related to DG implementation.

In a recent study, Lents and Allison (2000) determined the forms of DG that are most likely to improve environmental quality, and to reduce air pollution in California. The strategy they adopted was to comparatively analyze the level of pollutant emissions associated with a range of DG technologies and fuel types. The DG technologies considered in this study were: Micro-turbine generators, advanced turbine systems (ATS), conventional turbines, gas-powered internal combustion engines (ICE), diesel ICE, proton-exchange membrane (PEM) fuel cells, and solid oxide fuel cells. The study also considered home/commercial water heating systems to calculate the benefits of implementing CHP. They concluded that only the lowest-emitting DG technologies (e.g., fuel cells) with significant waste heat recovery are even marginally competitive with the emissions performance of modern, natural gas-fired, combined-cycle power

production from a criteria pollutant emissions perspective. However, in cases where waste fuel is being flared or directly emitted within the basin (e.g., in landfills), in-basin pollutant emissions can be reduced if this fuel is used to drive the DG units.

Ianucci et al. (2000) evaluated the net air emissions effects from the potential use of cost-effective distributed generation in California. First, the study used information on the available DG technologies and their costs to assess the economic market potential for DG, for both utilities and large commercial/industrial customers in years 2002 and 2010. Second, total emissions were calculated for the selected years, given the estimated market penetration levels for each type of DG, and compared with central-generation-only scenario. The study concluded that the current California central generation mix is so clean that virtually no cost-effective distributed generation source could lower net emissions, even when transmission and distribution electric line losses are included. Fuel cells achieved a marginal market penetration, as a result of their high cost, but showed great promise because fuel cell air emissions are much lower than central station generation.

Significantly, this previous research did not model impacts on air quality attributable to DG emissions. The results and conclusions of these studies were based purely on emissions assessments. Changes in emissions profiles affect the concentrations of primary and secondary atmospheric contaminants. These effects need to be evaluated with detailed air quality models that include chemical and physical processes that occur in the atmosphere. The research described in this report, was conducted by the Advanced Power and Energy Program (APEP) at the University of California, Irvine, and funded by the California Energy Commission under the Public Interest Energy Research (PIER) program. It sought to develop a set of realistic scenarios for DG application in the SoCAB and to assess the air quality impacts of DG with a detailed, three-dimensional Eulerian air quality model—the California Institute of Technology (CIT) model. This model includes atmospheric processes such as homogeneous and heterogeneous chemistry; advective and turbulent transport; and the spatial and temporal variability of the emissions and meteorology. The model is under continuous revision and development at University of California, Irvine, in collaboration with researchers from other institutions. The CIT model has been used in previous applications: e.g., to study control measures of NO_X and volatile organic compounds (VOCs) and the effect on particulate matter formation (Nguyen and Dabdub 2002b); and to assess the impact of chlorine chemistry in ozone formation over coastal urban environments (Knipping and Dabdub 2003).

The primary objectives of this study were to: (1) construct a set of distributed generation implementation scenarios for the SoCAB of California; (2) improve and validate an existing air quality modeling system for use in distributed generation analyses; and (3) determine the potential air quality impacts of DG in the SoCAB by application of these scenarios to a detailed air quality model for SoCAB.

The first part of this report presents the project approach, which includes three sections:

(1) **DG scenario development** strategy, which includes the methodology to define each DG scenario.
(2) **Air quality modeling** approach and results, which describes the inputs required for air quality simulations to determine impacts of DG and presents a comparison of simulation results with measurements.
(3) **Uncertainty and sensitivity** of the chemical mechanism and the full three-dimensional air quality model, including the methodology used to determine them.

The second part of this report presents the project outcome, which includes five sections:

(1) Final DG scenarios, which include the parameters that define each scenario and the net emissions resulting from DG implementation.
(2) Baseline air quality simulation results for the year of study 2010.
(3) Air quality modeling evaluation, which includes comparison of modeling results with simulations obtained by other models. In addition, this section presents improvements included in the air quality model to capture DG impacts and states the present understanding of model sensitivity to DG.
(4) Air quality impacts of DG scenarios, which includes impacts on ozone (O_3), nitric oxide (NO), and PM concentration.
(5) Uncertainty and sensitivity analysis results for the chemical mechanism and the full air quality model.

The final part of the report summarizes the conclusions extracted from this study. In addition, it includes final recommendations for the implementation of DG in the South Coast Air Basin and for future evaluations of DG implementation in other areas in California.

2. PROJECT APPROACH

2.1 Distributed Generation: Scenario Development

2.1.1 Characterization of DG Scenarios

To fully characterize how distributed generation (DG) resources may be implemented in the SoCAB, one must describe in detail a significant set of parameters that define the operating characteristics of the DG units, their spatial and temporal distribution throughout the basin, and other characteristics of the particular instance of DG use in the basin. In this project, a compilation of the entire suite of information and characteristics that are required to fully describe all of the DG characteristics as installed in the SoCAB is called a "DG Scenario."

The Advanced Power and Energy Program team has determined that the space required to fully define a DG Scenario can be characterized by a set of seven primary parameters and various factors that are subsets of those parameters. The seven parameters that have been identified to fully characterize a DG scenario are presented schematically in Figure 1. The seven parameters include: (1) the total fraction of SoCAB energy needs that are met by DG in the scenario, (2) the allocation of DG resources to meet that need, (3) the emissions associated with each DG unit type, (4) the spatial distribution of the DG in SoCAB, (5) the operational duty cycle of each DG, (6) the accounting for any emissions that are displaced by installation of the DG, and (7) other estimates that are required to account for the DG and relate the emissions to requirements of the air quality model (AQM). Each of the parameters may have several factors that are varied within the parameter space.

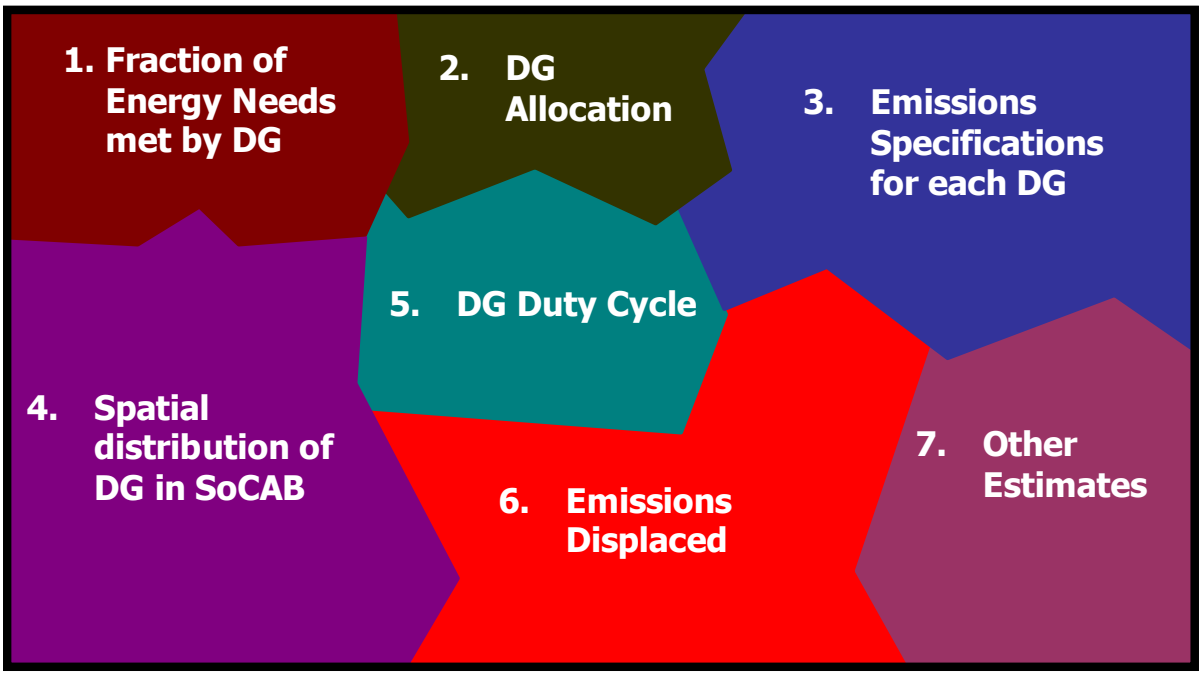

Figure 1. Schematic of the DG scenario parameter space

Table 1 presents more details of the parameter space and all of the factors that are considered in the development of the DG scenarios, including the overall outline of these parameters (highest level of characterization) and factors (lower-level variables). Note that the project team considers some of the parameters as fully characterized by variations in primary factors; whereas, other parameters require characterizations and variation of primary and secondary factors in their definition.

Table 1. List of parameters and factors that are required to be characterized to represent a full distributed generation scenario for the South Coast Air Basin

Main DG Parameter	Primary Factors	Secondary Factors
1. Fraction of energy needs met by DG	1.1. Limited (5% of increase in the power demand from 2002 to 2010)	
	1.2. Medium (10% of increase)	
	1.3. High (15%–20% of increase)	
2. DG allocation	2.1. Types of DG units	2.1.1. All NG large GT-DG (50 MW)
		2.1.2. Fuel Cell Only
		2.1.3. MTG only
		2.1.4. Renewables – yes, no
		2.1.5. Mix of DG (MTG, FC, NG-ICE, Stirling, hybrid, …)
		2.1.6. Mix of DG and large GT-DG (50 MW)
		2.1.7. Diesel included – yes or no
	2.2. Number of DG units of each type	2.2.1. Large DG unit size vs. small DG unit size
		2.2.2. Technology Mix Factors - High penetration of low-emissions technologies (strong regulation/policy drivers) - Low penetration of low-emissions technologies (either modest regulation or lack of technology advancement) - Zoning or land-use - Economic factors
3. Emissions specification for each DG	3.1. Current emissions factors	3.1.1. Known emissions factors – literature, data
		3.1.2. Estimated emissions factors
	3.2. Future advancements to meet regulatory requirements	3.2.1. Fraction that meets 2003 standards
		3.2.2. Fraction that meets 2007 standards

Table 1. (continued)

Main DG Parameter	Primary Factors	Secondary Factors
4. Spatial distribution of DG in SoCAB	4.1. Even	
	4.2. Population weighted	
	4.3. Population growth weighted	
	4.4. Land-use weighted	4.4.1. Classify land use
		4.4.2. Land-use energy adoption rate factors
		4.4.3. Land-use weighted technology adoption factors
	4.5. Electrical use weighted (need data from SCE/LADWP)	
	4.6. Freeway weighted	
5. DG duty cycle	5.1. Base-loaded	
	5.2. Peaking	
	5.3. Mix of base-loaded and peaking	
6. Emissions displaced	6.1. Port emissions	NOTE: Only if DG is installed in place of idling ships
	6.2. Landfill/digester/other flared or wasted gas use	NOTE: Most of these sources have already implemented emissions mitigation technology
	6.3. CHP	6.3.1. Displace old boilers and equipment
		6.3.2. Displace new boilers and equipment
		6.3.3. Percentage of CHP value recovered
	6.4. In-basin electricity emissions displaced	
7. Other estimates	7.1. Emissions assumptions	7.1.1. Speciation of total hydrocarbons into specific hydrocarbon compounds and PM into 8 size classes and 19 species of PM
	7.2. Performance degradation (yes or no)	
	7.3. Geometrical features (elevated emissions – yes or no)	
	7.4. DG commercial adoption rate	7.4.1. High early adoption (logarithmic increase of cumulative DG power from 2003 to 2010)
		7.4.2. Low early adoption (exponential increase of cumulative DG power)
		7.4.3. Medium early adoption (linear increase of cumulative DG power)

NG=natural gas; GT-DG=gas turbine-distributed generation; MTG=microturbine generation; FC==fuel cells; NG-ICE=natural gas-internal combustion engine; SCE=Southern California Edison; LADWP=Los Angeles Department of Water and Power

Once all of the parameters and factors of Table 1 are specified, the DG scenario is fully characterized and the corresponding DG emissions inventory for each of the discrete cells in the computational model can be developed for each instance in time. The model calculates the transport, chemical reaction, diffusion, and other aspects of all the species within the basin on an hourly averaged basis. As a result, DG emissions rates must be specified for, as listed in Table 1 for each cell and for each of the 24 hours of each day of the simulation. This DG emissions inventory is then formatted as a model input file and added to the baseline emissions inventory for use in the model to assess the air quality impacts of the DG emissions. The baseline emissions inventory includes the emissions forecasted for 2010 by the California Air Resources Board (CARB) and South Coast Air Quality Management District (SCAQMD) (Allen 2002, pers. comm.).

Two types of DG Scenarios were developed for this project:

- "Realistic" DG Implementation Scenarios
- "Spanning" DG Implementation Scenarios

These two categories segregate the DG Scenarios on the basis of the "likelihood" of the scenario. "Realistic" implementation scenarios for DG in the South Coast Air Basin are assessed by the APEP team and stakeholders who participated in the September 19, 2002 and May 20, 2003 workshops to be likely instances of DG installation in the SoCAB. However, for scientific completeness, for sensitivity analyses, and for determination of potential impacts for unexpected outcomes, "Spanning" scenarios are required. These spanning scenarios must not be considered realistic or probable. The spanning DG scenarios are not expected and are only used for purposes of garnering insights that may be useful.

2.1.1.1 Fraction of Energy Met by DG

The "Fraction of Energy Met by DG" parameter has a strong influence in the final air quality impact that a DG scenario exhibits. A high-penetration scenario implies that DG units throughout the basin meet a considerable portion of the total energy needs of the SoCAB. In this case, DG emissions extensively contribute to the total SoCAB pollutant emissions. However, for the same level of emissions, air quality impacts might be very different depending on other DG scenario characterization parameters such as spatial distribution of the DG power or duty cycle. In addition, these impacts are not easy to predict without a detailed and comprehensive model, because of the highly non-linear processes that govern the coupled transport and atmospheric chemistry of an air basin.

According to the California Energy Commission *Distributed Generation Strategic Plan* (Tomashefsky and Marks 2002), the forecasted adoption of DG in California for the year 2020 could be as high as 20% of the electricity load growth. The current DG scenarios are considered high-penetration scenarios if the power demand met by DG is greater than 15% of the increased SoCAB power. Medium and low penetration are assigned to cases with about 10% and 5%, respectively, of the increased power demands met by DG.

Because the fraction of energy met by DG is quite uncertain, a wide variety of DG penetration levels is investigated in the DG scenarios, to span the spectrum of possible air quality impacts.

2.1.1.2 DG Allocation

Based on input from the first industry stakeholders workshop held in September 2002 (see Appendix A for full details and results from this workshop), the current study includes distributed generators with power capacities that range from a few kilowatts (kW) up to 50 MW. The 50 MW limit is the maximum power that a generator can provide to be considered a DG installation in the SoCAB. The DG technologies that are likely to be implemented in the SoCAB include commercial technologies (natural-gas-fired combustion turbines (up to 50 MW) and natural-gas-fired reciprocating internal combustion engines (ICE)), and emerging technologies (solar photovoltaics (PV), fuel cells (proton exchange membrane fuel cell (PEMFC), molten carbonate fuel cells (MCFC), and solid oxide fuel cell (SOFC)), gas turbine fuel cell hybrids, natural-gas-fired microturbine generators (MTGs), and external combustion Stirling engines).

The specific mix of DG technologies that is likely to be installed in any one region of the SoCAB in 2010 is very difficult to forecast. The technology mix is dependent on the number and type of energy customers in that region as well as on a host of other economic and regulatory variables (e.g., electricity prices, gas prices, DG incentives, transmission constraints, emissions standards) that exist in that particular zone.

Every market segment can be preferentially associated with specific DG technologies that are likely to be predominant, mainly because their capacity and features are best suited to the energy demands of that segment. For example, residential applications in the range 1–5 kW will likely favor fuel cells and photovoltaics; commercial and small industrial sectors, with capacities ranges of 25–500 kW are more suited for PV, MTGs, small ICEs and FCs; large commercial and institutional sectors, in the range of 500 kW–2 MW, will likely favor natural gas reciprocating engines and gas turbines; and finally the large institutional and industrial sectors with 2–50 MW capacity will be mainly served by gas turbines. This relationship between DG type and market sector, together with spatial distributions of such in SoCAB, is used in some of the scenarios to estimate the distribution and duty cycle of technologies in each of the discretized cells of the model on the basis of land-use zoning classification data.

The DG scenarios developed in this effort are not based upon a detailed market penetration analysis for the various DG technologies in SoCAB, but rather upon studies that are currently available in the literature, APEP insights, and stakeholder feedback. The resources used include: (1) previous studies that determined a reasonable mix of technologies (e.g., Ianucci et al. 2000; Marnay et al. 2001), (2) input from the industry stakeholder workshops (see Appendix A and Appendix B), (3) current APEP understanding of technology features, (4) current penetration of certain technologies (e.g., MTGs), and (5) APEP intuition; engineering insight, and/or brainstorming.

Diesel- and petroleum-distillate-fueled units are not included in the current mix of DG technologies, because the SCAQMD does not currently permit them to run on a continual basis as distributed generators. These types of units are only permitted to run as backup generators.

2.1.1.3 Emissions Specifications

There is a wide range of emissions factors that are either available as measured data or estimated by various investigators for each of the DG technologies. Some DG technologies are environmentally friendly, with zero emissions (e.g., wind turbines, photovoltaics) or near-zero emissions (e.g., fuel cell systems using on-site natural gas reformation), while others may emit more pollutants than central station power plants. For the some of the spanning DG scenarios the emissions factors proposed by Allison and Lents (2002), which are best estimates from a compilation of sources, have been used directly. This data set, however, includes emissions factors that are higher than the current regulated limits for DG units permitted by SCAQMD (ICEs and GT) and the others certified by CARB (MG, FC, Stirling engines, and others with less than 1 MW capacity). Whenever this occurred, the values selected to characterize a specific DG unit were the applicable standards levels, instead of the emissions factors of Allison and Lents (2002). The emissions factors proposed by Allison and Lents (2002) for a collection of gas-driven DG technologies are presented in Table 2.

Table 2. Emissions factors and efficiencies for some DG technologies

Generation Type	Efficiency	CO	VOC	NO_x	SO_x	$PM_{2.5}$	CO_2
	Elec. Out / Energy In	lbs/kWh	lbs/kWh	lbs/kWh	lbs/kWh	lbs/kWh	lbs/kWh
Gas Turbine Combined-Cycle, central	0.52	1.70E-04	1.10E-04	1.30E-04	2.00E-05	2.00E-05	0.62
MTG	0.27	2.85E-03	5.00E-05	1.40E-03	2.00E-05	9.00E-05	1.25
Advanced Turbine	0.36	2.60E-03	3.00E-05	1.09E-03	2.00E-05	7.00E-05	0.95
Conventional Turbine	0.28	1.51E-03	4.00E-05	1.24E-03	3.00E-05	9.00E-05	1.2
Gas-Powered ICE	0.35	8.00E-03	1.70E-03	3.20E-03	1.00E-05	4.75E-04	0.97
Diesel ICE	0.44	3.00E-02	2.00E-03	1.70E-02	3.00E-04	3.00E-03	1.7
PEM Fuel Cell	0.36	0.00E+00	9.00E-04	2.00E-05	1.00E-05	0.00E+00	0.95
Direct Fuel Cell	0.4	0.00E+00	0.00E+00	0.00E+00	0.00E+00	0.00E+00	0.68

CO=carbon monoxide
(Source: Allison and Lents 2002)

For the realistic scenarios and to determine a more likely set of emissions for each of the DG technology types, the current study conducted an extensive literature search. This literature search, together with insights, reports, and feedback from agencies, industries, and colleagues has led the compilation of various emissions estimates, as presented in Table 3. Six primary sources are presented in Table 3, with each of the DG technologies that are covered by each reference, and a listing of the pollutant species emissions rates that are available in each study.

Appendix C presents the details of the emissions rates represented by the sources listed in Table 3. Note that there is wide variability of emissions factors among the currently available studies. Appendix C also presents the DG emissions standards for 2003 and 2007 and the current best available control technology (BACT) requirements of SCAQMD for DG in the SoCAB.

Table 3. DG technologies and pollutant species available in six literature references for DG emissions factors

Generation Type	NREL 2003	Nexus 2002	Allison and Lents, UCR 2002	Regulatory Assistant Project (RAP) 2001	Marnay et al., LBNL 2001	Ianucci et al., DUA 2000
Gas Turbine Combined-Cycle, central	N/A	N/A	CO, VOC, NO_x, SO_x, PM, CO_2	CO, VOC, NO_x, SO_x, PM, CO_2	N/A	N/A
Microturbine Generator	CO, NO_x, VOC, CO_2	CO, NO_x, VOC	CO, VOC, NO_x, SO_x, PM, CO_2	CO, VOC, NO_x, SO_x, PM, CO_2	CO, NO_x, PM	CO, VOC, NO_x, SO_x, PM, CO_2
Advanced Turbine	N/A	CO, NO_x, VOC	CO, VOC, NO_x, SO_x, PM, CO_2	CO, VOC, NO_x, SO_x, PM, CO_2	N/A	CO, VOC, NO_x, SO_x, PM, CO_2
Conventional Turbine	N/A	CO, NO_x, VOC	CO, VOC, NO_x, SO_x, PM, CO_2	CO, VOC, NO_x, SO_x, PM, CO_2	N/A	CO, VOC, NO_x, SO_x, PM, CO_2
Uncontrolled Gas Powered Lean Burn ICE	N/A	N/A	CO, VOC, NO_x, SO_x, PM, CO_2	CO, VOC, NO_x, SO_x, PM, CO_2	CO, NO_x, PM	CO, VOC, NO_x, SO_x, PM, CO_2
Uncontrolled Diesel ICE	N/A	N/A	CO, VOC, NO_x, SO_x, PM, CO_2	CO, VOC, NO_x, SO_x, PM, CO_2	CO, NO_x, PM	CO, VOC, NO_x, SO_x, PM, CO_2
PEMFC	N/A	CO, NO_x, VOC	CO, VOC, NO_x, SO_x, PM, CO_2	N/A	N/A	CO, VOC, NO_x, SO_x, PM, CO_2
DFC	N/A	CO, NO_x, VOC	CO, VOC, NO_x, SO_x, PM, CO_2	N/A	N/A	N/A
SOFC	N/A	CO, NO_x, VOC	N/A	NO_x, SO_x, PM, CO_2	N/A	N/A
3-way Catalyst Gas-Powered Rich-Burn ICE	N/A	CO, NO_x, VOC	N/A	CO, VOC, NO_x, SO_x, PM, CO_2	N/A	N/A
SCR-Controlled Diesel ICE	N/A	CO, NO_x, VOC	N/A	CO, VOC, NO_x, SO_x, PM, CO_2	N/A	N/A

DFC=direct fuel cell

Appendix C presents plots for emissions rates of different DG technologies for the main six air pollutants (CO, NO_X, VOC, SO_X, PM, and CO_2). Minimum, maximum, and average values of emissions estimates from all of the six literature sources presented in Table 3 are presented in Appendix C.

Table 4 and 5 present the recently approved California Air Resources Board emission standards (CO, VOC, NO_X, and PM limits) for type certification of DG. These standards apply to DG units that do not fall under the jurisdiction of SCAQMD for control of stationary point sources. The capacity limit for SCAQMD rules to apply is 1MW, below which the regulatory requirements presented in Table 4 and 5 apply.

Table 6 presents the SCAQMD best available control technology permitted levels for DG emissions. This project expended significant effort to study both the regulatory requirements of Table 4, Table 5, and Table 6, and all of the emissions estimates presented in Appendix C. This effort proved that significant disparities in the emissions rates and DG performance expectations exist, which adds uncertainty to the evaluation of DG environmental impacts. To address these disparities, this project included a sensitivity analyses effort to determine model output sensitivities to emissions rates, as well as to search out measurements and verifiable performance data to include in the analyses. At the same time, the best possible estimates that were deemed reasonable and feasible, and that do not violate current regulations, were used in the scenario development of this study.

In a couple of the spanning scenarios, DG emissions limits as currently set by CARB for 2003 and 2007, as well as SCAQMD best available control technology standards for DG, were used directly for all of the DG implemented. These spanning scenarios are presented as reference cases only.

Table 4. Approved ARB DG emissions standards for 2003

Pollutant / DG type	CO	VOC	NO_X	PM
	lbs/MWh	lbs/MWh	lbs/MWh	lbs/MWh
DG Unit not integrated with Combined Heat and Power	6.00	1.00	0.50	An emission limit corresponding to natural gas with sulfur content of no more than 1 grain per 100 standard cubic feet (scf)
DG Unit integrated with Combined Heat and Power	6.00	1.00	0.70	An emission limit corresponding to natural gas with sulfur content of no more than 1 grain per 100 standard cubic feet (scf)

Source: Chin et al. 2001

Table 5. Approved CARB DG emissions standards for 2007

Pollutant / DG type	CO lbs/MWh	VOC lbs/MWh	NO_X lbs/MWh	PM lbs/MWh
DG Unit not integrated with Combined Heat and Power	0.100	0.020	0.070	An emission limit corresponding to natural gas with sulfur content of no more than 1 grain per 100 standard cubic feet (scf)

Source: Chin et al. 2001

Table 6. SCAQMD BACT guidelines for gas turbines and internal combustion engines

Subcategory	VOC	NO_X	SO_X	CO	PM_{10}	Inorganic (NH_3)
NG GT < 3 MWe						
ppm@15% O_2		9	--	10	--	9
lbs/MMBtu	0.0026	0.0332	0.0008	0.0224	0.0066	0.012
lbs/MWh	0.0358	0.4638	0.0112	0.3137	0.0923189	0.170
NG GT ≥ 3 MWe and < 50 MWe						
ppm@15% O_2	2	3.6	--	10	--	5
lbs/MMBtu	0.0026	0.0133	0.0008	0.0224	0.0066	0.007
lbs/MWh	0.0243	0.1257	0.0076	0.2126	0.0626	0.064
Non-Emergency NG ICE, <2064 bhp						
ppm@15% O_2	32.42	11.28	--	74.18	--	--
lbs/MMBtu	0.0415	0.0415	0.0008	0.1663	0.0066	--
grams/bhp-hr	0.15	0.15	0.003	0.600	0.024	--
lbs/MWh	0.4431	0.4431	0.0085	1.7723	0.0704	--

NH_3=ammonia; MMBtu=million Btu; MW-hr=megawatt-hour; MWe=megawatt electric; bhp=brake horsepower
Source: SCAQMD 2000

Using the compilation of literature emissions factor data and the CARB and SCAQMD limits presented in Table 4, Table 5, and Table 6 as an upper bound, the APEP team constructed two tables with emissions factors for DG systems installed in the periods 2003–2006 and 2007–2010, respectively, as shown in Table 7 and Table 8. These sets of DG emission factors are the ones utilized in the development of DG implementation scenarios, both the spanning and the realistic scenarios, unless otherwise specified.

Table 7. Emissions factors used to develop DG Scenarios in the current study for DG units installed in the period 2003–2006

Generation Type	Efficiency (based on HHV)	CO	VOC	NOx	SOx	PM	CO_2	NH_3
		lbs/kWh	lbs/kWh	lbs/kWh	lbs/kWh	lbs/kWh	lbs/kWh	lbs/kWh
MTG	0.27	2.85E-03	5.00E-05	7.00E-04	1.01E-05	8.35E-05	1.50	0E+00
GT (<3 MW)	0.244	3.12E-04	3.58E-05	4.62E-04	1.12E-05	9.23E-05	1.66	1.70E-04
GT (>3 MW)	0.36	2.12E-04	2.43E-05	1.26E-04	7.59E-06	6.26E-05	1.13	6.42E-05
Gas ICE	0.32	1.77E-03	4.43E-04	4.43E-04	8.54E-06	7.04E-05	1.27	0.E+00
LT FC	0.36	1.00E-04	9.00E-04	7.00E-05	7.59E-06	6.26E-05	1.13	0.E+00
HT FC	0.48	1.00E-04	2.00E-05	7.00E-05	5.69E-06	4.69E-05	0.85	0.E+00
Stirling	0.27	6.00E-03	1.00E-03	5.00E-04	1.01E-05	8.35E-05	1.50	0.E+00
Hybrid	0.7	6.00E-03	1.00E-03	5.00E-04	3.90E-06	3.22E-05	0.58	0.E+00

LT FC= low-temperature fuel cell; HT FC = high-temperature fuel cell

Table 8. Emissions factors used to develop DG Scenarios in the current study for DG units installed in the period 2007–2010

Generation Type	Efficiency (based on HHV)	CO	VOC	NOx	SOx	PM	CO_2	NH_3
		lbs/kWh	lbs/kWh	lbs/kWh	lbs/kWh	lbs/kWh	lbs/kWh	lbs/kWh
MTG	0.27	1.00E-04	2.00E-05	7.00E-05	1.01E-05	8.35E-05	1.50	0.00E+00
GT (<3 MW)	0.244	3.12E-04	3.58E-05	4.62E-04	1.12E-05	9.23E-05	1.66	1.70E-04
GT (>3 MW)	0.36	2.12E-04	2.43E-05	1.26E-04	7.59E-06	6.26E-05	1.13	6.42E-05
Gas ICE	0.32	1.77E-03	4.43E-04	4.43E-04	8.54E-06	7.04E-05	1.16	0.00E+00
LT FC	0.36	1.00E-04	2.00E-05	7.00E-05	7.59E-06	6.26E-05	1.13	0.00E+00
HT FC	0.48	1.00E-04	2.00E-05	7.00E-05	5.69E-06	4.69E-05	0.85	0.00E+00
Stirling	0.27	1.00E-04	2.00E-05	7.00E-05	1.01E-05	8.35E-05	1.50	0.00E+00
Hybrid	0.7	1.00E-04	2.00E-05	7.00E-05	3.90E-06	3.22E-05	0.58	0.00E+00

The emissions factors presented in Table 7 and Table 8 indicate that the DG technologies that can be deployed in the SoCAB have relatively low criteria pollutant emissions rates (i.e., they are clean DG technologies). Nonetheless, if DG are widely adopted in the SoCAB, the contribution of DG emissions compared to total emissions estimates in the SoCAB for 2010 is important enough to be concerned about potential air quality impacts of DG deployment. For example, one of the spanning scenarios, characterized by an extra-high penetration (20% of total power met by DG) and a mix of DG technologies, produces DG NO_X emissions that account for 2% of the total SoCAB NO_X emissions inventory for 2010.

Figure 2 presents a comparison of DG criteria pollutant emissions (carbon monoxide, nitrogen oxides, reactive organic gases, and particulate matter) and the total basin emissions inventory for the SoCAB in 2010. The Figure 2 data represent the attainment emissions inventory (i.e., one that scales emissions for population and vehicle miles traveled growth and assumes additional

regulatory measures are adopted to meet attainment with ambient air quality standards (SCAQMD 2003)) compared to the high DG penetration scenario described above

Even though the realistic DG scenarios typically contain lower DG penetration and result in much smaller contributions of DG emissions to the inventory, the air quality impacts of these DG emissions may still be significant. First, many particular locations in the SoCAB are "on the edge" between compliance and non-compliance. Even a 1 ppb change in ozone concentrations in one location, for example, could result in the basin not achieving attainment. In addition, since the coupled transport and atmospheric chemistry interactions are of a highly non-linear nature, small changes in emissions fields could lead to substantial air quality impacts.

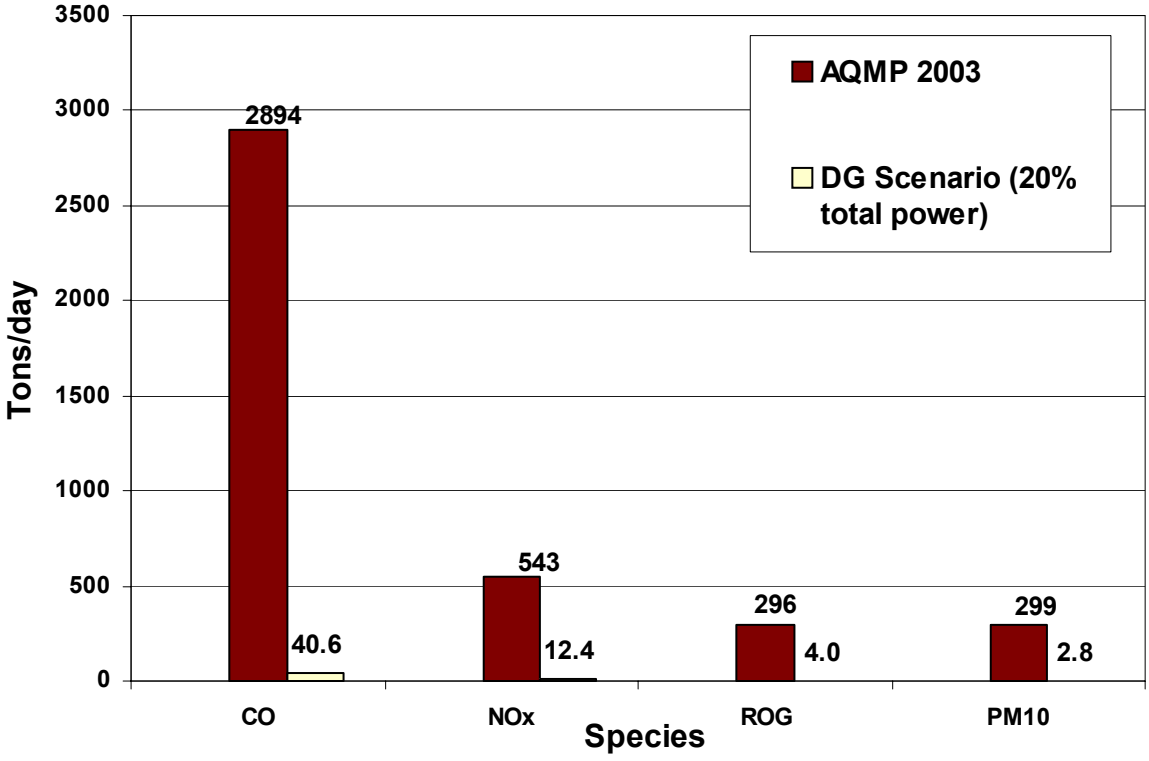

Figure 2. Comparison of total SoCAB emissions in 2010 and DG emissions from an extra high DG penetration scenario

2.1.1.4 Spatial Distribution of DG in SoCAB

It is important to capture the spatial distribution of emissions in an air basin in order to accurately determine species concentrations that contribute to air quality. The location of the emissions, together with meteorology, mass transport, photochemical reaction times, the mixture of chemical compounds (both gases and aerosols), radiation intensity, and other factors all contribute to the eventual air quality prediction (e.g., ozone, NO_X, PM_{10} concentrations). To estimate the spatial distribution of DG adoption accurately, a detailed market penetration study should be conducted at the scale of model resolution. However, this was beyond the scope of this study, so reasonable estimates of DG power in 2010 were developed based strictly upon

demographic and economic parameters that can be correlated to power (e.g., population data, population growth data, electricity consumption data, land-use data). In most of the DG scenarios developed in this effort (i.e., the spanning scenarios), the forecast of DG power in each cell is proportional to the number of inhabitants forecasted for 2010 in that cell—that is, the DG spatial distribution is population weighted. The other spatial distributions that are applied in this study are:

- even,
- population growth weighted,
- land-use weighted (used for all of the realistic scenarios),
- electrical use weighted (based on available data from Southern California Edison (SCE) and the Lost Angeles Department of Water and power (LADWP), and
- freeway weighted.

2.1.1.5 DG Duty Cycle

The DG duty cycle parameter accounts for the temporal variation of DG power production that leads to the overall capacity factor (number of hours operating/total hours) for each of the individual DG devices. The actual duty cycle for an individual DG unit depends upon maintenance schedules, economics, power demand, and many other factors. For a specific scenario some DG technologies (e.g., high-temperature fuel cells) will likely operate as base-loaded devices, i.e., they will operate essentially continuously. This is due to both economic factors (high efficiency and high capital cost portend continuous operation for a reasonable payback) and operational factors (high-temperature operation leads to long start-up and high thermal stresses associated with transients). On the other hand, many other DG technologies are expected to operate primarily during peak hours. The combined DG duty cycle of all DG units operating in each cell results in a different set of pollutant emissions for each hour of the simulation. The air quality model can assess the air quality impacts of this duty cycle, which is capable of accepting DG emissions profiles that vary on an hourly basis.

2.1.1.6 Emissions Displaced

Many of the DG technologies that are being and will be adopted in the SoCAB will be used in CHP applications, because the higher overall energy efficiency of CHP improves the economics of certain DG projects. Waste heat produced during electricity generation can be captured by a heat recovery system that provides useful heat to meet facility thermal loads, which can significantly decrease operating costs. As a result, DG/CHP can replace the heat produced by burning fuel in a boiler, leading to a reduction (displacement) of boiler-associated emissions in the basin. For retrofit DG/CHP applications, old, more-polluting boilers are likely to be displaced; whereas, for new applications displacement of emissions from new equipment (i.e., more efficient and lower polluting boilers) should be considered.

Emissions into the SoCAB can also be displaced by application of DG to waste gases from solid landfills, oil fields, or biomass gas emissions (e.g., dairy farm gaseous emissions). In these cases the DG application displaces either direct hydrocarbon emissions or flared gas emissions, depending upon the current status of the waste gas emission. According to Allison and Lents

(2002), all DG units in this type of application reduce ozone-related emissions, compared to a central station combined-cycle power plant. Because these units do reduce ozone-related emissions, and due to encouragement from the SCAQMD, most of the landfills in the SoCAB have already implemented DG (Lenssen 2001) to substitute for flares and produce on-site power and heat.

Other DG applications in which emissions could be displaced include the replacing of old central power plants in the basin and the substitution of lower-emitting DG technologies for the diesel generators that are extensively used in the Los Angeles port and its vicinity. All of the above potential displacements of emissions are taken into account in the development of realistic DG scenarios.

2.1.1.6.1 CHP emissions displacement

To assess the displaced boiler emissions and net DG emissions for each of the discretized model cells in scenarios in which CHP emissions displacement is considered, the following procedure was applied (see description of variables in Table 9):

Table 9. Description of variables used for calculation of CHP emission displacement

Variable	Description
f_{CHP}	Estimated fraction of DG with waste heat recovery
f_{HR}	Heat recovery utilization factor or heat recovery capacity factor
$f_{DG,i}$	Fraction of DG technology *i*, which can vary hourly
f_{old}	Fraction of old boilers
f_{new}	Fraction of new boilers
f_{boiler}	Avoidable boiler air emissions (lbs/Btu)
Q_{elec}	Electric energy produced by DG
Q_{HR}	Thermal heat recovered in each hour
Q_{fuel}	Offset fuel energy that would otherwise be burnt in the boilers
$\eta_{elec,i}$	Electrical efficiency of fuel driven DG technology *i*
$\eta_{total,i}$	Total efficiency of fuel driven DG technology *i*
ef_{old}	Old boilers efficiency
ef_{new}	New boilers efficiency
ef_{tot}	Total efficiency (mixed electricity and heat energy divided by fuel energy in)
ef_{elec}	Fuel-to-electricity conversion efficiency
ef_{boiler}	Fuel-to-heat conversion efficiency of boiler
$em_{old,i}$	Emission factors for pollutant species *i* for old boilers
$em_{new,i}$	Emission factors for pollutant species *i* for new boilers
$M_{CO,off}$	Displaced boiler CO emissions
$M_{CO,DG}$	DG CO emissions
$M_{CO,net}$	Net CO emissions from DG/CHP systems
DGHeatRate	Chemical energy of fuel divided by electrical output of DG [Btu/kWh]

1. Estimate a reasonable share of the DG implemented in the SoCAB that is installed with waste heat recovery equipment (e.g., f_{CHP} = 60% was suggested in the stakeholder workshop).
2. Assume an average heat recovery utilization factor or heat recovery capacity factor, which includes the lost waste heat due to supply and demand mismatch (e.g., f_{HR} = 50%).
3. Evaluate the total amount of thermal heat recovered in each hour, Q_{HR}, taking into account the electric energy produced by the DGs, Q_{elec}, the electrical and total efficiencies of each fuel-driven DG technology, $\eta_{elec,i}$ and $\eta_{total,i,}$ respectively, and the particular mix of DG, $f_{DG,i}$, which can vary hour by hour, depending on possible differences in duty cycle for each technology.

$$Q_{HR} = Q_{elec} \sum_{i}^{n} \left(f_{DG_i} \frac{\left(\eta_{total\,i} - \eta_{elec\,i}\right)}{\eta_{elec_i}} \right) \cdot f_{CHP} \cdot f_{HR} \tag{1}$$

4. Assume a reasonable mix of old, inefficient, dirty boilers (associated with retrofit DG/CHP) and new, clean, more efficient boilers (associated with new DG/CHP projects). Example: f_{old} = 30%: f_{new} = 70%.
5. Evaluate the total amount of offset fuel that would otherwise be burnt in the boilers to produce the same quantity of thermal energy delivered by the DG/CHP units. Consider both old boilers and new boilers efficiencies (e.g.: ef_{old} = 0.8 and ef_{new} = 0.9).

$$Q_{fuel} = \frac{Q_{HR}}{\left(ef_{old} f_{old} + ef_{new} f_{new}\right)} \tag{2}$$

6. Use both emissions factors for old (em_{old}) and new boilers (em_{new}) and calculate the avoided emissions in each cell. As an example, the expression for displaced boiler CO emissions is presented below:

$$M_{CO,off} = Q_{fuel}\left(em_{old,CO} f_{old} + em_{new,CO} ef_{new}\right) \tag{3}$$

7. Determine the net flux of emissions for each pollutant in a cell due to DG, subtracting the displaced boiler emissions from the total DG emissions contribution. In the case of CO, the net DG emissions can be written as follows:

$$M_{CO,net} = M_{CO,DG} - M_{CO,off} \tag{4}$$

2.1.1.6.2 Emissions factors for boilers

New and old SCAQMD values for avoidable boiler air emissions are presented in Table 10. The avoided emissions per kWh of electric generation for a particular DG-CHP technology can be written as:

$$DGHeatRate(Btu_{in} / kwh_e) \cdot \frac{\left(ef_{tot} - ef_{elec}\right)}{ef_{boiler}} \cdot f_{boiler}(lbs / Btu) \tag{5}$$

Table 10. Typical boiler air emissions

	CO lbs/MMBtu	VOC lbs/MMBtu	NO_x lbs/MMBtu	SO_x lbs/MMBtu	$PM_{2.5}$ lbs/MMBtu	CO_2 lbs/MMBtu
New	2.35E-02	5.39E-03	1.5E-02	5.90E-04	7.45E-03	118
Old	8.24E-02	5.39E-03	3.6E-02	5.90E-04	7.45E-03	118

Source: Ianucci et al. 2000; Kay 2003

2.1.1.6.3 Analysis of maximum potential emissions displacement for each DG technology

This section assesses the reduction in emissions for four representative DG technologies in the case when the heat recovery unit is running continuously, 24 hours a day, and is fully utilized. This case represents the maximum theoretical emissions displacement, when both the share of CHP and the heat recovery capacity factor are equal to 100%. Therefore, this exercise gives an upper bound of emissions offsets that DG implementation scenarios would be able to provide if all DG installations included CHP. Table 11 shows CO, VOC, NO_X, and CO_2 emissions reductions when CHP is applied to four DG types (fuel cells, natural gas ICEs, diesel ICEs, and MTGs). Table 11 presents boiler emissions displacements for both new and retrofit applications.

Table 11. Maximum emission displacements for four types of CHP units

Type of DG	Type of application	CO			VOC			NO_x			CO_2		
		DG (lbs/kWh)	Boiler (lbs/kWh)	% Red.	DG (lbs/kWh)	Boiler (lbs/kWh)	% Red.	DG (lbs/kWh)	Boiler (lbs/kWh)	% Red.	DG (lbs/kWh)	Boiler (lbs/kWh)	% Red.
Fuel cell (PEM)	Retrofit	0.0001	0.00048	**478.4**	0.0009	3.1E-05	**3.5**	7E-05	0.00021	**298.6**	1.16	0.685	**59.1**
	New	0.0001	0.00012	**121.2**	0.0009	2.8E-05	**3.1**	7E-05	7.7E-5	**110.6**	1.16	0.609	**52.5**
Natural gas ICE	Retrofit	0.0018	0.00058	**32.2**	0.00044	3.8E-05	**8.6**	0.00044	0.00025	**57.3**	1.27	0.834	**65.6**
	New	0.0018	0.000148	**8.3**	0.00044	3.4E-05	**8.6**	0.00044	9.4E-5	**21.2**	1.27	0.741	**58.3**
Diesel ICE	Retrofit	0.0077	0.00033	**4.3**	0.0014	2.1E-05	**1.5**	0.013	0.00014	**1.1**	1.3	0.469	**63.9**
	New	0.0077	8.3E-05	**1.1**	0.0014	1.9E-05	**1.4**	0.013	5.3E-5	**0.4**	1.3	0.417	**32.1**
MTG	Retrofit	0.00285	0.00076	**26.5**	0.00005	4.9E-05	**98.8**	0.0007	0.00033	**47.12**	1.5	1.081	**72.1**
	New	0.00285	0.00019	**6.7**	0.00005	4.4E-05	**87.8**	0.0007	0.00012	**17.45**	1.5	0.961	**64.1**

Note that for natural gas and diesel ICEs with higher pollutant emission footprints (see Allison and Lents (2002) for ICE emissions and Table 7 for the other DG emissions), boiler emission displacements are not very high (0%–32%). The only exception is the 57.3% reduction in NO_X emissions for a natural gas ICE displacing an old boiler. On the other hand, when cleaner-fuel-driven DGs such as MTGs or fuel cells are considered, significant reductions are achieved, resulting in some cases in a negative net emissions flux (such as when NO_X emissions for fuel cells with CHP are used). Furthermore, all natural-gas-driven CHP technologies yield to significant displacement (52%–72% reduction) of global warming CO_2 emissions.

All of the CHP technologies of Table 11 were considered with different adoption rates and with different heat recovery capacity factors that were all significantly less than 100% to account for losses, temporal non-coincidence, and end-use thermal requirements. In realistic DG scenarios, where diesel ICE CHP was not included, only small reductions in air pollutant emissions in the

range 0%–20% are expected. On the other hand, reductions in CO_2 emissions may be higher, in the range of 20%–40%.

2.1.1.7 Other Estimates

Some of the DG technologies are just emerging in the marketplace, so certain features of these technologies—including accurate pollutant emissions rates and emissions speciation—are not readily available. In addition, understanding of features such as continuous versus peak power applicability, size of equipment, fuel availability, emissions stack height, and others may need to be estimated for the current study. Currently the APEP group is carrying out a detailed emissions measurement process for various DG types in a DG testing facility, which is being used to complete some of the missing data. When data are still not available, however, reasonable estimates or assumptions are applied only as required for compatibility with the simulation software.

One significant factor that must be estimated for the current study is the degradation rate for technologies installed in the earlier years between now and the study year of interest. All DG technologies experience some degradation in efficiency performance and many may also degrade in the pollutant emissions performance. However, measurements of DG performance degradation are still limited, and therefore, a degradation rate due to operation of DG must be estimated. The adoption cumulative curve of DG power in the following year is also uncertain and various curves (exponential, linear, etc.) are considered. Finally, some technologies are expected to substantially improve their emissions and efficiency performance over the next several years. This performance improvement must also be estimated for accurate development of a DG scenario.

2.1.1.8 Speciation of criteria pollutants

Emissions from DG are estimated on a basis of a limited set of generic pollutants: NO_X, SO_X, VOC, and PM. To make the emissions fluxes from any DG scenario compatible with the input required by the air quality model, one must provide emissions fluxes for all species that the model currently considers in its detailed chemical mechanism. Consequently, emissions of these generic pollutants have to be speciated into a finer level of detail. Table 12 shows the speciation and weighting factors used for each of the species for which this procedure was required. The codes presented in Table 12 for the species in VOC and PM are the same as those used in the Caltech Atmospheric Chemical Mechanism (CACM). Table 13 also lists the chemical name associated with each code.

Table 12. Speciation used for criteria pollutants from DG scenarios

Criteria Pollutant	Species							Comments
NO_x	**NO**			**NO_2**				APEP estimates
% Weight	95			5				
SO_X	**SO_2**			**SO_3**				APEP estimates
% Weight	95			5				
VOC	**CH_4**	**HCHO**	**ALKL**	**AROH**		**AROL**		VOC Speciation from CARB data for gas external combustion boiler profile (www.arb.ca.gov/emisinv/speciate/speciate.htm)
% Weight	58	8	29	4		2		
PM	**EC**	**OC**	**Cl**	**Sf**	**Nt**	**K**	**Ca**	PM Speciation from CARB data for gas ICE profile (www.arb.ca.gov/emisinv/speciate/speciate.htm)
% Weight	20	26	7	45	1	1	1	

Table 13. Chemical names for species considered in VOC and PM CACM speciation

Species	Species ID in CACM	Chemical Name	Criteria Pollutant
HCHO	4	Formaldehyde	VOC
ALKL	10	C2-C6 Alkanes	VOC
AROH	19	High Yield Aromatics	VOC
AROL	20	Low Yield Aromatics	VOC
EC	29	Elemental Carbon	PM
OC	30	Unresolved Organic Carbon	PM
Cl	32	Chloride ion	PM
Sf	34	Sulfur (VI)	PM
Nt	35	Nitrate	PM
K	37	Potassium	PM
Ca	38	Calcium	PM

2.1.1.8.1 Low early adoption of DG power

In all spanning scenarios except one (#S5 HEAPW20%), a realistic low early adoption of DG power is assumed. This implies that the curve of the annual rate of DG power adoption over the period 2003–2010 increases each year (exponentially or parabolic) until the DG power estimated for 2010 is achieved. Quantitatively, this means that only about 2% of the total DG power adopted in the period 2003–2010 will be implemented before 2007. For the remaining 98% of DG power that will be installed after 2007, those small units under the CARB certification program will have to meet the more stringent 2007 CARB emissions limits (see Table 5).

2.1.1.9 Performance Degradation and Geometrical Features

Only one of the spanning scenarios accounts for performance degradation of the DG units. This spanning scenario includes a decrease of efficiency and an increase in emissions that occurs over the years with all of the DG units. The emissions degradation is allowed to proceed for all DG units up to the applicable regulatory requirement. The remainder of the spanning scenarios assumes no degradation. Moreover, all of the scenarios included in the present study consider DG emissions to occur at ground level (i.e., no elevated emissions). A small number of DG may be installed on rooftops of tall buildings, but, this fact is not included in the DG scenarios.

2.1.1.10 Scenarios that Include Emissions Displacement from In-basin Power Plants

The approach used to develop DG emissions inventories for scenarios that include emissions displacement from in-basin power plants is as follows:

Randomly locate one or more power plants in the SoCAB with approximately the same amount of power as the estimated DG power implemented for 2010 (1060 gigawatts(GW) when 20% of the increased demand is met by DG). The database consulted is the one available in the website of the California Energy Commission for power plants in California (CEC 2001). Two combustion turbine/steam turbine power plants situated in Long Beach and Huntington Beach with a total aggregated online capacity of 1090 GW were selected for the 20% of increased demand case, for example. Table 14 presents the main characteristics of these plants.

Table 14. Main characteristics of selected power plants in the SoCAB

Name	Address	Primary fuel	Technology	Online capacity (MW)	Cogen	Date Online	Type
Long Beach	2665 Seaside Blvd., Long Beach, CA 91770	Natural Gas	Combustion Turbine, Steam Turbine	530	NO	1/1/1976	Base loaded
Huntington Beach	21730 Newland St., Huntington Beach, CA 92646	Natural Gas, Distillate	Steam Turbine, Combustion Turbine	563	NO	6/1/1958	Base loaded

1. Determine the most recent emissions flux rates for each of the selected power plants from the CARB website (CARB 2000). Continuing with the same example, the values for criteria pollutant emissions from the Long Beach and Huntington Beach power plants in 2000 are shown below in Table 15.

Table 15. Emissions from selected power plants in the SoCAB

Name	Year	CO (tons/year)	NO_x (tons/year)	VOC (tons/year)	SO_x (tons/year)	PM (tons/year)	NH_3 (tons/year)
Long Beach	2000	80.8	159	366.8	0.5	10.8	-
Huntington Beach	2000	56.5	290.7	39.7	2.8	9.2	0.18

2. Identify the model cells where the power plants are installed. For this purpose the APEP team used the web map tool developed in the first stages of this project (see Appendix D), which allows the user to click in any particular point in a SoCAB map and get the air quality model coordinates as well as the Universal Transverse Mercator (UTM) coordinates of that point. In the case of the current example, the X and Y model coordinates for Huntington Beach and Long Beach power plants are (41,10) and (35,12), respectively.
3. Determine the power plant emissions in the suitable units of the model. To do that, the APEP researchers assumed a capacity factor for both power plants of 80%, a reasonable value for base-loaded power plants.
4. Evaluate the net emissions from the DG scenario in each cell of the computational domain. The only cells that have different emissions from the ones in Scenario #S1 are precisely those cells with displaced emissions from the power plants. For the current example, the 2 cells that represent Huntington Beach and Long Beach power plants contain negative emissions fluxes in the DG scenario because emissions from the power plants is significantly higher than the emissions from the DG units implemented in those same cells. However total emissions of this scenario plus the baseline emissions are still positive.

2.1.1.11 Business as usual DG Scenario development

To develop a "business as usual" scenario, one can assume a linear extrapolation of DG power and DG mix from the current trends in the SoCAB area as documented in the years 2001 and 2002. Data for current trends of DG power in California under 1 MW were extracted from the report, *Self-Generation Incentive Program. Second Year Impacts Evaluation Report* (CPUC 2003). Table 16 shows the evolution of active programs in terms of kW for the different incentive levels of the program. The levels presented in Table 16 correspond to the following DG incentives:

Level 1: The lesser of 50% of project costs, or $4.50/watt for photovoltaics, wind turbines, and fuel cells operating on renewable fuels;
Level 2: The lesser of 40% of project costs, or $2.50/watt for fuel cells operating on non-renewable fuel and utilizing sufficient waste heat recovery,
Level 3-R: The lesser of 40% of projects costs, or $1.50/watt for microturbines, internal combustion engines, and small gas turbines utilizing renewable fuel.
Level 3-N: The lesser of 30% of project costs, or $1.00/watt for the above combustion technologies operating on non-renewable fuel, utilizing sufficient waste heat recovery and meeting certain reliability criteria.

Table 16. Active DG California Public Utility Commission (CPUC) projects in 2001 and 2002

Incentive Level	Total Active 2001 (kW)	Total Active 2002 (kW)
Level 1	2291	26875
Level 2	200	600
Level 3N	15452	57625
Level 3R	-	1585
Total	17943	86685

It was also roughly assumed that only the DG projects administered by SCE and Southern California Gas Company (SoCal Gas) are to be implemented in the SoCAB, which accounts for 51% of the total DG power in the SoCAB. No data on DG power installed in the service territory of the other large electricity company in the SoCAB (LADWP) is available. As a result, an assumption has been made that the total DG power installed in 2001 and 2002 in the LADWP service territory is 35% of that installed in SCE territory. This level of DG penetration directly corresponds to the ratio of LADWP to SCE power delivered in the SoCAB in 2002.

The distribution of power among the DG types under 1 MW is also based on the CPUC data for the business-as-usual cases. This assumption leads to adoption of DG types as follows: 32% PV, 1.2% FC, 7.5% MTG, and 59.3% ICE. This DG mix is considered constant in the extrapolation of DG power up to 2010 for all business-as-usual cases. For the LADWP DG power, the APEP team estimated the same mix of DG types as that reported by SCE and SoCal Gas.

In years 2001 and 2002, two peak power plants with less than 50 MW total capacity each were installed in the SoCAB (CEC 2003). Consequently, an installation rate of one 49 MW-unit per year was assumed in this business-as-usual case. This adoption rate, in conjunction with the adoption rates of the other DG technologies mentioned above, results in the following technology mix for the business-as-usual cases predicted for the year 2010: 59% GT, 25% ICE, 13% PV, 3% MTG, and 0.5% FC.

Figure 3 shows the projected linear trends for accumulated DG power in the period 2001–2010, based on real data in years 2001 and 2002. A total DG power capacity of 936 MW is projected for the year 2010, which requires a total installation of 680 MW additional DG capacity in the period 2003–2010.

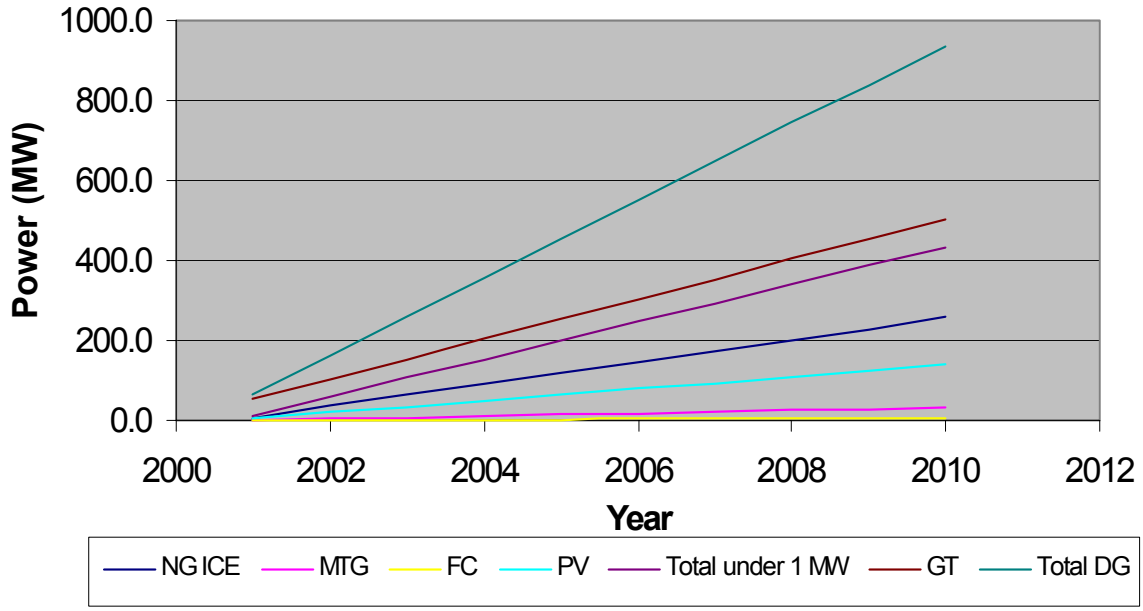

Figure 3. Projected DG power trends in the SoCAB according to CPUC Self-Generation Program DG data for 2001 and 2002 using a linear fit

Alternatively, one could apply an increasing parabolic extrapolation of the DG power data of 2001 and 2002 instead of a linear extrapolation by assuming zero DG power was installed in the year 2000. In this case, more DG power and more emissions from DG would be expected. Projections of DG power for this case are shown in Figure 4. Note that this set of assumptions for DG adoption in the business-as-usual cases leads to a total installed capacity of DG that is almost 1800 MW in the year 2010.

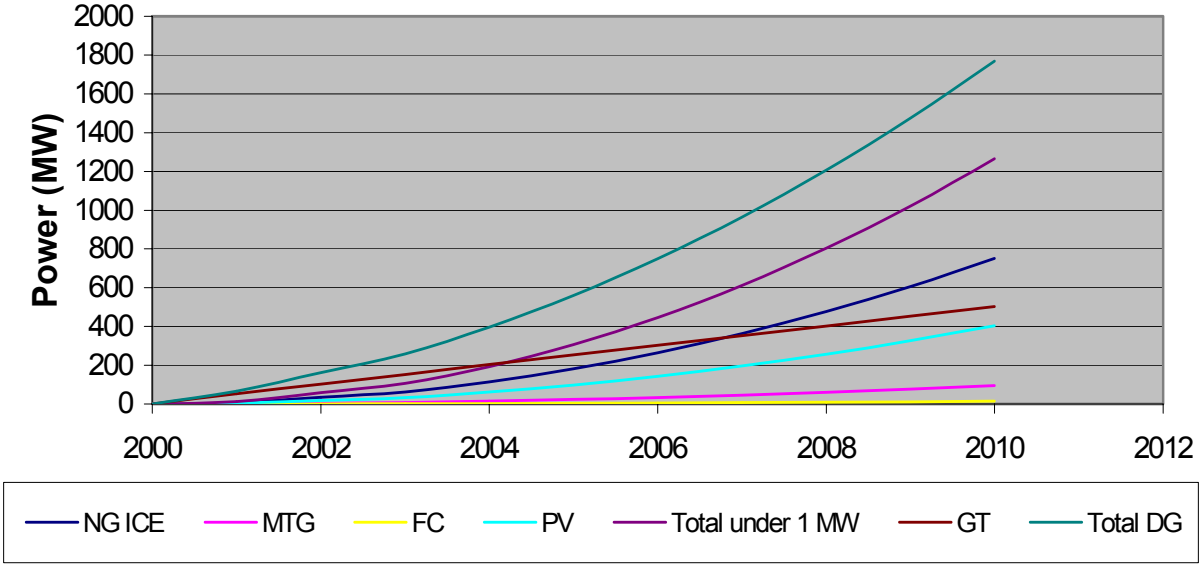

Figure 4. Projected DG power trends in the SoCAB according to CPUC Self-Generation Program DG data for 2001 and 2002, using a parabolic fit

2.1.2 DG Scenario Screening Criteria

If one decided to investigate all possible permutations of the parameters and factors identified above, one would need to simulate 2.04×10^{46} (= 39! = 39 factorial) scenarios. To accomplish the simulation of air quality in SoCAB for such a large number of cases is not feasible. In addition, the APEP team sought to narrow the scope of the current investigations by focusing on the appropriate parameters and factors of concern. As a result, the team proposes an approach for systematically screening the number of scenarios to a much smaller number by using screening criteria.

By requirement of the contract with the California Energy Commission, the criteria used to screen the scenarios and select a more reasonable number of computations in this study must be presented in both draft and final form in deliverable documents to the Energy Commission. In order to meet this contractual obligation, APEP decided to develop the criteria, present the criteria to experts in the air quality modeling and DG communities (in both public workshops and in coordination meetings with the SCAQMD, CARB, and California Energy Commission) and to subsequently submit these criteria in a draft screening criteria document. As a result of our initial criteria development, and modifications of such as suggested by the coordination group and experts in public workshops, APEP staff are able to present the final screening criteria used in this program as follows.

Table 17 presents the final screening criteria for selecting a limited number of DG Scenarios from the list of possible scenarios that could be comprised of variations in all of the parameters and factors identified in Table 1. Table 17 presents seven primary screening criteria and a description of each. Note that the description of each criterion is stated in the affirmative. Any set of parameter variations that positively meets any one of the screening criteria of Table 17, as a result, has been retained in the current study.

The criteria of Table 17 were applied to the parameter and factor space outlined above and their application resulted in the selection of about 100 DG Scenarios. This number of scenarios is still too large to reasonably accomplish in the current effort. As a result and with feedback and encouragement from the industry stakeholder workshop participants, APEP was able to develop two additional criteria that were further used to screen the scenarios. These two criteria, presented in Table 18, were used to cast a deciding vote on whether or not a scenario is included in this study. Note that the criteria A and B are subjective, however, they are applied and based upon all the literature reviewed to-date, all of the expertise of the APEP team, and insights garnered from CARB, AQMD, and industrial participants in the stakeholder workshops. This process is briefly described in the descriptions of each criterion in Table 18.

Table 17. Final screening criteria

Criterion Number	Criterion	Description
1	Likelihood of implementation	Are the variations in the parameters and factors considered realistic or not realistic based upon team and stakeholder input? If they are realistic or possible, then the variation is included in the current study.
2	Variety of implementation	Are the variations in the parameters and factors required to span the spectrum of possible implementations and/or technologies of interest? If yes, then the scenario should be included in the current study.
3	Potential for socio-political forcing	Is there a potential for social demand, regulatory requirements, energy crises or other socio-political forcing functions to support the variations in the parameters and factors considered for a specific DG Scenario? If yes, then the scenario should be included in the current study.
4	Fundamental understanding	Does inclusion of the DG Scenario provide insight into any specific aspect of the air quality results or model itself (e.g., atmospheric chemistry, mass transport, DG emissions)? If yes, then the scenario should be included in the current study.
5	Data acquisition or additional funding required	Is the inclusion of the scenario consistent with the contract, the funding level provided, and is sufficient information to characterize the scenario already available? If yes, then the scenario should be included in this study. If additional funding or data acquisition is required to develop or include the scenario then the scenario is rejected.
6	Availability of resources	Are sufficient resources such as published results, stakeholder insights, Energy Commission studies, or APEP measurements and expertise available to develop and support the validity of the variations in the parameters and factors considered for a specific DG Scenario? If yes, then the scenario should be included in the current study.
7	Required for determining specific sensitivity of the model	Is the specific DG Scenario required to conduct an appropriate sensitivity analysis or to provide insight regarding model sensitivity to simulation parameters? If yes, then the scenario should be included in the current study.

Table 18. Additional screening criteria

Criterion Letter	Criterion	Description
A	***Is the DG scenario realistic?***	A subjective determination is made regarding whether or not a DG scenario is realistic. This determination is made on the basis of literature review, APEP expertise, and industry and other stakeholder insights. If the scenario is deemed to be realistic or probable, then the scenario is included in the current study.
B	***Does the investigation of the DG scenario contribute to increased understanding?***	An assessment is made of the value of including the DG scenario, even if Criterion A is not met. The assessment is based upon whether or not the team believes increased understanding of DG air quality impacts may be garnered by inclusion of the scenario. If the scenario is deemed to have merit in this regard, then it is included in the current study.

2.1.3 Extraction and Processing of GIS Land-use Data

The use of a realistic means of defining the spatial distribution of DG in the SoCAB is critically important to the realistic prediction of air quality impact. In addition, the first industry stakeholder workshop strongly recommended spatial allocation of the DG technologies throughout the basin according the actual electrical and thermal demand anticipated for 2010 and the type of end-use for each spatial location. The sort of information required to accomplish such a realistic spatial allocation is only available from special sources. These sources include the local utilities, which have spatially resolved data on electricity consumption, and local governmental agencies that have geographical information systems (GIS) information for SoCAB.

The Southern California Area Governments (SCAG) generously donated GIS land-use data for the following counties: Los Angeles, Orange, San Bernardino, Riverside, Imperial, and Ventura. The latest data in this GIS data set were collected in the year 2000. Figure 5 shows how the computational domain of the air quality model for the SoCAB includes partially or wholly the counties of Orange, Los Angeles, Riverside, San Bernardino, and Ventura.

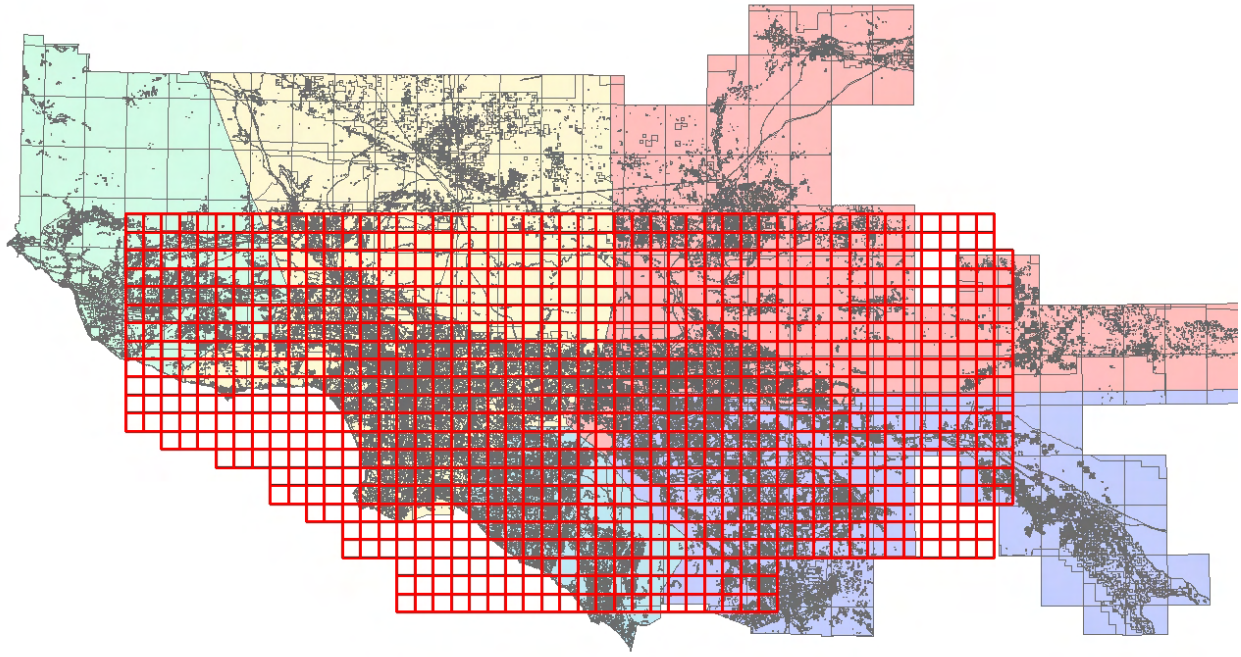

Figure 5. Southern California counties with land-use GIS data and the computational grid of the air quality model (in red lines)

These data consist of each of the counties divided into land parcels (polygons) of different area and shape. The number of parcels per county is rather large. For example, the total number of individual land parcels in Los Angeles County alone is more than 40,000. The land parcels have a resolution of 2 acres (0.0081 km^2). Each of the polygons has associated with it a database that contains an ID number, total area, and zone classification code. Figure 6 presents a picture of a small region near Long Beach to illustrate the typical number and resolution of the land parcel polygons. The location of the 5 km x 5 km model cells and corresponding resolution of the air quality model in this same region are represented by the red lines of Figure 6.

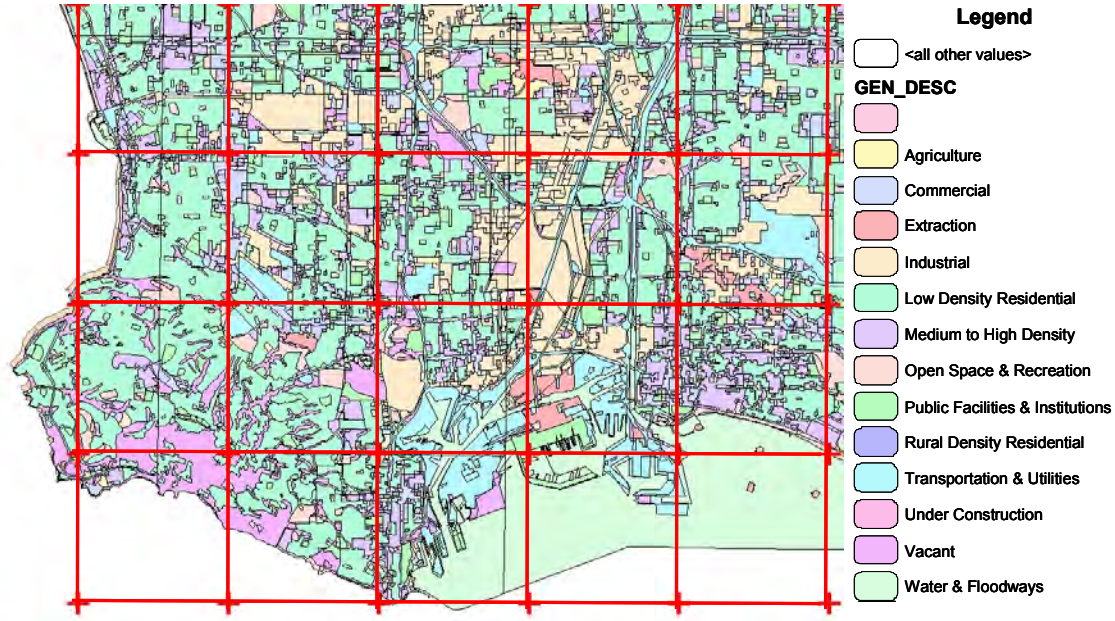

Figure 6. Example of generic land-uses in Long Beach area

The GIS database contains 132 different specific land-use types that are aggregated into 13 generic land use types. The 13 generic land use types are the only types presented in Figure 6. Table 19, on the other hand, shows both the specific land-use types and the generic types that are contained in the GIS database.

Table 19. Land-use codes and descriptions

LU CODE	LAND USE DESCRIPTION	GENERIC LAND USE TYPE
1000	Urban or Built-up	
1100	Residential	Low Density Residential
1110	Single Family Residential	Low Density Residential
1111	High Density Single Family Residential	Low Density Residential
1112	Low Density Single Family Residential	Low Density Residential
1120	Multi-Family Residential	Medium to High Density Residential
1121	Mixed Multi-Family Residential	Medium to High Density Residential
1122	Duplexes, Triplexes & 2 or 3 Unit Condos & Townhomes	Medium to High Density Residential
1123	Low-Rise Apartments Condominiums and Townhouses	Medium to High Density Residential
1124	Medium-Rise Apartments and Condominiums	Medium to High Density Residential
1125	High-Rise Apartments and Condominiums	Medium to High Density Residential
1130	Mobile Homes and Trailer Parks	Medium to High Density Residential
1131	Trailer Parks and Mobile Home Courts High Density	Medium to High Density Residential
1132	Mobile Home Courts and Subdivisions Low Density	Medium to High Density Residential
1140	Mixed Residential	Medium to High Density Residential
1150	Rural Residential	Low Density Residential
1151	Rural Residential High Density	Low Density Residential
1152	Rural Residential Low Density	Rural Density Residential
1200	Commercial and Services	Commercial
1210	General Office Use	Commercial

Table 19. (continued)

LU CODE	LAND USE DESCRIPTION	Generic Land Use Type
1211	Low- and Medium-Rise Major Office Use	Commercial
1212	High-Rise Major Office Use	Commercial
1213	Skyscrapers	Commercial
1220	Retail Stores and Commercial Services	Commercial
1221	Regional Shopping Mall	Commercial
1222	Retail Centers, Non-Strip Contiguous Interconnected Off-Street	Commercial
1223	Modern Strip Development	Commercial
1224	Older Strip Development	Commercial
1230	Other Commercial	Commercial
1231	Commercial Storage	Commercial
1232	Commercial Recreation	Commercial
1233	Hotels and Motels	Commercial
1234	Attended Pay Public Parking Facilities	Commercial
1240	Public Facilities	Public Facilities & Institutions
1241	Government Offices	Public Facilities & Institutions
1242	Police and Sheriff Stations	Public Facilities & Institutions
1243	Fire Stations	Public Facilities & Institutions
1244	Major Medical Health Care Facilities	Public Facilities & Institutions
1245	Religious Facilities	Public Facilities & Institutions
1246	Other Public Facilities	Public Facilities & Institutions
1247	Non-Attended Public Parking Facilities	Public Facilities & Institutions
1250	Special Use Facilities	Public Facilities & Institutions
1251	Correctional Facilities	Public Facilities & Institutions
1252	Special Care Facilities	Public Facilities & Institutions
1253	Other Special Use Facilities	Public Facilities & Institutions
1260	Educational Institutions	Public Facilities & Institutions
1261	Pre-Schools Day Care Centers	Public Facilities & Institutions
1262	Elementary Schools	Public Facilities & Institutions
1263	Junior or Intermediate High Schools	Public Facilities & Institutions
1264	Senior High Schools	Public Facilities & Institutions
1265	Colleges and Universities	Public Facilities & Institutions
1266	Trade Schools	Public Facilities & Institutions
1270	Military Installations	Public Facilities & Institutions
1271	Base Built-up Area	Public Facilities & Institutions
1272	Vacant Area	Vacant
1273	Air Field	Public Facilities & Institutions
1300	Industrial	Industrial
1310	Light Industrial	Industrial
1311	Manufacturing Assembly and Industrial Services	Industrial
1312	Motion Picture and Television Studio Lots	Industrial
1313	Packing Houses and Grain Elevators	Industrial
1314	Research and Development	Industrial
1320	Heavy Industrial	Industrial
1321	Manufacturing	Industrial
1322	Petroleum Refining and Processing	Industrial
1323	Open Storage	Industrial
1324	Major Metal Processing	Industrial

Table 19. (continued)

LU CODE	LAND USE DESCRIPTION	Generic Land Use Type
1325	Chemical Processing	Industrial
1330	Extraction	Extraction
1331	Mineral Extraction - Other Than Oil and Gas	Extraction
1332	Mineral Extraction - Oil and Gas	Extraction
1340	Wholesaling and Warehousing	Industrial
1400	Transportation Communications and Utilities	Transportation & Utilities
1410	Transportation	Transportation & Utilities
1411	Airports	Transportation & Utilities
1412	Railroads	Transportation & Utilities
1413	Freeways and Major Roads	Transportation & Utilities
1414	Park and Ride Lots	Transportation & Utilities
1415	Bus Terminals and Yards	Transportation & Utilities
1416	Truck Terminals	Transportation & Utilities
1417	Harbor Facilities	Transportation & Utilities
1418	Navigation Aids	Transportation & Utilities
1420	Communication Facilities	Transportation & Utilities
1430	Utility Facilities	Transportation & Utilities
1431	Electrical Power Facilities	Transportation & Utilities
1432	Solid Waste Disposal Facilities	Transportation & Utilities
1433	Liquid Waste Disposal Facilities	Transportation & Utilities
1434	Water Storage Facilities	Transportation & Utilities
1435	Natural Gas and Petroleum Facilities	Transportation & Utilities
1436	Water Transfer Facilities	Transportation & Utilities
1437	Improved Flood Waterways and Structures	Transportation & Utilities
1438	Mixed Wind Energy Generation and Percolation Basin	Transportation & Utilities
1440	Maintenance Yards	Transportation & Utilities
1450	Mixed Transportation	Transportation & Utilities
1460	Mixed Transportation and Utility	Transportation & Utilities
1500	Mixed Commercial and Industrial	Industrial
1600	Mixed Urban	Industrial
1700	Under Construction	Vacant
1800	Open Space and Recreation	Open Space & Recreation
1810	Golf Courses	Open Space & Recreation
1820	Local Parks and Recreation	Open Space & Recreation
1821	Local Park Developed	Open Space & Recreation
1822	Local Park Undeveloped	Open Space & Recreation
1830	Regional Parks and Recreation	Open Space & Recreation
1831	Regional Park Developed	Open Space & Recreation
1832	Regional Park Undeveloped	Open Space & Recreation
1840	Cemeteries	Open Space & Recreation
1850	Wildlife Preserves and Sanctuaries	Open Space & Recreation
1860	Specimen Gardens and Arboreta	Open Space & Recreation
1870	Beach Parks	Open Space & Recreation
1880	Other Open Space and Recreation	Open Space & Recreation
1900	Urban Vacant	Vacant
2000	Agriculture	Agriculture
2100	Cropland and Improved Pasture Land	Agriculture
2120	Non-Irrigated Cropland and Improved Pasture Land	Agriculture
2200	Orchards and Vineyards	Agriculture

Table 19. (continued)

LU CODE	LAND USE DESCRIPTION	Generic Land Use Type
2300	Nurseries	Agriculture
2400	Dairy and Intensive Livestock	Agriculture
2500	Poultry Operations	Agriculture
2600	Other Agriculture	Agriculture
2700	Horse Ranches	Agriculture
3000	Vacant	Vacant
3100	Vacant Undifferentiated	Vacant
3200	Abandoned Orchards and Vineyards	Vacant
3300	Vacant With Limited Improvements	Vacant
3400	Beaches (Vacant)	Open Space & Recreation
4000	Water	Water & Floodways
4100	Water	Water & Floodways
4200	Harbor Water Facilities	Water & Floodways
4300	Marina Water Facilities	Water & Floodways
4400	Water Within a Military Installation	Water & Floodways
4500	Area of Inundation (High Water)	Water & Floodways

2.1.3.1 GIS data extraction

The first step required to make effective use of the land-use GIS data in our DG scenarios was to correlate (i.e., scale-up) the resolution of the GIS data with the 5 km x 5 km resolution of the air quality model grid. This task proved to be quite challenging, requiring the assistance of a skilled computer programmer with expertise in graphical data extraction. In this process, Tony Soeller, staff member of the Network and Academic Computing Services (NACS) at UCI, and an expert in GIS data management and manipulation, assisted APEP staff.

After some weeks of intensive work, the APEP team, working with Tony Soeller, came up with a 15-step procedure that uses the GIS software ArcMap to satisfactorily map the GIS data to the air quality model grid. This strategy for integrating GIS data with the AQM is described in this section of the report.

Table 20 presents a small cross-section of the model grid as a sample of the type of data now available to use for all of the cells in the model. The *X* and *Y* coordinates of the model are presented in Table 20, followed by the square kilometers (km^2) of area within each cell that correspond to Agriculture, Commercial, Extraction, Industrial, Low Density Residential, and other land use types. Issues that had to be resolved in the process of extracting GIS data included:

- How does one define and create the 5 x 5 km cell layer in GIS?
- How does one identify the location of each polygon with respect to the cells?
- How can one determine if land-use polygons are entirely inside one cell or shared among cells?
- How can one account for land-use polygons that occupy more than one cell?
- How can the GIS data be exported in a convenient way to use in the Excel scenario development files?

All of these issues have been resolved to the satisfaction of the APEP team.

Table 20. Detail of some cells with GIS land-use data extracted

		Agriculture	Commercial	Extraction	Industrial	Low Density Residential
Ymodel	Xmodel	A_{Agric} km^2	A_{Comm} km^2	A_{Ext} km^2	A_{Ind} km^2	A_{Lowres} km^2
26	19	1.335	0.000	0.549	0.000	0.031
26	20	0.012	0.000	0.503	0.000	0.000
26	21	0.175	0.000	0.000	0.000	0.000
26	22	5.147	0.000	0.000	0.000	0.000
26	23	0.043	0.000	0.026	0.000	0.000
26	24	0.040	0.000	0.137	0.000	0.000
26	25	1.453	0.000	0.136	0.000	0.000
26	26	0.044	0.000	1.310	0.000	0.000
26	27	0.545	0.000	1.116	0.000	0.586
26	28	2.896	0.868	1.498	1.128	0.685
26	29	3.212	0.151	0.000	1.520	4.766
26	30	0.650	0.125	0.000	0.120	5.810
26	31	0.180	0.319	0.000	0.173	1.779
26	32	0.123	0.008	0.932	0.037	2.120
26	33	0.028	0.000	0.388	0.000	0.000
26	34	0.090	0.000	0.000	0.018	0.000

In the process of extracting the GIS data, the APEP team isolated each of the 13 generic land-use categories. These generic land-use categories are listed in Table 21. Reducing the total number of land use types to the 13 generic land use types allowed reasonable identification of the spatial distribution of land use types in the SoCAB. Maps with the locations of all the parcels belonging to each land-use type are presented in Appendix E.

Table 21. Generic land-use categories

LU CODES	GENERIC LAND USE TYPE
1000–1112, 1150–1151	Low Density Residential
1120–1140	Medium to High Density Residential
1152	Rural Density Residential
1200–1234	Commercial
1240–1273	Public Facilities & Institutions
1300–1325, 1340, 1500, 1600	Industrial
1330–1332	Extraction
1400–1460	Transportation & Utilities
1700, 1900, 3000, 3100, 3200, 3300	Vacant
1800 – 1880, 3400	Open Space & Recreation
2000 – 2700	Agriculture
4000 – 4500	Water & Floodways

Figure 7 presents a bar chart with the total areas for the 13 generic land-use categories. Note that the "Vacant" area is by far the largest land-use category with more area (greater than 12,000 km^2, or 4,600 square miles ($miles^2$)) associated with it than any other category. The vacant area is followed by the "Low Density Residential" land use category with about 3,000 km^2 (1,200 $miles^2$) in the SoCAB. The third and forth land-use categories with significant area in the SoCAB are "Agriculture" and "Transportation and Utilities," respectively. For perspective on the land-use categories with smaller total areas, Figure 8 presents the total areas for the 12 of the 13 generic land-use categories. All but the "Vacant" land-use categories are presented in Figure 8.

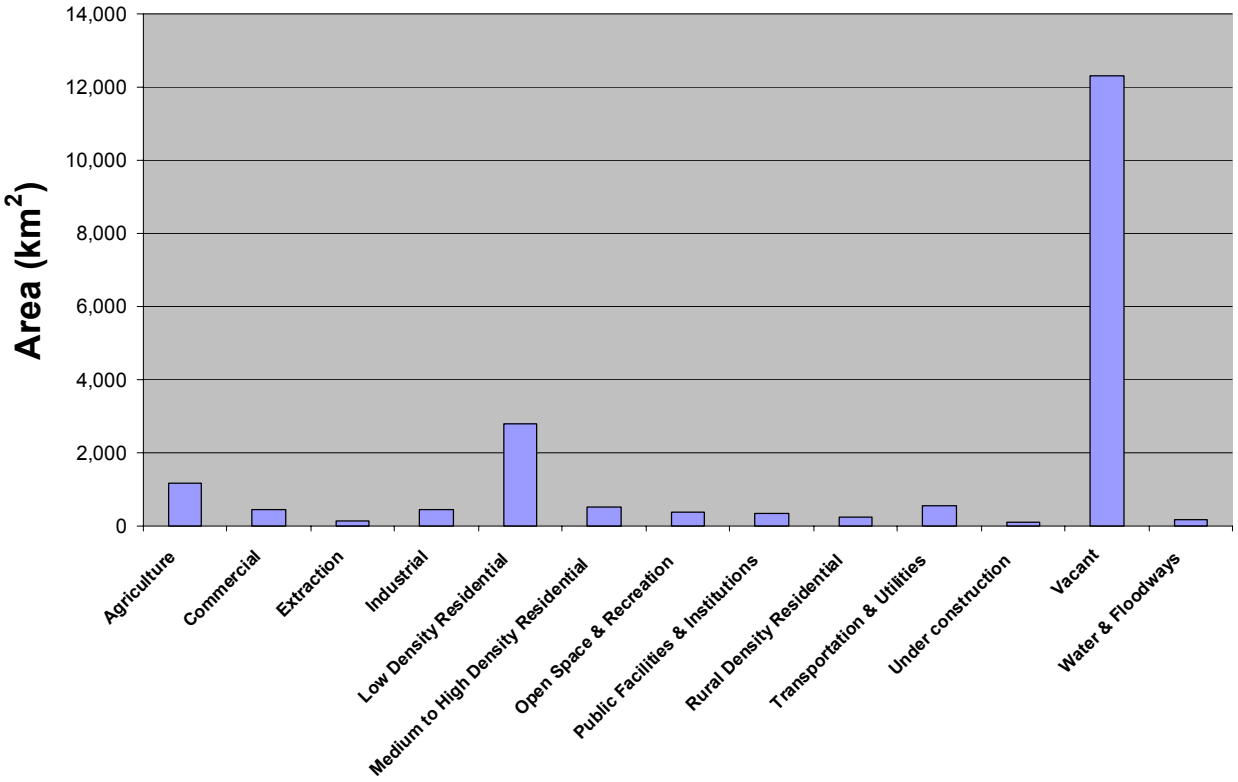

Figure 7. Total land-use areas in the 13 generic land use categories in SoCAB

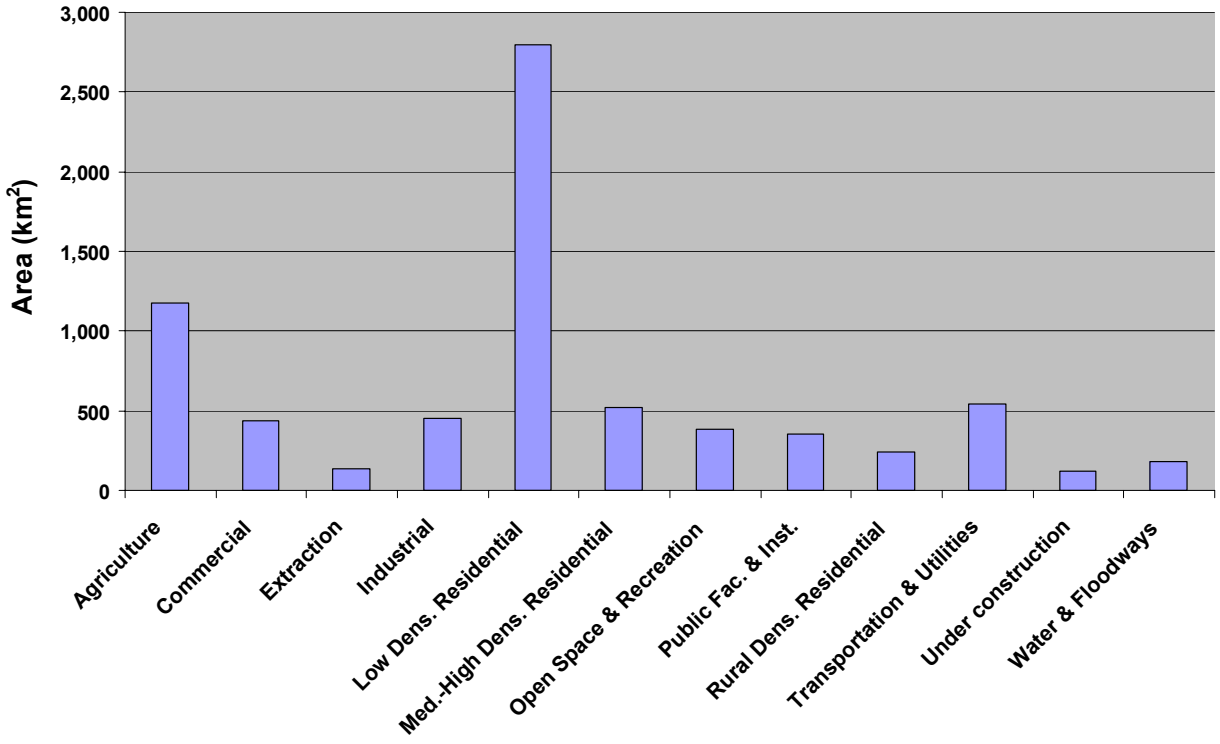

Figure 8. Total land-use areas in 12 of the 13 generic land use categories in SoCAB (vacant category not plotted).

2.1.3.2 Approach to relate land-use data to DG power and DG mix

After extracting the areas in each cell for the 13 generic land-use categories, the next step was to design a strategy to relate land-use areas to the amount of DG power and to the mix of DG technologies assigned to each cell of the grid. Since the land-use categories generally refer to a sector of the economy that is expected to use DG (of various types and to varying degrees in various applications), the label used for groupings of land-use categories in this section is "sector."

A systematic approach to relate DG power and DG mix to land-use data has been developed that is well-grounded in and fully based upon the most recent data and reports that are currently available. The approach presented herein was well received by the stakeholders in the second workshop (May 21, 2003), organized specifically to discuss the scenario development tasks and to receive a critique and feedback from DG stakeholders.

The systematic approach consists of a 10-step procedure that is described in this section of the report. The nomenclature used in the equations that define the approach is presented in Table 22, together with definitions for each variable.

Table 22. Nomenclature used in the equations that define the systematic approach for developing realistic DG scenarios

$A_{i,k}$	Area of sector i in cell k
$S_{i,j}$	Relative area of sector i in size category j
$A_{i,j,k}$	Area of sector i in size category j in cell k
A_{SoCAB}	Total area in the SoCAB
$D_{i,h}$	Duty cycle factor in sector i and hour of the day h
$R_{i,j}$	Adoption rate relative intensity (in terms of DG power/square foot) for sector i in size category j
$F_{power,k}$	Factor accounting for the total DG power in each cell
$P_{Tot,k}$	Total DG power (in MW) assigned to each cell
$P_{Tot,SoCAB}$	Total DG power (in MW) estimated for the SoCAB in 2010
$P_{i,j,k}$	DG power (in MW) of specific sector i in size category j in cell k
$W_{l,i,j}$	Relative weight for DG type l in sector i and size category j
$T_{l,k}$	Relative contribution to DG power of DG type l in cell k
$T_{l,k,h}$	Relative contribution to DG power of DG type l in cell k at hour h
$P_{l,k}$	DG power (in MW) of DG type l in cell k
$P_{l,k,h}$	DG power (in MW) of DG type l in cell k at hour h
$e_{l,X}$	Emission factor for species X of DG type l
$[X]_{emiss,k}$	Total DG emissions of species X in cell k

In reading this section of the report one should periodically refer back to Table 22. Note that the subscript i refers to the sector type (i.e., groupings of land-use categories), the subscript j refers to the DG size class, and the subscript k refers to the AQM model cell. The subscript h refers to the hour of the day and the subscript l refers to the type of DG technology. These subscripts are consistent throughout the derivation presented in this section. Note that to develop a realistic DG implementation scenario, one must consider a large number of factors as shown in Table 22.

The development of a realistic scenario based on land-use data, DG size, DG type, and other available data and insights is presented in this section as a 10-step procedure. This process has been derived, honed, and developed by the APEP team through many internal iterations and brainstorming sessions. This process has been vetted by colleagues; the California Energy Commission; SCAQMD and CARB staff; and the DG stakeholders who participated in the workshops (see Appendix A and Appendix B). The ten-step procedure is defined as follows.

STEP 1. The starting point for the DG scenario development is the extracted land-use data in 5x5 km resolution. These data consist of the areas (in square kilometers) of all 13 of the generic land use types for each of the 994 cells of the model grid. The 13 land-use area types are aggregated into six different sectors (i.e., low-density residential, medium-to-high-density residential, commercial, industrial, agriculture, and others), as shown in Table 23. The amount of square kilometers of a sector type in any specific cell is represented by A_i. Figure 9 presents a representative picture of the aggregated GIS land-use categories as integrated into the six economic sectors for the Central Los Angeles area.

Table 23. Integration of land-use types into energy sectors

Sector	Land use types considered in that sector *
Low Density Residential	***Low Density Residential***
	Rural Density Residential
Medium to High Density Residential	***Medium to High Density Residential***
Commercial	***Commercial***
Industrial	***Industrial***
Agriculture& Water Pumping	***Agriculture***
Other	***Extraction***
	Public Facilities & Institutions
	Transportation & Utilities
	Under Construction

**** The rest of the land use categories (Vacant, Water and Flood Ways, and Open Space and Recreation) assumed to adopt zero DG power***

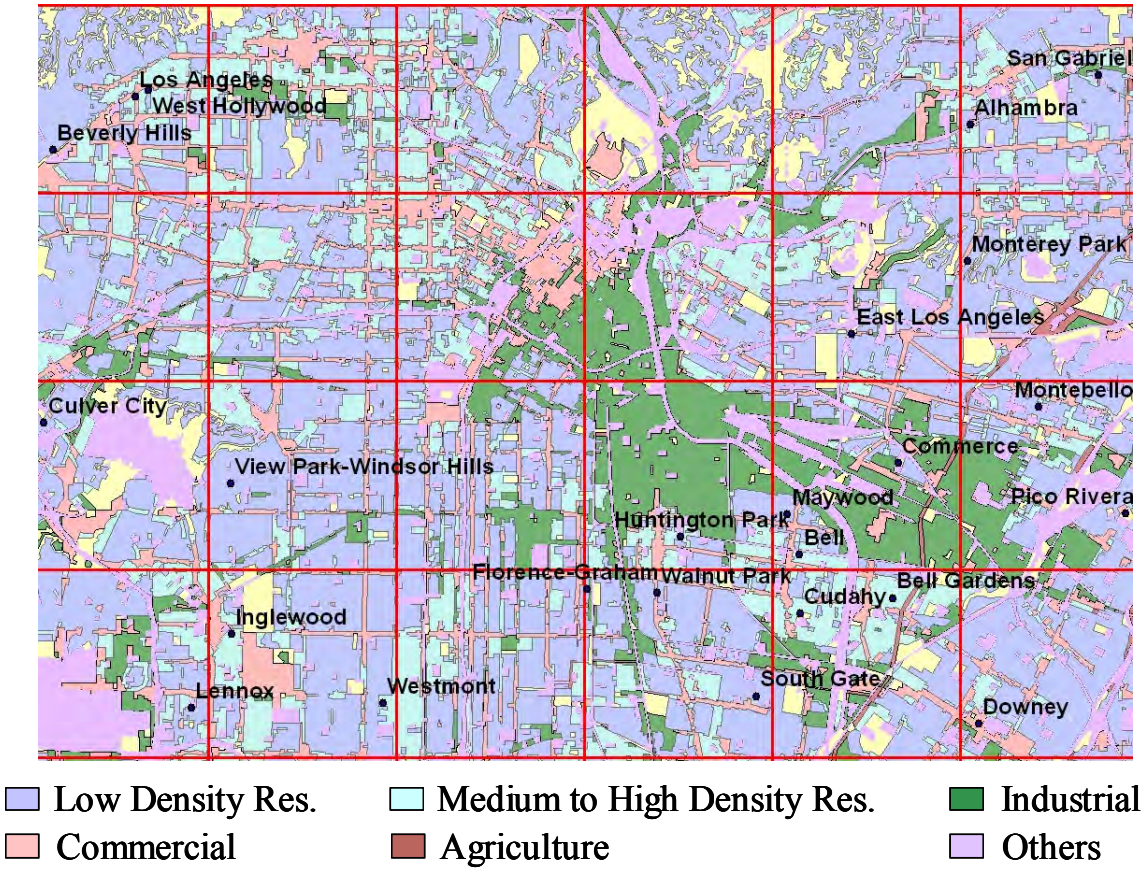

Figure 9. Land use parcels in central Los Angeles aggregated into 6 energy sector categories

STEP 2. The second step is to disaggregate each of the sector areas in each cell into six (6) sub-categories according to DG size capacity. The six DG size classes that are used are:

- < 50 kW,
- 50–250 kW,
- 250–1,000 kW,
- 1–5 MW,
- 5–20 MW, and
- 20–50 MW.

The bases of this disaggregating process are several reports on energy consumption surveys in the commercial, residential, and manufacturing sectors by the Energy Information Agency (1999a, 1999b, 2000). These reports relate total floor space of various establishment types in each sector to the annual electricity consumption. From these data, the average power demand for each establishment is estimated and the potential for each sector to adopt DG in each of the six size classes is determined. The results of these analyses are normalized by dividing the area of each size-category by the total area in that sector to get a relative area per sector (i) and per size category (j), which is represented by $S_{i,j}$. Two of the sectors (Agriculture and Other) required the development of estimated S_{ij}, because no data is currently available for these sectors. Reasonable estimates were made based on the S_{ij} of the other sectors and insights of the APEP team. The equation that relates total area to area per size category for each of the sectors considered is:

$$A_{i,j,k} = S_{i,j} \cdot A_{i,k} \tag{6}$$

Table 24 shows the resulting normalized area factors that are applied to disaggregate (split) the sectors (groups of GIS land-use areas) into specific areas for each DG size category.

Table 24. Normalized area factors for each DG size category for the different sectors ($S_{i,j}$)

Size category	Low Density Residential	Medium and high density residential	Commercial	Industrial	Agriculture	Other
< 50 kW	99%	95%	55%	0%	80%	0%
50-250 kW	1%	5%	17%	5%	10%	5%
250-1,000 kW	0%	0%	20%	15%	10%	15%
1-5 MW	0%	0%	8%	22%	0%	22%
5-20 MW	0%	0%	0%	30%	0%	30%
20-50 MW	0%	0%	0%	28%	0%	28%
Total	100%	100%	100%	100%	100%	100%

STEP 3. The third step is to determine DG power in each of the disaggregated (DG size class dependent) areas in each cell of the model based on a third factor included in this approach. This third factor is called the "Adoption Rate Relative Intensity" factor and has the units of DG power per square kilometer. This relative adoption rate intensity is a function of both the sector and the DG power size category, and is represented by $R_{i,j}$ in the current approach. The adoption rate relative intensity factor, $R_{i,j}$, accounts for the fact that a certain amount of land that is occupied by a certain economic sector will adopt DG technology at a rate that differs from that of other sectors.

The adoption rate relative intensity factor, $R_{i,j}$, is determined in the current approach as a function of both size category and sector based on a report that describes CHP penetration in the commercial and industrial sectors in California (CEC 1999). Note that this report only provides combined market penetration of DG with CHP and includes both the industrial and the commercial sectors. The relative adoption rates for DG in other sectors are estimated from comparison to these data, from other DG market penetration studies (see Table 3) and from APEP team insights. Table 25 presents the current estimates for these intensity factors, normalized to the smallest non-zero entry of the table (other sector; < 50kW).

The factors should be interpreted as follows: if the DG power penetration in a square kilometer of the low-density residential sector is 1.6 MW in the size category < 50 kW, the corresponding DG power penetration in the same area for the industrial sector in the range capacity 20–50 MW is 567.2 MW. The adoption rate relative intensity factors of Table 25 are well grounded in the literature and APEP insights that are currently available. However, these factors can be refined and modified at any time as additional detailed market penetration studies are completed and as information becomes available for DG market penetration in California (especially in the SoCAB).

Table 25. Adoption Rate Relative Intensity ($R_{i,j}$) per size category and per sector

Size category	Low Density Residential	Medium and high density residential	Commercial	Industrial	Agriculture	Other
< 50 kW	*1.6*	*16.4*	*7.9*	*7.9*	*3.2*	*1.0*
50-250 kW	*8.3*	*208.1*	*151.7*	*151.7*	*8.6*	*19.1*
250-1,000 kW	*0.0*	*0.0*	*141.5*	*141.5*	*8.6*	*17.9*
1-5 MW	*0.0*	*0.0*	*221.5*	*221.5*	*0.0*	*27.9*
5-20 MW	*0.0*	*0.0*	*0.0*	*376.9*	*0.0*	*47.6*
20-50 MW	*0.0*	*0.0*	*0.0*	*567.2*	*0.0*	*71.6*

As a result of the above development of areas and factors, one can determine the total DG power in each cell as a sum of the areas per sector and per size category ($A_{i,j,k}$) multiplied by the adoption rate relative intensity. This factor F_{power} is determined for each individual cell of the air quality model as follows:

$$F_{power,k} = \sum_i \sum_j A_{i,j,k} R_{i,j} \tag{7}$$

The total DG power in real units (MW) assigned to each cell k of the model is then determined as a function of the assumed total implementation of DG power in the SoCAB (portion of increased power demand met by DG) and the normalized power factor as follows:

$$P_{Tot,k} = \frac{F_{power,k}}{\sum_k F_{power,k}} \cdot P_{Tot,SoCAB} \tag{8}$$

Once the total DG power in each cell is determined, DG power associated with each of the size categories in each sector can be described by the following equation:

$$P_{i,j,k} = \frac{A_{i,j,k} R_{i,j}}{F_{power}} P_{Tot,k} \tag{9}$$

Finally then, the total DG power per sector and per cell can be written as:

$$P_{i,k} = \frac{\sum_j A_{i,j} R_{i,j}}{F_{power}} P_{Tot,k} \tag{10}$$

STEP 4. At this point one must consider the operational duty cycle of DG units. The temporal variation of the DG power due to the variety of duty cycles of the units is introduced into this procedure as a function of the particular sector that the DG units are serving. Average load profiles are calculated for each sector based on hourly electric data obtained from the Southern California Edison web page (refer to Appendix F for details). To apply the sector-specific duty cycle, one must determine a normalized vector factor, $D_{i,h}$, which describes the hour-by-hour duty expected in each sector. The total power for a particular sector in a cell is presented in equation 10 as $P_{i,k}$. This factor is considered the peak DG power output that can occur at any one hour of the day in a particular sector. Thus, multiplying the normalized duty cycle by the peak sector power in each cell produces the total power per sector and per cell as a function of the time of the day as:

$$P_{i,k,h} = P_{i,k} D_{i,h} \tag{11}$$

The next step consists of determining the relative contribution to total power in a cell by each of the DG types considered (namely, low temperature (LT) fuel cells, high

temperature (HT) fuel cells, MTGs, NG ICEs, PV, conventional gas turbine (CGT), advanced gas turbine (AGT), Stirling engines, and Hybrid fuel cell systems). To accomplish this, six tables must be developed (one for each sector), in which the relative expected contribution of each DG type in each size category, $W_{i,l,,j}$, is presented. And the total DG power in each cell supplied for each of the DG types considered is:

$$P_{l,k,h} = T_{l,k,h} \cdot P_{Tot,k,h} \tag{12}$$

STEP 5. Table 26 below presents the relative contributions of DG technology types ($W_{i,l,j}$) for the industrial sector as an example. Tables presenting $W_{i,l,j}$ for all the sectors are included in Appendix G. The relative contribution factors all six sectors are based on market penetration of DG technology types in the industrial sector (Little 2000), utility sector (Ianucci et al. 2000), and building sector (Boedecker et al. 2000) and APEP team or other expert estimates on market distribution of DG technology types in each of the size categories.

As a result, the equation that determines the relative contribution of each DG technology in each cell for a particular hour of the day, $T_{l,k,h}$, is given by:

$$T_{l,k,h} = \frac{\sum_i \sum_j W_{i,l,j} \cdot P_{i,j,k,h}}{P_{Tot,k,h}} \tag{13}$$

And the total DG power in each cell supplied for each of the DG types considered is:

$$P_{l,k,h} = T_{l,k,h} \cdot P_{Tot,k,h} \tag{12}$$

Table 26. Estimated relative contributions of DG technology types ($W_{i,l,j}$) in the Industrial sector as a function of size class

Size categories	% LT Fuel cells	% HT Fuel cells	% MTGs	% NG ICEs	% PV	% CCT	% AGT	Stirling	Hybrid
< 50 kW	0.0%	0.3%	0.7%	0.0%	0.0%	0.0%	0.0%	0.0%	0.0%
50-250 kW	0.0%	2.1%	13.6%	0.0%	0.0%	0.0%	0.0%	0.0%	0.0%
250-1,000 kW	0.0%	2.9%	0.0%	10.1%	0.0%	9.7%	0.0%	0.0%	2.5%
1-5 MW	0.0%	0.0%	0.0%	10.1%	0.0%	9.7%	0.0%	0.0%	2.5%
5-20 MW	0.0%	0.0%	0.0%	0.0%	0.0%	9.7%	13.0%	0.0%	0.0%
20-50 MW	0.0%	0.0%	0.0%	0.0%	0.0%	0.0%	13.0%	0.0%	0.0%
Total	0.0%	5.2%	14.4%	20.1%	0.0%	29.2%	26.0%	0.0%	5.0%

STEP 6. At this point, an estimate of the spatial distribution of DG power and the mix of DG technologies in each cell of the model—and the power that each is producing at each

hour of the day—has been determined. The sixth step to consider is a weighting factor for relative DG adoption rates that is a function of the location within the basin that one is considering. The systematic procedure presented thus far uses average DG adoption factors for all cells throughout the basin. No local information on forecasted DG penetration in certain zones of the SoCAB as the result of any potential driver (e.g., transmission or distribution constraints in utility grid, strong DG incentives in particular cities, or anticipated larger DG installations) has been included in the approach thus far.

Since data was not available to suggest preferential DG adoption at any particular location or set of locations in the SoCAB, the APEP team decided to retain average adoption rates. However, if at any time preferential DG adoption rates that apply to the spatial distribution of DG in the SoCAB become available, one should apply a normalized adoption rate factor in this step. So far no local data is available and, therefore, no modification to the first five steps of this systematic approach is applied in this analysis.

STEP 7. The seventh step is to calculate pollutant emissions in each cell and each hour of the day, based on the emissions factors for each of the DG types, e_l. As explained in Section 2.1.1.3 Emissions Specifications, the emissions factors, e_l, for each of the DG types are determined from literature sources (Ianucci et al. 2000; Marnay et al. 2001; Allison and Lents 2002) and APEP measurements of emissions from various DG technologies. Note that, based on current emission factors gathered from literature in Table 2, some DG technologies do not meet the applicable emission standards (summarized in Table 4, Table 5, and Table 6). However, in all cases the emissions from DG are never allowed to exceed the applicable CARB and SCAQMD emissions limits, since any DG unit must comply with the emission standards to be installed in the basin. In other words, if a certain DG technology is to be installed in the SoCAB, but has emission factors that exceed the standards, the applicable emission standards are assumed, instead of its corresponding emission factor to calculate DG emissions. The emissions for all the DG pollutants considered in a given cell of the model can be determined through the following equations:

$$[CO]_{emiss,k,h} = \sum_{l} P_{l,k,h} \cdot e_{l,CO} \tag{14}$$

$$[NOx]_{emiss,k,h} = \sum_{l} P_{l,k,h} \cdot e_{l,NOx} \tag{15}$$

$$[VOC]_{emiss,k,h} = \sum_{l} P_{l,k,h} \cdot e_{l,VOC} \tag{16}$$

$$[SOx]_{emiss,k,h} = \sum_{l} P_{l,k,h} \cdot e_{l,SOx} \tag{17}$$

$$[PM]_{emiss,k,h} = \sum_{l} P_{l,k,h} \cdot e_{l,PM} \tag{18}$$

$$[CO_2]_{emiss,k,h} = \sum_{l} P_{l,k,h} \cdot e_{l,CO2} \tag{19}$$

Although CO_2 emissions do not contribute to the atmospheric chemistry, they are accounted in this step to ascertain the possible global warming impacts of DG implementation in the SoCAB.

STEP 8. To fully characterize the emissions coming from potential DG operation in the SoCAB at the level required by the air quality model, a further speciation of the above criteria pollutants (i.e., NO NO_X, CO, VOC, SO_X, and PM) must be applied. This step requires that one directly correlate each of the pollutant emissions calculated in the previous seven steps to the pollutant flux rates that are required by the particular chemical mechanism that the AQM is using. In this particular case, the species that are considered in the AQM are those associated with the CACM mechanism. Use of the CACM mechanism requires splitting of NO_X emissions into NO and NO_2; SO_X emissions into SO_2 and SO_3; characterization of the VOCs as five distinct hydrocarbon compounds; and supplying a distribution of particulate matter that is comprised of 19 species and eight size classes. The process of accomplishing this is presented in more detail in Section 2.1.1.8.

STEP 9. The effects of any emissions displacement that may occur as a result of DG installations in the SoCAB are accounted for in Step 9. Once the speciated emissions from the DG realistic scenario are known, the process described in Section 2.1.1.10 to account for displaced emissions due to the operation of CHP DG units (or other emissions displacement) is applied. The resulting net emissions fluxes are calculated in this step by direct subtraction of emissions fluxes that account for displaced emissions.

STEP 10. The last step that is required to complete the development of a realistic scenario based upon land-use data is to take into account other realistic factors that can affect the final emissions levels for the particular date that one desires to simulate. The factors that can be included are first the date of the simulation (upon which all factors above must be scaled) together with an adoption rate curve, or any performance degradation that one wants to include for the installed DG systems.

With regard to the adoption rate, both a realistic exponential increase and a less realistic linear increase of the accumulated DG power installed in the period 2003–2010 have been implemented in this study, as shown in Section 2.1.1.11 of this report. The performance degradation can include both an increase of criteria pollutant emissions and a decrease of electrical efficiency that will likely occur throughout the lifetime of any DG unit. As practically no public data on DG performance degradation are currently available, the APEP team suggests a 10% annual increase in criteria pollutant emissions. According to the estimated adoption rate, two average years of installation for the DG units are determined—one for the DG fleet as adopted in the period 2003–2006, and the other for the one introduced in 2007–2010. The corrections of net emissions for both the 2003–2006 and the 2007–2010 DG fleets due to selected annual performance degradation are determined, according to their average year of installation. See Section 2.1.1.11 for more details of this procedure.

2.2 Air Quality Modeling: Approach and Results

2.2.1 Input Considerations

Simulations of air quality episodes with a three-dimensional model require a series of input parameters used to compute the numerical solution of the atmospheric diffusion/advection equation (Equation 20).

$$\frac{\partial Q_m^k}{\partial t} + \nabla \cdot \left(u Q_m^k\right) = \nabla \cdot \left(K \nabla Q_m^k\right) + \left(\frac{Q_m^k}{\partial t}\right)_{sources/\sin ks} + \left(\frac{Q_m^k}{\partial t}\right)_{aerosol} + \left(\frac{Q_m^k}{\partial t}\right)_{chemistry} \quad (20)$$

Input data needed include the meteorological conditions and the emissions inventory. In particular, the following fields describe the meteorological data in the model: temperature, relative humidity, solar radiation, three-dimensional wind fields, and inversion height. Gas-phase reactions and aerosol-phase conversion processes are included in the model through a state-of-the-art chemical mechanism and a comprehensive aerosol-phase formation module. Finally mixing and transport of pollutants are also considered.

2.2.1.1 Meteorological conditions

The Southern California Air Quality Study (SCAQS) completed a comprehensive campaign of atmospheric observations in the SoCAB during August 27–29, 1987. The campaign collected an extensive set of meteorological and air quality data that has been used widely to validate air quality models (Moya 2002 et al.; Griffin et al. 2002b; Knipping et al. 2002; Meng et al. 1998). During SCAQS, temperature, humidity and winds vertical profiles were obtained along with the temporal and spatial distribution of these fields. Further analysis of these measurements has provided a complete set of gridded meteorological data readily available to be used in air quality simulations. Zeldin et al. (1990) found that August 28, 1987, falls within a "reasonable central met-class tendency," and makes it suitable for modeling. In addition, the August 27–29, 1987, episode was found statistically within the top 10% most severe ozone-forming meteorological conditions (SCAQMD 2003a). Furthermore, this episode is also used by the AQMD to show that air pollution control strategies proposed in the 2003 Air Quality Management Plan (SCAQMD 2003b) will lead to ozone attainment by 2010. Hence, this episode is selected in this study to evaluate the air quality impacts of DG during severe smog conditions.

During a typical day, the dominant direction followed by the winds in the SoCAB is from west to east. The San Gabriel and San Bernardino Mountains form a natural barrier that enhances accumulation of air pollutants, especially in downwind locations, such as Riverside and San Bernardino. In addition, warm and sunny conditions together with lack of natural scavenging processes, such as rain, promote the formation of photochemical smog and ozone.

The SCAQS episode in August 27–29, 1987, was characterized by a weak onshore pressure gradient and warming temperatures aloft. The wind flow was characterized by a sea breeze during the day and a weak land-mountain breeze at night. The presence of a well-defined diurnal inversion layer at the top of neutral and unstable layers near the surface, and a slightly stable nocturnal boundary layer, facilitated the concentration of pollutants over the SoCAB and lead to an episode with high ozone concentrations.

2.2.1.2 Emissions inventory

The SCAQMD and CARB have prepared the gridded emission inventories used in this report. Back-casting of emissions has lead to emission inventories used for modeling purposes. Emission inventories for the years 1987 and 1997 are used to compare simulation results with measured data. Forecasting of emissions is used to generate emission inventories for the year 2010. Forecasted emissions are required by state agencies to evaluate emission control measures that might lead to attainment of ozone federal air quality. Two different emission inventories have been prepared: (1) a 2010 baseline emission inventory, which accounts for increase in population and does not consider any future emissions control measures (Figure 10 and Figure 12), and (2) a 2010 attainment scenario, which includes all the control measures proposed by state agencies to accomplish ozone federal air quality standards attainment by 2010 (Figure 11 and Figure 13).

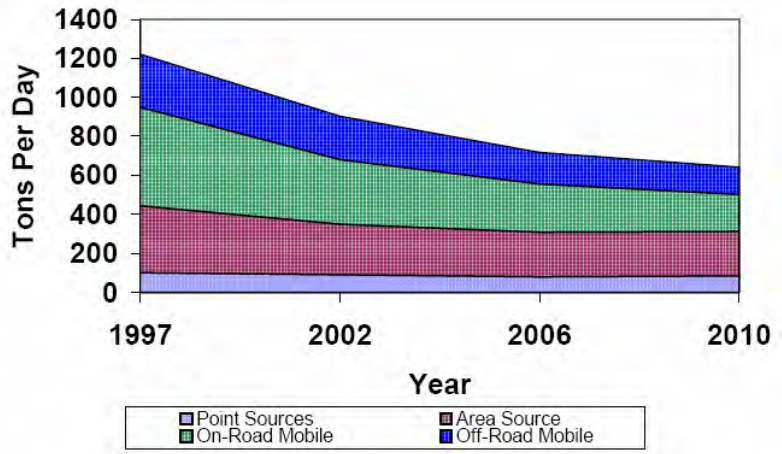

Source: SCAQMD 2003b

Figure 10. Baseline VOC emissions

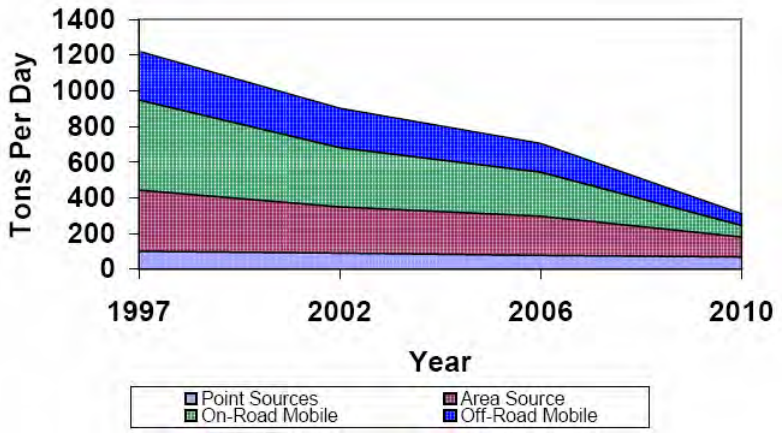

Source: SCAQMD 2003b

Figure 11. Attainment VOC emissions

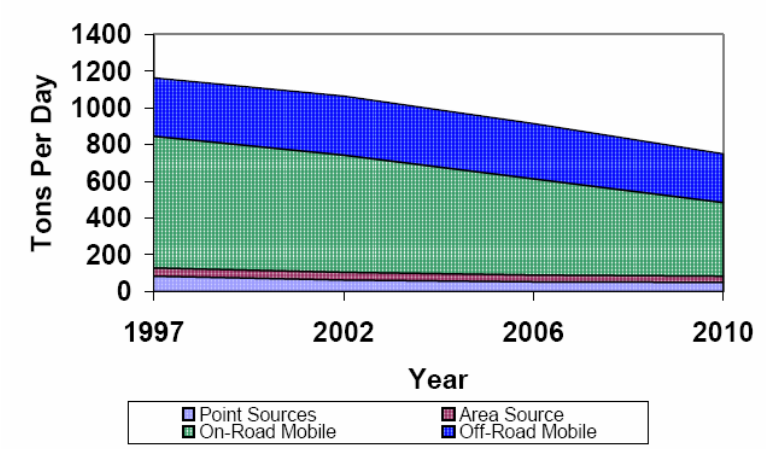

Source: SCAQMD 2003b

Figure 12. Baseline NO_X emissions)

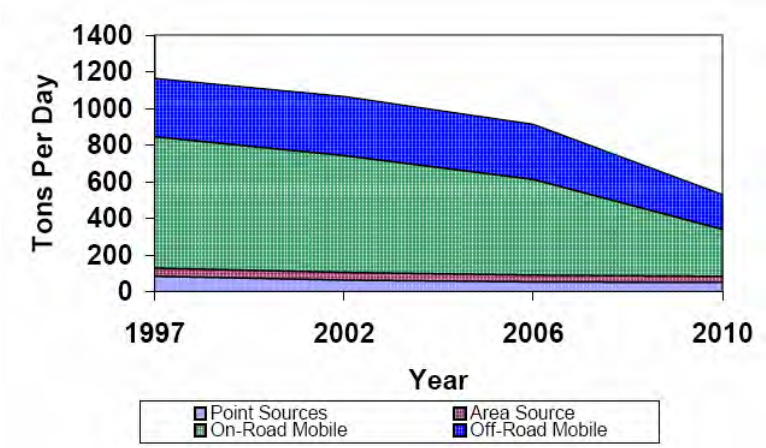

Source: SCAQMD 2003b

Figure 13. Attainment NO_X emissions

Determination of DG air quality impacts depends on the emission inventory used for the simulations. VOCs and NO_X in the attainment emission inventory are lower than those of the baseline scenario by 40% and 27%, respectively. As a result, air quality impacts due to DG on the attainment scenario may be significantly greater than impacts on the baseline scenario. Results in this work, however, are based on the baseline emission inventory, since the attainment emission inventory is under ongoing development. A section reporting air quality impacts of DG using the attainment emissions inventory is included in this study, to discuss the effects of base emissions on DG air quality impacts.

2.2.1.3 Chemical mechanism

The gas-phase chemical mechanism used in the present simulations is the Caltech Atmospheric Chemical Mechanism (CACM, see Griffin et al. 2002b). This mechanism is based on the work of Stockwell et al. (1997); Jenkin et al. (1997); and SAPRC-97 and SAPRC-99 (available from W.P.L. Carter at http://pah.cert.ucr.edu/~carter/). It includes O_3 chemistry and a state-of-the-art

mechanism of the gas phase precursors of secondary organic aerosol (SOA). The full mechanism consists of 361 chemical reactions and 191 gas-phase species which describe a comprehensive treatment of VOCs oxidation.

2.2.1.4 Aerosol-phase dynamics

Inorganic aerosol formation is calculated using the Simulating Composition of Atmospheric Particles at Equilibrium 2 model (SCAPE2, Meng et al. 1995). SCAPE2 has been modified to account for the interaction between organic ions present in the aqueous phase and the inorganic aerosol components.

The model used to determine the partitioning of secondary organic compounds is the Model to Predict the Multiphase Partitioning of Organics already built in the CIT Airshed model (MPMPO, Griffin et al. 2002b). MPMPO allows the simultaneous formation of SOA in a hydrophobic organic phase and a hydrophilic aqueous phase. The module consists of 37 size-resolved aerosol-phase species, in 8 different size bins ranging from 0.04 to 10 micrometers. The integrated module allows particulate matter to undergo advection, turbulent diffusion, condensation/evaporation, nucleation, emissions, and dry deposition processes.

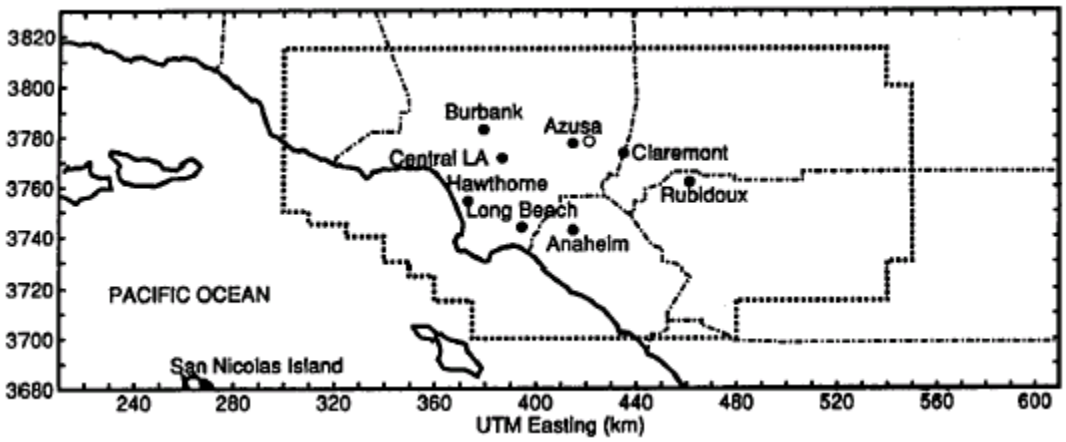

Source: Griffin et al. 2002a

Figure 14. CIT Airshed domain

2.2.1.5 Mixing and transport mechanism

The California Institute of Technology (CIT) Airshed Model is used as the host model for the chemical and aerosol mechanisms (Harley et al. 1993; Griffin et al. 2002a; and Meng et al. 1998). The grid used by the CIT model encompasses Orange County and part of Los Angeles, Ventura, San Bernardino, and Riverside counties (Figure 14). The grid consists of cells with an area of 5 km by 5 km (3 miles by 3 miles), with a vertical resolution defined by five vertical layers of increasing thickness from ground level up to 1100 meters (3600 feet) of altitude. The respective five layers thicknesses are 38.5, 115.5, 154, 363, and 429 meters (126, 378.9, 505, 1,190, and 1,407 feet) from the bottom to the top layer.

2.2.2 Comparison of Simulation Results with Measured Data

Model performance needs to be analyzed and compared with available observations since simulation of an air quality episode requires various input parameters, each one subject to different sources of uncertainty. Griffin et al. 2002a validated results obtained with the CIT model and the CACM chemical mechanism using the August 27–29, 1987, meteorology and emissions inventory (see Figure 15). Griffin et al. 2002a also reported comparisons between observed and simulated data at Pasadena and Riverside. In general, ozone concentrations in Pasadena were under-predicted each day; whereas, NO concentrations at this location compared reasonably well with observation, except for the third day. In Riverside, ozone concentrations agreed with observed data for the second and third day. However, NO concentrations were under-predicted during the daylight hours and over-predicted at nighttime. A statistical analysis was conducted to determine the overall performance of the model versus observed data (see Table 27). Results show a typical level of agreement for current three-dimensional air quality models.

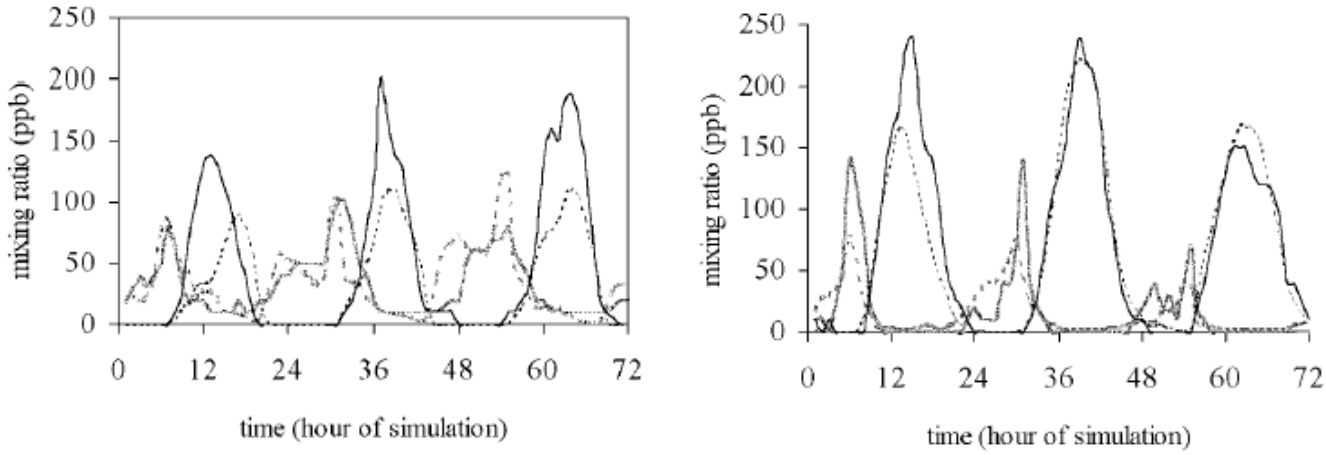

Source: Griffin et al. 2002a

Figure 15. Comparison of simulated (dashed line) and measured (solid line) NO (shaded) and O_3 (black) mixing ratio in Pasadena (left) and Riverside (right) during August 27–29, 1987

Table 27. Statistical analysis of model performance versus observed data on August 28, 1987, for O_3 and NO_2

Statistical Measure	O_3	NO_2
Bias, ppb	15.9	-0.4
Normalized bias, %	21.7	12.6
σ of residuals, ppb	55.3	28.1
Gross error, ppb	39.5	21.4
Normalized gross error, %	41.1	51.6

Source: Griffin et al. 2002a

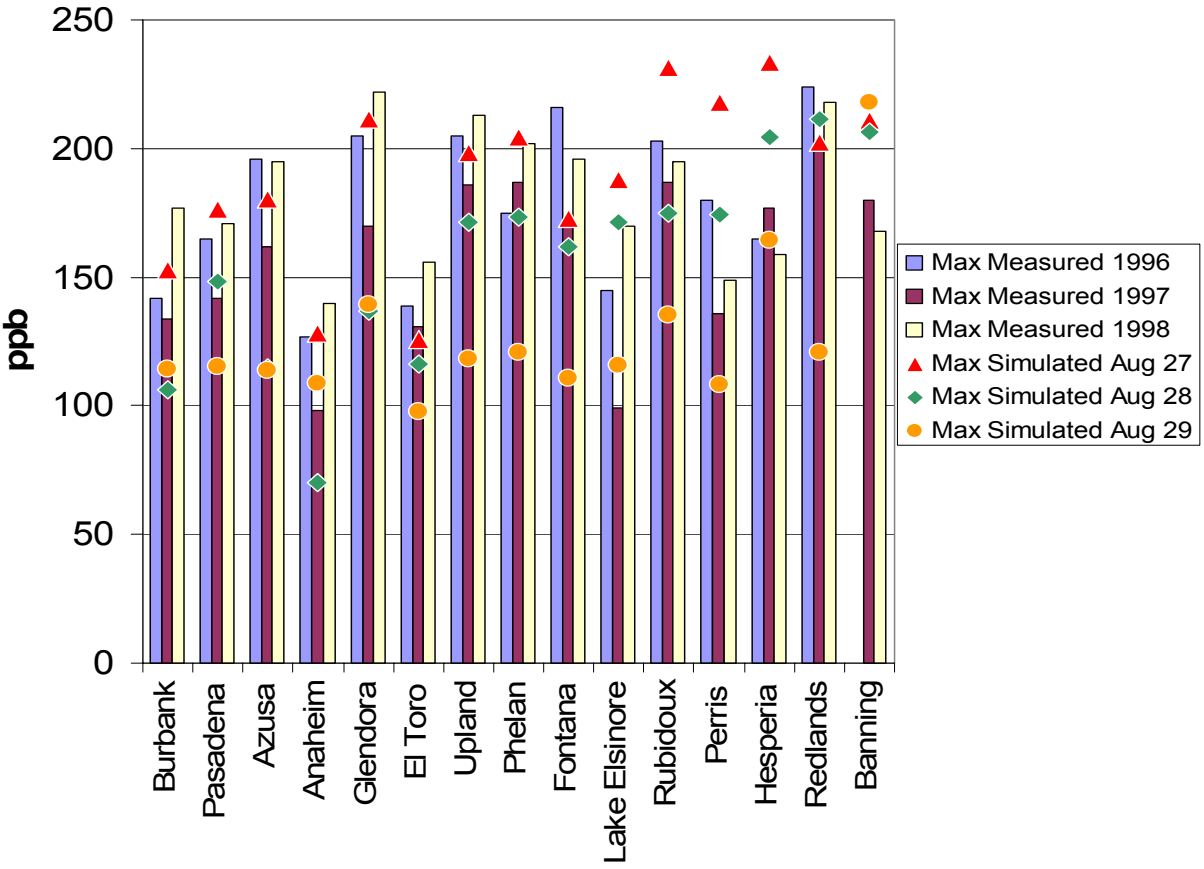

Figure 16. Comparison between measured maximum concentration of ozone in years 1996–1998, and concentration of ozone simulated using 1997 emission inventory and a high ozone-forming potential episode (SCAQS August 27–29, 1987, meteorology)

Figure 16 shows a comparison between model predictions and observations of maximum ozone concentrations at different monitoring stations using August 27–29 meteorology and the emission inventory for year 1997. Measured maximum ozone concentrations reported in Figure 16 correspond to observations in the period from 1996 to1998 at the selected stations. Note that simulated data refers to a specific episode; whereas, measured data refers to maximum concentrations during the entire year. This comparison shows that simulation results fall within the range of measured ozone values at each station. Although not a strict validation, this kind of comparison establishes an additional sense of confidence in the simulation results, specially needed when different emission inventories will be used.

2.3 Uncertainty and Sensitivity Analysis

2.3.1 Importance and Background

Air quality models are instrumental to assess the potential air quality impacts of DER within urban basins. Only through the use of a detailed AQM can one assess the effects of increased DG emissions on the complex, non-linear, and concurrent processes of transport, mixing, heterogeneous, and homogeneous chemistry that lead to criteria pollutant concentrations of interest. However, numerical predictions from mathematical models are subjected to various sources of uncertainty. A quantitative analysis of AQM responses to different input parameters is a prerequisite to characterize these sources of uncertainty. Additionally, such an analysis also identifies those input parameters and simulation conditions responsible for most of the model output variation.

Emissions inventories represent the largest uncertainties associated with output concentrations in three-dimensional urban/regional air quality models (Griffin et al. 2002b). However, the gas-phase chemical mechanism could introduce significant uncertainties in model predictions. Sources of uncertainty in chemical mechanisms lie in the rate constants, the product yields, and the mechanisms of degradation of reaction products. Mathematical procedures to analyze uncertainty and sensitivity of complex photochemical mechanisms have been evaluated thoroughly. For instance, Dunker (1981, 1984); Milford et al. (1992); and Gao et al. (1995) used direct decoupled methods; Rabitz et al. (1983) and Rabitz and Hales (1995) employed the Green's Function or Adjoint Green's Function methods; whereas, Carmichael et al. (1997) favored automatic differentiation techniques.

Monte Carlo methods that examine uncertainties in chemical parameters have been applied also to gas-phase chemistry and photochemical box models (Stolarski et al. 1978; Ehhalt et al. 1979; Thompson and Stewart 1991; Gao et al. 1995; Yang et al. 1996). Monte Carlo methods are statistical simulation methods, where sequences of random numbers are used together with multiple trials (simulations in this case) and statistical analyses of variance to determine sensitivities. Monte Carlo methods are widely used because they can be applied to problems with a large number of input parameters. Furthermore, Monte Carlo methods have the advantage that estimates of the uncertainties in model outputs are calculated with systematic runs of the model with standard statistical tests that can be applied to output results.

This section presents the approach selected by the University of California, Irvine research team to conduct sensitivity analyses of the atmospheric chemical mechanism (CACM) and the full AQM (the CIT Airshed model) used to determine the air quality impacts of DG. This section begins with a presentation of the results of the uncertainty and sensitivity analysis performed on the CACM (Griffin et al. 2002a,b; Pun et al. 2002). The CACM includes state-of-the-art treatment of ozone formation, but more importantly, is the first detailed atmospheric chemistry mechanism that includes explicit prediction of semivolatile products formation. These semivolatile products have the potential to be constituents of SOA and are significant precursors to SOA formation in the SoCAB.

A global sensitivity analysis of the chemical mechanism is performed and presented herein using Monte Carlo techniques combined with Latin hypercube sampling to vary simultaneously all

chemical parameters over their full ranges of uncertainty. Uncertainties in rate parameters are propagated through box model simulations with CACM for three summer cases. The cases cover a range of initial concentrations of reactive organic gases and nitrogen oxides that represents various episodes of high ozone levels in polluted urban areas.

This section describes the methodology used in the sensitivity analysis performed on the CACM as an introduction to the methodology selected for the current project. The same methodology is applied to the complete air quality model and chemical mechanism used in this project. Different approaches and evaluations have been used to understand the sensitivity and uncertainty of air quality models (Yang et al. 1997; Hanna et al. 1998, 2001; Moore and Londergan 2001; Hanna and Davis 2002; Vardoulakis et al. 2002; Hakami et al. 2003; Sax and Isakov 2003). However, the present analysis focuses on some specific aspects unique to this study. First, it examines the response of specific AQM predictions in order to separate the DG air quality impacts from the uncertainty of the model to various input parameters. Second, it provides a measure of the error bounds for model concentrations of ozone and particulate matter less than 2.5 micron ($PM_{2.5}$). Finally, this analysis explores the error spatial variation to determine those areas in the SoCAB of California where the model predictions display the largest uncertainties.

2.3.2 Chemical Mechanism Sensitivity

2.3.2.1 Methodology

Sensitivity and uncertainty analyses are accomplished using statistical methods to identify reaction parameters whose changes present the largest effect on both the concentration of selected key species and their associated errors. This section describes the statistical sampling used, the multiple regression approach to estimate sensitivity coefficients, and the corresponding uncertainty assessment under the simulation conditions established.

2.3.2.1.1 Latin hypercube sampling

A conventional approach to address uncertainty assessment is to apply Monte Carlo techniques. This particular methodology has been applied extensively in the study of regional-scale gas-phase mechanisms (Derwent and Hov 1988; Gao et al. 1996; Phenix et al. 1998; Bergin et al. 1999; Grenfell et al. 1999; Hanna et al. 2001; Vuilleumier et al. 2001a). Monte Carlo analysis investigates the response of model output (species mixing ratio) when the input variables (reaction rates) are changed by repeated sampling from some assumed joint probability distribution. The probability distribution of the species mixing ratio along with its mean, variance, and other characteristics are obtained from the evaluation of model output for each sample.

Monte Carlo analysis using random sampling yields reasonable estimates for the mixing ratio probability distribution if the sample size is large. However, acquiring a large number of samples (distinct randomly perturbed instances of running the full model in this case) is computationally expensive. An alternative approach, which yields more precise estimates, is to use a constrained Monte Carlo sampling scheme. One such scheme is Latin Hypercube Sampling (LHS) (McCay et al. 1979), a stratified sampling technique that has been compared extensively

with other techniques (Iman and Helton 1984), and that is proven to be more efficient than simple random sampling.

Latin hypercube sampling selects n different values from each of the N_p total number of parameters treated as random variables in the following manner. The range of each variable is divided into m non-overlapping intervals on the basis of equal probability. One value from each interval is selected at random with respect to the probability density in the interval. This value is randomly paired with the n values of the other N_p variables. Thus, the m N_p -tuplets constructed in this manner form the Latin hypercube sample. It is convenient to think of this sample as an $n \times N_p$ input matrix where the l^{th} row contains specific values of each of the N_p input variables used on the l^{th} run of the computer model.

The proper size of an LHS sample is a compromise between the number of runs and the required accuracy. In this study, sample sizes ranging from 100 to 3,880 runs are used to test the convergence of the means and the corresponding standard deviations of selected species. Study of these sample sizes resulted in the selection of 1150 samples for the sensitivity analyses of the CACM box model. Results reported thereafter are obtained with a sample size of 1150 computational runs of the box model. Even though the random variables are sampled independently and paired randomly, the sample correlation coefficient of any of the m N_p-tuplets is not zero, due to sampling fluctuations.

The input parameters in this study are treated as independent variables, and the correlation coefficients determined by the sensitivity analyses for the samples used never exceeded a value of 0.015. As a result, the assumption of independence is a good one. Sensitivity of the model output to the input parameters is determined with multiple linear regression analysis techniques in a manner similar to Derwent and Hov (1988) and Gao et al. (1996).

2.3.2.1.2 Simulation conditions

Computational runs performed in a box model with CACM as the chemical mechanism are the starting point for the proposed Monte Carlo analysis. The box model includes time-varying photolysis rates at a latitude of 34°N, approximately that of the Los Angeles basin. A 12-hour period that spans from 600 to 1800 (local time) is chosen to study an episode where photolysis plays a major role in the formation of important species such as ozone.

Initial conditions used represent those of an urban environment. Initial conditions for all species are obtained from typical data provided by the three-dimensional CIT model (Harley et al. 1993; Meng et al. 1998). The cell (box) in the CIT model that was selected represents Riverside because this location exhibits large ozone concentrations in the SoCAB. Typical VOC to NO_X ratios in this and similar urban regions vary from 6:1 to 50:1 (Baugues 1986). Urban summer ground-level conditions for VOC/NO_X ratio range from 6:1 to 24:1 with 1000 ppbC total VOC mixing ratio (Gao et al. 1995). The value of the initial VOC/NO_X ratio in the chosen cell is 8.6 with 1534 ppb carbon (C) total VOC. However, different cases for the VOC/NO_X ratio are analyzed by changing the NO_X mixing ratio.

Three cases are examined. First, the VOC/NO_X ratio is set at 8:1 corresponding to a regime in which ozone increases as NO_X gets reduced. Second, the optimal ratio for maximum ozone

production is set at 17:1. Finally, a ratio of 32:1 corresponding to the regime where decreasing NO_X results in O_3 reduction is applied.

All rate parameters are treated as random variables. Uncertainty estimates for the kinetic parameters of the chemical mechanism (CACM in this case) are compiled mostly from published reviews (DeMore et al. 1990; Gao et al. 1996), and from the Summary of Evaluated Kinetic and Photochemical Data for Atmospheric Chemistry (available from Atkinson et al. on the World Wide Web server for the IUPAC Subcommittee for Gas Kinetic Data Evaluation, http://www.iupac-kinetic.ch.cam.ac.uk/index.html).

2.3.3 Air Quality Model Sensitivity

2.3.3.1 Description

This study investigates the uncertainty and sensitivity of key species to variations in selected input parameters related to DG by use of a Monte Carlo methodology. Monte Carlo analysis has been applied to study the uncertainty of regional-scale gas-phase mechanisms (Derwent and Hov 1988; Gao et al. 1996; Phenix et al. 1998; Bergin et al. 1999; Grenfell et al. 1999; Hanna et al. 2001; Vuilleumier et al. 2001a). Also, previous work is based on calculations of the California Institute of Technology (CIT) Airshed model over the SoCAB. Although responses of aerosol and gas-phase species to changes in NO_X, VOC, and ammonia (NH_3) emissions have been investigated by (Meng et al. 1997; Nguyen and Dabdub 2002b), these studies focus on simulation scenarios for the SCAQS on August 27, 28, and 29, 1987.

Sensitivity results presented use the 2010 baseline emissions inventory described in other parts of this report. This inventory helps to establish a baseline scenario, which accounts for the increase in population by the year 2010. Additionally, an improved model is used in the present work. For instance, the current CIT model incorporates the CACM (Griffin et al. 2002a,b; Pun et al. 2002), a detailed atmospheric chemical mechanism directed toward explicit prediction of semi-volatile products formation with the potential to be constituents of SOA. The potential air quality effects of DG implementation by the year 2010 motivate the current study. After performing various model evaluations, statistical analysis methods are used to identify the input parameters with the largest effect on both, concentrations of selected key species and their associated errors. This section describes the chosen statistical sampling, the multiple regression methodology used to estimate the sensitivity coefficients, and the corresponding uncertainty assessment for the simulation conditions established.

2.3.3.1.1 Latin hypercube sampling

Monte Carlo methods examine the changes in modeled output (species mixing ratio) when repeated sampling from an assumed joint probability distribution varies a pre-selected set of input variables. The probability distribution of species mixing ratio along with the mean and other relevant statistics are evaluated from each sample of model output. Latin Hypercube Sampling is proven to be more efficient than straight Monte Carlo sampling when the use of large samples is computationally costly. The LHS technique employed for the full air quality model is identical to that described in Section 2.3.2.1.1, used for the chemical mechanism sensitivity analysis.

2.3.3.1.2 Multiple linear regression

Model sensitivity to variation of selected input parameters is explored using multiple linear regression analysis (Derwent and Hov 1988; Gao et al. 1996; Hanna et al. 2001). However, when many input variables are involved, the direct construction of a regression model containing all input variables may not be the most adequate approach. Moreover, only a small number of input variables typically have an impact on the output variable. Thus, stepwise regression (Helton 1993) is used as an alternative to construct a regression model containing all the input variables. With this approach, a sequence of regression models is constructed. Namely, the first regression model contains the single input variable with the largest impact on the output uncertainty. The second regression model contains the two input variables with the largest impact, including the variable from the previous model. Additional models in the sequence are defined until a point is reached at which subsequent models are unable to increase meaningfully the amount of variation that can be accounted in the output variable. This study reports the results obtained in the last model of the sequence.

2.3.3.1.3 Simulation conditions

Investigation of uncertainties in complex three-dimensional air quality models poses a major challenge, because a large number of computational simulations is required. Additionally, statistical tools are essential to derive a few useful conclusions from the numerous three-dimensional, time-dependent simulation results (modeled concentrations). An important step in the analysis is the selection of input variables that: (1) have the potential to affect the concentrations predicted by the model, and (2) reflect changes as the result of DG implementation. This selection typically includes parameters such as the meteorology, the chemical reaction rates, and the initial conditions. The implementation of DG, however, will result in significantly different emissions profiles from those of central generation. Therefore, this study aims to understand whether changes in emission inventories similar to those caused by DG make a difference, and to what extent this difference is significant in the predictions of the air quality model. It is also important to characterize the temporal and spatial domain-wide differences in model uncertainties. This characterization will distinguish the numerical uncertainties of the model from the simulated air quality impacts of DG.

Table 28 presents the variables considered in this study and the values of their uncertainty ranges. The probability density function of the variables considered in the sensitivity analysis is assumed to follow a lognormal distribution. Values for the uncertainty ranges are compiled from published studies (Hanna et al. 1998, 2001). Table 28 reflects the careful selection of those quantities, such as boundary conditions and emissions, which drive spatial variation and affect the implementation of DG in the basin. The number of parameters is limited to less than 20 for three main reasons. First, this analysis focuses on the model sensitivity and uncertainty of ozone and particulate matter; thus, only input variables that affect these species are considered. Second, the number of input variables chosen is restricted in order to decrease the computational demands of the analysis, which requires large numbers of simulations when various input variables are considered. Third, not all chemical reaction rates need to be included since a comprehensive sensitivity and uncertainty analysis of CACM (Rodriguez and Dabdub 2003) shows that only a subset of reactions is the most influential in the formation of ozone. Moreover,

the reactions included in Table 28 are consistently the most important over different VOC:NO_X ratios explored in the box model calculations (Rodriguez and Dabdub 2003).

Computational runs, performed with the CIT model, are the starting point for the Monte Carlo analysis. Results reported in this study are obtained with a sample size of 50 computational model runs. The number of simulations is adequate, given the number of input variables (Hanna et al. 1998, 2001). Each model run represents a period of three simulation days (72 hours). However, this work only considers data results from the third day of simulations to lessen the influence of initial conditions. Lagrangian models confirm (Nguyen and Dabdub 2002b) that more than 90% of the initial conditions leave the computational domain by the second day of simulation. Moreover, direct sensitivity analysis of multidimensional models (Yang et al. 1997) estimates that ozone peak sensitivity values to initial conditions are 12 times higher on the first day, compared to values on the second and subsequent days. After simulations are performed, calculation of probability density functions for each output variable provides a way to characterize the uncertainty of predicted species concentrations. Sensitivity is based on the regression coefficients estimated with multiple linear regression as detailed in the previous section.

Table 28. Uncertainty ranges and associated sigmas for the Airshed input variables in the Monte Carlo runs

Variable Type	Input Variable	Range of Uncertainty (σ_g log-normal)
Boundary Concentrations	1. Top Ozone	1.23
	2. Top NO_x	1.73
	3. Top VOC	1.73
	4. Top NH_3	1.73
	5. Side Ozone	1.23
	6. Side NO_x	1.73
	7. Side VOC	1.73
	8. Side NH_3	1.73
Emissions Rates	9. Domain-wide NO_x	1.41
	10. Domain-wide VOC	1.41
	11. Domain-wide NH_3	1.41
Chemical Reactions	12. $NO_2 + h\nu$	1.30
	13. $NO + O_3 \rightarrow NO_2 + O_2$	1.10
	14. $NO_2 + OH + M \rightarrow HNO_3$	1.10
	15. $HCHO + h\nu$	1.40
	16. Alkenes + $OH \rightarrow RO_2$	1.13
	17. Aldehydes + $h\nu$	1.40

OH = hydroxyl radical; HNO_3 = nitric acid; RO_2 = organic peroxy radical

3. PROJECT OUTCOMES

3.1 Final DG Scenarios

Through application of the criteria presented in this report and use of all of the data and information that is currently available to the APEP team, it was determined that only a very limited number of realistic scenarios can be developed and included in the current study. This is because all available information and resources for well defining each of the parameters and factors is used to develop a "realistic" DG Scenario. The APEP team has sought and is including all possible information resources to ground these few "realistic" DG scenarios and is then including several parametric variations (excursions) on these scenarios that either complete or complement the overall analysis of air quality impacts of DG in SoCAB.

In addition, the APEP team is following the recommendation provided in the Industrial Stakeholder Workshops held on September 19, 2002, and May 21, 2003, to classify each of the DG scenarios in two categories according to the "likelihood" of the scenario. Some of the scenarios that were developed in this effort are therefore classified as "realistic" implementation scenarios for DG in the South Coast Air Basin. However, for scientific completeness, for sensitivity analyses, and for determination of potential impacts for unexpected outcomes, the APEP team developed a series of scenarios that "span the spectrum." These scenarios are classified as "spanning" DG Scenarios.

These spanning scenarios should in no way be considered realistic or probable. The authors strongly caution readers to accept these spanning or "unrealistic" scenarios only in as much as they provide increased understanding or fundamental insight into DG air quality impacts. Under no circumstances do the authors suggest that the predicted impacts of a spanning scenario are realistic or expected due to the installation of DG in SoCAB. The spanning DG scenarios are not expected and are only used for purposes of garnering insights that may be useful.

The list of DG scenarios that is recommended includes: (1) three baseline scenarios without DG emissions, (2) five realistic DG scenarios, and (3) twenty one spanning DG scenarios. These recommended DG Scenarios are presented and described below.

3.1.1 Baseline Scenarios

Three baseline scenarios were included in this study. Recall that these baseline scenarios are not perturbed by the addition emissions from the DG scenarios. DG scenario emissions were added to a baseline scenario to determine relative air quality impacts of the DG emissions. In each of the baseline scenarios, the emissions inventory for the South Coast Air Basin was not modified from that which was received by APEP from the California Air Resources Board. The 1987 Baseline Scenario is included as a reference case for checking the model and comparing results with real measured emissions and air quality measurements. Two Baseline Scenarios for the year 2010 were used in this study. The APEP team focused on the year 2010 to evaluate the air quality impacts of DG in the SoCAB. The year 2010 was the deadline for the SoCAB to comply with the NAAQS of ozone. As a result, emission projections for this year were already available from the California Air Resources Board. In addition, the California Energy Commission

estimates in its DG strategic plan projected a substantial market penetration of DG by 2010 (Tomashefsky and Marks 2002).

3.1.1.1 Scenario #B1: 1987 Baseline

No parameters or factors are changed from the 1987 Emissions Inventory obtained from the California Air Resources Board. This inventory has been tested against measured emissions and basin-wide air quality measurements by many research groups in hundreds of air quality studies.

3.1.1.2 Scenario #B2: 2010 Baseline

No parameters or factors are changed from the emissions inventory projected by the California Air Resources Board for the year 2010. The emissions inventory used herein was obtained from the CARB in May of 2003. Emissions in this scenario are assumed to be scaled for growth in population, industrial and commercial activity, vehicle miles traveled, and other factors, with the expectation that no additional regulatory requirements are instituted between now and 2010.

3.1.1.3 Scenario #B3: 2010 Attainment Baseline

No parameters or factors are changed from the 2010 emissions inventory projections obtained from the California Air Resources Board in 2003. Emissions in this scenario are those of the 2010 Attainment scenario used by the SCAQMD in their 2003 Air Quality Management Plan for demonstration of ozone National Ambient Air Quality Standards (NAAQS) attainment (http://www.aqmd.gov/aqmp/AQMD03AQMP.htm).

3.1.2 Realistic Scenarios

As a result of applying the screening criteria described above, and using all the data that are currently available, the APEP team recommends a limited number of realistic DG Scenarios (5), which are included in this study. The full characterization of these realistic scenarios uses all available reports, studies, measurements, APEP team insights, stakeholder comments, and other information that were available on DG characteristics, performance, market penetration, and application compatibility at the time of this report writing.

All of the realistic scenarios incorporate the recently acquired GIS land-use data of the SoCAB as a cornerstone to spatially distribute the DG throughout the basin. In addition, all of the latest studies regarding the potential application of various DG to certain applications, the degree of market penetration expected and the size, electrical performance, efficiency and emissions characteristics of each DG type are used in the realistic scenarios. A listing of these resources is presented in the References section. In addition, a detailed description of the GIS data and a systematic approach of scenario development based on these and other DG data and resources can be found in the report, *Final DG Scenario Development Report,* available on the Energy Commission website (www.energy.ca.gov/distgen_oii/documents/dgwg/R+D-7.pdf).

3.1.2.1 Scenario #R1

This realistic scenario #R1 is the basis for the other four realistic scenarios, which only incorporate a slight variation in one of the major factors that define Scenario #R1. Scenario #R1 makes use of all the resources available to justify DG overall penetration, DG power, and DG mix in each of the discretized cells of the air quality model. For this particular scenario, a medium early adoption for DG is assumed, which implies that the cumulative DG power implemented and operating in the SoCAB follows a linear trend from 2003 to 2010. Scenario #R1 also assumes a limited DG penetration (5% of the increased power requirements by 2010). This scenario contains a realistic duty cycle based on metered average electric hourly profiles for various energy sectors, a displacement of emissions due to the heat recovery mode of most of the units installed, and a low performance degradation of the DG units with time. Only in one of the spanning scenarios is an unrealistically high performance degradation considered (see Section 3.1.4.20). The high rate of performance degradation is considered unrealistic because it will likely not be allowed by air quality regulations.

Table 29 presents the primary factors that contribute to the overall definition of the realistic scenario #R1. Note that the actual mix of technologies, detailed descriptions of the approach for use of GIS data, and other descriptions of the factors in Table 29 are presented in the *Final DG Scenario Development Report* produced and submitted to the California Energy Commission under this same contract.

Table 29. Factors that contribute to the definition of realistic scenario #R1

Factor 1.1	Limited DG penetration, 5% of increased power
Factor 2.1.6	Different mix of Permitted and Certified DG in each cell based on the systematic approach to relate GIS data to DG mix
Factor 2.2.2.1	High penetration of low-emission technologies (strong regulation/policy drivers)
Factor 3.1.1	Known emissions factors – literature, data, permitted/certified levels (upper bound)
Factor 4.4	Different DG power in each cell based on the systematic approach to relate land use GIS data to spatial distribution of DG power
Factor 5.3	Realistic Duty Cycle for every sector
Factor 6.3	CHP Emissions Displaced
Factor 7.1.1	PM and VOC speciation from CARB data
Factor 7.2	Low performance degradation (3% increase of emissions per year)
Factor 7.3	No geometrical features
Factor 7.4.3	Medium early adoption of DG power (linear trend)

3.1.2.2 Scenario #R2: Medium Penetration (10%) Version of #R1

Scenario #R2 is defined by all of the same factors and parameters as Scenario #R1, except for a variation in DG Penetration. The DG Penetration parameter is set to a higher, still realistic value of 10% of the increased power demand being met by DG in 2010.

3.1.2.3 Scenario #R3: High Penetration (20%) Version of #R1

The same parameters and factors that apply to Scenario #R1 are applied to #R3. In this case, a DG Penetration parameter is set to an even higher value (20% of the increased power demand is met by DG in 2010) to account for the uncertainty associated with the future implementation of DG in the SoCAB. In addition, this high DG Penetration is consistent with the current rate of DG adoption and recommendations made by some of the stakeholders in the industry stakeholder workshop of May 21, 2003.

3.1.2.4 Scenario #R4: Low Early Adoption Version of #R1

The same parameters and factors that apply to Scenario #R1 are applied to #R4. The only variation is that a relatively low early adoption of DG is assumed, i.e., for #R4 most of the DG units operating in the SoCAB in 2010 will have been installed after the year 2007. Thus, the emissions signatures for the portion of the DG units that are smaller than 1 MW are set to be less or equal to the stricter CARB DG 2007 emissions standards.

3.1.2.5 Scenario #R5: No Emissions Displaced Version of #R1

The same parameters and factors that apply to Scenario #R1 apply also to #R5. However, in the case of #R5, emissions displacements that the implementation of DG in the SoCAB may produce are assumed to be zero. That is, no current basin emissions are removed as the result of DG installations. This realistic case is included to account for the possibility that no net emission offsets occur because credits might be sold to other entities, or the market for credits could end up not being robust enough, or the demands for energy are so significant that they require additional in-basin emissions that cannot be offset by reductions elsewhere in the basin.

3.1.3 Resulting Spatial Distribution of DG Power

The APEP team followed the procedure described in Section 2.1.3 that relates DG implementation to power per sector and DG technology mix, based on land-use GIS data, to produce a spatial distribution of DG power in the SoCAB for the year 2010. Figure 17 presents a contour plot of the DG power (on a log scale) for a DG scenario with a 5% of the increased power in the basin being met by DG. This type of spatial distribution, called a land-use weighted spatial distribution, is typical of the realistic DG scenarios that have been developed in the current program.

Figure 18 presents a comparison of the land-use weighted spatial distribution of DG power and other spatial distributions used in this study; namely, population-weighted, population growth-weighted, and freeway density-weighted spatial distributions. Except for the non-realistic freeway density spatial distribution of DG power, the other three distributions show relatively

similar patterns with some differences that are worthy of note. Both the population-weighted and the population growth-weighted spatial distributions have higher DG power peaks localized in the central part of Los Angeles. On the other hand, the land-use based distribution spreads DG power to more locations (e.g., south of Riverside) and reduces the power peak in central Los Angeles. Note also that the locations of peak power production occur in slightly differing regions of the SoCAB, representing zones permitted for industrial use and residential use for the land-use weighted and population- and population growth-weighted cases, respectively.

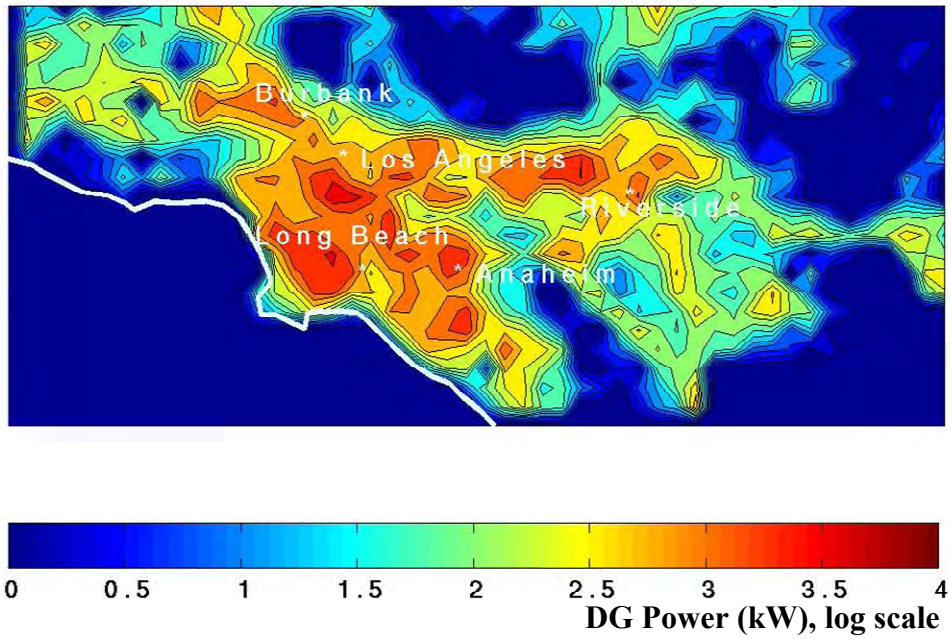

Figure 17. Spatial DG power distribution based on land-use GIS data

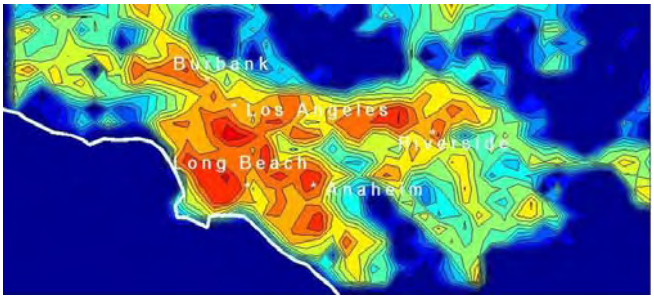

(a)

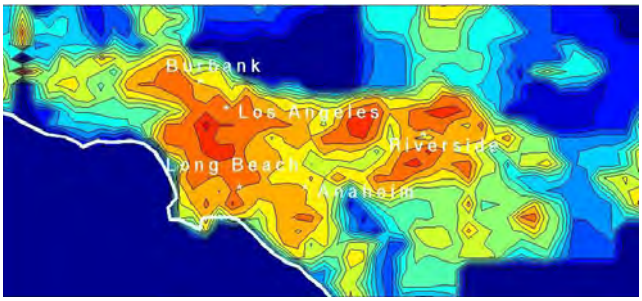

(b)

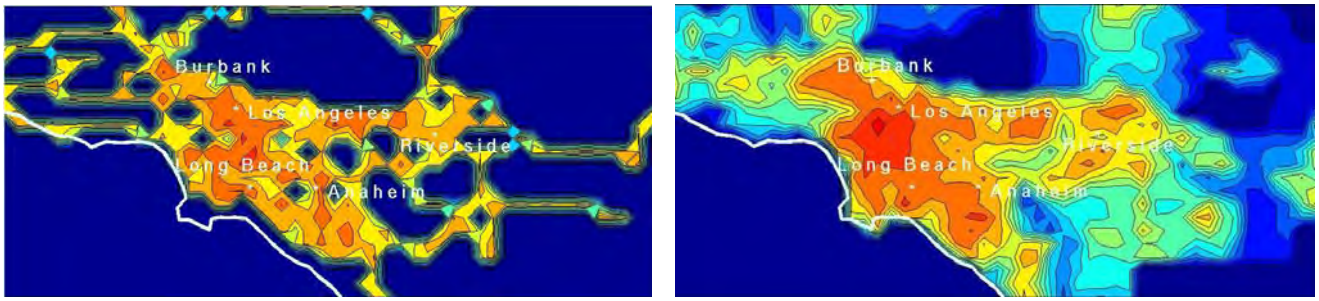

(c) (d)

Figure 18. Comparison among four spatial distributions of DG power in the SoCAB: (a) land-use-weighted; (b) population-weighted; (c) freeway density-weighted; (d) population growth-weighted

The application of the 10-step systematic approach for developing realistic DG implementation scenarios provides a reasonable distribution of DG power among sectors and among DG types in the SoCAB for 2010. Figure 19 presents the total DG power distribution among the various sectors considered in the current study. About 60% of total DG power is implemented in the industrial sector, and more than 30% is going to the commercial-institutional sector (the sum of categories "commercial" and "other"). Only a small fraction of the DG power that is anticipated for installation in the SoCAB by 2010 is installed to meet power demands in the residential sectors.

Figure 20 presents the relative contribution of each type of DG technology considered in the current study for the systematic approach for developing a DG scenario outlined above. According to this approach, almost 50% of the DG market is being met by gas turbines; whereas ICEs, MTGs, PV, and FC account for 17%, 15%, 5%, and 10% of the total 2010 DG power market, respectively. These figures are presented on a total power contribution basis, therefore they do not accurately reflect the number of units installed, but rather the contribution to total power demands that are met by each type of DG technology. For example, one large industrial gas turbine contributes much more to the power demand (and emissions) than does a host of small fuel cells installed in the residential sector.

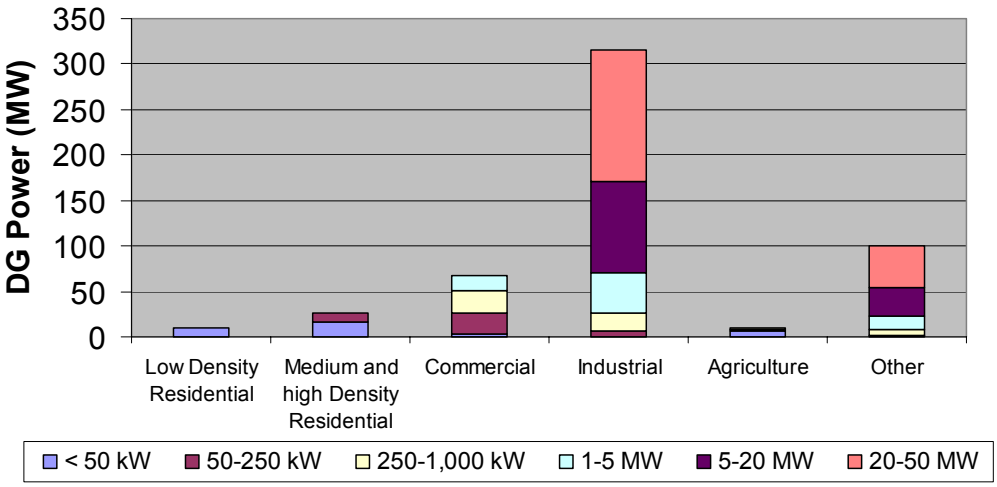

Figure 19. Total DG power distribution among sectors

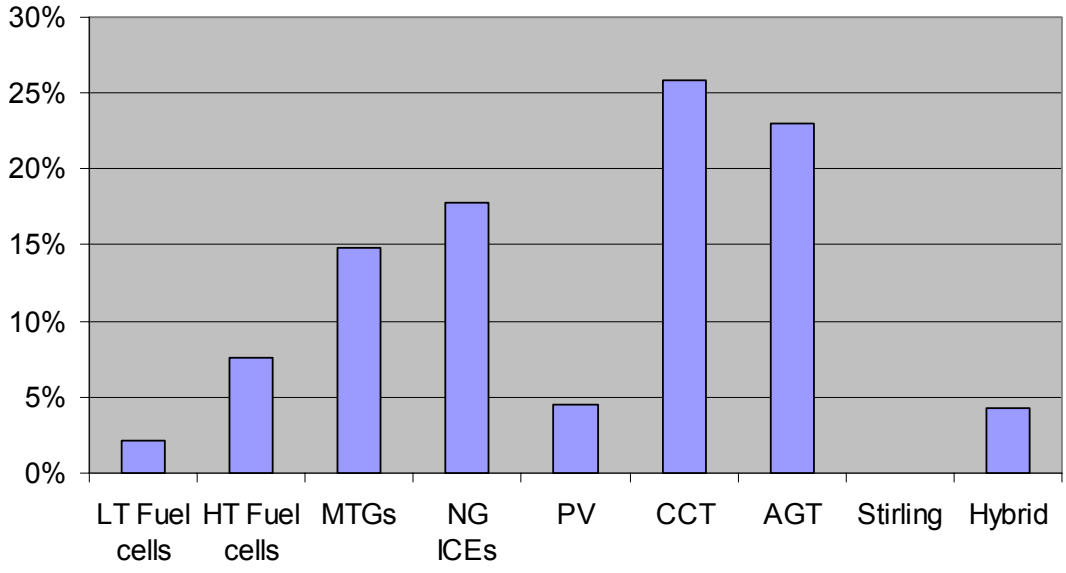

Figure 20. Total power distribution by DG type

3.1.4 Spanning DG Scenarios

In the spanning DG scenarios, most of the complexity of a realistic, very detailed scenario is skipped to develop relatively quickly scenarios that can be insightful for scientific completeness, sensitivity analyses, and/or the determination of potential impacts for unexpected outcomes. In all, the screening process has led to the selection of 21 spanning cases that are included in the current study. The 21 spanning DG scenarios are listed below, each with a simple one-sentence description of the scenario purpose. For a more thorough description of these and all of the scenarios, please see *Final DG Scenario Development Report*.

3.1.4.1 Scenario #S1: Population Weighted 2010 (PW2010)

Scenario #S1 contains a population-weighted spatial distribution of emissions from an "aggregated mix" of DG technologies with an overall DG penetration of 20% of the increase in power demand between now and 2010.

3.1.4.2 Scenario #S2: CARB 2003 Emissions Standards (2003ES)

Scenario #S2 is identical to scenario #S1, except that all DG are assumed to emit pollutants at exactly the CARB 2003 Emissions Standard.

3.1.4.3 Scenario #S3: CARB 2007 Emissions Standards (2007ES)

Scenario #S3 is identical to scenario #S2, except that all DG are assumed to emit pollutants at exactly the CARB 2007 Emissions Standard.

3.1.4.4 Scenario #S4: Permitted levels for ICEs (PermICEPW20%)

Scenario #S4 contains a population-weighted spatial distribution of emissions from DG technologies that are all assumed to emit pollutants at the current best available control technology (BACT) level approved by the SCAQMD in SoCAB.

3.1.4.5 Scenario #S5: High Early Adoption (HEAPW20%)

Scenario #S5 contains a population-weighted spatial distribution of emissions from an "aggregated mix" of DG technologies with an overall DG penetration of 20% of the increase in power demand between now and 2010. The rate of DG adoption is such that 98% of DG are installed before 2007, and 2% are installed between 2007 and 2010.

3.1.4.6 Scenario #S6: Peaking Scenario (PeakPW)

Scenario #S6 assumes that all of the DG technologies ("aggregate mix" of various technologies) are operating as peaking units (operating only between noon and 6 p.m.) with an installed capacity that equals 20% of the increase in power demand between now and 2010.

3.1.4.7 Scenario #S7: Large Gas Turbines without Ammonia Slip (LDG20%)

Scenario #S7 assumes that all DG are relatively large (50 MW) gas turbines that have emissions consistent with a $SCONO_X$ approach to emissions reduction (i.e., no ammonia emissions).

3.1.4.8 Scenario #S8: Large Gas Turbines with Ammonia Slip (NH3_20%)

Scenario #S8 assumes that all DG are relatively large (50 MW) gas turbines that have emissions consistent with a selective catalytic reduction (SCR) approach to emissions reduction (i.e., ammonia emissions are included).

3.1.4.9 Scenario #S9: Population Growth Weighted 2010 (PGW2010)

Scenario #S9 is similar to #S1, except that the spatial distribution of DG is determined by population growth between now and 2010, versus population for 2010.

3.1.4.10 Scenario #S10: Land use Weighted 2010 (LU2010)

Scenario #S10 is similar to #S1, except that the spatial distribution of DG is determined by land use designations, versus population for 2010.

3.1.4.11 Scenario #S11: Freeways (Free20%)

Scenario #S11 distributes all DG along the freeways in SoCAB.

3.1.4.12 Scenario #S12: All Fuel Cells (FCPW20%)

Scenario #S12 contains a population-weighted spatial distribution of emissions from DG that are assumed to be all fuel cells (of various types).

3.1.4.13 Scenario #S13: All MTGs (MTGPW20%)

Scenario #S13 contains a population-weighted spatial distribution of emissions from DG that are assumed to be all microturbine generators (of various types).

3.1.4.14 Scenario #S14: All CHP (DGCHP)

Scenario #S14 contains a population-weighted spatial distribution of DG that are all assumed to use CHP with appropriate emissions displacement for such technology being applied.

3.1.4.15 Scenario #S15: All Electricity emissions displaced (DGEED)

Scenario #S15 assumes that the operation of DG in SoCAB is one-for-one offset by a reduction in the electricity demanded from an in-basin power plant, reducing emissions from these power plants.

3.1.4.16 Scenario #S16: Technology distribution with 10% of the increased demand (TDPW10%)

Scenario #S16 contains a population-weighted spatial distribution of emissions from a distribution of various DG technologies with an overall DG penetration of 10% of the increase in power demand between now and 2010.

3.1.4.17 Scenario #S17: Business as usual with linear trend (BAU)

Scenario #S17 assumes that the adoption rate of DG proceeds linearly throughout the SoCAB as it has been reported to occur in the years 2001 and 2002 by Southern California Edison and Los Angeles Department of Water and Power.

3.1.4.18 Scenario #S18: Business as usual with parabolic trend (BAU_par)

Scenario #S18 assumes that the adoption rate of DG proceeds exponentially throughout the SoCAB as it has been reported to occur in the years 2001 and 2002 by Southern California Edison and Los Angeles Department of Water and Power.

3.1.4.19 Scenario #S19: Extremely High Penetration (EHP)

Scenario #S19 assumes an extremely high DG penetration that accounts for meeting of 20% of the total power requirements in 2010.

3.1.4.20 Scenario #S20: High Performance Degradation (HPD)

Scenario #S20 assumes a high rate of DG performance degradation just to the point of non-compliance for all DG technologies.

3.1.4.21 Scenario #S21: Peaking Total Power (PeakPW-2)

Scenario #S21 assumes that all of the DG technologies ("aggregate mix" of various technologies) are operating as peaking units (operating only between noon and 6 p.m.) with a total power produced that equals 20% of the increase in power demand between now and 2010.

3.1.5 Summary of Emissions from Spanning Scenarios

A brief description of DG scenarios is presented in Table 30.

Table 30. Brief description of DG scenario parameters

DG Scenario	Parameters that describe each scenario
Realistic	
#R1	• 5% of increased power demand from 2002 to 2010 met by DG • Technology mix according to activity sector distribution • High penetration of low-emission technologies • Spatial distribution according to GIS land-use distribution • Realistic duty cycle per each sector • CHP emission displaced • Low performance degradation (3% increase of emissions per year) • Linear trend for DG power adoption (Medium early adoption of DG Power)
#R2	• 10% of increased power demand from 2002 to 2010 met by DG • Same assumptions as in #R1 for the rest of parameters
#R3	• 20% of increased power demand from 2002 to 2010 met by DG • Same assumptions as in #R1 for the rest of parameters
#R4	• Low early adoption of DG Power (98% of DG installed in 2007 or after) • Same assumptions as in #R1 for the rest of parameters
#R5	• No CHP emissions displaced • Same assumptions as in #R1 for the rest of parameters
Spanning	
PW2010	• 20% of increased power demand from 2002 to 2010 met by DG • Technology Mix – mix of permitted and certified DG: 28.9% large GT (> 3 MW), 1.1% small GT (< 3 MW), 30% ICE, 25% MTG, 8% PV, 4.9% HTFC, 2.1% LTFC • GT distributed in populated areas with high industrial activity, population-weighted spatial distribution for the rest of DG • Base-loaded duty cycle • No emission displacement • No performance degradation • Low early adoption of DG Power
2003ES	• Technology Mix - all DG are certified under CARB 2003 Emission Standards • Population-weighted spatial distribution • Same assumptions as in PW2010 for the rest of parameters

Table 30. (continued)

DG Scenario	Parameters that describe each scenario
Spanning (continued)	
2007ES	• Technology Mix - all DG are certified under CARB 2007 Emission Standards • Same assumptions as in 2003ES for the rest of parameters
PermICEPW	• Technology Mix - all DG are ICE operating under BACT criteria • Same assumptions as in 2003ES for the rest of parameters
HEAPW20%	• High Early Adoption of DG Power: 95% of DG is installed before 2007 • Same assumptions as in PW2010 for the rest of parameters
PeakPW	• Peaking duty cycle (6 hours a day) • Peak power demand is equal to base load demand in PW2010 (20% of increased power demand from 2002 to 2010) • Total power delivered by DG during duty cycle • Technology Mix - mix of permitted and certified DG: 33.9 % large GT (> 3 MW), 1.4% small GT (< 3 MW), 35.3% ICE, 29.4% MTG • Same assumptions as in PW2010 for the rest of parameters
LDG20%	• Technology Mix – all DG are 49 MW GT • No ammonia emissions from DG considered • GT distributed in populated areas with high industrial activity • Same assumptions as in PW2010 for the rest of parameters
NH3_20%	• Ammonia emissions from GT considered • Same assumptions as in LDG20% for the rest of parameters
PGW2010	• GT distributed in populated areas with high industrial activity, population growth-weighted spatial distribution for rest of DG • Same assumptions as in PW2010 for the rest of parameters
LUW20%	• GT distributed in populated areas with high industrial activity, land use-weighted spatial distribution for rest of DG • Same assumptions as in PW2010 for the rest of parameters
Free20%	• GT distributed in populated areas with high industrial activity, freeway-weighted spatial distribution for rest of DG • Same assumptions as in PW2010 for the rest of parameters
FCPW20%	• Technology Mix – All DG are fuel cells • Population-weighted spatial distribution • Same assumptions as in PW2010 for the rest of parameters
MTGPW20%	• Technology Mix – All DG are certified MTG • Population-weighted spatial distribution • Same assumptions as in PW2010 for the rest of parameters

Table 30. (continued)

DG Scenario	Parameters that describe each scenario
Spanning (continued)	
DGCHP	• CHP emissions displaced • Same assumptions as in PW2010 for the rest of parameters
DGEED	• All electricity emissions displaced from in-basin electricity generators • Same assumptions as in PW2010 for the rest of parameters
TDPW10%	• 10% of increased power demand from 2002 to 2010 met by DG • Technology Mix – 34% NG ICE, 46% MTG, 10% FC, 10% PV • Population-weighted spatial distribution • Fuel cells are base loaded, rest of DG operates in a 6-hour duty cycle (from 12 p.m. to 6 p.m.) • Same assumptions as in PW2010 for the rest of parameters
BAU	• Linear extrapolation from current data on 2001 and 2002 DG installations in the SoCAB to determine total DG power installed in 2010 • Technology Mix – Mix of permitted and Certified DG from current DG mix data • Medium early adoption of DG Power • Same assumptions as in PW2010 for the rest of parameters
EHP	• Extra-high DG penetration: 20% of total power met by DG • Same assumptions as in PW2010 for the rest of parameters
BAU_par	• Parabolic extrapolation from current data to determine total DG power installed in 2010 • Same assumptions as in BAU for the rest of parameters
HPD	• High performance degradation: 10% increase of emissions per year • Same assumptions as in PW2010 for the rest of parameters
PeakPW-2	• Peaking duty cycle (6 hours a day) • Peak power demand is 4 times the base load demand in PW2010 so that the total cumulative electricity delivered by DG during the duty cycle equals the DG electricity in the PW2010 • Technology Mix - mix of permitted and certified DG: 33.9 % large GT (> 3 MW), 1.4% small GT (< 3 MW), 35.3% ICE, 29.4% MTG • Same assumptions as in PW2010 for the rest of parameters

Figure 21 shows a comparison of criteria pollutant emissions rates resulting from the various DG spanning scenarios. Because scenarios #S9 (PGW20%), #S10 (LUW20%), and #S11 (Free20) present exactly the same amount of total DG emissions as #S1 (PW2010), but with a different spatial distribution, they are not all presented in the bar chart of Figure 21. One of the realistic scenarios, #R3 is included for comparison purposes. Note that the emissions flux rates are presented on a log scale. Presented in this manner, one should observe that the differences in overall, basin-wide DG emissions among the various DG implementation scenarios are not in orders of magnitude. Most of the DG scenarios contain DG emissions rates that are within an order of magnitude of the typical emissions fluxes. Exceptions to this are the EHP case, with significantly higher CO_2 emissions and the DGEED case with significantly lower CO_2 emissions.

The same DG scenario emissions results that are presented in Figure 21 are presented in Figure 22. In Figure 22, however, the scale on which emissions fluxes are plotted is linear (versus the logarithmic scale of Figure 21). Notice that there are significant differences among the DG scenarios that are more obvious when the data are plotted on a linear scale.

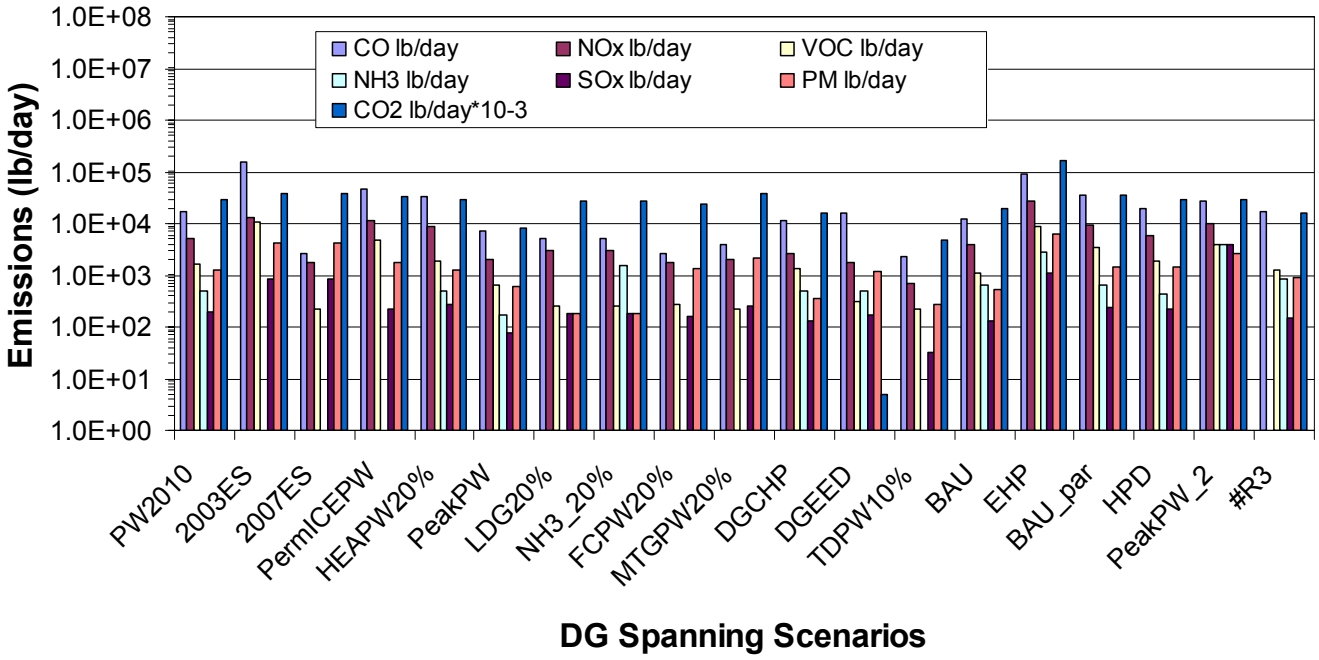

Figure 21. Comparison of criteria pollutant emissions among DG spanning scenarios (logarithmic scale)

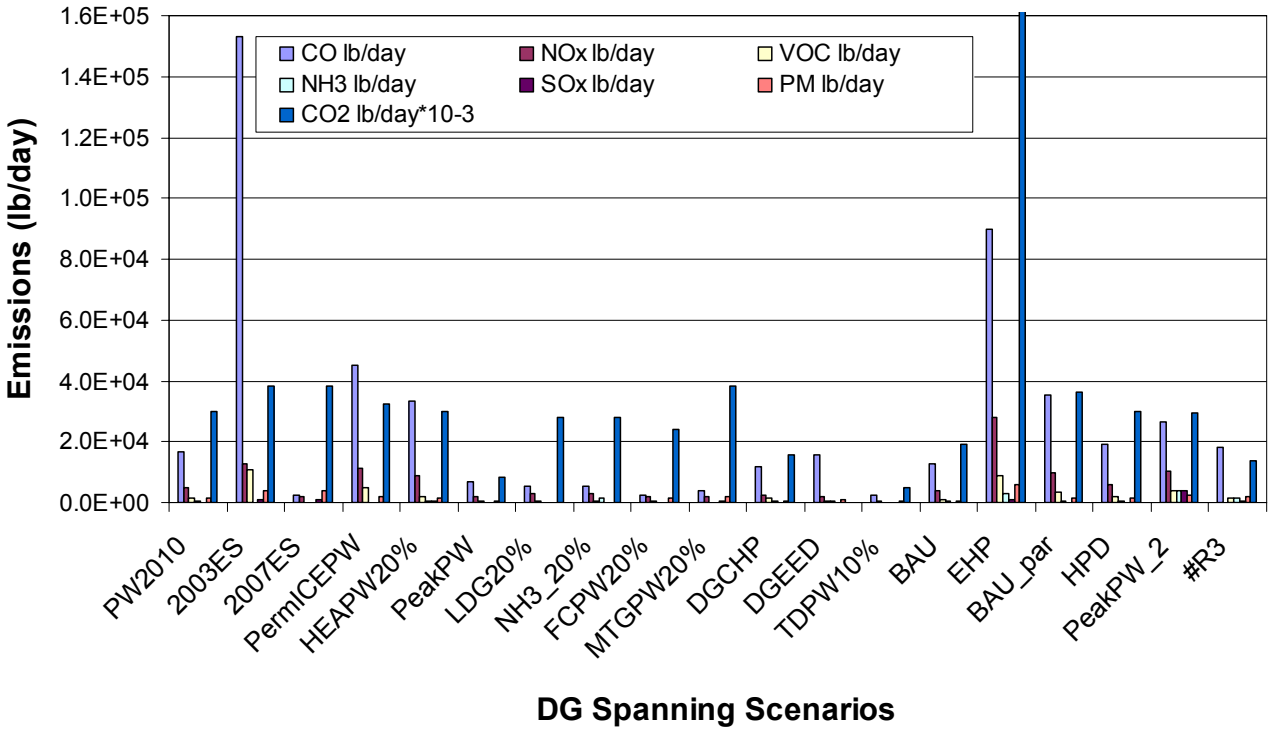

Figure 22. Comparison of criteria pollutant emissions among DG spanning scenarios (linear scale)

3.2 Simulation results: 2010 Baseline Scenario

This section presents simulation results using the baseline emission inventory for the year 2010 and the meteorological conditions of the August 27–29, 1987, episode. Table 31 shows a summary of the basin-wide emissions used for the simulation. Also, Table 32 reports the maximum concentrations of some criteria pollutants.

Table 31. Summary of Basin-wide baseline emissions for 2010

Species	tons/day
Anthropogenic NMHC*	649
Biogenic NMHC	232
NO_X	407
CO	3,268
PM	580
SO_x	88
NH_3	168

*NMHC= Non-Methane Hydrocarbons

Table 32. Simulated concentration of some criteria pollutants: Maximum hourly average concentration of O_3, NO_2, and CO and 24-hour average concentration of $PM_{2.5}$ (2010 baseline scenario)

Species	Maximum	Location	Average	Time
O_3	238 ppb	San Bernardino	1-hr average	1300
NO_2	158 ppb	Ontario	1-hr average	0500
CO	3.0 ppm	Los Angeles	1-hr average	0800
$PM_{2.5}$	115 $\mu g/m^3$	Riverside	24-hr average	N/A

ppm=parts per million; $\mu g/m^3$=micrograms per cubic meter

Simulation results for the baseline case show that ozone, NO_2, and $PM_{2.5}$ concentrations peak at locations downwind from places, like Los Angeles, where maximum emission occur (Figure 23). On the other hand, CO concentrations peak in Central Los Angeles. This difference is primarily because ozone, NO_2, and $PM_{2.5}$ are secondary pollutants; whereas, CO is a primary pollutant and its concentrations depend mainly on direct emissions. Ozone and $PM_{2.5}$ concentrations exceed the established air quality standards (Table 33). The emissions inventory used in this simulation does not include prospective air pollution control measures to be implemented before the year 2010 but accounts for population growth and the corresponding increase in anthropogenic emissions. The introduction of new air pollution control strategies will lead to reductions in emissions of ozone precursors, and consequently, to reductions in ozone concentrations. The SoCAB must reach maximum ozone concentrations of 120 ppb or lower by November of 2010 to comply with ozone federal air quality standards.

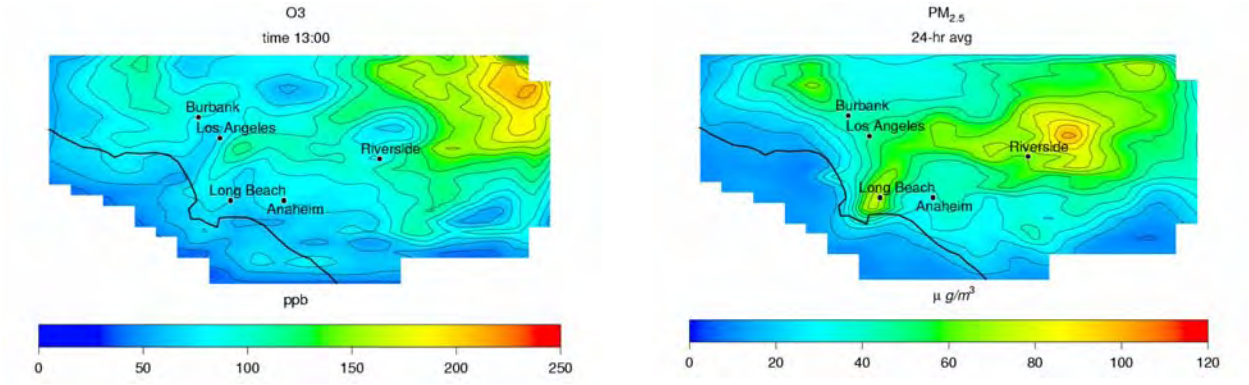

(a) (b)

Figure 23. Concentration of criteria pollutants: (a) Ozone concentration at hour 1300, (b) 24-hour average concentration of $PM_{2.5}$

The South Coast Air Quality Management District's estimates of peak ozone concentration for 2010 are lower than the values reported in this work. The AQMD predicts an ozone peak of 134 ppb, using the meteorological episode of August 27–29, 1987, and baseline emissions inventory. Discrepancies among predictions arise from different chemical mechanisms used for the simulations. For instance, the AQMD uses the carbon bond IV (CB-IV) chemical mechanism in their simulations. However, Jimenez et al. (2003) showed that models that use CACM tend to exhibit significantly higher ozone formation than those that use CB-IV. Because

of high solar radiation during the simulated episode, the tropospheric sinks of CO and NO_2 are enhanced. As a result, concentrations of CO and NO_2 are below air quality standard values.

Table 33. California and Federal Air Quality Standards for some criteria pollutants

Species	State standard	Federal standard	Averaging time
O_3	90 ppb	120 ppb	1 hr
NO_2	250 ppb	–	1 hr
CO	9 ppm / 20 ppm	9 ppm / 35 ppm	8 hr / 1 hr
$PM_{2.5}$	–	65 $\mu g/m^3$	24 hr

3.3 Air Quality Modeling: Evaluation

The CIT model has been used to analyze the air quality impacts produced by deployment of DG in the SoCAB (Medrano et al. 2003; Carreras et al. 2004). Installation of DG introduces new emission sources throughout the basin. Changes in pollutant emissions affect the concentrations of both primary and secondary atmospheric contaminants. These effects need to be evaluated using a detailed air quality model that includes most of the chemical and physical processes that occur in the atmosphere, such as homogeneous and heterogeneous chemistry; advective and turbulent transport; spatial and temporal variability of emissions; and meteorology. The performance of the CIT model has been partially analyzed in the past (Rodriguez and Dabdub 2003; Griffin et al. 2002a) and features all the atmospheric processes mentioned above. The model is in continuous development at University of California, Irvine, in collaboration with researchers from the California Institute of Technology and other institutions.

Russell and Dennis presented a comprehensive review of the state of the art in air quality modeling (Russell and Dennis 2000). The review identified all the important pieces in an air quality model, and reported the relative importance of each element on air quality simulation results. The present work focuses on the CIT Airshed model, shows the sensitivity of baseline year 2010 simulations to input variables and to model components, and identifies the parameters and elements that most influence air quality predictions. In addition, simulation results were compared with predictions shown in the 2003 Air Quality Management Plan using Urban Airshed (UAM) and CALGRID air quality models. Furthermore, this project analyzed the sensitivity of the CIT model to emissions changes from weekday-weekend variation and DG implementation.

3.3.1 Elements for Air Quality Modeling

Simulation of an air quality episode with an air quality model requires a series of inputs that are used to compute the numerical solution of the atmospheric diffusion/advection equation (Equation 20).

$$\frac{\partial Q_m^k}{\partial t} + \nabla \cdot \left(u Q_m^k\right) = \nabla \cdot \left(K \nabla Q_m^k\right) + \left(\frac{Q_m^k}{\partial t}\right)_{sources/sinks} + \left(\frac{Q_m^k}{\partial t}\right)_{aerosol} + \left(\frac{Q_m^k}{\partial t}\right)_{chemistry} \quad (20)$$

Among the inputs needed for the simulation, there are meteorological conditions, and area and point emissions. Meteorological parameters include: temperature, relative humidity, solar radiation, three-dimensional wind fields, and inversion height. Chemical mechanisms and aerosol-phase formation mechanisms are required to account for gas-phase reactions and particulate matter formation in the atmosphere. Mechanisms of mixing and transport of pollutants are required to account for advective transport and diffusion of pollutants throughout the air shed considered.

3.3.1.1 Meteorological conditions input

A comprehensive campaign of atmospheric measurements (SCAQS) was carried out in the SoCAB in August 27–29, 1987, in Southern California. The study collected a very extensive set of meteorological and air quality data that has been widely used to validate air quality models (Moya 2002 et al.; Griffin et al. 2002a; Knipping and Dabdub 2002; Meng et al. 1998). During SCAQS, vertical profiles of temperature, humidity, and wind were obtained, along with their temporal and spatial distribution. Posterior treatment of these measurements allowed researchers to obtain a complete set of gridded meteorological data to be used in air quality simulations. Zeldin et al. (1990) conducted a study entitled *A Meteorological and Air Quality Assessment of the Representativeness of the 1987 SCAQS Intensive Days*. They found August 28, 1987, of "reasonable central met-class tendency," which makes it suitable for modeling. In addition, August 27–28, 1987, episode was found statistically within the top 10% of severe ozone-forming meteorological conditions (SCAQMD 2003a). Furthermore, this episode is also used by AQMD to show that air pollution control strategies proposed in the 2003 Air Quality Management Plan (SCAQMD 2003b) will lead to ozone attainment by 2010. Hence, this episode was used to evaluate the air quality impacts of DG during a reasonably severe smog episode.

The dominant winds in the SoCAB are from west to east during a typical day. The San Gabriel and San Bernardino Mountains form a natural barrier that enhances accumulation of air pollutants, especially over downwind locations, such as Riverside and San Bernardino. In addition, warm and sunny conditions and lack of natural scavenging processes, such as rain, favors the formation of photochemical smog and ozone.

The SCAQS episode in August 27–29, 1987, was characterized by weak onshore pressure gradient and warming temperature aloft. The wind flow was characterized by a sea breeze during the day and a weak land-mountain breeze at night. The presence of a well-defined diurnal inversion layer at the top of neutral and unstable layers near the surface, and a slightly stable nocturnal boundary layer facilitated the concentration of pollutants over the SoCAB and lead to an episode of high ozone concentration.

3.3.1.1.1 Temperature

This section presents the impact of temperature on ozone concentration. Previous studies have evaluated the effect of temperature on the concentration of atmospheric pollutants (Sillman and Samson 1995; Bärtsch-Ritter et al. 2003). Ozone concentration is mainly affected by the strong temperature-dependence of peroxyl acetyl nitrate (PAN) decomposition. High temperatures favor decomposition of PAN, and consequently NO_X concentrations increase, which tends to form more ozone. Sillman and Samson (1995) suggest that increasing temperatures are correlated to higher biogenic VOC emissions and higher UV radiation, which would contribute

to enhance ozone formation. They also suggest that high temperatures could be correlated to higher anthropogenic emissions and stagnant circulation conditions. Bärtsch-Ritter et al. 2003 studied the effects of meteorological conditions on the air quality of Milan, Italy. Based on simulation results, the study shows that increasing temperature leads to an increase of VOC-limited areas, mostly because of lower PAN formation. If VOC-limited areas increase, ozone concentrations are less sensitive to a change in NO_X emissions. Therefore, temperature is potentially an important factor for the design of an air pollution control strategy.

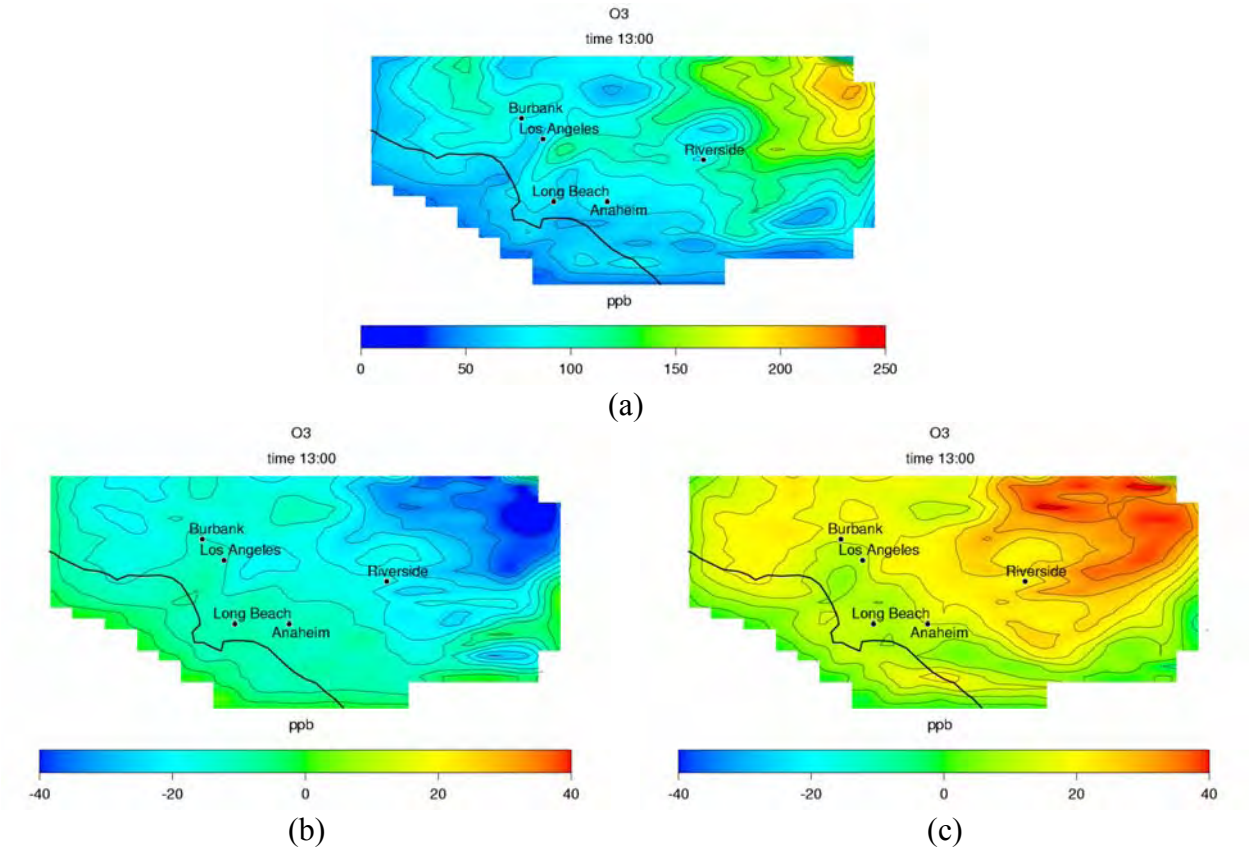

Figure 24. Effect of temperature in ozone concentration: (a) Ozone concentration in base case simulation, and difference in ozone concentration (in ppb) at hour 13 of the third day of simulation between a study case and the base case for: (b) reduction of temperature by 5°C, (c) increase of temperature by 5°C

During August 27–29, 1987, temperature ranged from moderate temperatures at night (around 15°C–20°C, or 59°F–68°F) to high temperatures at downwind locations in the early afternoon (maximum temperature: 42°C, or 108°F). Two scenarios are presented in this section to evaluate the effect of temperature on ozone concentration in the SoCAB: (a) temperature is decreased by 5°C (9°F) in each cell of the domain and at every hour, and (b) temperature is raised by 5°C (9°F) in each cell and every hour. While scenario (a) could represent a warm episode during spring with temperatures ranging from 10°C–35°C (50°F–95°F), scenario (b) presents temperatures extremely high in certain regions of the domain, reaching temperatures over 45°C (113°F). However, these two cases are useful for clearly illustrating the effect of temperature on ozone concentration. Figure 24 presents the difference in ozone concentration at hour 1300 of the third

day of simulation between scenarios (a) and (b) and the baseline case. A decrease of 5 ^{o}C (9^{o}F) (scenario (a)) results in decreases over 40 ppb in ozone concentration, particularly in the northeast part of the domain. In addition, peak ozone concentration decreases from 238 ppb to 188 ppb. An increase of 5 ^{o}C (9^{o}F) (scenario (b)) results in increases over 40 ppb in ozone concentration, and the peak ozone reaches 277 ppb.

As suggested in previous studies, an increase in temperature could imply an increase in both biogenic and anthropogenic emissions, more stagnant conditions and more intense insolation. These parameters—not included in this section—could lead to even higher impacts.

3.3.1.1.2 UV radiation

Ozone formation is controlled by photolysis of NO_2 by UV radiation. As described in Harley et al. (1993), solar ultraviolet radiometers were operated at five locations in the SoCAB, for the August 27–29, 1987, episode. Measurements of UV irradiance were used to obtain NO_2 photolysis rates. On the other hand, "clear sky" photolysis rates can be obtained as a function of the solar actinic flux, which depends on the solar zenith angle, the elevation and the wavelength. For the baseline simulation, UV scaling factors are calculated as a ratio of actual photolysis rates to "clear sky" values, for each monitoring station. These scaling factors are calculated for each hour, and then extrapolated for the rest of the domain. Typical UV scaling factors at midday for this episode are 1.0 at Central Los Angeles, 0.8 at Claremont, 0.65 at Rubidoux, and 1.2 at Mount Wilson. Harley et al. (1993) evaluated the effect of UV scaling factors on ozone concentration by considering only "clear sky" photolysis rates. In this scenario, in which scaling factors may be incremented by 50% with respect to the baseline in areas such as Rubidoux, ozone concentration increased by 10–30 ppb.

In this section, two scenarios in which the UV radiation is scaled by a constant factor are presented: (a) a scaling factor of 0.8 is applied throughout the basin and during the three days of simulation, and (b) scaling factor of 1.2 is applied throughout the basin and during the three days of simulation. Figure 25 shows the difference in ozone concentration at hour 1300 of the third day of simulation between scenarios (a) and (b) and the baseline case. Reduction of UV radiation by 20% (scenario (a)) leads to reductions of over 20 ppb in ozone concentration at northeastern locations, and to a decrease in the absolute peak ozone of 20 ppb. Increase of UV radiation by a 20% (scenario (b)) leads to a maximum increase in ozone concentration of 20 ppb and to an increase in the peak ozone concentration of 17 ppb. Impacts from scenario (b) are comparable to the ones reported by Harley et al. (1993).

Vuilleumier et al. (2001b) studied the factors that contribute to UV optical depth in Los Angeles area. Results from the study suggested that light scattering and absorption contributed up to 90% in reducing actinic flux. A secondary factor was light absorption by ozone, which contributed up to 10% in the reduction of solar UV radiation. These results imply that changes in ozone and aerosol concentrations resulting from air pollution control strategies could have a feedback effect on UV scaling factor, and hence, on ozone formation.

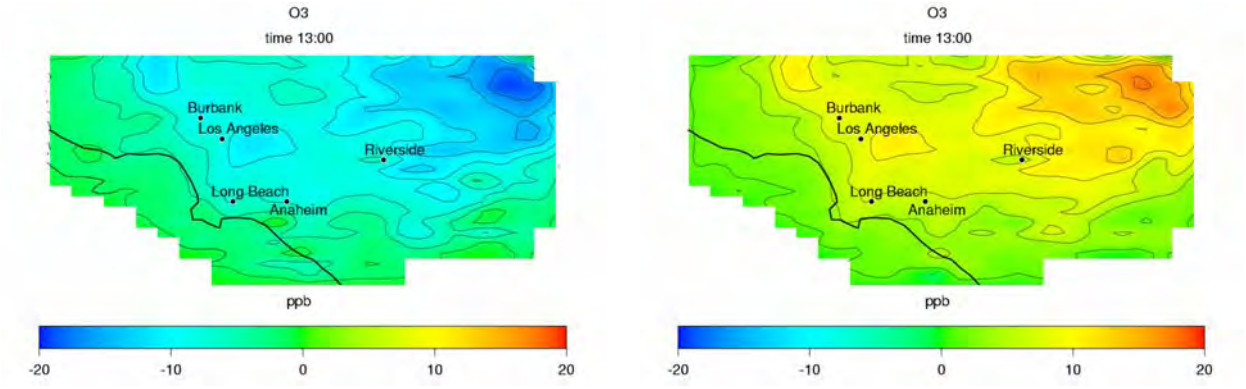

(a) (b)

Figure 25. Effect of UV radiation on ozone concentration (in ppb). Difference in ozone concentration at hour 13 of the third day of simulation between a study case and the base case for UV radiation scaling factor of (a) 0.8, and (b) 1.2

3.3.1.1.3 Mixing height

The height of the mixing layer determines the vertical dispersion of pollutants. As described in Harley et al. (1993), during the SCAQS episode, upper air soundings were performed in eight sites that covered coastal and inland regions. Mixing heights were derived from potential temperature plots that were obtained from upper air sounding measurements. During the episode, a well-defined inversion layer was developed on the top of neutral/unstable layers close to the surface. Mixing heights ranged approximately from 50 m (164 ft) at night, to 1100 m (3600 ft) in the afternoon.

Previous studies have evaluated the impact of mixing height on pollutant concentrations. Harley et al. 1993 simulated the 1987 SCAQS episode and doubled the mixing height. The result was small increments in the ozone concentration. Other works focused on the effect of mixing height on pollution control strategies. Sistla et al. (1996) compared results from control strategies in the area of New York City between scenarios with variable mixing height and with fixed mixing height. The study showed that to reduce ozone concentration, it would be more effective to reduce NO_X emissions than it would be to reduce VOC emissions, if a uniform mixing height was used. The use of a variable mixing height showed the opposite trend. Li et al. (1998) studied the effect that mixing heights have on the efficiency of NO_X emission control towards ozone reduction in the New York area. The study showed that NO_X emission controls were significantly more effective when the mixing height was reduced by 50%, with respect to baseline values.

This section presents two scenarios: (a) mixing height is scaled by a factor of 0.8 and (b) mixing height is scaled by a factor of 1.2. Although these factors are applied evenly throughout the domain and during the three days of simulation, there are two limiting conditions that set minimum mixing height to 50 m (164 ft) and maximum height to 1100 m (3600 ft). Figure 26 presents the difference in ozone concentration at hour 1300 of the third day of simulation between scenarios (a) and (b) and the baseline case. Reduction of the mixing height (scenario (a)) produces both positive and negative impacts on the ozone concentration, leading to differences of ±30 ppb. However, the peak ozone concentration only changes by -2 ppb. Increase of mixing height (scenario (b)) leads to increases in ozone concentration of the order of

10–35 ppb, over the north-central part of the domain. Reductions in ozone concentration produced by the increase in mixing height occur near the eastern boundary of the domain, and reach values of 30 ppb. In this scenario, the peak ozone concentration decreases by 5 ppb.

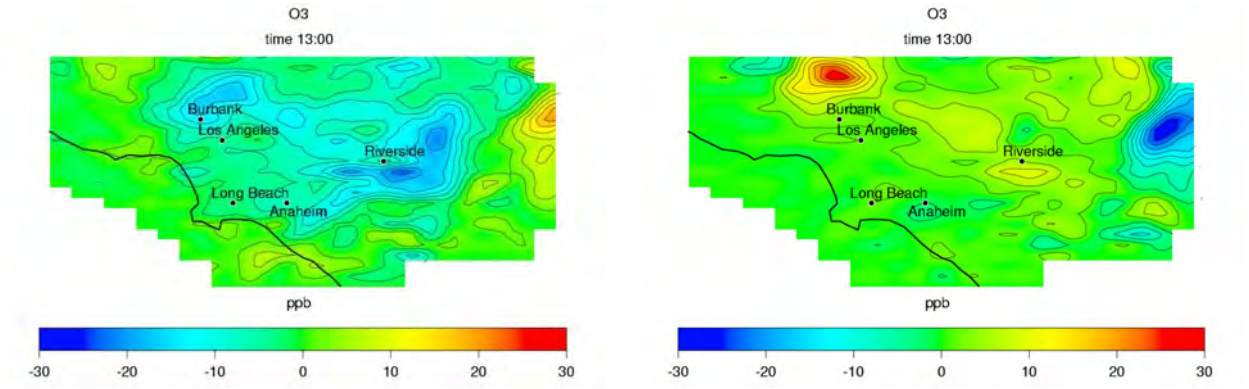

Figure 26. Effect of mixing height on ozone concentration. Difference in ozone concentration (in ppb) at hour 1300 of the third day of simulation between a study case and the base case for: mixing height scaling factor of (a) 0.8, (b) 1.2

3.3.1.1.4 Wind fields

Previous studies have explored the effect of wind velocity on pollutant concentration (Harley et al. 1993; Dabdub et al. 1999; Bärtsch-Ritter et al. 2003). Results from these studies showed that an increase in wind velocity increases the effect of the upwind boundary conditions and tends to dilute pollutant concentration. On the other hand, a decrease in wind velocity provides stagnant conditions that tend to accumulate air pollutants in the domain, increasing their concentration. This section presents how wind fields transport pollutants over the basin. In addition, it presents two scenarios, in which baseline wind velocity is modified by a factor of 0.5 and by a factor of 2.

Baseline wind field was obtained by interpolation of measured data during the SCAQS episode in August 27–29, 1987. As it is shown in the sequence of plots presented in Figure 27, pollutants are transported from west to northeast. Figure 27 shows the transport of two different shapes of 120-ppb ozone puffs over a background concentration of 20 ppb. Pollutant concentrations at the boundaries are zero, which tends to dilute the basin and ultimately removes any contaminant present in the basin. Both cases show that in this episode stagnant conditions prevailed until noon. After hour 1200 offshore winds started to blow in the northeast direction, transporting air pollutants towards the San Bernardino Mountains, which acted as a natural barrier and contained pollutants inside the basin. After 24 hours, the puffs had not fully disappeared, and pollutants remained in the basin during the early morning until winds started blowing faster again at around noon. This wind regime is characteristic of smog episodes that occur in the South Coast Air Basin, and that tend to accumulate ozone around the northeastern part of the basin.

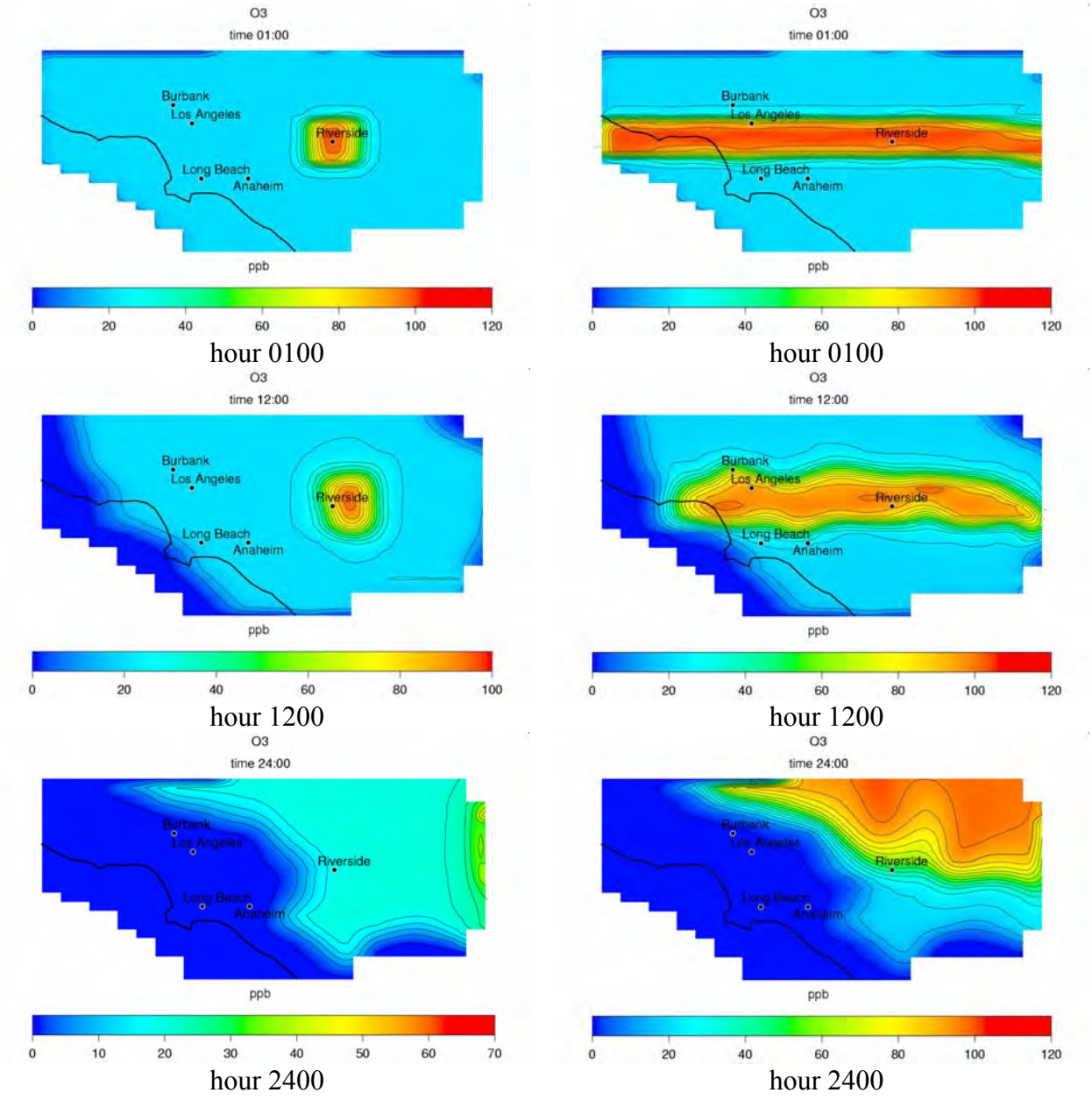

Figure 27. Transport of a 120-ppb ozone puff in a background of [O_3]=20 ppb and zero ozone concentration at the boundaries. Left – square puff; right – horizontal band puff.

Harley et al. 1993 studied the effect of wind velocity using meteorological data and emissions for the August 27–29, 1987, episode. They reported an increase of 50 ppb in ozone peak concentration by reducing wind velocity by 50%. Figure 28 presents the results of two scenarios using the same meteorology used by Harley et al. 1993, and 2010 baseline emissions, and with: (a) wind velocity increased by a factor of two, and (b) wind velocity scaled by a factor of 0.5. Peak ozone concentration in scenario (a) is 177 ppb, which is 61 ppb lower than in the base case. In addition, ozone concentration is reduced by up to 150 ppb in other areas. Scenario (b) predicts a peak ozone concentration of 311 ppb, which is 73 ppb higher than the baseline simulation. It is interesting to note that scenario (b), with slower winds, produces the ozone peak

closer to the main source of emissions and later in time (at hour 1800). On the other hand, higher wind velocities, as in case (a), transport the ozone peak farther downwind. In addition, the peak ozone concentration is produced earlier.

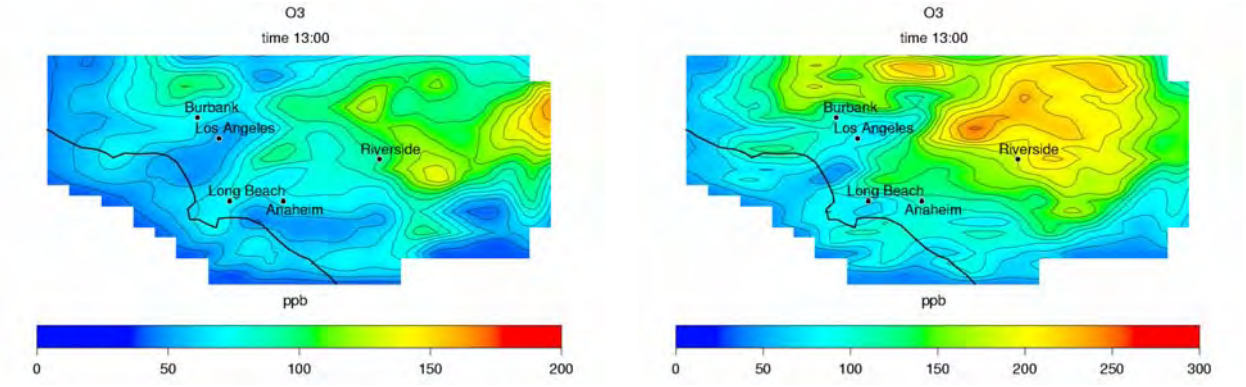

(a) $[O_3]_{max}$= 177 ppb (b) $[O_3]_{max}$= 311 ppb

Figure 28. Ozone concentration (in ppb) using two different wind fields: (a) baseline wind velocity scaled by 2.0, (b) baseline wind velocity scaled by 0.5

3.3.1.2 Boundary conditions

Typically, the region is defined by three general boundaries: (1) the ground surface, which is defined by specific topography Z = h(X, Y), (2) the time-varying upper boundary Z = H(X, Y, t), that is the base of the inversion layer, and (3) lateral boundary conditions at the horizontal extremes of the domain.

The boundary condition at the ground surface used in the simulations is:

$$K_{zz}\frac{\partial c_i}{\partial z} = \upsilon_{d,i} c_i \tag{21}$$

where K_{zz} is the eddy diffusivity in the vertical direction and $\upsilon_{d,i}$ is the deposition velocity of species i.

The boundary condition atop is:

$$K_{zz}\frac{\partial c_i}{\partial z} = 0 \tag{22}$$

The lateral boundary conditions are given by the following expressions:

$$\begin{aligned} [uc_i - K\nabla c_i]\cdot\vec{n} &= (uc_i^b)\cdot\vec{n}, \qquad u\cdot\vec{n} \le 0 \\ -[\nabla c_i]\cdot\vec{n} &= 0, \qquad\qquad u\cdot\vec{n} > 0 \end{aligned} \tag{23}$$

where c_i^b is the concentration of species i outside the modeling region, $\vec{n}$ is the unit outward normal to the time varying airshed domain. Note that for the latter boundary condition, specific values of pollutant concentration at the boundaries are required to solve Equation 20.

3.3.1.2.1 Lateral boundary conditions

The CIT Airshed model has been evaluated with the August 27–28, 1987, SCAQS episode. For "backcasting" smog episodes, interpolated values from measurements are typically used as boundary conditions. For future year conditions, specific values of pollutant concentration have to be assumed. To minimize the impact of inadequate conditions for lateral boundaries on air quality predictions, boundaries should be located far away from the main area of study. However, the size of the domain is typically constrained by data availability and computational capacity.

Previous studies have tried to analyze the effect of boundary conditions on air quality simulation results. Winner et al. 1995 compared ozone isopleths produced by two different sets of boundary and initial conditions: the first case used interpolated values from data measured during the August 27–28, 1987, SCAQS episode for both boundary and initial conditions. The second case used "clean air" values for both boundary and initial conditions. The study showed that using values based upon measurements it would be virtually impossible to reach peak ozone concentrations lower than the federal air quality standard (1-hour average concentration = 120 ppb). On the other hand, the study showed that if clean air values were used, the ozone federal air quality standard would be attained by reducing reactive organic gases (ROG) emissions by 50%. There are some indications based on previous studies that concentration of pollutants over the ocean to the west of the Los Angeles area (prevailingly upwind area) is affected by emissions from downwind onshore emissions (Benkovitz et al. 1994). Hence, concentration at the boundaries will be affected by a significant reduction of emissions at downwind locations. Particularly, concentration at the boundaries would tend to reach "clean air" conditions when continental anthropogenic emissions tend to zero.

Dabdub et al. 1999 showed the impact of boundary conditions on the air quality predictions in the San Joaquin Valley. Ozone formation in this area is not as strongly dominated by in-basin emissions as in the Los Angeles area, and hence boundary conditions affect more significantly air quality simulation results. Results showed that ozone concentration at locations near the inflow boundary (west boundary) was more sensitive to ozone boundary condition than to NO_X-VOC boundary condition. On the other hand, ozone concentration at downwind locations, far from the inflow boundary, was more sensitive to NO_X-VOC boundary condition.

The same approach used by Dabdub et al. 1999 and Winner et al. 1995 is pursued here in order to determine the sensitivity of ozone concentration in the Los Angeles area to boundary conditions. Six different scenarios are simulated: (1) baseline case, (2) zero all boundary conditions, (3) zero ozone boundary condition, (4) zero NO_X boundary condition, (5) zero VOC boundary condition and (6) "clean air" boundary conditions as described in Winner et al. 1995. Table 34 presents the boundary conditions used in the simulation of case (1) and (6). Figure 29 shows the 1-hour average concentration of ozone at hour 1300 (time when ozone peaks in the baseline case) of the third day of simulation using the different sets of boundary conditions.

Table 34. Boundary conditions used for the simulation of the base case and the "Clean air" case (in ppb)

		Baseline case					"Clean air" case				
		Vertical layer in model					Vertical layer in model				
Species	**Boundary**	**Surface**	**Lev 2**	**Lev 3**	**Lev 4**	**Lev 5**	**Surface**	**Lev 2**	**Lev 3**	**Lev 4**	**Lev 5**
NO_2	N, S, W	1	1	1	1	1	1	1	1	1	1
NO_2	E	aq[a]	aq	1	1	1	1	1	1	1	1
NO	N, S, W	1	1	1	1	1	1	1	1	1	1
NO	E	aq	aq	1	1	1	1	1	1	1	1
O_3	N	aq	70	70	70	60	40	40	40	40	40
O_3	E	aq	aq	60	70	70	40	40	40	40	40
O_3	S, W	40	40	40	40	40	40	40	40	40	40
RHC	N	aq	100	100	100	100	10	10	10	10	10
RHC	E	aq	aq	100	100	100	10	10	10	10	10
RHC	S, W	100	100	100	100	100	10	10	10	10	10
HCHO	N, E	aq	aq	3	3	3	3	3	3	3	3
HCHO	S, W	3	3	3	3	3	3	3	3	3	3
ALD2	N, E	aq	aq	5	5	5	5	5	5	5	5
ALD2	S, W	5	5	5	5	5	5	5	5	5	5
MEK	N, E	aq	aq	4	4	4	4	4	4	4	4
MEK	S, W	4	4	4	4	4	4	4	4	4	4
CO	N, E	aq	200	200	200	200	120	120	120	120	120
CO	S, W	200	200	200	200	200	120	120	120	120	120

[a]*aq* refers to values based upon measurements obtained during Aug 27–29, 1987, SCAQS episode. These values are scaled down so that the maximum boundary value is 120 ppb of ozone.

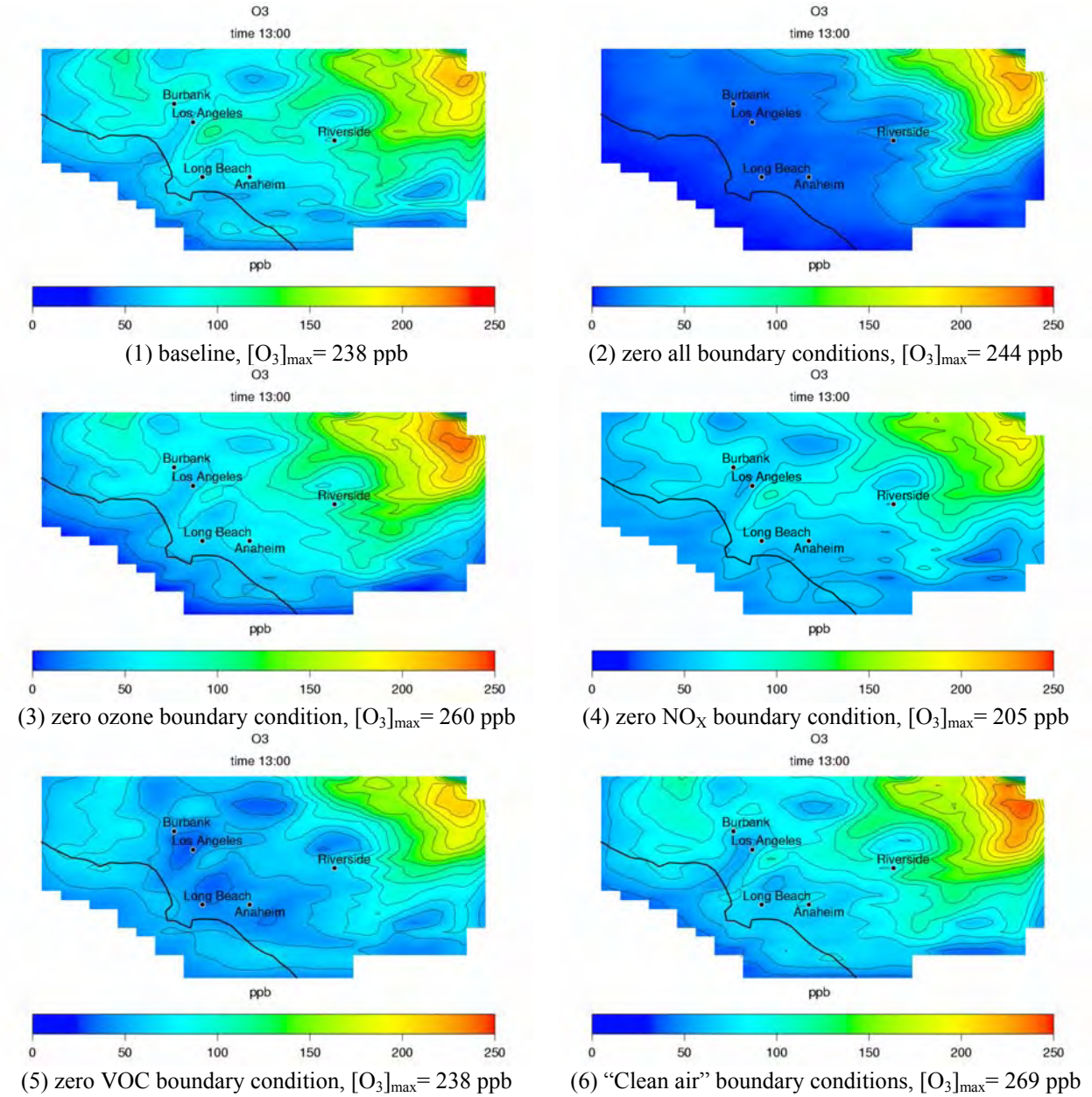

(1) baseline, $[O_3]_{max}$= 238 ppb

(2) zero all boundary conditions, $[O_3]_{max}$= 244 ppb

(3) zero ozone boundary condition, $[O_3]_{max}$= 260 ppb

(4) zero NO_X boundary condition, $[O_3]_{max}$= 205 ppb

(5) zero VOC boundary condition, $[O_3]_{max}$= 238 ppb

(6) "Clean air" boundary conditions, $[O_3]_{max}$= 269 ppb

Figure 29. Ozone concentration (in ppb) in the South Coast Air Basin at time 1300 of the third day of simulation (August 29, 1987), using different sets of boundary conditions

Boundary conditions equal to zero are used purely diagnostically, because even in the cleanest air, concentrations of ozone, NO_X or VOC are not zero. Since the west boundary is predominantly an inflow boundary that transports air masses towards the eastern boundary, one would expect locations close to the western part of the domain to experience the largest impact in ozone concentration. Case (2)—zero all boundary conditions—shows a decreases of the order of 130 ppb in ozone concentration over the western and central part of the domain, due to dilution produced by an inflow boundary with zero pollutant concentration. However, peak ozone concentration increases by 6 ppb. Comparison of cases (3), (4), and (5)—zero O_3, NO_X

and VOC boundary conditions, respectively—shows that VOC boundary condition affects the most ozone concentration in the central part of the basin. These results confirm that formation of ozone near Los Angeles is VOC-limited. On the other hand, zeroing NO_X boundary condition leads to the largest decrease in 1-hour peak ozone concentration, of 33 ppb with respect to the baseline case. Zero ozone boundary conditions lead only to an increase of 22 ppb in the peak ozone concentration with respect to the base case, although in the central part of the domain, ozone concentration decreases by up to 80 ppb. As mentioned earlier, locations near the west boundary, which is predominantly an inflow boundary, are more affected by boundary conditions than downwind locations closer to the eastern boundary. Finally, case (6)—"clean air" boundary conditions—presents an increase in the ozone peak of 30 ppb, but overall ozone concentrations over the central area are comparable to the one achieved in the base case.

3.3.1.2.2 Height of the top boundary condition

Air quality models used by SCAQMD use vertical layers that extend up to 3000 m (9800 ft), whereas the CIT Airshed model considers a maximum height of 1100 m (3600 ft). Although the mixing height is typically below 1100 m (3600 ft) during the episode chosen for the simulations, ozone concentration predicted by the model is affected by the presence of extra layers atop the 1100 m (3600 ft) limit. The questions that may be answered then are: (1) how the increase in the top boundary height affects ozone concentration, and (2) how sensitivity of ozone to a change in emissions is affected by increasing the domain's height. A host of cases has been simulated to address these two questions: (a) the base case, in which the domain has five layers that add up to 1100 m (3600 ft), (b) Case 2, in which one extra layer of 900 meters (3000 ft)has been added to the base case domain, and (c) Case 3, in which an extra layer of 1200 meters (3900ft) has been added to Case 2. Additionally, three other cases have been simulated using the three different domains mentioned above, and applying an emission reduction of 40% for NO_X and 25% for VOC.

Table 35 summarizes the effect of adding extra layers at the top of the computational domain of the CIT model. In the ground-level layer (layer 1), peak ozone concentration decreases by 17 ppb if a sixth layer is added, and the hourly ozone concentration in other areas is reduced by up to 27 ppb. Adding a seventh layer decreases peak ozone concentration by 5 ppb more, and maximum decreases of the hourly ozone concentration are up to 30 ppb with respect to the case with five layers. On the other hand, concentration of ozone decreases dramatically in the fifth layer if a sixth layer is added. This is because adding an extra layer facilitates dilution of the fifth layer, because of air entrainment from the layer atop. Adding a seventh layer decreases ozone concentration only slightly further. This indicates that the height assumed by CIT model is not enough to disregard the effect of boundary conditions on top of the modeling domain. A low modeling height promotes pollutant accumulation and hence, model results tend to overestimate ozone concentration.

Table 35. Impact of adding extra layers on O_3 concentration: 6 (Case 2) and 7 layers (Case 3) versus 5 layers (Base case) (in ppb)

	Layer 1				Layer 5			
	Peak O_3	Time	Max ΔO_3[(a)]	Time	Peak O_3	Time	Max ΔO_3	Time
Base case	238	13	-	-	312	16	-	-
Case 2	221	13	-27	17	222	16	-167	17
Case 3	216	13	-30	17	213	16	-170	17

[(a)]Change in O_3 is with respect to the base case

Table 36 compares different predictions of ozone concentration using 6 and 7 layers in the vertical direction. As already discussed above, ozone concentration predicted using 6 or 7 layers varies by less than 10 ppb. Thus, ozone concentration in layers one through five is not very sensitive to adding extra layers to the sixth one.

Table 36. Impact of adding extra layers on O_3 concentration: 7 layers (Case 3) versus 6 layers (Case 2) (in ppb)

	Layer 1				Layer 5			
	Peak O_3	Time	Max ΔO_3[(a)]	Time	Peak O_3	Time	Max ΔO_3	Time
Case 2	221	13	-	-	222	16	-	-
Case 3	216	13	-7	16	213	16	-10	7

[(a)]Change in O_3 is with respect to the Case 2

Table 37 shows the impacts on ozone concentration of a certain emissions reduction using 5, 6, and 7 layers. Although, as seen before, absolute ozone concentration changes when extra layers are added atop the fifth layer, impacts of the same emission reduction are not very different in each case. Peak ozone concentration decreases by 25 ppb, 18 ppb, and 17 ppb, if 5, 6, and 7 layers are used, respectively. In addition, maximum changes in hourly ozone concentration are 44 ppb, 42 ppb, and 41 ppb. Consequently, even though an extra layer added to the CIT model may affect moderately absolute ground-level ozone concentrations, it does not affect the impact on ozone concentration of changes in emissions. Specifically, impacts of DG on air quality will not change significantly if an extra sixth layer is added to the CIT model.

Table 37. Impact on ozone sensitivity to an emission change due to additional layers (units in ppb)

	Baseline emissions		Controlled emissions			
Case	Max O_3	Time	Max O_3	Time	Max ΔO_3	Min ΔO_3
Base case	238	13	213	13	44	-35
Case 2	221	13	203	13	42	-35
Case 3	216	13	199	13	41	-35

3.3.1.3 Initial conditions

Previous works assumed that simulation of two-day episodes would be sufficient in order to minimize the effect of initial conditions on air quality modeling (Winner et al. 1995; SCAQMD 2003b; Griffin et al. 2002b). In addition, use of longer episodes is limited by data availability.

This section presents the effect of initial conditions on air quality predictions. Two simulations are conducted: (1) 10-day episode with baseline initial conditions, and (2) 10-day episode with zero initial conditions for all species. Because there is no data from an episode that long, meteorological conditions used from third day to tenth day are the ones corresponding to the second day. Since all parameters are equal for the third and subsequent days—meteorology, emissions, boundary conditions—one would expect that concentration of pollutants reached a stationary cycle after some days of simulation. In addition, one would expect that concentration of pollutants in the case of zero initial condition would tend to the levels reached in the base case when time advances.

Figure 30 presents the evolution of ozone concentration at six different locations, for the two cases studied: baseline case and zero initial conditions (IC) case. Figure 30 (a) and (b) show ozone concentration in Central Los Angeles and Long Beach. These two points represent upwind locations strongly dominated by direct emissions. As a result, concentration of ozone in the zero IC case recovers with respect to the baseline case by the second day of simulation. Figure 30 (c) and (d) show ozone concentration in Riverside and San Bernardino. These two cities are located at downwind locations, and although they are important contributors of local emissions, the air quality in this region is dominated by transport of pollutants from the central area of Los Angeles. Since local emissions are not as important as in the previous upwind cities, ozone concentration in the zero IC case needs two days to recover with respect to the baseline case. This result is particularly important because maximum concentrations of ozone are usually found over these regions, and control strategies are mainly designed based on peak concentrations. Consequently, this work suggests that three days of simulation should be used, if possible, for air pollution control studies. Finally, Figure 30 (e) presents ozone in Hesperia, which is a location close to the northeastern boundary, where the maximum ozone concentration is formed, and (f) presents ozone in Palm Springs, which is located far downwind from Los Angeles and from main anthropogenic emissions. For these two locations, recovering ozone concentration in the zero IC case with respect the baseline case takes three days. In conclusion, the farther a location is from the central area—where major emissions occur—the longer the effects of the initial conditions are. In addition, in contrast to what previous works assumed, this study suggests that control strategies should be based upon simulations of three days, in order to minimize the impact of initial conditions over the areas where ozone concentration is typically the highest.

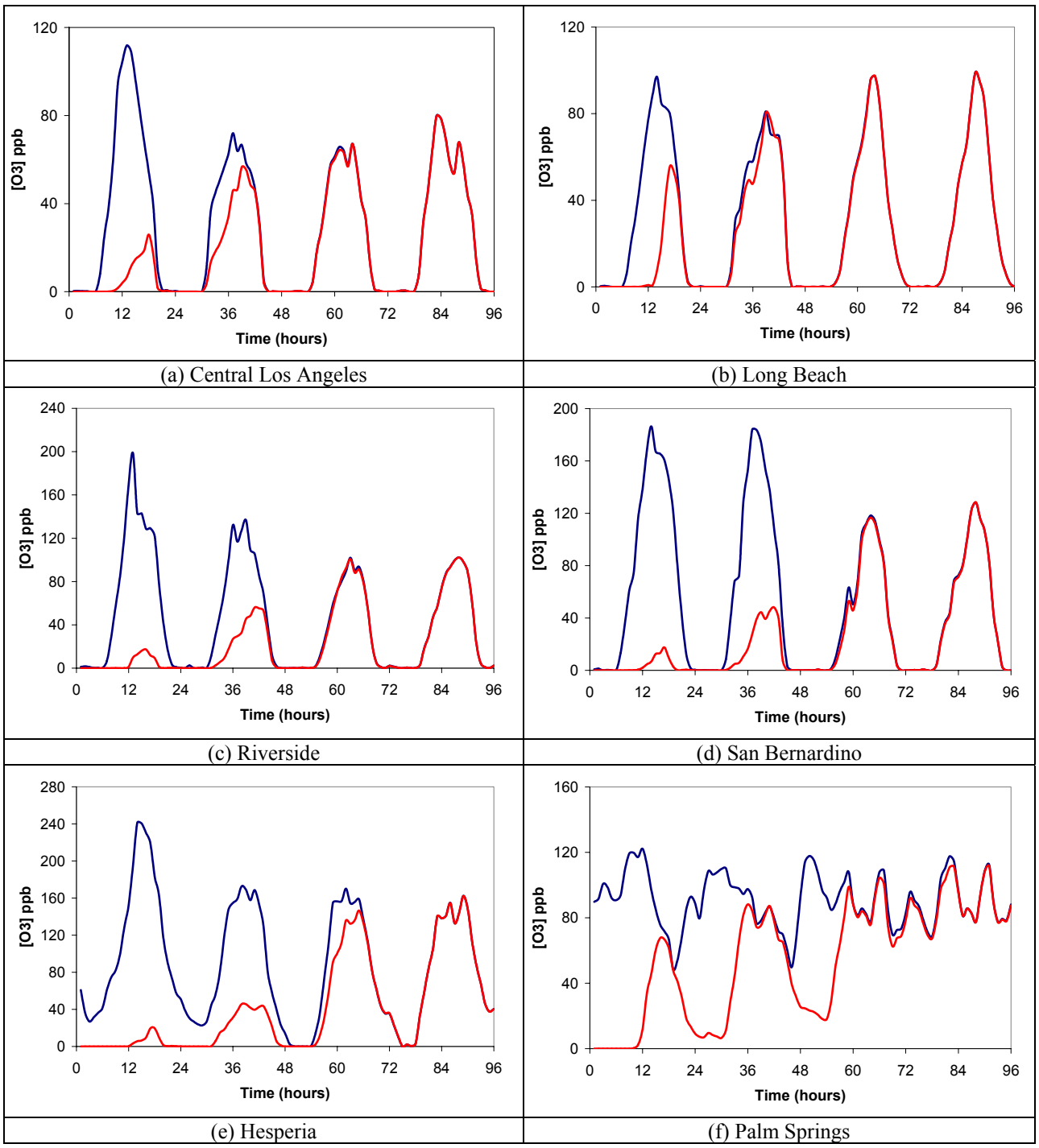

Figure 30. Evolution of ozone concentration (in ppb) at six different locations during four days of simulation (baseline case in blue; zero initial conditions case in red).

3.3.1.4 Advection solver

The advection equation is one of the component operators in the solution of the atmospheric diffusion equation (Equation 20) by operator splitting schemes. Numerical solution of the advection equation by various solvers leads to numerical dispersions and oscillations. Previous studies have evaluated the effect of the advection solver on air quality modeling. Chock (1991), Chock and Winkler (1994), and Dabdub and Seinfeld (1994) reported that the Accurate Space Derivative scheme (ASD) is the best algorithm in terms of peak preservation properties, mass conservation, and average absolute error. Dabdub and Seinfeld (1994) also reported that the finite-element Galerkin solver was the second-best advection scheme, and significantly less CPU-intensive than the ASD method. According to various studies (Dabdub and Seinfeld 1994; Chock and Winkler 1994), the Smolarkiewicz method, which is used for ozone attainment demonstration with the UAM model (SCAQMD (2003b), gives the least accurate results and consequently authors suggest using other methods for air quality modeling. Figure 31 show the numerical solution of the advection equation for a rotating wind field (as described in Dabdub and Seinfeld 1994) using the three different numerical schemes.

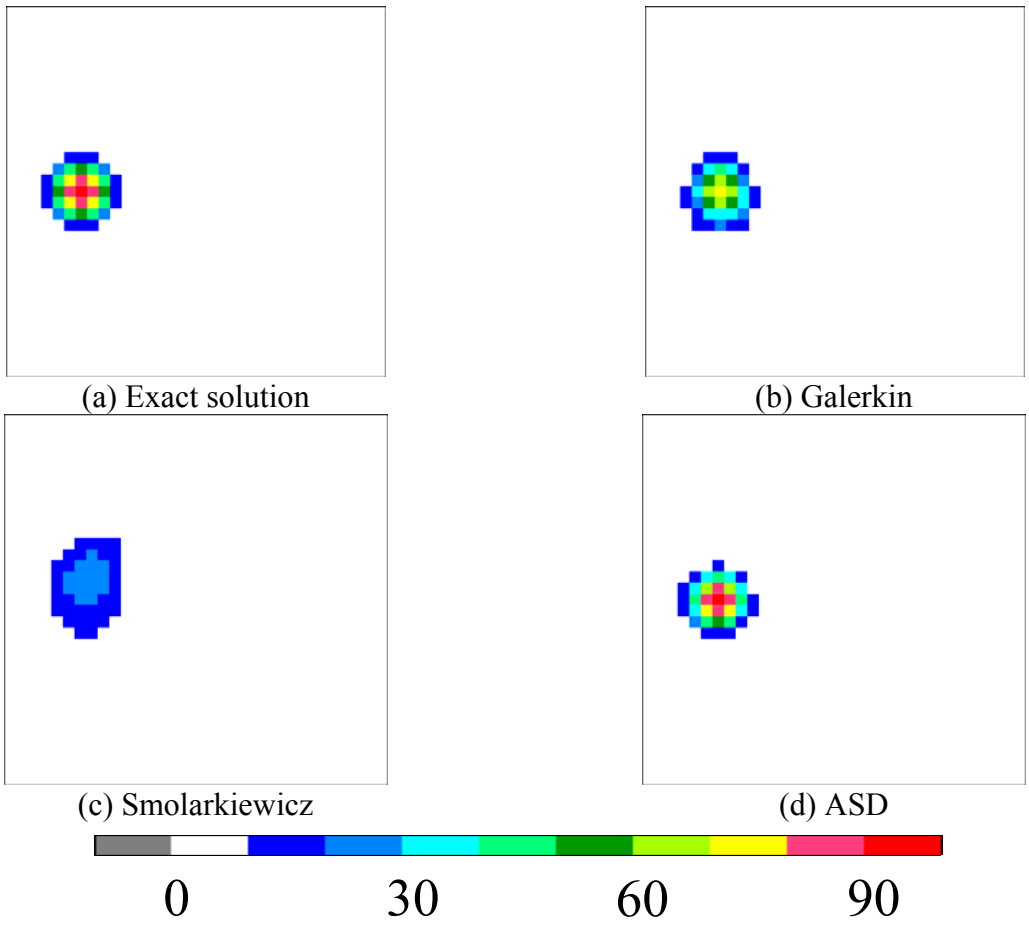

Figure 31. Solution of the advection equation for a rotating wind field using three different advection schemes. Plots show calculated concentration after one complete revolution.

Nguyen and Dabdub (2001) presented a new advection solver—the Quintic Spline Taylor-series expansion (QSTSE)—that is comparable with the Galerkin scheme in terms of CPU expenses, but it improves predicted peak ozone concentrations in a full model by 27.5%. QSTSE is significantly faster than ASD, although it produces similar peak retention, and maintains mass conservation and positive definiteness.

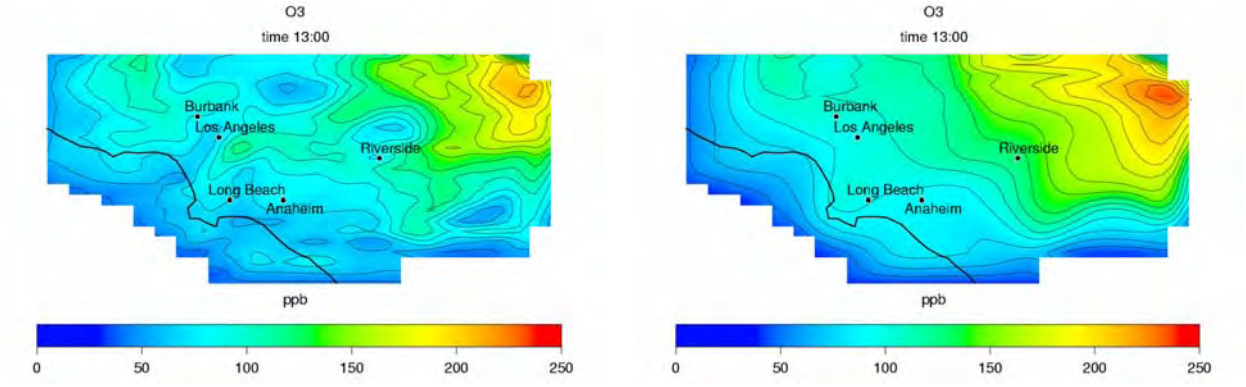

(a) baseline – using QSTSE (b) Galerkin

Figure 32. Ozone concentration (in ppb) in the South Coast Air Basin at hour 1300 of the third day of simulation: (a) baseline case using QSTSE, and (b) using Galerkin finite-element scheme

This section compares the simulation of the SCAQS episode using the QSTSE scheme (scenario (a)) and the Galerking scheme (scenario (b)). The Galerkin scheme is used with the CALGRID model for the SCAQMD's 2003 Air Quality Management Plan, to support ozone attainment demonstration by the UAM model. Figure 32 presents the ozone concentration at hour 1300 of the third day of simulation for scenarios (a) and (b). Simulations with the Galerkin scheme produces lower ozone concentrations is over the central part of the domain and the ozone peak is transported towards the northeastern boundary. The maximum concentration of ozone in scenario (b) is 246 ppb, which is 8 ppb higher than in scenario (a). In addition, in scenario (b) ozone concentration over central areas is up to 90 ppb larger than in scenario (a). These differences are mainly because Galerkin provides a smoother solution of the advection equation, compared to the QSTSE scheme, although QSTSE has a better peak retention than Galerkin. Having higher peak retention does not necessarily mean that predicted peak ozone concentration will be higher, since peak retention affects all species, including NO_X, that may enhance ozone destruction. As shown in Figure 33, Galerkin disperses NO_X concentration more than QSTSE, and because Los Angeles is typically under a VOC-limited regime, ozone concentrations predicted by Galerkin in this area are higher than the values predicted by QSTSE.

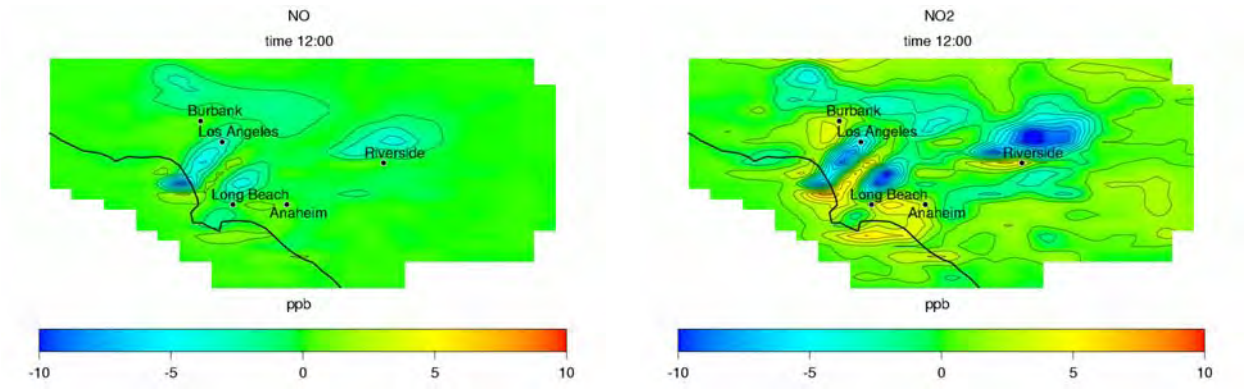

(a) (b)

Figure 33. Difference in the predicted NO_X concentration (in ppb) by the Galerkin and by QSTSE advection solvers (Galerkin—QSTSE) at hour 1200 of the third day of simulation: (a) difference in NO concentration, and (b) difference in NO_2 concentration

3.3.1.4.1 Mass conservation of advection solver

One important quality that determines the accuracy of an advection solver is the capacity to conserve mass. Previous studies (Chock and Winkler 1994; Dabdub and Seinfeld 1994; and Nguyen and Dabdub 2001) have assessed mass conservation of the advection solvers mentioned above. According to Nguyen and Dabdub (2001), QSTSE, ASD, and Galerkin advection solvers achieve mass conservation in the simulation of a rotating cosine hill, after two revolutions. This test enables assessing mass conservation in a divergence-free field. Typically, urban air quality models assume that atmosphere has constant density. Consequently, these models require divergence-free wind fields so that mass conservation can be imposed from the continuity equation. However, obtaining wind fields with zero divergence from meteorological data is difficult. As a result, these wind fields include a residual divergence that has to be minimized. Nguyen and Dabdub (2001) tested various advection schemes in a divergent field, and found that QSTSE conserves mass satisfactorily under such conditions. Galerkin and ASD advection solvers showed 6% and 36% mass loss, respectively, under the same conditions.

Application of any advection solver into an air quality model has to take into account the residual divergence that a wind field may have. From advection equation (Equation 24), the term $\nabla\vec{u}$ must be accounted for unless the wind field is completely divergence-free (Equation 25). Dismissing this term when the wind field is slightly divergent may impact dramatically mass conservation. Figure 34 shows the mass conservation with time of a puff being transported throughout the CIT Airshed domain, without leaving it. The meteorology used in this experiment is from August 27, 1987. No losses or sources of any kind—such as chemical production or loss, deposition or emission—have been considered. Galerkin, QSTSE, and QSTSE assuming $\nabla\vec{u} = 0$ are compared. As in the study by Nguyen and Dabdub (2001), QSTSE proves to be the scheme with better mass conservation. The Galerkin scheme also performs well during the first hours, although at around hour 18 it starts adding extra mass in the system. This mass addition comes from the numerical filter, which has to compensate for negative concentrations generated by the numerical solution of the advection equation. Since QSTSE is positive definite, no extra mass is added, because no filter is needed. The problem with divergent wind fields arises if the term $\nabla\vec{u}$ is assumed to be zero. As Figure 34 depicts, assuming

divergence-free wind fields causes the total mass to decrease dramatically during the first hours, and later to increase suddenly, artificially adding mass to the system. Consequently, divergence of a wind field has to be taken into account to maintain mass conservation.

$$-\frac{\partial c}{\partial t} = \nabla(uc) = u \cdot \nabla c + c \cdot \nabla u \tag{24}$$

$$-\frac{\partial c}{\partial t} = \nabla(uc) = u \cdot \nabla c \tag{25}$$

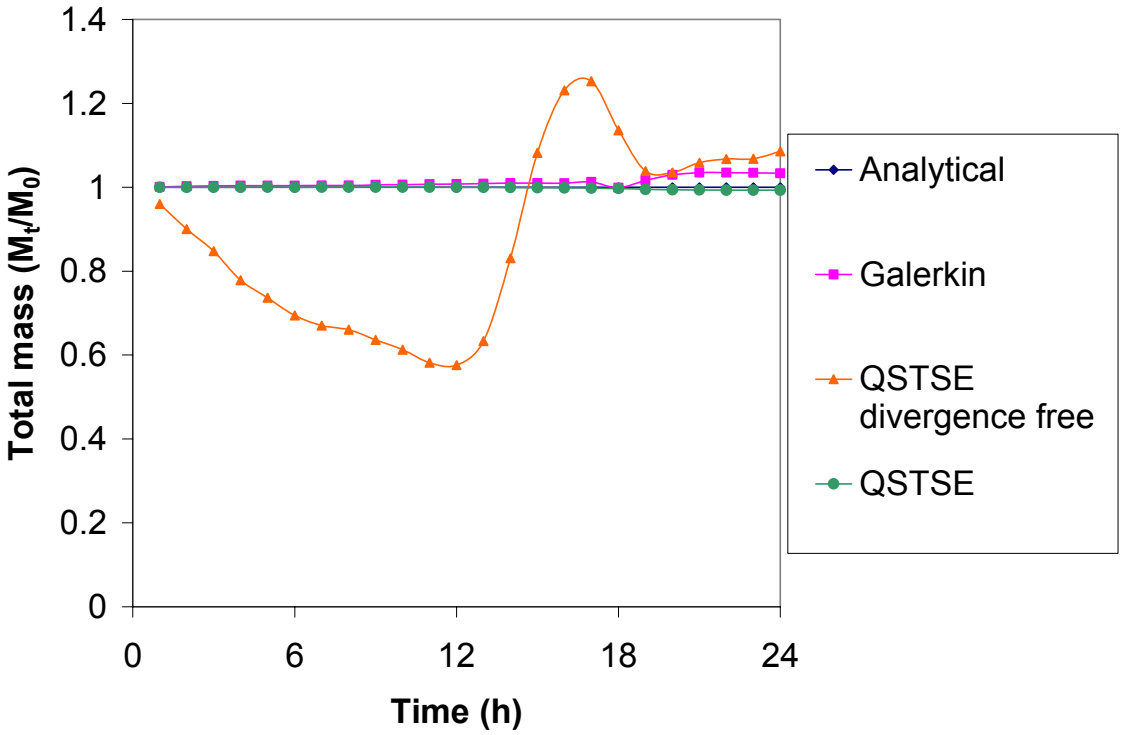

Figure 34. Mass conservation of different advection solvers applied to the CIT Airshed model. Values represent the total mass at time *t* (M_t) divided by the initial mass (M_0) of a puff transported throughout the domain, with no chemistry, no deposition, and no other loss. Meteorology of August 27, 1987.

3.3.1.5 Chemical mechanism

The chemical mechanism is one of the major components of an air quality model. As discussed in Atkinson (2000), there are a large number of components in the atmosphere that can undergo innumerable reactions. A chemical mechanism is an approximate representation of all the chemical processes that take place, and is limited by the information available for each reaction, and the products that result from them. In addition, use of more complex chemical mechanisms may be limited by computational constraints. Russell and Dennis (2000) listed the Regional Acid Deposition Model (RADM), the Regional Atmospheric Chemistry Mechanism (RACM), the Carbon Bond IV (CB-IV), and the Statewide Air Pollution Research Center model (SAPRC-90), as the most commonly used chemical mechanisms in air quality modeling. The SAPRC

model has been continuously updated to newer versions (SAPRC-97 and SAPRC-99). Both SAPRC-99 and CB-IV are used in the SCAQMD's 2003 AQMP, for ozone attainment demonstration.

The chemical mechanism used in the present work for baseline simulations is the CACM (see Griffin et al. 2002a for an extensive description). The gas-phase mechanism is based on the RADM/RACM work of Stockwell et al. (1997); Jenkin et al. (1997); SAPRC-97 and SAPRC-99 (available from W.P.L. Carter at http://pah.cert.ucr.edu/~carter/). It includes O_3 chemistry as well as chemistry of SOA precursors. The model consists of 361 chemical reactions and 191 gas-phase species—120 fully integrated species, 67 pseudo-steady-state species, and 4 species that have fixed concentration—and includes a comprehensively resolved treatment of VOC oxidation.

Jimenez et al. (2003) conducted a comparison among SAPRC-99, CB-IV, and CACM, as well as other mechanisms (see Table 38 for main features of each mechanism). The comparison was based on box model simulations of remote atmosphere conditions. Neither emissions nor deposition were considered. As Jimenez et al. 2003 emphasized, it is impossible to know which mechanism is the "correct" one. Measurements from smog chamber experiments could be used to complement their work, but these smog chamber experiments also represent limited systems. On the contrary, Jimenez et al. 2003 based the comparison between mechanisms on the average value obtained using all the mechanisms. One limitation of this work is that comparisons are based on one set of initial conditions. Simulations in three-dimensional models usually start from a large set of initial conditions. Study of other initial conditions could reveal different results from the comparisons.

Jimenez et al. 2003 reported that CACM and the Lurmann, Coyner, and Carter (LCC) mechanism are the mechanisms that produce the highest ozone concentration. CACM produced a difference in ozone peak concentration of +41% with respect to the average, and LCC produced a difference of +18.2% (see Figure 35).

Table 38. Main features of three different photochemical mechanisms: CBM-IV, SAPRC-99, and CACM

	CBM-IV	SAPRC-99	CACM
# reactions	81	237	361
# species	33	72	191
# organics	11	39	129

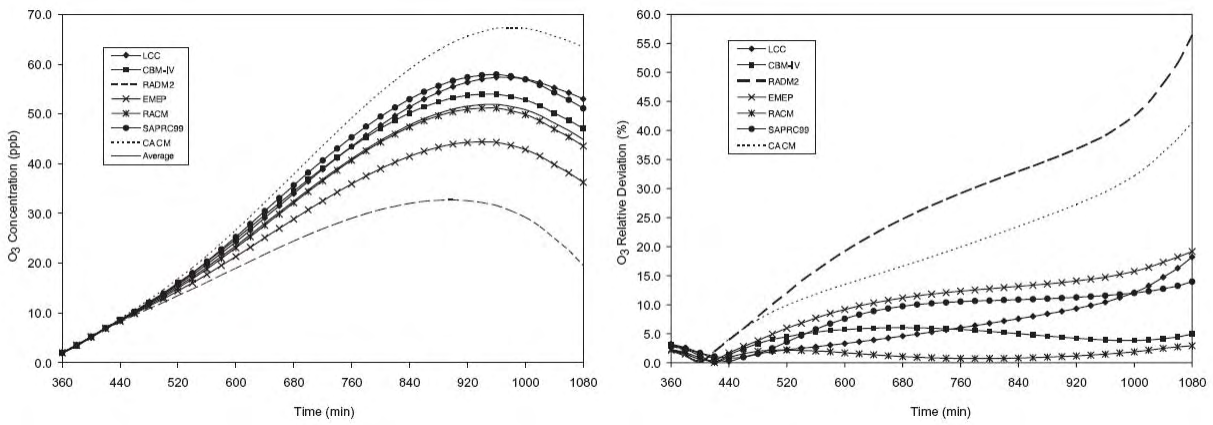

Source: Jimenez et al. 2003

Figure 35. Comparison of ozone formation simulated by different photochemical mechanisms used in a box model

This section extends this comparison to the three-dimensional model and contrasts results from simulations of a three-day episode using CACM and LCC mechanisms. Figure 36 presents the ozone concentration at hour 1300 of the third day of simulation using: (a) a CACM mechanism, and (b) an LCC mechanism. As obtained by Jimenez et al. 2003, the CACM mechanism produces a higher ozone peak than the LCC. Maximum ozone concentration in case (a) is 238 ppb; whereas, in case (b), it is 150 ppb. In addition, distribution of ozone concentration in each case differs significantly—an effect that box model analyses cannot predict. CACM mechanism produces the peak ozone concentration over the northeastern region of the domain, at downwind locations; whereas, the LCC mechanism produces the peak ozone concentration over the east part of Riverside, much closer to main sources. The difference between cases may be mainly caused by faster ozone removal considered in the LCC mechanism. As reported in Jimenez et al. 2003, nitric acid (HNO_3) concentration produced by LCC is higher than CACM. In addition, formation of PAN is slower for CACM. As a result, PAN is transported farther downwind, and therefore peak ozone concentrations move toward the east.

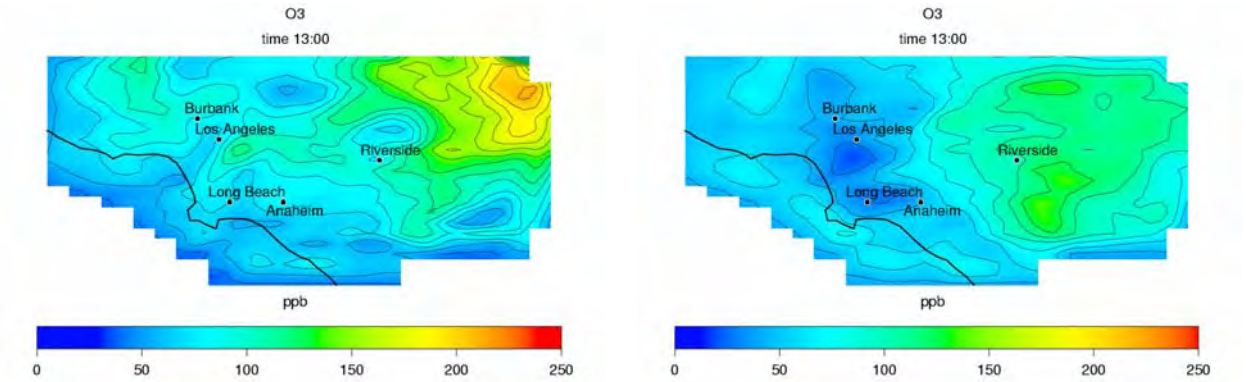

(a) CACM chemical mechanism (baseline) (b) LCC mechanism

Figure 36. Ozone concentration (in ppb) in the South Coast Air Basin at hour 1300 of the third day of simulation: (a) baseline case, and (b) using LCC mechanism

3.3.2 Comparison Between CIT, CALGRID and UAM Simulations

One of the major applications of an air quality modeling is to set bases for air pollution control strategies. The SCAQMD has been developing continuously plans to reduce emissions and hence comply with the NAAQS. To demonstrate that the measures proposed in the AQMP produce the desired pollutant reduction, SCAQMD uses two different air quality models: (1) UAM with the CB-IV chemical mechanism, and (2) CALGRID with the SAPRC-99 chemical mechanism. This section compares results obtained with the models used by SCAQMD with the CIT Airshed model, used by the authors in previous works (Medrano et al. 2003; Carreras et al. 2004). Besides different chemical mechanisms and other features listed in Table 39, the models encompass areas of different size. The SCOS97 domain extends from 275 km to 595 km UTM Easting (171 mi to 370 mi UTM Easting) and from 3670 km to 3870 km UTM Northing (2280 mi to 2405 mi UTM Northing). CIT domain has a smaller size and is not completely rectangular, but approximately extends from 300 km to 550 km UTM Easting (186 mi to 342 mi UTM Easting) and from 3700 km to 3810 km UTM Northing (2300 mi to 2367 mi UTM Northing). Because CALGRID and UAM use a domain size different than the CIT model, different boundary conditions are needed. From conclusions in previous sections, different boundary conditions are a source of discrepancies among simulation results.

Resolution in the vertical direction is different in each model. UAM and CIT models consider five vertical layers with variable height, with finer resolution at ground level, and coarser resolution at the top layer. Although considering a larger number of vertical layers, CALGRID assumes a fixed vertical height. As a result, CALGRID provides coarser resolution than UAM and CIT at the ground level.

Two main aspects that are different in the three models are chemical mechanism and advection solver. Regarding the chemical mechanism, UAM uses CB-IV; CALGRID uses SAPRC-99; and CIT uses CACM. As mentioned above, CB-IV has the lowest ozone-forming potential, and CACM has the highest ozone-forming potential. Regarding advection solver, UAM uses a Smolarkewicz scheme, which was found to be significantly less accurate than the Galerkin scheme and the QSTSE, used in CALGRID and in CIT, respectively.

Table 39. Comparison of CALGRID, UAM, and CIT modeling systems

Parameter	CALGRID[a]	UAM[a]	CIT
Modeling system			
Domain size	SCOS97	SCOS97	CIT
Grid size	5 km (3 miles)	5 km (3 miles)	5 km (3 miles)
Vertical Layer Structure	Fixed 16 layers	Variable 5 layers	Variable 5 layers
Region Top	5000 m (3.1 miles)	2000 meters (1.2 miles)	1100 meters (0.7 miles)
Boundary/top/initial conditions	Modified EPA Clean*	Modified EPA Clean*	Based on historical values
Modeling coordinate system	Lambert Conformal	UTM	UTM
Emissions			
Emissions inventory	2010 CARB/District	2010 CARB/District	2010 CARB/District
Chemistry			
Basic Module	SAPRC-99	CB-IV	CACM
Chemical Solver	Quasi Steady States analysis (QSSA) or Hybrid Solver	Quasi-steady state assumptions with Crank-Nicholson algorithm	Quasi Steady States analysis (QSSA) or Hybrid Solver
Photolysis rates	Radiation Extinction as height above sea level	One-dimensional based on Zenith angle	Radiation Extinction as height above sea level
Meteorology			
Meteorological data	1987 SCAQS	1987 SCAQS	1987 SCAQS
Wind model	MM5-4DDA	CALMET	
Advection	Chapeau function based scheme with Forester filter	Forward-upstream diffusive-corrected algorithm of Smolarkewicz	Quintic spline Taylor-series expansion
Vertical Diffusivity/ Diffusion	Horizontal diffusion-based on stability class with adjusted wind speed, (Smagorinsky method) Vertical diffusivity – Combination of various methods depending on stability and layer height	Vertical diffusivity coefficient is calculated internally	Horizontal diffusion-based on stability class with adjusted wind speed, (Smagorinsky method) Vertical diffusivity – Combination of various methods depending on stability and layer height
Dry Deposition	Surface Resistance model	Roughness length, stability, wind, speed, deposition factor	Surface Resistance model
Mixing Heights	CALMET	Holsworth	
Cloud cover	Yes	None	None
Mass continuity adjustment	NONR	O'Brien scheme	Included in QSTSE

[a] SCAQMD 2003c

* Modified EPA Clean include NO= 0ppb, NO2= 2ppb, and VOC= 10ppbv

Table 40 presents the maximum ozone concentration simulated by different air quality models. Among the models discussed above, CALGRID estimates the lowest peak ozone concentration, using meteorology of August 5–6, 1997. Although UAM uses a chemical mechanism that tends to produce less ozone and an advection solver that tends to diffuse more pollutant concentration than the scheme used in CALGRID, UAM estimates a higher peak ozone concentration than

CALGRID does, using the same meteorological episode. One reason for this difference could be attributable to different consideration of solar radiation and cloud cover. UAM does not consider cloud cover, or radiation extinction. As shown in Section 3.3.1.1.2, stronger radiation tends to produce higher ozone concentration. Other factors such as difference in calculation of deposition or vertical transport not discussed in this work could also contribute to differences in the peak ozone predictions. CIT model estimates much higher peak ozone concentration than the other two models. Main causes of such difference are attributable to the chemical mechanism and the advection solver, as discussed in previous sections. An additional simulation using the CIT model with a similar chemical mechanism and advection solver used by CALGRID is summarized in Table 40. The peak ozone concentration obtained by this simulation is in concordance with the results obtained by CALGRID. Note that CIT is used with a different meteorological episode than the one used with CALGRID. As a result, peak ozone concentration estimated by CIT with LCC/Galerkin advection solver is a slightly lower than the one predicted by CALGRID.

Table 40. Comparison of peak ozone concentrations simulated using different air quality models

	(1) UAM[a]	(2) UAM[a]	(3) CALGRID[b]	(4) CIT	(5) CIT with LCC/Galerkin
Episode	August 5–6, 1997	August 27–28, 1987	August 5–6, 1997	August 27–28, 1987	August 27–28, 1987
Peak ozone	153 ppb	136 ppb	134 ppb	263 ppb	127 ppb

[a] from AQMP 2003
[b] from AQMP 2003, Appendix V

3.3.3 Weekend Effect

The term *weekend effect* refers to the consistent increase in ozone concentration during weekends with respect to weekdays. A variety of causes have been identified as possible reasons for its occurrence. Decrease in NO_X emissions in areas where NO_X concentrations are typically high is known to produce an increase in ozone concentration. In an area such as the SoCAB, where NO_X emissions are very high, lower NO_X emissions during weekends (with respect to weekdays) are thought to be a cause of higher ozone concentration during weekends. Qin et al. (2004a) reported weekly trends for ozone variation in the AQMD. They showed that over the period from 1992 to 2001, the number of times that 1-hour and 8-hour O_3 air quality standards were exceeded during weekends was statistically larger than on weekdays. Qin et al. (2004b) reported also weekly trends of ozone precursor concentrations, PM_{10} concentration, and light scatter for the same period of time and region. In particular, they reported concentration values for NO_X, CO, non-methane hydrocarbons (NMHC) and PM_{10}, and light scatter at morning rush hour (0600 pacific standard time (PST) for NO_X and O_3, and 0500 PST for NMHC and CO) and at peak ozone time. Data consistently showed a decrease in ozone precursor concentrations and light scatter on weekends with respect to weekdays: 37%, 18%, 15%, 14%, and 9% decrease in NO_X, CO, NMOC, PM_{10}, and light scatter, respectively, at morning rush hour; 29%, 13%, 24%, 17% and 17% decrease in NO_X, CO, NMHC, PM_{10} and light scatter, respectively, at peak ozone time. On the other hand, peak ozone concentration and 8-hour average maximum concentration

on weekends were on average 20% and 22%, respectively, higher than during weekdays. Based on these observations, Qin et al. 2004b concluded that lower NO_X emissions and light scattering on weekends with respect to weekdays are the main contributors to the weekend effect.

As discussed in Section 3.3.1.1.2, based upon model simulations, increase in UV radiation by 20% leads to maximum increases of 20 ppb in ozone concentration. This correlation corroborates one of the conclusions by Qin et al. 2004b that identifies less light scattering over the weekends as a cause for the weekend effect. However, other factors must be considered, because impacts from changing UV radiation cannot fully explain observations reported by Qin et al. 2004b: increasing UV radiation alone (which is a way of decreasing light scatter) increases ozone concentration in downwind locations more significantly than in central areas, whereas reported data show the opposite trend.

Modeling of the weekend effect requires the use of an emissions inventory for weekends that takes into account emissions reductions due to the decrease of industrial activity and daily commute. However, such inventories are scarce. As an alternative, this section presents a scenario in which emission reductions are applied to a baseline weekday inventory. Reductions are applied following the weekday-weekend trends of ambient concentrations of ozone precursor reported by Qin et al. 2004b (see Table 41). Although changes in pollutant ambient concentrations do not necessarily correlate to changes in pollutant direct emissions, this scenario is a first approximation to the conditions that define a weekend episode.

Table 41. Reductions applied to the baseline weekday emissions inventory and baseline light scatter to simulate a weekend episode

Pollutant	Reduction (%)
NO	45
NO_2	22
VOC	20
CO	15
PM	15
Light Scatter	15

Qin et al. 2004b show that differences in ozone concentration between weekdays and weekends, in percentage, are bigger at 0600 than at the ozone peak hour. Simulation results also show that in the early morning ozone concentration changes from weekdays to weekends by a greater percentage, since concentration at 0600 are already very low (see Figure 37). However, in absolute values, changes in ozone concentration in the early morning are comparable to the ones occurring at peak ozone time. In addition, measurements reported by Qin et al. 2004b show that at far downwind locations, such as Palm Springs, and at upstream locations, such Santa Clarita, there are no significant increases in ozone concentration due to the weekend effect. As it appears in Figure 37, simulation results also show no significant increases in ozone concentration at far downwind locations and upstream locations on the west part of the domain.

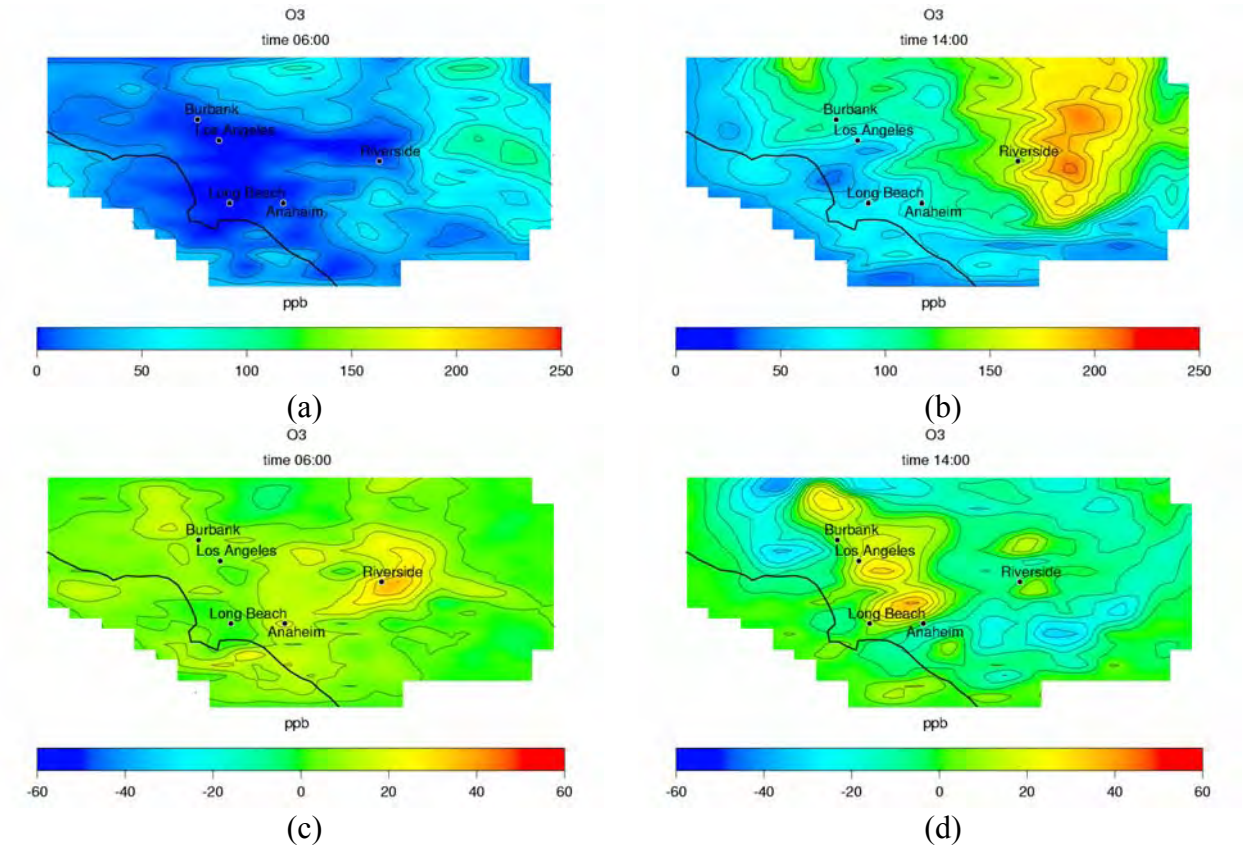

Figure 37. Weekend effect. Baseline weekday ozone concentration (in ppb) during the second day of simulation (a) at 0600, (b) at 1400; difference in ozone concentration (in ppb) during second day of simulation (weekend – weekday): (c) at 0600, and (d) at 1400.

Increases in ozone concentration obtained from simulations using weekend effect data range up to 60 ppb at peak ozone time. On the other hand, values reported by Qin et al. 2004b indicate more moderate increases from the weekend effect, around 20 ppb, because these values are averages obtained for a period of seven summers of data collection (June–October, 1995–2001). Nonetheless, simulation results show good agreement with measured data and suggest that the air quality model can predict satisfactorily air quality impacts resulting from emission changes. Consequently, CIT can also be used with confidence to determine air quality impacts of emissions increase due to DG.

3.3.4 Model Improvements to Capture DG Impacts

A preliminary study of the air quality impacts of DG in the SoCAB was presented by Medrano et al. (2003). Simulations of air quality impacts were performed with the CIT model using the LCC mechanism and a Galerkin scheme for the numerical solution of advection. In addition, a two-day episode was used to evaluate those impacts. In a posterior study, modifications were introduced to the CIT model based on the analyses presented above.

3.3.4.1 Improvements in initial conditions handling

Major air quality impacts potentially occur at downwind locations, on the eastern portion of the SoCAB. As shown in Section 3.3.1.3, the effect of initial conditions on pollutant concentration at these locations is still important after two days of simulation. Consequently, a three-day episode was chosen to study air quality impacts of DG, as opposed to using a two-day episode. In addition, previous simulations assumed same initial concentration at upper levels other than ground level for each day of simulation. In present simulations, initial concentrations for the second and third day of simulations are the concentrations at the last hour of the previous day, for all five vertical levels of the computational domain.

3.3.4.2 Improvements in the chemical mechanism

Preliminary results in Medrano et al. (2003) showed that DG deployment in the SoCAB would impact not only ozone concentration, but also secondary aerosols. These preliminary results were obtained using the LCC mechanism. The CACM mechanism includes comprehensive treatment of oxidation paths that lead to ozone formation, based on RADM, SAPRC-97, and SAPRC-99 chemical mechanisms, which are more recent models than LCC. Hence, these three mechanisms and CACM use updated and more complete chemistry and chemical kinetics than LCC does. In addition, CACM includes chemistry of VOC oxidation that leads to formation of SOA precursors. Consequently, the CACM chemical mechanism was chosen to determine air quality impacts of DG in the SoCAB, so that the impacts on ozone and aerosol formation were better captured.

3.3.4.3 Improvements in the advection solver

Previous versions of the CIT model used a Galerkin-type of numerical scheme for the solution of the advection equation. As reported in Section 3.3.1.4, previous studies showed that the ASD scheme and the QSTSE scheme obtain better accuracy than the Galerkin method in the solution of sample advection problems. The ASD is the most accurate, although it is significantly more expensive than the QSTSE in terms of computational demand. Thus, the QSTSE scheme is used in the CIT model simulations of air quality impacts from DG deployment.

3.3.5 Current Understanding of Model Sensitivity to DG

Monte Carlo analyses help identify the uncertainty of the air quality model predictions to the variation of given input parameters. However, there are differences between Monte Carlo and spatial sensitivity analyses. For instance, the Monte Carlo methodology considers changes in the intensity of emissions through multiplicative factors, but their spatial distribution is not modified. This procedure, although important, does not explore the spatial sensitivities of emissions and their relevance to predictions. Moreover, the influence of DG installation in the SoCAB needs to be addressed more directly. In particular, the type of variations produced in simulation results when DG is placed in specific parts of the basin. To investigate spatial sensitivities, this section presents a methodology in which only changes to DG emissions added to the baseline are systematically considered.

The development of a set of scenarios to investigate spatial sensitivities is based partly in the general methodology devised by Carreras et al. (2004). The total mass emissions selected for this

sensitivity study correspond to the Extra High Penetration (EHP) scenario, for which Carreras et al. (2004) found one of the largest impacts on ozone concentrations due to DG implementation. The daily increases in emissions of NO_X, CO, VOC, NH_3, SO_X, and PM in this scenario are 2.0%, 1.3%, 0.7%, 0.7%, 0.4%, and 0.8%, respectively. Instead of using an arbitrary spatial distribution of emissions, five scenarios were developed to separate the adoption of DG by counties in the SoCAB using GIS land-use data. For all scenarios, base-loaded emissions from the EHP scenario were added to the baseline for each county. Specifically, 50 cells of the computational domain were selected by using the non-vacant areas provided by the GIS land-use data. This method ensures that the emissions variations are done equally in all scenarios and that the simulated effects are not due to more or less DG adoption in each county. Figure 38 shows the areas in each county where additional DG emissions are placed.

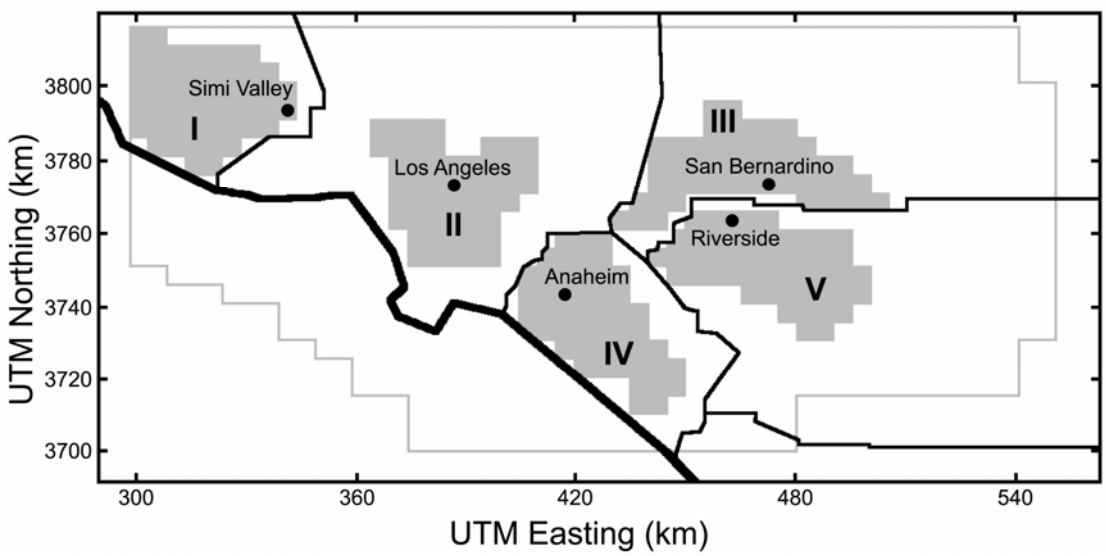

Figure 38. Regions where DG emissions for spatial sensitivity scenarios are placed in each county of the SoCAB

Figure 39 presents the 1-hr average ozone concentrations difference between each scenario and the 2010 base-case at hour 1300. This hour is selected to compare the impacts of the scenarios because it is when domain-wide ozone concentrations peak. Nonetheless, the largest differences may occur at different times. In general ozone impacts range from -36 to 39 ppb, which are significant differences, compared to the EHP scenario impacts (± 8 ppb). Furthermore, this exhibits the importance of DG spatial accumulation, because both the EHP and county scenarios input the same amount of emissions mass to the basin. Areas where emissions are typically low (such as Ventura) present the largest impacts. Ozone increases with respect to the base case can be as large as 39 ppb. In this region, increases in NO_X emissions reduce ozone formation locally during the nighttime. However, as the sun rises at around 0800 the differences start to become positive, indicating an increase in ozone concentrations. At night, NO from DG emissions scavenges ozone. During the day, the VOC to NO_X ratios are such that Ventura is in a NO_X-limited region where NO increases lead to higher ozone concentrations. Additionally, the meteorology of this episode shows that the ozone impacts elsewhere in the basin are not

significant when DG is placed in Ventura. In Central Los Angeles the introduction of distributed generation NO_X emissions has the effect of decreasing ozone concentrations locally and downwind. Central Los Angeles is a VOC-limited region; therefore, increases in NO_X emissions decreases ozone concentrations. In fact, results show that the largest decreases in ozone occur during the peak of the daylight cycle. Another aspect this scenario exhibits is that with the given meteorology, the placement of DG in Los Angeles County does not directly impact the ozone concentration in the east side of the basin. For the scenario in which DG emissions are established in San Bernardino, simulations predict that ozone concentrations decrease locally, but they increase downwind from the sources. Results show that the decrease is more pronounced during the nighttime—not presented in the figures—but during the peaks of the daylight hours, especially after 1200 hours, ozone increases up to 16 ppb. The mixing of pollutants downwind and the large VOC-to-NO_X ratios leads to more ozone at higher NO_X emissions. Placement of DG in Riverside produces a similar behavior in the ozone formation, as in San Bernardino. Namely, local decreases during the night; downwind increases during the day. Although the decreases are similar in both counties, the increase in ozone concentration produced by allocating all DG in Riverside is 50% larger than the increase in ozone concentration produced by placing all DG in San Bernardino. However, one of the most prominent impacts is observed when DG is located near coastal areas such as Orange County. With the exception of the Ventura scenario, it represents the largest ozone increases from all scenarios explored. The positive and negative impacts have approximately the same magnitude, although they do not occur at the same time. As in the case of Riverside and San Bernardino, the largest decreases occur locally at nighttime, in particular just at before sunrise at 0700 hours. The largest increases, downwind from sources, occur at around 1600 hours. Finally, the effects of placing DG in Orange County can be felt as far as the east side of Riverside.

Figure 40 presents the 24-hr average $PM_{2.5}$ aerosol concentrations impacts for each county scenario. In general these impacts range from -2 to 14 $\mu g/m^3$. Also, the positive impacts on aerosol concentrations have larger magnitudes than the negative ones, which imply that the influence of DG on $PM_{2.5}$ is to increase aerosol concentrations. With the exception of Central Los Angeles, all the other scenarios produce impacts comparable to those observed in the EHP scenario. Impacts on aerosol concentrations for the Los Angeles scenario show increases of $PM_{2.5}$ concentrations north to the sources (± 3 $\mu g/m^3$). The largest impacts occur for the Ventura scenario, since in the base-case no major emissions are associated with this region. These impacts, however, are seen locally and indicate that DG installation in this region does not have an effect in others in the SoCAB. The effect of placing DG in both Riverside and San Bernardino is very similar; those impacts do not exceed 7.5 $\mu g/m^3$. Typically, these regions have very high particulate matter concentrations, however, the contribution of additional DG places additional concentrations locally but not downwind. The Orange county scenario puts most of the $PM_{2.5}$ impacts far from the sources, suggesting that this aerosol is the product of gas to aerosol conversion from gas-phase precursors. Therefore, the placement of DG in coastal areas shows to be of utmost importance for impacts in regions that already have high aerosol concentrations.

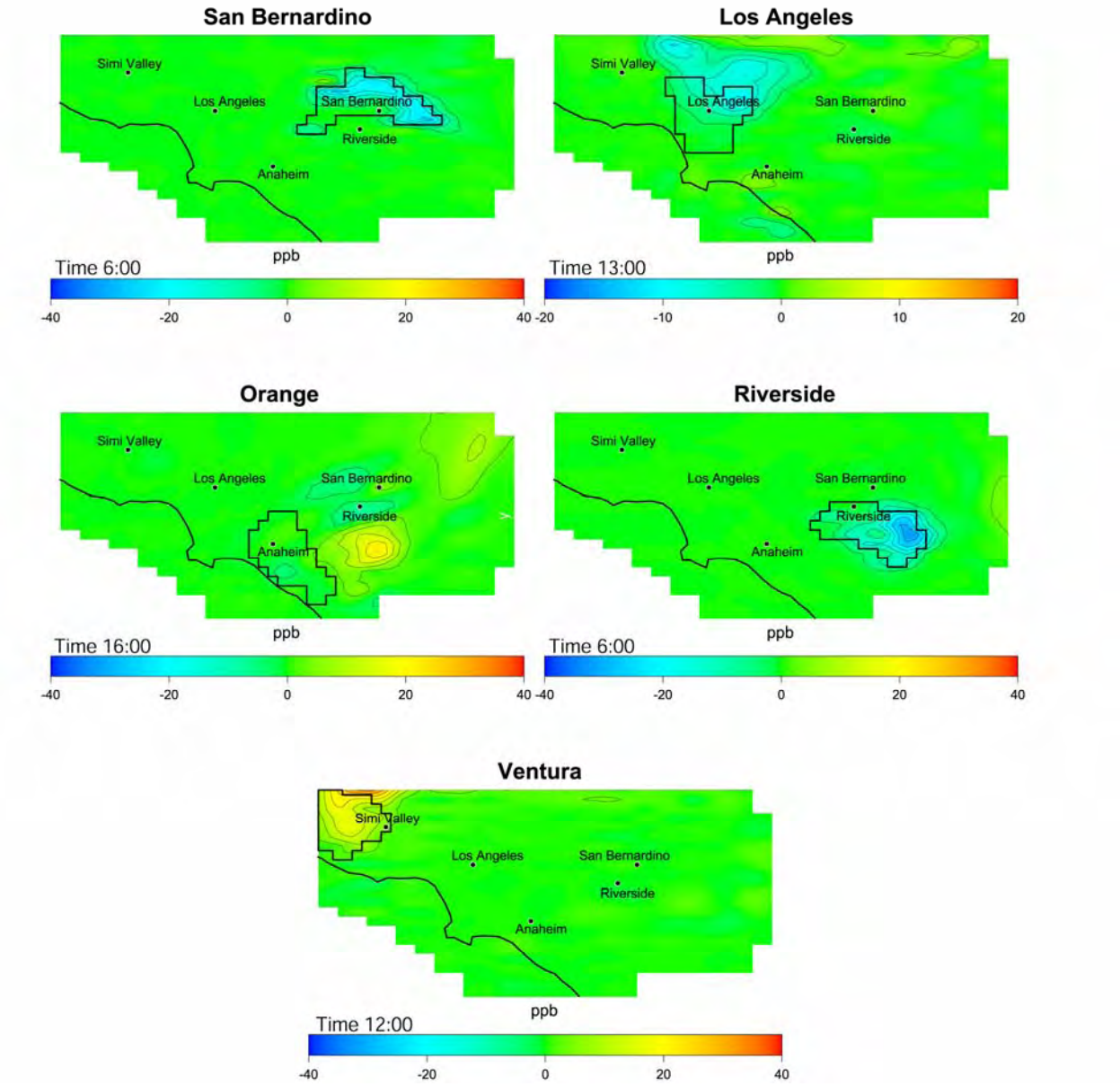

Figure 39. Difference between spatial sensitivity scenarios and baseline ozone concentrations at hours of maximum impact

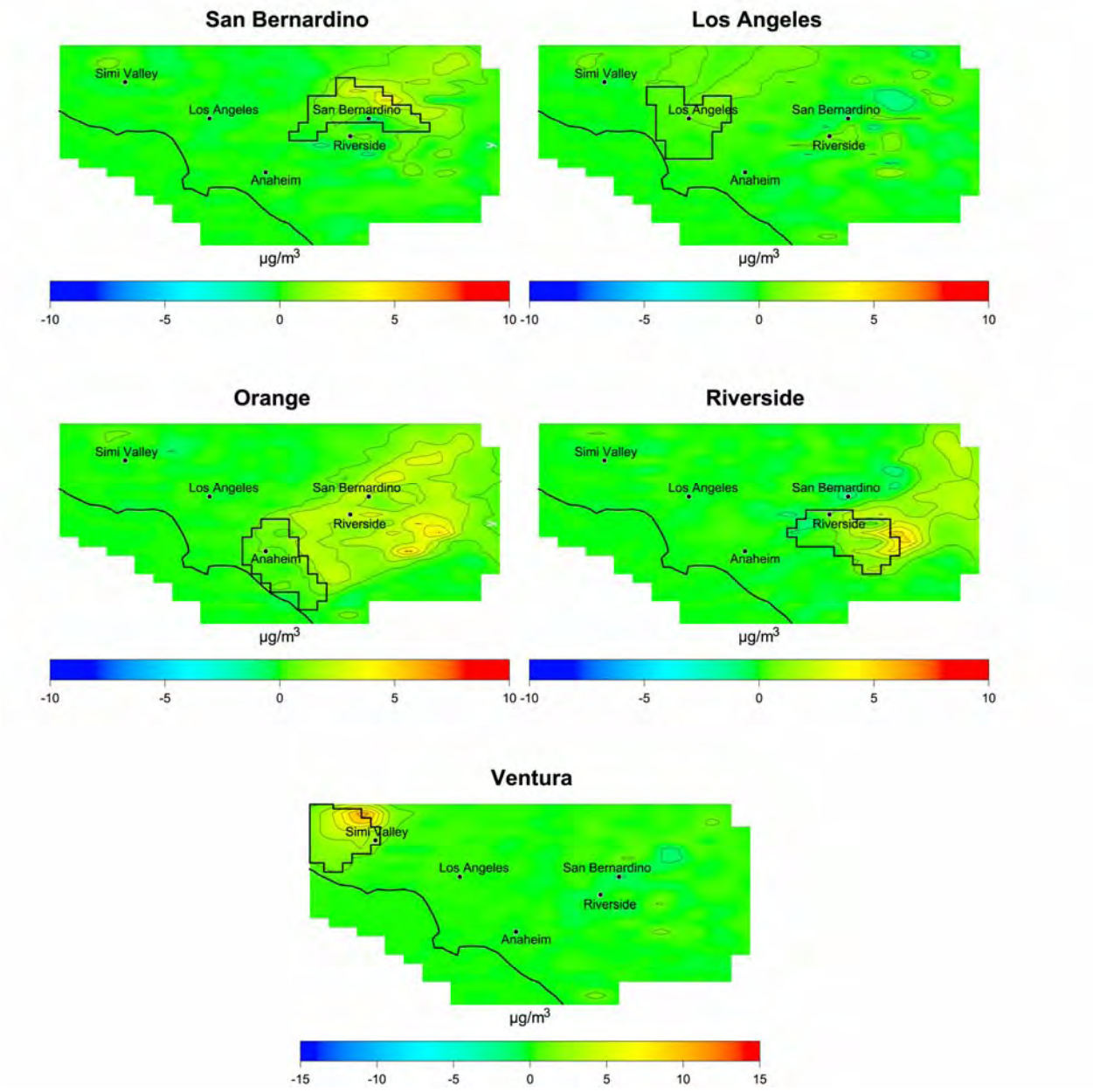

Figure 40. Difference between spatial sensitivity scenarios and baseline for 24-hr average $PM_{2.5}$ aerosol concentrations

3.4 Air Quality Impacts of DG Scenarios

This study presents an assessment of air quality impacts caused by the deployment of DG systems throughout the SoCAB. Installation of such technologies by the year 2010 will depend upon market penetration for each DG type. Factors that will influence the degree of market penetration include the application for which DG is required, the cost of installation, and the ability of each technology to comply with pollutant emission standards. A set of 26 DG scenarios has been developed (Samuelsen et al. 2003) and divided into two categories: (1) realistic scenarios, and (2) spanning scenarios. Realistic DG scenarios are developed to reflect an expected level of DG deployment in 2010. Spanning DG scenarios are developed for scientific completeness, for sensitivity analyses, and for determination of potential impacts due to unexpected outcomes. Additionally, spanning scenarios help to set upper bounds for air quality impacts resulting from DG installation. Section 2.1 presents a detailed description of the DG scenario development.

The process for developing DG implementation scenarios is a very significant advance of the current effort. This process, which is especially rigorous for the development of realistic DG implementation scenarios, resulted in the development of more than 100 DG implementation scenarios. After screening these scenarios, 5 realistic and 21 spanning scenarios were studied in detail. A brief description of the parameters that define each of these scenarios is presented in Table 30. More detailed information on these scenarios can be found in Samuelsen et al. 2003.

Deployment of DG in most cases implies an increase of primary pollutants from in-basin emissions. Some scenarios also account for emissions displacement, which leads to a decrease in the emission of certain pollutants. Table 42 shows the increase in criteria pollutant emissions for each DG scenario. Table 43 presents the increase due to DG implementation as a percentage of pollutant emissions relative to the total in-basin emissions. Spanning Scenarios 2 (2003ES) and 18 (EHP) present the highest increase in pollutant emissions; whereas, spanning Scenario 16 (TDPW10%) presents the lowest increase in emissions, except for NO_X. Realistic Scenario #R3 has the lowest NO_X emissions, because #R3 assumes the highest net decrease in NO_X emissions due to CHP emissions displacement. In general, the increase of emissions with respect to the baseline in all DG implementation scenarios is less than 1%, for all species. Scenarios 22 through 25 consider a net in-basin decrease of NO_X emissions due to emissions displacements that result from CHP use.

Although the increase of basin-wide emissions in all cases is relatively small compared to total emissions, each scenario considers the implementation of a different DG technology mix, and DG units are installed to operate according to different duty cycles. In addition, each DG technology has different emission factors and is implemented differently according to its use by activity sector. As a result, chemically resolved emissions vary widely in space and time. Furthermore, the effects of emissions fluxes on ambient concentrations depend upon a host of coupled processes, including bulk transport, diffusion, and chemical and photochemical reactions. Hence, localized air quality impacts can be determined only through use of the three-dimensional air quality models. Detailed results, including variations in predicted criteria pollutants as a function of space and time are presented in the following sections for both realistic and spanning DG implementation scenarios.

Table 42. Basin-wide absolute increase of primary criteria pollutant emissions per each DG scenario

DG Scenario Name	DG Scenario #	CO	NO_X	VOC	NH_3	SO_X	PM
		ton/day	ton/day	ton/day	ton/day	ton/day	ton/day
PW2010	**1**	8.19	2.54	0.80	0.25	0.10	0.61
2003ES	**2**	75.65	6.30	5.32	0.00	0.43	2.04
2007ES	**3**	1.26	0.88	0.11	0.00	0.43	2.04
PermICEPW	**4**	22.37	5.59	2.36	0.00	0.11	0.88
HEAPW20%	**5**	16.44	4.43	0.93	0.25	0.13	0.61
PeakPW	**6**	3.45	1.03	0.33	0.09	0.04	0.30
LDG20%	**7**	2.58	1.54	0.13	0.00	0.09	0.09
NH3_20%	**8**	2.58	1.54	0.13	0.78	0.09	0.09
PGW2010	**9**	8.19	2.54	0.80	0.25	0.10	0.61
LUPW20%	**10**	8.19	2.54	0.80	0.25	0.10	0.61
Free20%	**11**	8.09	2.52	0.78	0.26	0.10	0.81
FCPW20%	**12**	1.26	0.88	0.13	0.00	0.08	0.65
MTGPW20%	**13**	1.90	1.03	0.11	0.00	0.13	1.05
DGCHP	**14**	5.79	1.31	0.66	0.25	0.06	0.18
DGEED	**15**	7.67	0.86	0.16	0.25	0.09	0.60
TDPW10%	**16**	1.12	0.34	0.11	0.00	0.02	0.13
BAU	**17**	6.19	1.96	0.54	0.33	0.06	0.26
EHP	**18**	44.35	13.76	4.31	1.37	0.54	3.01
BAU_par	**19**	17.37	4.78	1.65	0.33	0.12	0.72
HPD	**20**	9.49	2.86	0.93	0.22	0.11	0.71
PeakPW-2	**21**	13.19	5.02	1.95	1.94	2.00	1.31
#R1	**22**	2.26	-0.09	0.16	0.20	0.03	0.24
#R2	**23**	4.53	-0.18	0.32	0.40	0.06	0.49
#R3	**24**	9.06	-0.35	0.64	0.80	0.12	0.97
#R4	**25**	1.22	-0.29	0.11	0.18	0.03	0.24
#R5	**26**	2.79	0.75	0.19	0.20	0.04	0.28

Table 43. Basin-wide relative increase of primary criteria pollutant emissions per each DG scenario

DG Scenario Name	DG Scenario #	CO %	NO_X %	VOC %	NH_3 %	SO_X %	PM %
PW2010	**1**	0.25	0.37	0.13	0.13	0.08	0.16
2003ES	**2**	2.30	0.93	0.84	0.00	0.34	0.55
2007ES	**3**	0.04	0.13	0.02	0.00	0.34	0.55
PermICEPW	**4**	0.68	0.82	0.37	0.00	0.09	0.24
HEAPW20%	**5**	0.50	0.65	0.15	0.13	0.11	0.16
PeakPW	**6**	0.10	0.15	0.05	0.05	0.03	0.08
LDG20%	**7**	0.08	0.23	0.02	0.00	0.07	0.02
NH3_20%	**8**	0.08	0.23	0.02	0.42	0.07	0.02
PGW2010	**9**	0.25	0.37	0.13	0.13	0.08	0.16
LUPW20%	**10**	0.25	0.37	0.13	0.13	0.08	0.16
Free20%	**11**	0.25	0.37	0.12	0.14	0.08	0.22
FCPW20%	**12**	0.04	0.13	0.02	0.00	0.06	0.17
MTGPW20%	**13**	0.06	0.15	0.02	0.00	0.10	0.28
DGCHP	**14**	0.18	0.19	0.10	0.13	0.05	0.05
DGEED	**15**	0.23	0.13	0.02	0.13	0.07	0.16
TDPW10%	**16**	0.03	0.05	0.02	0.00	0.01	0.04
BAU	**17**	0.19	0.29	0.09	0.18	0.05	0.07
EHP	**18**	1.35	2.02	0.68	0.74	0.43	0.81
BAU_par	**19**	0.53	0.70	0.26	0.18	0.10	0.19
HPD	**20**	0.29	0.42	0.15	0.12	0.09	0.19
PeakPW-2	**21**	0.40	0.74	0.31	1.05	1.60	0.35
#R1	**22**	0.07	-0.01	0.03	0.11	0.02	0.07
#R2	**23**	0.14	-0.03	0.05	0.22	0.05	0.13
#R3	**24**	0.27	-0.05	0.10	0.43	0.10	0.26
#R4	**25**	0.04	-0.04	0.02	0.10	0.02	0.07
#R5	**26**	0.08	0.11	0.03	0.11	0.03	0.08

3.4.1 Air Quality Impacts of Realistic DG Scenarios

Scenarios that consider the realistic implementation of DG introduce small emission increments of 0.43% and less. Distribution of these new sources is based on land-use data, which concentrates DG technologies close to industrial zones, such as Long Beach, Los Angeles, and Riverside. In contrast, population distribution places higher DG concentration in the central area of Los Angeles (see Figure 41). Although basin-wide emission increments are small, the additional emissions by DG are distributed throughout the basin and are especially installed in industrialized regions, where they have the potential to discernibly impact air quality.

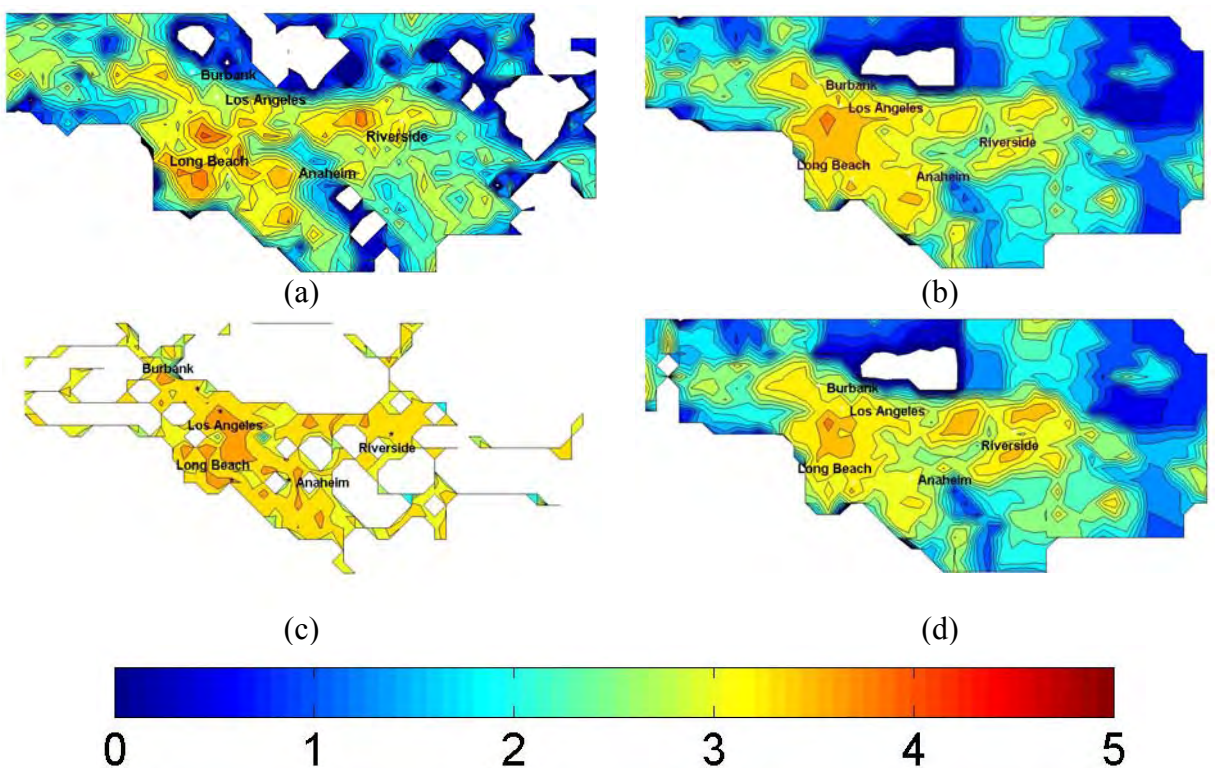

Figure 41. Comparison among 4 spatial distribution of DG power (in kW, Log scale) in the SoCAB in: (a) land use-based; (b) population-based; (c) freeway density-based; (d) population growth-based

In the realistic scenario #R1, 5% of the increased power demand from 2002 to 2010 is met by DG. The distribution of DG throughout the basin is based on land-use data, and DG operation follows realistic duty cycles corresponding to different activity sectors present in each cell of the computational domain. Thus the amount of emissions introduced by DG varies geographically and temporally. In addition, each DG technology is deployed differently, depending on the activity area in which DG is installed. Therefore, the fraction of different pollutants introduced varies in each cell of the domain.

Realistic scenarios #R2 and #R3 have the same emissions spatial distribution as scenario #R1. However, #R2 and #R3 present DG penetration of 10% and 20% of the increased power demand during the years 2002 through 2010. Hence, increase in emissions of CO, VOC, PM, NH_3, and SO_X in scenario #R2 is twofold the increase in #R1; whereas, the increase in #R3 is 4 times higher than that of #R1. On the other hand, NO_X emissions are reduced with the same ratios in #R2, #R3, and #R1, because the increase in emission displacement due to CHP applications is proportional to DG penetration.

Realistic scenario #R4 also presents the same DG distribution as #R1. However, the DG adoption rate for this scenario is assumed nonlinear with time. This assumption means that DG technologies will be installed at a higher rate after the year 2007. As a result, a higher fraction of DG technologies installed by 2010 will produce lower emissions, in compliance with the approved CARB emission standards for 2007. #R4 is the realistic scenario with the lowest CO

and VOC emissions, and only #R3 has lower NO_X emissions, since #R3 has higher NO_X emissions displacement than #R4.

Finally, realistic scenario #R5 presents the same DG distribution as #R1, but it neglects the emission displacement from CHP. Therefore, #R5 is the realistic scenario with the highest NO_X emissions.

Table 44, Table 45, and Table 46 present the overall basin-wide impacts of realistic DG implementation scenarios on O_3, NO_2, and $PM_{2.5}$ concentrations, respectively. The domain-wide maximum ozone concentrations do not change among the different realistic scenarios (Table 44) and are equal to that of the baseline. This could suggest that compliance with ozone standards will not likely be affected by implementations of DG that are similar to the realistic scenarios of this study, since peak, basin-wide, 1-hour ozone concentration is the parameter upon which compliance with current federal standards is determined. However, increases in ozone concentration of the order of 2 ppb occur in areas where baseline concentrations exceed the air quality standards. Therefore, implementation of DG may contribute to the already poor air quality in certain downwind locations. The domain-wide maximum NO_2 concentration is also similarly not affected by any of the realistic DG scenarios (Table 46). However, the largest hourly changes in NO_2 concentrations range from -3 ppb to +3 ppb.

Table 44. Maximum O_3 concentration, and maximum decrease and increase in O_3 concentration for simulation of each realistic DG scenario (State standard: 90 ppb; Federal standard: 120 ppb)

Scenario	Basin-Wide Max (ppb)	Time	Max Increase (ppb)	Baseline reference (ppb)	Time, Max Increase	Max Decrease (ppb)	Baseline reference (ppb)	Time, Max Decrease
#R1	238	13	3	46	13	-2	60	12
#R2	238	13	5	45	14	-9	152	13
#R3	238	13	5	89	12	-4	178	13
#R4	238	13	3	70	11	-8	178	13
#R5	238	13	2	88	12	-8	178	13

Table 45. Maximum NO_2 concentration, and maximum decrease and increase in NO_2 concentration for simulation of each realistic DG scenario (State standard: 250 ppb)

Scenario	Basin-Wide Max (ppb)	Time	Max Increase (ppb)	Baseline reference (ppb)	Time, Max Increase	Max Decrease (ppb)	Baseline reference (ppb)	Time, Max Decrease
#R1	158	5	2	93	1	-1	60	1
#R2	158	5	2	83	1	-3	57	18
#R3	158	5	2	83	1	-3	49	21
#R4	158	5	3	49	6	-3	6	18
#R5	158	5	1	18	23	-1	60	1

The domain-wide hourly maximum $PM_{2.5}$ concentration obtained in all realistic scenarios is equal to the baseline $PM_{2.5}$ peak, except for scenario #R2, in which the maximum is 1 $\mu g/m^3$ higher. However, hourly $PM_{2.5}$ concentrations decrease 33 $\mu g/m^3$ in #R1 and increase 17 $\mu g/m^3$ in scenario #R5 with respect to the baseline. On the other hand, changes in 24-hour average $PM_{2.5}$ concentrations fall within the range ± 3 $\mu g/m^3$. The 24-hour average $PM_{2.5}$ results from simulation of all of the realistic DG implementation scenarios are presented in Table 47. Since current regulations are based upon the 24-hour average of particulate matter (PM_{10} in current regulations), the results of Table 47 suggest a potential slight improvement in compliance due to DG installation. This is the case because observed decreases in $PM_{2.5}$ occur in locations of high baseline 24-hour average $PM_{2.5}$ concentration.

Table 46. Maximum hourly $PM_{2.5}$ concentration, and maximum decrease and increase in hourly $PM_{2.5}$ concentration for simulation of each realistic DG scenario

Scenario	Basin-Wide Max ($\mu g/m^3$)	Time	Max Increase ($\mu g/m^3$)	Baseline reference ($\mu g/m^3$)	Time, Max Increase	Max Decrease ($\mu g/m^3$)	Baseline reference ($\mu g/m^3$)	Time, Max Decrease
#R1	248	3	15	17	6	-19	113	3
#R2	249	3	15	72	4	-14	96	4
#R3	248	3	13	59	6	-15	65	22
#R4	248	3	16	24	7	-15	88	4
#R5	248	3	17	54	7	-33	207	6

Table 47. Maximum 24-hour average $PM_{2.5}$ concentration, and maximum decrease and increase in 24-hour average $PM_{2.5}$ concentration in each realistic scenario (Federal standard: 65 $\mu g/m^3$)

Scenario	Max ($\mu g/m^3$)	Max Increase ($\mu g/m^3$)	Baseline reference ($\mu g/m^3$)	Max Decrease ($\mu g/m^3$)	Baseline reference ($\mu g/m^3$)
#R1	115	3	45	-2	44
#R2	115	2	58	-2	81
#R3	114	2	39	-2	70
#R4	114	2	39	-2	69
#R5	112	3	39	-3	115

For scenario #R1, the maximum difference in ozone concentrations compared to the baseline case for any location at any time is on the order of 3 ppb (see Table 44). This difference occurs in areas where ozone concentrations are already lower than the peak concentration, so these changes will not affect compliance with ozone standards. However, the decreases in ozone concentration of Table 44 (for all realistic cases) occur in regions of relatively high baseline ozone concentration; whereas, increases occur in regions of relatively low baseline ozone concentration. Thus, the simulation of realistic DG implementation scenarios suggests no impact of DG on basin compliance with air quality standards, but a potential to slightly decrease ozone in areas of relatively high ozone concentration.

Figure 42 presents the spatially resolved impacts on ozone concentration at 1300, the hour when ozone concentrations reach their maximum for scenario #R1. Figure 42 shows the difference in ozone predictions between the realistic and the baseline cases. At this particular hour, increases and decreases in ozone concentration range from -2 to +2 ppb. Although this range is small, some of the increases occur downwind from Riverside, where ozone concentration is typically exceeding the air quality standards.

Impacts of scenario #R1 on NO_2 concentration range between -1 to +2 ppb, as shown in Table 45. The largest impacts occur at night and early morning, when NO_2 is not photolyzed yet and concentrations are still high. At night, NO_2 reacts with remaining ozone to form NO_3, which is the predominant atmospheric oxidant for unsaturated hydrocarbons and a precursor for particular matter. As a result, the maximum increase in particulate matter occurs in the early morning after NO_2 peaks. On the other hand, although wide ranges of change in hourly $PM_{2.5}$ concentrations occur in the basin, as shown in Table 46, there are no significant impacts on the $PM_{2.5}$ 24-hour average concentration.

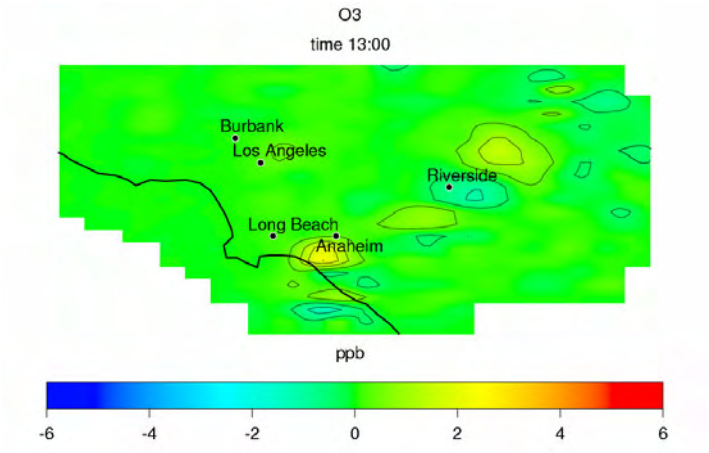

Figure 42. Difference in O_3 concentration (in ppb) between #R1 and Baseline at hour 1300

Differences in the $PM_{2.5}$ 24-hr average concentrations between the realistic DG scenario #R1 and the baseline scenario range from -2 to +3 $\mu g/m^3$, as shown in Figure 43. The largest differences in $PM_{2.5}$ 24-hour concentration are located near San Bernardino and Riverside, where maximum concentrations of particulate matter are typically observed.

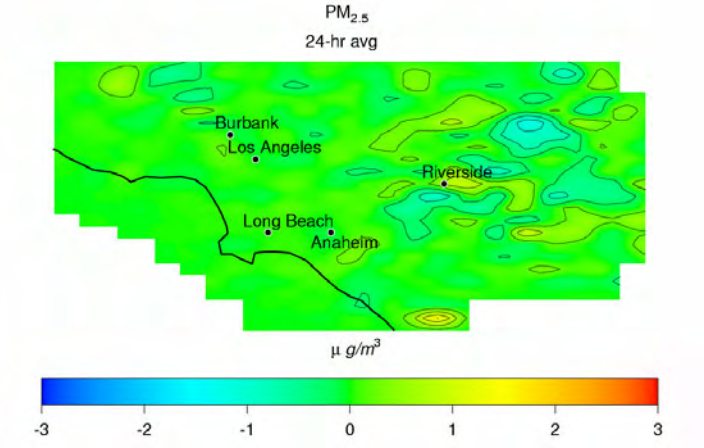

Figure 43. Difference in $PM_{2.5}$ 24-hour average concentration (in $\mu g/m^3$) between #R1 and Baseline

Impacts on ozone and $PM_{2.5}$ concentrations are also analyzed at two specific locations in the SoCAB: Riverside and Central Los Angeles. Riverside is characterized as one of the regions with the poorest air quality in the basin, with respect to both ozone and particulate matter. On the other hand, Central Los Angeles is typically in compliance with the ozone air quality standard, but it suffers from high particulate matter concentrations. Furthermore, air quality poses the most significant health risks in Central Los Angeles, since it is the most populated region in the basin.

Figure 44 presents the entire two-day time evolution of ozone and $PM_{2.5}$ concentrations in Riverside and Los Angeles. In the realistic scenario #R1, ozone concentrations are not affected significantly at either location. Impacts on $PM_{2.5}$ concentrations are more significant in Riverside than Central Los Angeles (Figure 44). Differences in $PM_{2.5}$ concentrations in Riverside reach values of ± 5 $\mu g/m^3$. Major changes in $PM_{2.5}$ at Riverside are due to available nitric acid transported from central areas and local ammonia emissions. Both species combine and form secondary particulate matter.

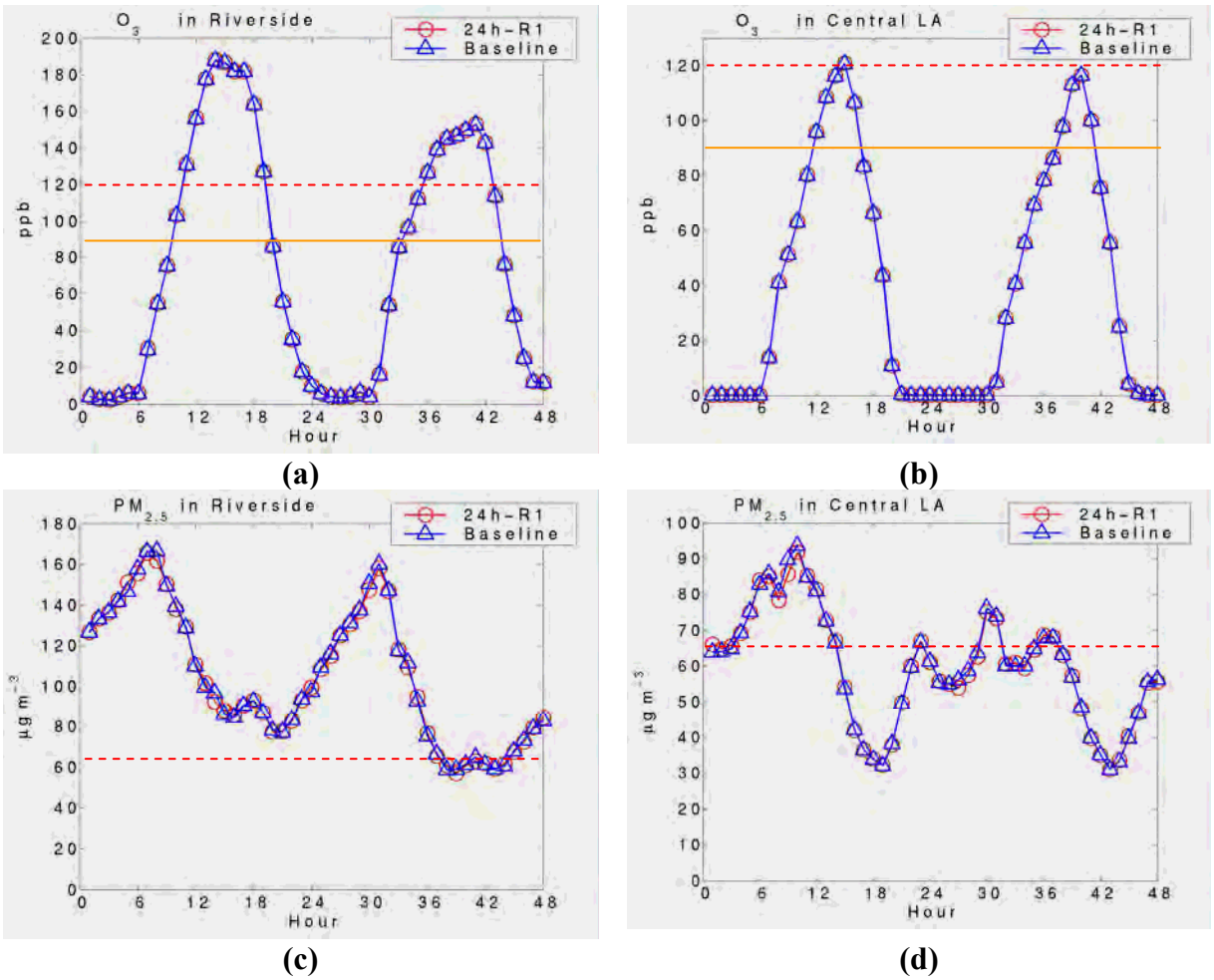

Figure 44. Impact on O_3 (in ppb) and $PM_{2.5}$ (in $\mu g/m^3$) concentrations at two different locations during the second and third day of simulation (Δ Base, O #R1, Federal standard: red discontinuous line, State standard: orange line): (a) O_3 at Riverside, (b) O_3 at Central LA, (c) $PM_{2.5}$ at Riverside, and (d) $PM_{2.5}$ at Central Los Angeles

Appendix H presents the two-day time evolution of $PM_{2.5}$, NO_2, and O_3 for all of the DG scenarios investigated in this study for six locations in the SoCAB: (1) central Los Angeles, (2) Riverside, (3) San Bernardino, (4) Long Beach, (5) Burbank, and (6) Simi Valley. These results are presented in Appendix H for completeness. Note that the differences between the two-day time evolution of the baseline case and any DG scenario case are typically small enough that it is difficult to discern from the time series (as in Figure 44 above).

Figure 45 and Figure 46 show the effects of an increase in DG market penetration on ozone and $PM_{2.5}$ concentrations, respectively. Maximum changes in ozone concentration range from -9 to +5 $\mu g/m^3$ in all three scenarios (#R1, #R2, and #R3) (Figure 45). In addition, increases of 2–3 ppb in ozone concentration occur at near Riverside, where ozone levels exceed air quality standards. However, due to progressively higher DG penetration in #R2 and #R3, the area in which ozone concentrations are impacted becomes larger. The effects in $PM_{2.5}$ concentrations produced by increasing DG penetration are less evident than the effects in ozone concentrations (compare Figure 46 for $PM_{2.5}$ to Figure 45 for ozone).

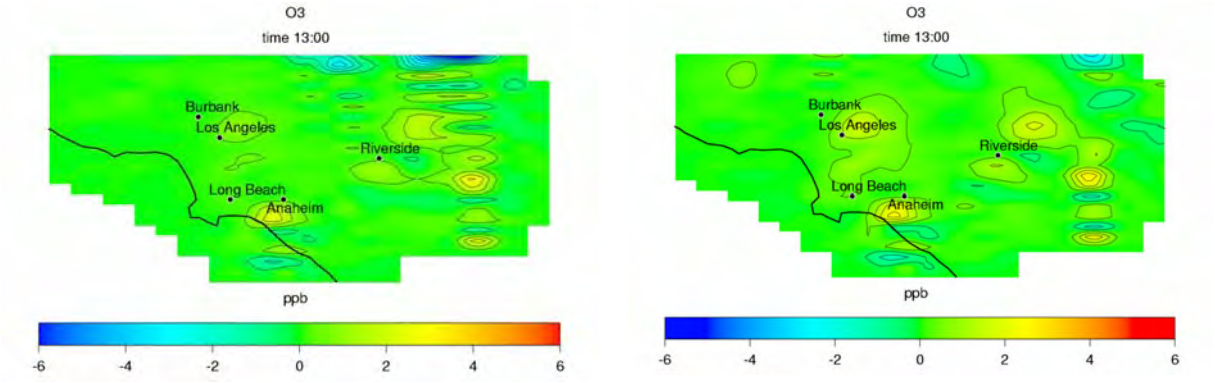

Figure 45. Effect of DG penetration on O_3 concentration (in ppb) at hour 1300: (a) #R2, 10% of increased power demand met by DG, (b) #R3, 20% of increased power demand met by DG

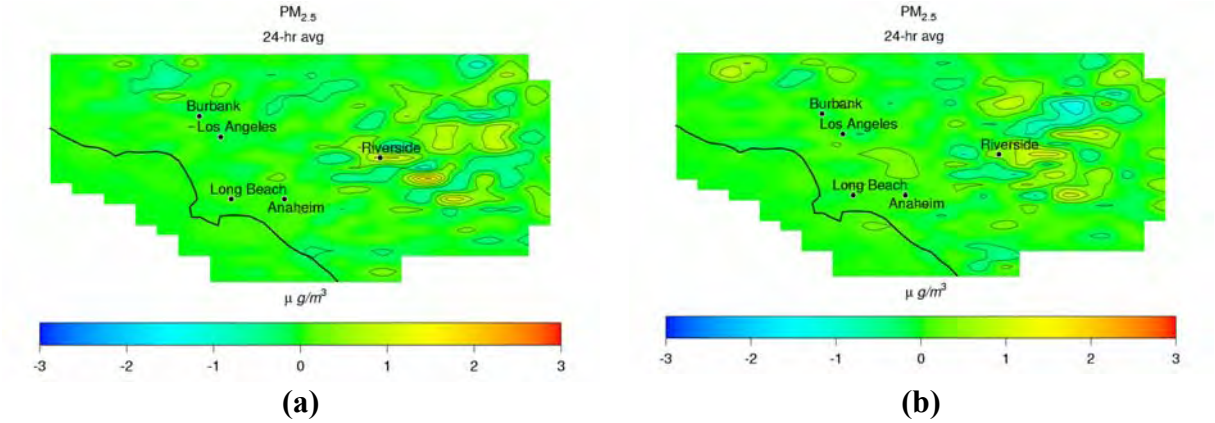

Figure 46. Effect of DG penetration on 24-hour average $PM_{2.5}$ concentration (in $\mu g/m^3$): (a) #R2, 10% of increased power demand met by DG, (b) #R3, 20% of increased power demand met by DG

Similar impacts on $PM_{2.5}$ concentration are observed for all five realistic scenarios. None of the changes among the realistic scenarios significantly changes the impact of DG on $PM_{2.5}$ concentrations in the SoCAB. As a matter of fact, the majority of all DG scenarios did not show significantly differing impacts of DG emissions on the ground-level distribution of $PM_{2.5}$. As a result, $PM_{2.5}$ plots are included in the body of this report only for cases in which the $PM_{2.5}$ impacts of DG emissions vary from the trend presented in Figure 46. Otherwise, plots of ground level 24-hour average $PM_{2.5}$ that result from all of the DG scenarios investigated in this study are presented in Appendix I (for completeness).

Realistic scenario #R4 introduces slightly lower emissions than #R1 (Figure 47a). As a result, impacts in both ozone and $PM_{2.5}$ concentrations are very similar. Realistic scenario #R5 does not account for emissions displacement, and therefore, NO_X emissions increase. This increase in NO_X emissions, which occur mainly in the central area of the basin, leads to slight reductions in ozone concentrations at hour 1300 (Figure 47b). This decrease is due to the characteristic high NO_X/VOC ratio in the Los Angeles area. In this region, ozone production is "VOC limited,"

thus, the increase in NO_X emissions produced by DG leads to a reduction in ozone concentrations. Nevertheless, impacts on ozone concentration are small.

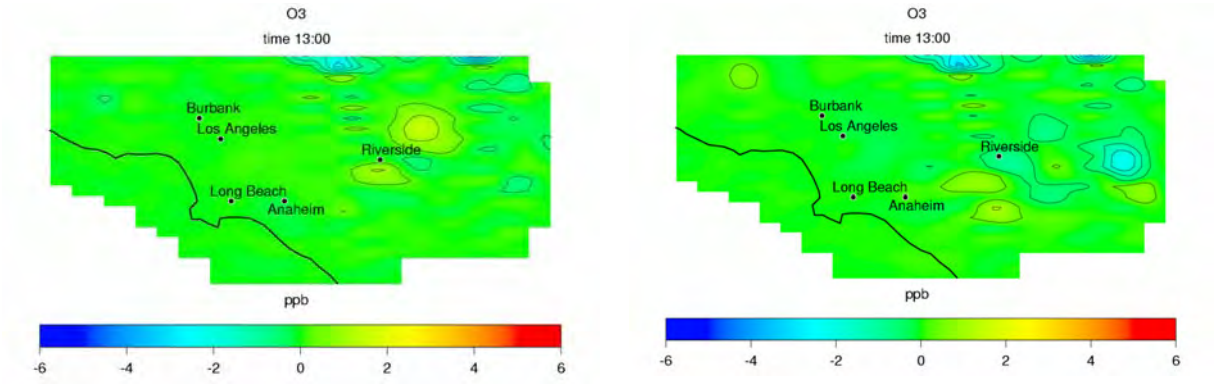

(a) **(b)**

Figure 47. Impact on O_3 concentration (in ppb) at hour 1300: (a) #R4 - Base, (b) #R5 – Base

3.4.2 Air Quality Impacts of Spanning DG Scenarios

The aim of simulating spanning scenarios is to set bounds for the air quality impacts of DG. These scenarios are not meant to represent likely future installations of DG in the SoCAB. However, results from the investigation of spanning scenarios can provide insights into the sensitivity of the results to our assumptions for realistic scenarios, insights into scenarios that are unexpected, and/or estimates of air quality impacts produced in years beyond 2010. Table 48 presents a summary of the key features of each of the spanning DG implementation scenarios.

Most of the spanning DG implementation scenarios assume that distribution of DG throughout the SoCAB is proportional to population density. To determine the effects of DG allocation on air quality impacts, three scenarios have been developed to take into consideration other types of distribution: PGW2010 assumes DG distribution proportional to the population growth from 2000 to 2010; LUW20% assumes a distribution based on land-use data similar to #R3, but it does not estimate the DG mix in each cell based on land use, and it does not account for emission displacement, nor for duty cycles; and Free20% considers a DG distribution proportional to freeway density.

All scenarios except for EHP, TDPW10, BAU, and BAU_par, assume that a 20% of the increased demand from 2002 to 2010 will be met by DG. TDPW10% considers a DG penetration of 10% of the increased power demand (this scenario introduces the lowest emissions from DG among spanning scenarios, except for NO_X, since no CHP was considered). EHP assumes that DG supply 20% of the total electricity demand. In BAU and BAU_par, linear and parabolic extrapolation of the market actual evolution during 2001 and 2002 is applied to calculate DG penetration and technology mix. Scenarios PeakPW, PeakPW-2, and TDPW10% are the only spanning scenarios that account for duty cycles. For the remaining spanning scenarios, DG units are set to operate constantly, 24 hours a day. Finally, different technology mixes are considered, including scenarios in which only fuel cells, MTG, gas turbines, or ICE permitted under BACT criteria are operated exclusively (scenarios FCPW20%, MTGPW20%, LDG20% and PermICEPW, respectively).

Table 48. Summary of the key features of the spanning scenarios

#	DG Scenario	Penetration	Distribution	Technology Mix
1	**PW2010**	20% inc.	PW[a]	30% GT, 30% ICE, 25% MTG, 7% FC, 8% PV
2	**2003ES**	20% inc.	PW	100% 2003 CARB Standards
3	**2007ES**	20% inc.	PW	100% 2007 CARB Standards
4	**PermICEPW**	20% inc.	PW	100% Permitted ICE (BACT)
5	**HEAPW20%**	20% inc.	PW	30% GT, 30% ICE, 25% MTG, 7% FC, 8% PV
6	**PeakPW**	20% inc.	PW	35% GT, 35% ICE, 30% MTG
7	**LDG20%**	20% inc.	HIA[b]	100% GT
8	**NH3_20%**	20% inc.	HIA	100% GT
9	**PGW2010**	20% inc.	PGW[c]	30% GT, 30% ICE, 25% MTG, 7% FC, 8% PV
10	**LUW20%**	20% inc.	LUW[d]	30% GT, 30% ICE, 25% MTG, 7% FC, 8% PV
11	**Free20%**	20% inc.	FreeW[e]	30% GT, 30% ICE, 25% MTG, 7% FC, 8% PV
12	**FCPW20%**	20% inc.	PW	100% FC
13	**MTGPW20%**	20% inc.	PW	100% MTG
14	**DGCHP**	20% inc.	PW	30% GT, 30% ICE, 25% MTG, 7% FC, 8% PV
15	**DGEED**	20% inc.	PW	35% GT, 35% ICE, 30% MTG
16	**TDPW10%**	10% inc.	PW	34% ICE, 46% MTG, 10% FC, 10% PV
17	**BAU**	Linear	PW	28% ICE, 4% MTG, 1% FC, 15% PV, 52% GT
18	**EHP**	20% Total	PW	30% GT, 30% ICE, 25% MTG, 7% FC, 8% PV
19	**BAU_par**	Parabolic	PW	28% ICE, 4% MTG, 1% FC, 15% PV, 52% GT
20	**HPD**	20% inc.	PW	30% GT, 30% ICE, 25% MTG, 7% FC
21	**PeakPW-2**	20% inc.	PW	35% GT, 35% ICE, 30% MTG

[a] PW – Population-based distribution for all DG except for GT. GT are distributed in areas with high industrial activity.
[b] HIA – Distribution following highly industrialized areas
[c] PGW – Population growth-based distribution for all DG except for GT. GT are distributed in areas with high industrial activity.
[d] LUW – Land-use-based distribution
[e] FreeW – Freeway density-based distribution

Table 49, Table 50, Table 51, and Table 52 show the summary criteria pollutant results for the simulation of the spanning DG implementation scenarios. The domain-wide maximum concentration and the maximum change in the concentration of ozone, NO_2, and $PM_{2.5}$ are presented in Table 49, Table 50, and Table 51, respectively. Table 52 presents the domain-wide

maximum 24-hour $PM_{2.5}$ concentration and the maximum change in such for each of the spanning scenarios. Table 49 shows that maximum basin-wide ozone concentration in scenarios 2003ES, HEAPW20, BAU_par, PeakPW2, and EHP increases by 1 ppb, suggesting an impact on compliance with ozone standards (even though the impact is small). On the other hand, simulation of scenario LDG20 results in a decrease in maximum basin-wide ozone concentration of 1 ppb. For the other spanning scenarios, maximum basin-wide ozone concentration remains unchanged. For the majority of DG scenarios, the largest differences between DG scenario and baseline ozone concentrations at any time and in any place throughout the basin range from -8 to +8 ppb. In half of the scenarios, maximum increases in ozone concentration occur in areas where baseline ozone concentrations are below the California Ambient Air Quality Standard (CAAQS, 90 ppb); whereas, the rest of scenarios exhibit maximum increases where baseline ozone concentrations already exceed the CAAQS. On the other hand, maximum decreases in ozone concentration occur mainly in areas and hours where baseline ozone concentration is low. Maximum concentration of NO_2 remains unchanged in all spanning scenarios except for scenario PeakPW2, in which NO_2 peak concentration increases by 1 ppb. Changes in 1-hour average maximum $PM_{2.5}$ concentrations range from -1 to +1 $\mu g/m^3$.

Table 49. Summary of impacts on O_3 concentration for all spanning DG scenarios: Maximum hourly average O_3 concentration, maximum increase and decrease in hourly average O_3 concentration, and baseline (reference) hourly average O_3 concentration where maximum differences occur

Scenario	Max (ppb)	time	Max Increase (ppb)	Baseline reference (ppb)	Time, Max Increase	Max Decrease (ppb)	Baseline reference (ppb)	Time, Max Decrease
PW2010	238	13	4	46	13	-3	5	5
2003ES	239	13	6	100	13	-4	12	6
2007ES	238	13	5	100	13	-7	66	11
PermICEPW20	238	13	7	100	13	-3	12	6
HEAPW20	239	13	6	100	13	-3	5	5
PeakPW	238	13	5	100	13	-13	24	5
LDG20	237	13	8	46	11	-7	66	11
NH3-20	238	13	3	73	12	-7	66	11
PGW20	238	13	6	108	14	-2	5	5
LUW20	238	13	5	134	13	-3	5	5
Free20	238	13	6	89	12	-3	54	22
FCPW20	238	13	3	53	12	-1	146	12
MTGPW20	238	13	5	89	12	-2	90	13
DGCHP	238	13	4	134	13	-2	60	12
DGEED	238	13	34	7	22	-14	73	14
TDPW10	238	13	5	89	12	-2	60	12
BAU	238	13	4	134	13	-4	146	12
EHP	239	13	8	46	14	-8	15	6
BAU_par	239	13	6	108	14	-7	66	11
HPD	238	13	6	100	13	-3	5	5
Peak_2	239	13	8	10	2	-26	29	2

For most scenarios, maximum hourly changes in NO_2 concentrations fall within the range of ±10 ppb (Table 50). Only scenarios PeakPW and PeakPW_2 produce larger increases, of up to 14 ppb and 30 ppb, respectively, and scenario DGEED produces larger decreases of up to -39 ppb. None of these changes imply an impact of DG installation on air quality that would affect SoCAB compliance with NO_X air quality standards. Nonetheless some of these changes are very significant, especially when considering the small amount of emissions that DG introduces into the basin.

Maximum hourly changes in $PM_{2.5}$ concentration, presented in Table 51, range from –27 $\mu g/m^3$ to +23 $\mu g/m^3$. However, the maximum changes in 24-hour average $PM_{2.5}$ concentrations (Table 52) are on the order of -4 to +6 $\mu g/m^3$ for all of the spanning DG implementation scenarios. This is a significant change that could impact SoCAB compliance with air quality standards if a scenario would emerge that is well represented by these spanning scenarios (especially the EHP and Peak_2 spanning scenarios, which introduce the most concentrated DG emissions).

Table 50. Summary of impacts on NO_2 concentration for all spanning DG scenarios: Maximum hourly average NO_2 concentration, maximum increase and decrease in hourly average NO_2 concentration, and baseline (reference) hourly average NO_2 concentration where maximum differences occur

Scenario	Max (ppb)	time	Max Increase (ppb)	Baseline reference (ppb)	Time, Max Increase	Max Decrease (ppb)	Baseline reference (ppb)	Time, Max Decrease
PW2010	158	5	3	29	5	-3	6	18
2003ES	158	5	5	31	6	-3	6	18
2007ES	158	5	2	49	6	-3	6	18
PermICEPW20	158	5	4	31	6	-3	6	18
HEAPW20	158	5	4	29	5	-3	6	18
PeakPW	158	5	14	9	5	-3	24	2
LDG20	158	5	6	13	6	-3	6	18
NH3-20	158	5	6	13	6	-3	6	18
PGW20	158	5	3	29	5	-3	6	18
LUW20	158	5	3	29	5	-3	6	18
Free20	158	5	4	34	23	-3	6	18
FCPW20	158	5	2	61	5	-3	6	18
MTGPW20	158	5	2	49	6	-1	1	11
DGCHP	158	5	2	80	23	-3	6	18
DGEED	158	5	10	26	1	-39	45	23
TDPW10	158	5	2	80	23	-3	6	18
BAU	158	5	3	29	5	-4	46	1
EHP	158	5	9	2	5	-3	46	1
BAU_par	158	5	4	29	5	-3	6	18
HPD	158	5	3	29	5	-3	6	18
Peak_2	159	5	30	7	4	-8	24	2

Table 51. Summary of impacts on hourly $PM_{2.5}$ concentration for all spanning DG scenarios: Maximum hourly average $PM_{2.5}$ concentration, maximum increase and decrease in hourly average $PM_{2.5}$ concentration, and baseline (reference) hourly average $PM_{2.5}$ concentration where maximum differences occur

Scenario	Max ($\mu g\ m^{-3}$)	time	Max Increase ($\mu g\ m^{-3}$)	Baseline reference ($\mu g\ m^{-3}$)	Time, Max Increase	Max Decrease ($\mu g\ m^{-3}$)	Baseline reference ($\mu g\ m^{-3}$)	Time, Max Decrease
PW2010	248	3	18	54	7	-16	58	21
2003ES	248	3	17	54	7	-18	207	6
2007ES	249	3	16	100	8	-19	145	6
PermICEPW20	248	3	14	115	3	-16	68	18
HEAPW20	249	3	19	54	7	-15	112	6
PeakPW	248	3	17	54	7	-15	62	21
LDG20	247	3	17	54	7	-17	147	4
NH3-20	248	3	13	59	6	-27	137	3
PGW20	248	3	18	54	7	-22	108	5
LUW20	248	3	14	115	3	-21	106	8
Free20	249	3	14	56	4	-15	97	3
FCPW20	249	3	17	17	7	-18	122	1
MTGPW20	248	3	17	54	7	-16	105	5
DGCHP	248	3	17	54	7	-13	61	22
DGEED	249	3	14	104	3	-21	136	6
TDPW10	248	3	18	54	7	-22	207	6
BAU	248	3	17	17	7	-16	96	4
EHP	248	3	20	100	8	-14	34	7
BAU_par	248	3	14	104	3	-22	148	4
HPD	248	3	16	24	7	-20	132	7
Peak_2	249	5	23	100	8	-19	87	22

Table 52. Summary of impacts on 24-hour average $PM_{2.5}$ concentration for all spanning DG scenarios: Maximum 24-hour average $PM_{2.5}$ concentration, maximum increase and decrease in 24-hour average $PM_{2.5}$ concentration, and baseline (reference) 24-hour average $PM_{2.5}$ concentration where maximum differences occur

Scenario	Max ($\mu g\ m^{-3}$)	Max Increase ($\mu g\ m^{-3}$)	Baseline reference ($\mu g\ m^{-3}$)	Max Decrease ($\mu g\ m^{-3}$)	Baseline reference ($\mu g\ m^{-3}$)
PW2010	114	3	78	-1	90
2003ES	113	3	45	-2	67
2007ES	114	3	45	-4	81
PermICEPW20	114	2	82	-2	69
HEAPW20	117	3	39	-2	69
PeakPW	114	3	45	-2	83
LDG20	115	3	39	-2	94
NH3-20	113	2	39	-2	82
PGW20	115	3	39	-1	62
LUW20	115	3	45	-2	17
Free20	114	3	39	-2	55
FCPW20	115	2	64	-2	87
MTGPW20	114	3	59	-2	104
DGCHP	114	3	39	-2	79
DGEED	113	2	59	-4	81
TDPW10	114	3	39	-2	46
BAU	115	3	45	-2	104
EHP	115	4	45	-2	17
BAU_par	115	2	78	-2	17
HPD	114	2	39	-2	69
Peak_2	116	6	75	-2	14

In the following sections, results from simulating all of the spanning scenarios are compared within different subcategories that allow a parametric evaluation of air quality impacts. These subcategories are chosen to permit comparisons between cases in which specific parameters that describe a DG scenario are changed one at a time. The comparisons are based on the impacts on ozone concentration at hour 1300, when the maximum value occurs. In some other cases, differences in the formation of $PM_{2.5}$ are also highlighted.

3.4.2.1 Spatial distribution

Ozone and $PM_{2.5}$ are secondary pollutants. Hence, their formation in the atmosphere not only depends upon precursor emissions, but also on other physical and chemical processes, governed by meteorological parameters. As a result, formation of ozone and $PM_{2.5}$ is influenced by the location of emissions sources.

This section presents four scenarios—PW2010, PGW2010, LUW20, and Free20—in which the same technology mix and DG penetration is assumed. These four scenarios introduce the same total basin-wide emissions. The only parameter that is varied among these scenarios is the geographic distribution of DG throughout the basin.

Figure 48 shows the difference in O_3 concentration between simulations of each scenario and the baseline case at hour 1300. In general, there is an overall reduction in ozone concentration of less than 3 ppb in the central area of the basin (near Los Angeles), due to the already high NO_X/VOC ratio. On the other hand, ozone concentration increases by up to 6 ppb in some areas on the eastern part of the basin, downwind from the central area.

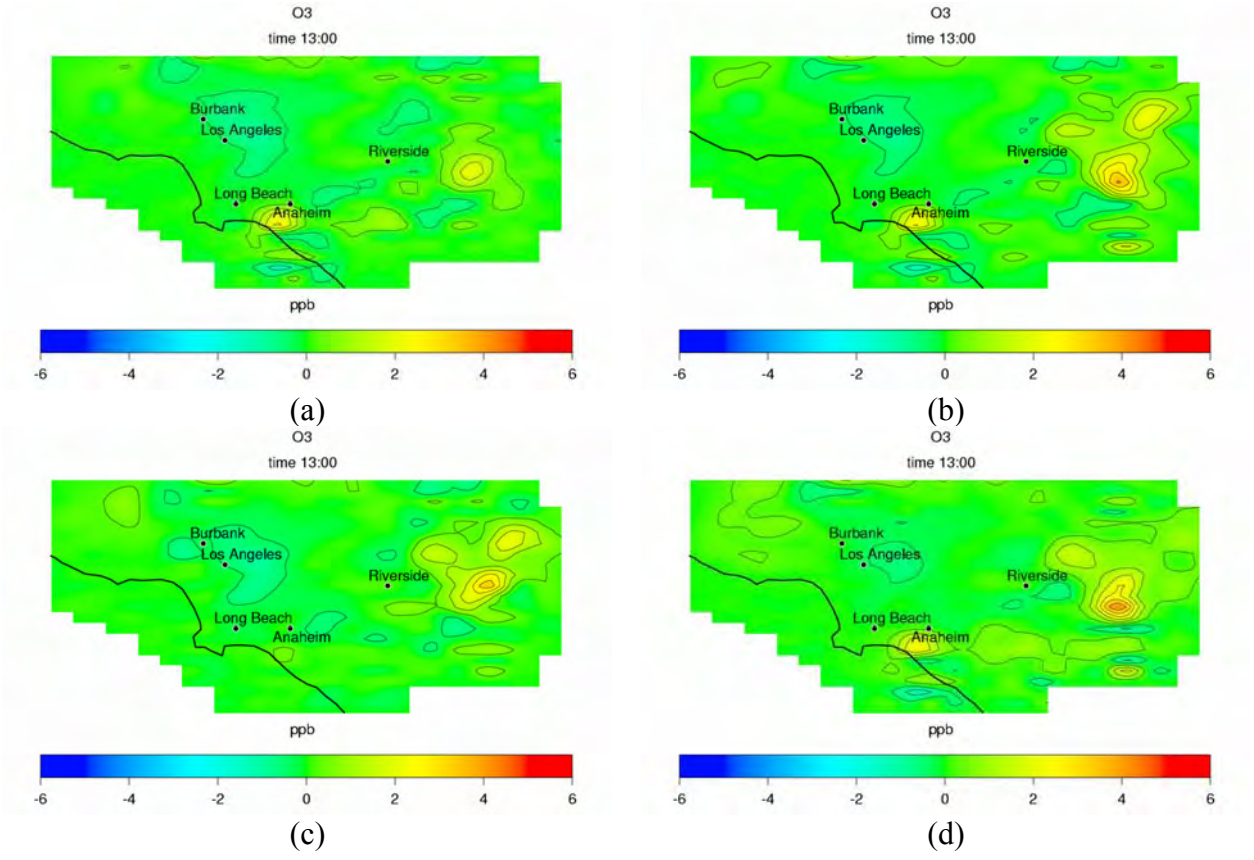

Figure 48. Difference in O_3 concentration (in ppb) at hour 1300 between DG scenarios and the baseline for scenarios: (a) PW2010, (b) PGW2010, (c) LUW20, and (d) Free20%

Although there are differences between these four scenarios, the results of Figure 48 show primarily that the level of emissions introduced by DG scenarios (0.37% of total NO_X, 0.13% of total VOC) consistently results in a similar and small ozone air quality impact. The different distributions of emission sources presented in Figure 48 show that scenario Free20% is the scenario with the highest impact. This scenario considers a distribution proportional to the freeway density. As shown in Figure 41, freeway density distribution is the one that concentrates DG emissions the most, leaving bigger areas in the basin free of DG. As a result, scenario Free20% produces higher increases in ozone concentration attributable to the spatial distribution.

The air quality impact of concentrating DG emissions in certain locations in the basin is a discernable feature revealed by the model in Figure 48 and in several other computational results. This is a significant result of the current effort, suggesting that attention should be paid to the spatial distribution of emissions in the basin. This result suggests that if DG is to be widely used in the basin, then it should not be concentrated in a small area. DG scenarios with a higher penetration will likely show an even more pronounced dependence upon spatial distribution.

3.4.2.2 CARB and SCAQMD standards

Three scenarios were developed to evaluate DG emission standards by assuming that all DG in the scenario emit pollutants at exactly the level of the standard. Scenarios 2003ES and 2007ES introduce DG technologies that emit at the level of the emission standards approved by CARB for the years 2003 and 2007. Scenario 2003ES introduces 2.3%, 0.93%, and 0.84% increases in CO, NO_X, and VOC emissions, respectively. Emission standards for 2007 are far more stringent, resulting in emission increases of 0.04%, 0.13%, and 0.02% for CO, NO_X, and VOC. Scenario PermICEPW20% assumes that all DG are internal combustion engines permitted by SCAQMD under current best available control technology (BACT) regulations. These three scenarios are compared with PW2010 in Figure 49.

In general, simulations of Figure 49 show a decrease in ozone concentrations in the central area, and an increase at downwind locations at hour 1300. As explained above, the primary difference between central areas and surrounding locations is with regard to VOC/NO_X ratios. Scenarios 2003ES and PermICEPW20 show increases in ozone concentrations up to 7 ppb at hour 1300. These impacts are bigger than the ones produced by scenarios PW2010 and 2007ES, due to the difference in emissions introduced by DG. Emission standards for the year 2007 are more stringent than standards applied in other scenarios. Hence, scenario 2007ES shows the lowest impacts on ozone.

Both decreases and increases in ozone concentrations throughout the basin become larger as NO_X emissions from DG increase. Among the four cases, scenario 2003ES presents the largest decrease in ozone concentration, since it introduces the largest NO_X emissions. Decreases due to scenario PermICEPW20 are very similar to the ones obtained by scenario 2003ES, because they introduce a similar percentage of NO_X emissions. Increases in downwind ozone, however, are the most significant for the PermICEPW20 case, which introduces the highest CO and VOC emissions levels in this comparison (see Figure 49).

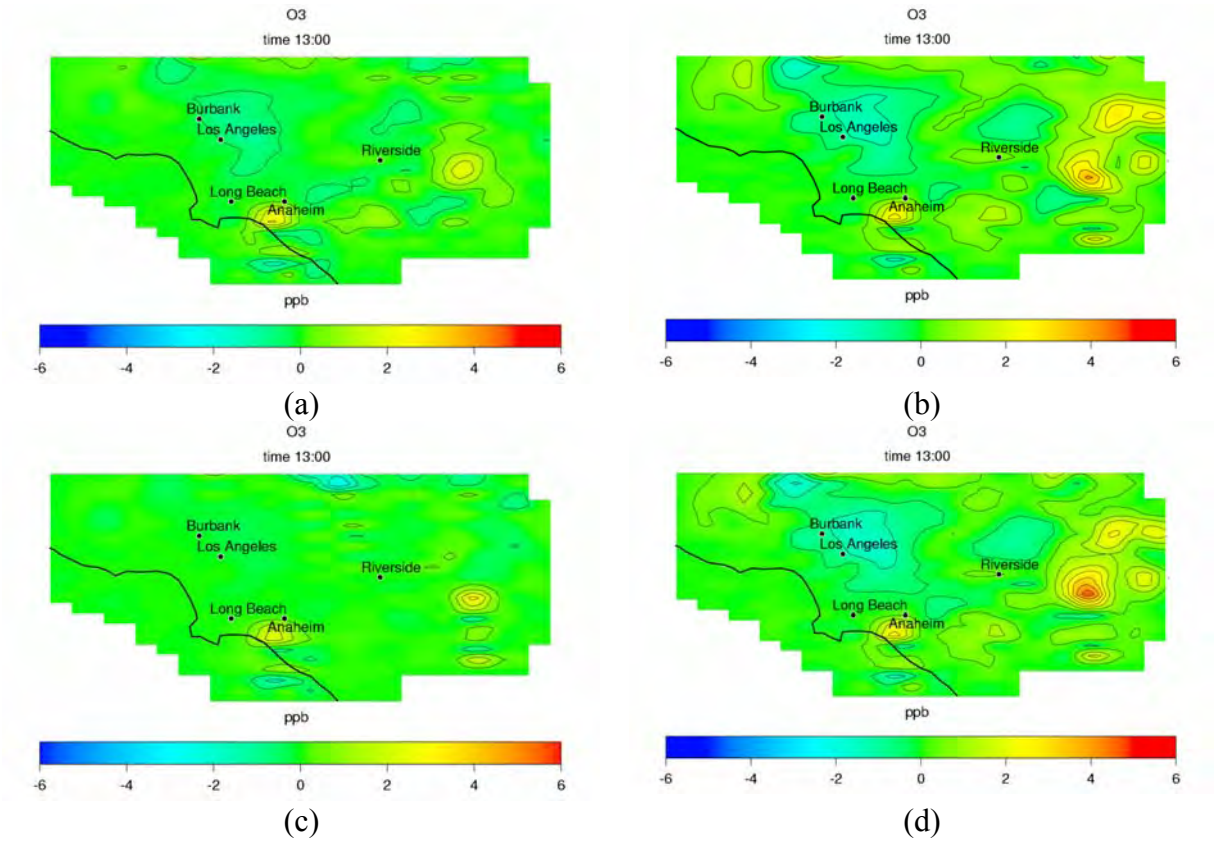

Figure 49. Difference in O_3 concentration (in ppb) at hour 1300 between DG scenarios and baseline: (a) PW2010, (b) 2003ES, (c) 2007ES, and (d) PermICEPW20%

3.4.2.3 Adoption curve of DG technologies

The adoption rate of DG technologies from 2002 to 2010 will affect the level of emissions by the end of this period. If DG is adopted with a high rate during the first years, they are not required to comply with more stringent emission standards in 2007. In addition, if a constant degradation rate of DG technologies is considered, emissions will increase as DG systems are adopted earlier. Scenario HEAPW20% assumes a high early adoption rate for DG deployment. Figure 50 presents the differences in air quality impacts between PW2010, a scenario with a low early DG adoption rate (98% of DG installed in the period 2007–2010) and HEAPW20% (a case with higher early adoption of DG).

Scenario HEAPW20% introduces 75% more NO_X, 13% more VOC, and 100% more CO emissions than scenario PW2010. As a result, impacts on ozone concentration in scenario HEAPW20% are more noticeable than the impacts observed for the PW2010 scenario. In particular, the decrease of ozone concentration near central Los Angeles is more widespread, and increases in ozone concentration are also bigger in the eastern part of the basin, in comparison to scenario PW2010. This is consistent with the previous finding and expectations that higher DG emissions rates lead to a larger ozone air quality impact. Whether this more significant impact on ozone will likely have a negative affect on compliance with air quality standards is a more

complicated question, since both increases and decreases in ozone are more significant with the increased DG emissions.

Some insight into this can be garnered from Table 49. Note that for both the PW2010 and HEAPW20 scenarios, the increases in ozone occur at locations with already higher ozone concentration, suggesting that the negative impact of emissions levels on ozone compliance is more likely. Note also, however, that the peak ozone concentrations are significantly higher than those in the regions where the maximum (positive and negative) impact is observed. Also, peak ozone concentration does not change significantly by the levels of DG emissions introduced in the current study. Finally, the authors caution that one should not draw general conclusions based only on the spanning DG scenario simulations of this effort.

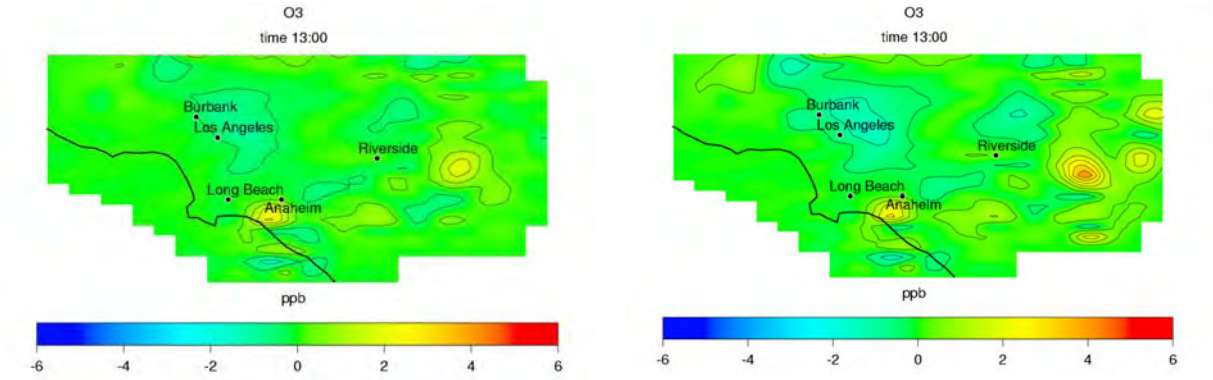

(a) (b)

Figure 50. Difference in O_3 concentration (in ppb) at hour 1300 between DG scenarios and baseline: (a) PW2010, and (b) HEAPW20%

3.4.2.4 Duty cycle

NO_X emissions in the SoCAB peak at rush hours during the morning and evening; whereas, VOC emissions are related to industrial activity. Nevertheless, NO_X and VOC emissions are high during the day and decrease dramatically at night. Scenarios PeakPW and PeakPW_2 assume that DG units operate for only six hours a day, from hour 1200 to 1800. Therefore, DG systems emit when baseline emissions are peaking. Scenario PeakPW considers that all DG installations have the capacity to supply 20% of the increased power demand from 2002 to 2010. Scenario PeakPW_2 assumes that, in six hours of operation, the amount of energy supplied by DG is the same amount supplied by DG in Scenario PW2010 during the 24 hours of base-load mode. Thus, DG power capacity in Scenario PeakPW_2 is four times higher than in PW2010. The energy supplied by DG in scenario PeakPW_2 is four times the electricity supplied by DG in scenario PeakPW. Both scenarios consider that emissions from DG at the first hour of operation are three times the normal emissions, due to the start-up process. Figure 51 presents a comparison between the impacts on ozone concentrations produced by a scenario in which all DG are base-loaded, and the two scenarios in which DG units are peaking six hours a day.

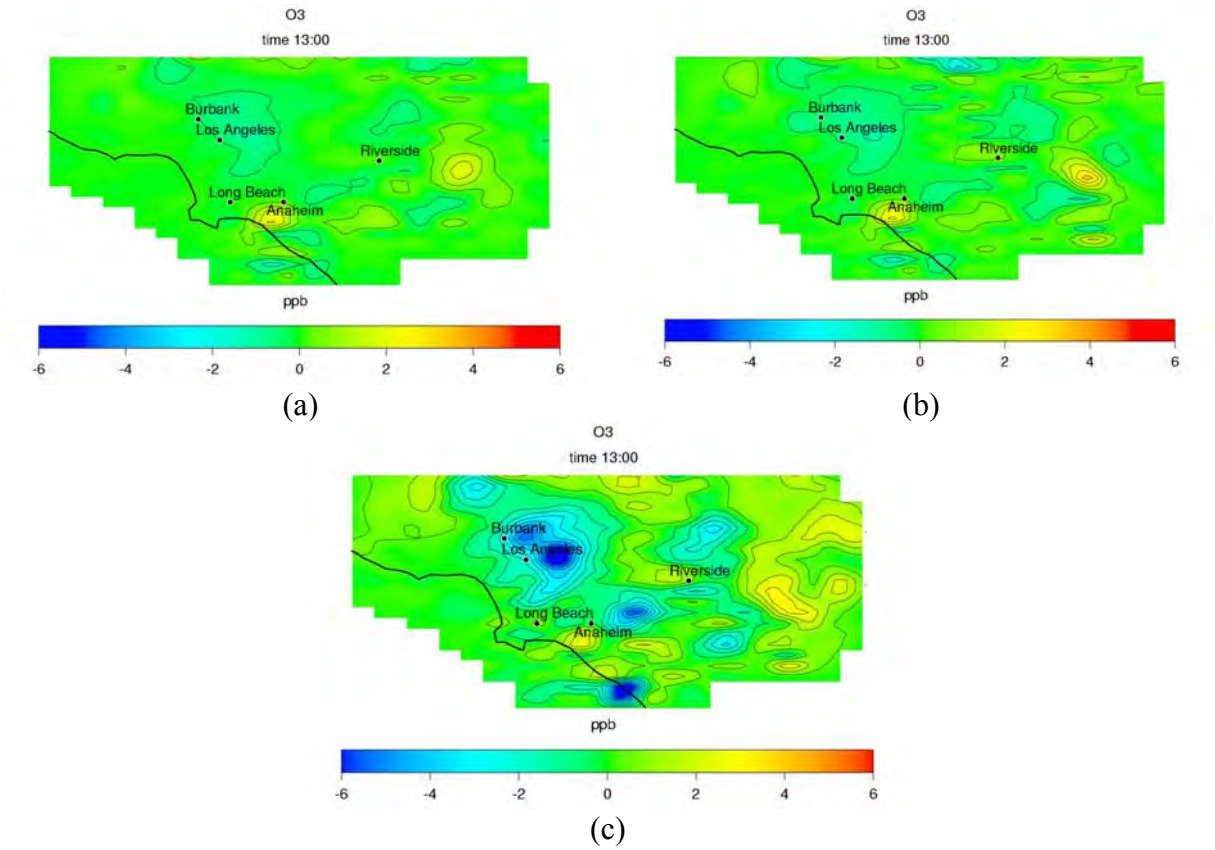

Figure 51. Difference in O_3 concentration (in ppb) at hour 1400 between DG scenarios and baseline: (a) PW2010, (b) PeakPW, and (c) PeakPW_2

Although Scenario PeakPW introduces lower emissions than PW2010, it produces similar changes on ozone concentration. Therefore, when the same amount of total emissions is considered, ozone concentrations are affected more significantly if emissions rates increase during the day (when ozone production is significantly higher), or are concentrated in time. Scenario PeakPW_2 introduces approximately four times the DG emissions of scenario PeakPW. It is observed that larger decreases in ozone concentration occur in the central area of the basin.

It should be noted that NO_X emissions in scenario PeakPW_2 are 20% lower than those of scenario 2003ES. However, impacts on ozone concentration—both increases and decreases—are more pronounced in scenario PeakPW_2 and ozone concentrations increase by up to 4 ppb over downwind locations in the eastern portion of the basin. In conclusion, if the same emissions are introduced, scenarios that concentrate emissions based on afternoon duty cycles have the potential to impact ozone concentrations more significantly, compared to cases in which emissions are introduced constantly during 24 hours. Both reductions in the central part of the basin and increases in downwind locations are more significant when emissions are concentrated in time.

3.4.2.5 Large scale DG/ammonia slip

Scenario LDG20% assumes that all DG units are large gas turbines. Because these units produce 49 MW of power, only 21 gas turbines are needed to supply the 20% of increased power demand from years 2002 to 2010. These 21 gas turbines are installed near industrialized regions.

NO_X emissions from gas turbines are typically controlled by selective catalytic reduction (SCR) of NO_X using ammonia introduced over a catalyst bed at a certain temperature. One consequence of this process is ammonia emissions (often called "ammonia slip") that result from excess ammonia used in the catalytic reaction. Ammonia is one of the gas-phase precursors involved in the formation of secondary particulate matter. Thus, the current effort developed spanning scenario NH3_20%, which has the same assumptions as scenario LDG20%, but with the inclusion of ammonia emissions from the SCR process at each of the 21 large (49 MW) plants installed in the SoCAB.

The locations of the 49 MW power plants are shown as red dots in Figure 52, which presents the difference in ozone concentration between (a) the LDG20% scenario and the baseline, and (b) the NH3_20% scenario and the baseline.

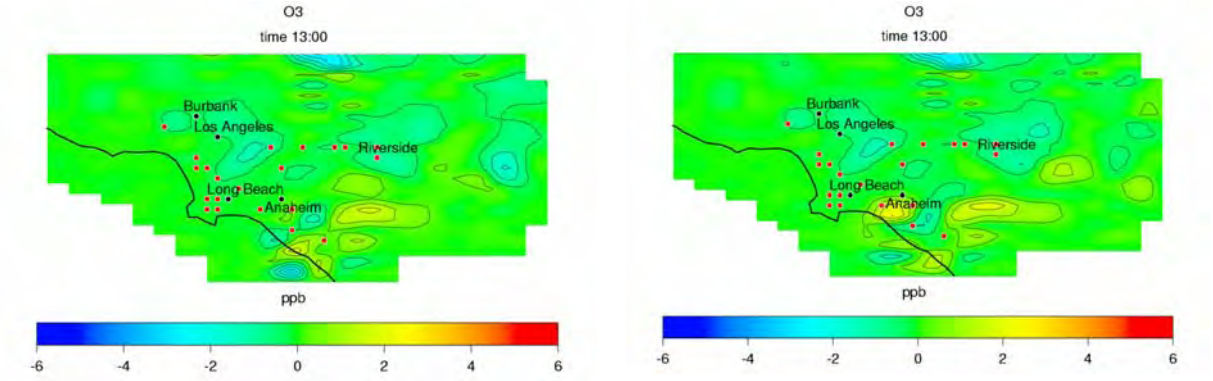

(a) (b)

Figure 52. Difference in O_3 concentration (in ppb) at hour 1300 between DG scenarios and baseline: (a) LDG20%, (b) NH3_20% (the red dots indicates the locations of large DG)

Figure 52 shows the impacts on ozone concentrations produced by both scenarios. Because emissions of ozone precursors (NO_X and VOC) are the same in both scenarios, ozone concentrations are affected similarly. Small differences are due to the reaction of nitric acid with the excess ammonia. This reaction consumes some nitric acid that would otherwise react with OH. This results in higher OH concentrations that are available to oxidize hydrocarbons present in the atmosphere to produce slightly more ozone in the NH3_20% case.

Figure 53 presents the difference in the 24-hour average concentration of $PM_{2.5}$ between the DG scenarios and the baseline. A priori, increase in ammonia emission would lead to an increase in $PM_{2.5}$ concentration. However, at the level of the emissions introduced in these two scenarios, differences between LDG20% and NH3_20% are very small.

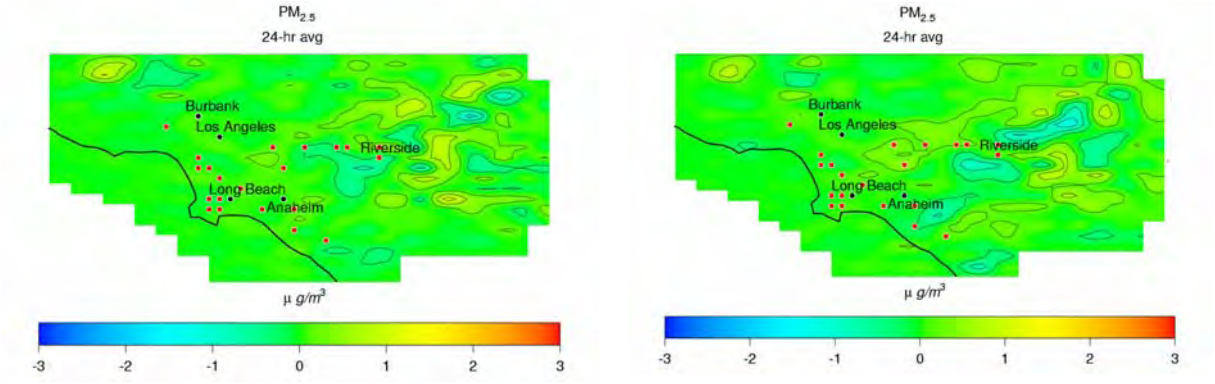

(a) (b)

Figure 53. Difference in $PM_{2.5}$ 24-hour average concentration (in $\mu g/m^3$) between DG scenarios and baseline: (a) LDG20%, (b) NH3_20%

3.4.2.6 DG technology mix

Emissions levels from DG implementation depend upon the types of DG technology considered. Fuel cells typically have the lowest emissions compared to the other combustion-driven DG technologies. This section presents the effects of DG technology types and mix of technology types.

Scenario FCPW20% assumes that all the DG power is supplied by fuel cells; whereas, scenario MTGPW20% considers that all the DG units are MTGs. Scenario NH3_20% assumes that all DG are relatively large (49MW) gas turbine power plants (21 total power plants). Scenario TDPW10% considers a DG technology mix that includes natural gas internal combustion engines, fuel cells, microturbine generators, and larger gas turbine power plants. Scenario TDPW10% introduces the lowest emissions of all spanning scenarios primarily because the power supplied by DG in this scenario is 10% of the increased power demand from 2002 to 2010.

Figure 54 shows the difference in O_3 concentration at hour 1300 between the DG scenarios (a) NH3_20%, (b) FCPW20%, (c) MTGPW20%, and (d) TDPW10% and the baseline case. Because the level of emissions introduced in the four cases is low relative to total basin-wide emissions, only small differences were observed regarding the impact of DG technology type on O_3 concentrations throughout the basin. For all cases, the impact of DG on ozone concentration is relatively low (between -2 and +3 ppb). Clearly, however, the fuel-cell-only case (Figure 54b) has the least significant impact on ozone concentrations, due to the very low emissions levels of these fuel cell systems. Note that the emissions from fuel cells in this case (FCPW20%) are based on natural gas operation and include total system emissions (i.e., all emissions from the fuel cell and natural gas reformation processes).

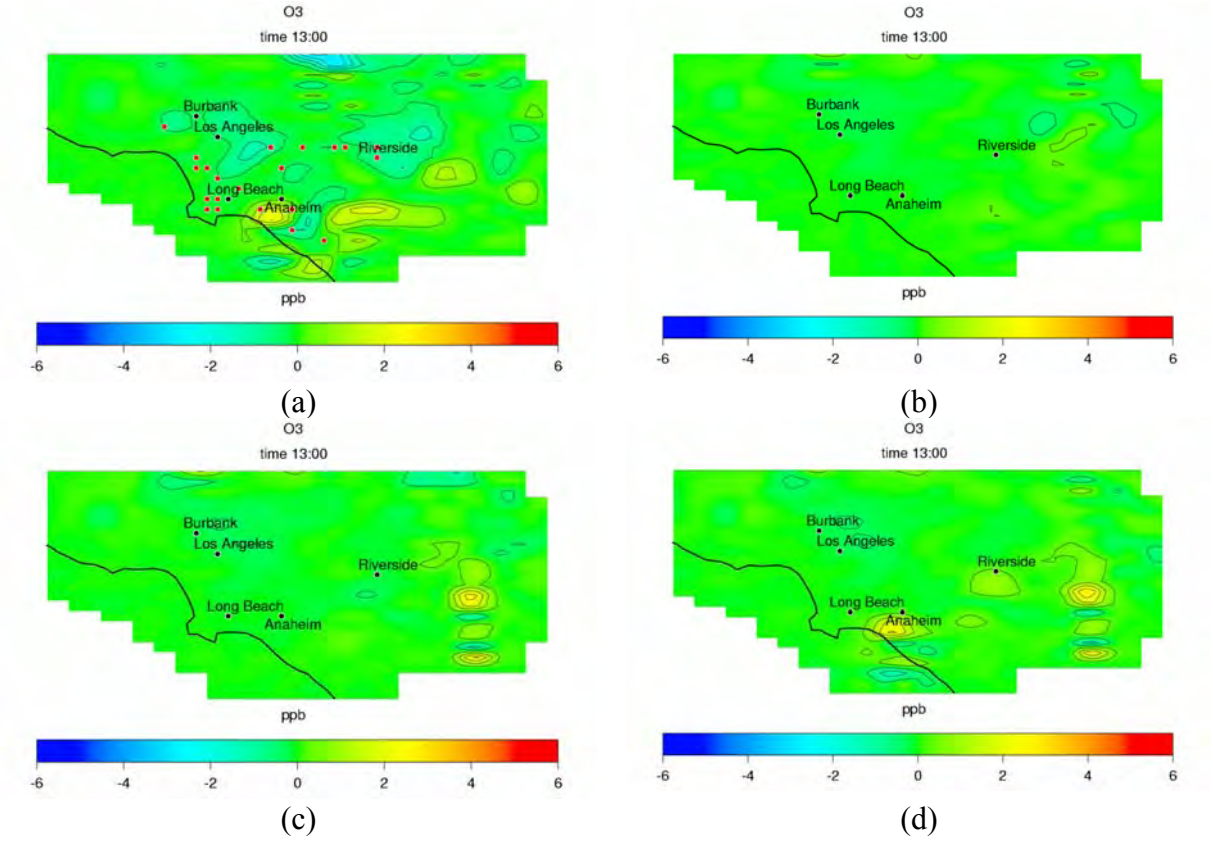

Figure 54. Difference in O_3 concentration (in ppb) at hour 1300 between DG scenarios and baseline: (a) NH3_20%, (b) FCPW20%, (c) MTGPW20%, (d) TDPW10%

3.4.2.7 Emissions displacement due to CHP

The use of CHP in combination with DG increases the overall efficiency of electricity production. In addition, CHP eliminates the need for a heat source (i.e., a boiler) for domestic water and heating, and therefore reduces emissions of pollutants. Scenario DGCHP examines the effects of CHP on air quality. This scenario makes the same assumptions as scenario PW2010, but it also accounts for emissions displacement due to CHP.

NO_X emissions in scenario DGCHP are 50% lower than scenario PW2010; whereas, VOC emissions are reduced by 25%. As in previous cases, a reduction in emissions leads to smaller decreases in ozone concentration in the central areas, and to smaller increases in ozone concentrations in the surrounding areas of the basin (Figure 55).

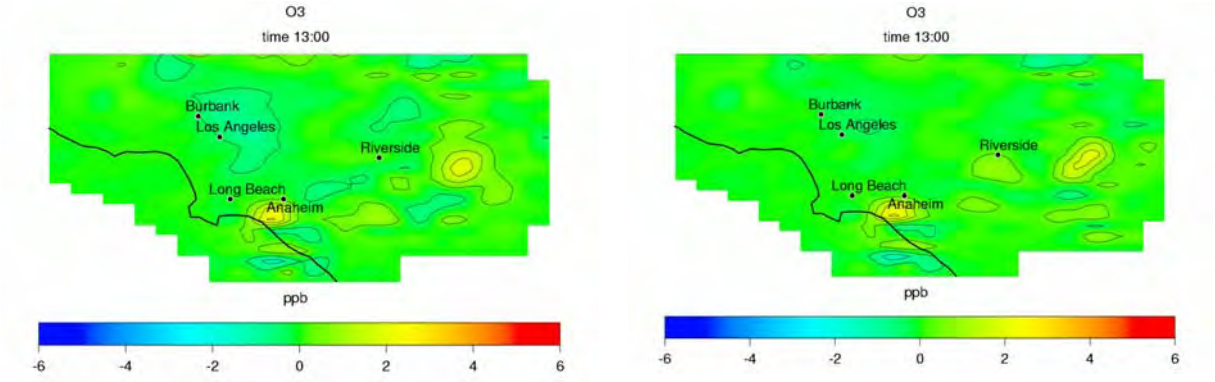

(a) (b)

Figure 55. Difference in O_3 concentration (in ppb) at hour 1300 between DG scenarios and baseline: (a) PW2010, and (b) DGCHP

3.4.2.8 In-basin large power plants displaced by DG

Implementation of DG most likely will help meet a portion of the new power demand, and will not displace any of the existing in-basin central power plants. Nevertheless, a scenario is presented to explore this possibility. The DGEED scenario assumes the same DG penetration and technology mix assumed in the PW2010 scenario. In addition, two central natural gas-fired power plants, one in Long Beach another in Huntington Beach, are turned off. As a result, net emissions of NO_X and VOC introduced by scenario DGEED are 65% and 85% lower than the net emissions introduced by scenario PW2010.

Figure 56 shows how the impact on ozone concentrations in scenario DGEED differs from PW2010. Although scenario DGEED has NO_X and VOC emissions levels similar to those of scenario FCPW20%, impacts on ozone concentrations are different. This difference is a consequence of a localized reduction in emissions at two coastal cells. The power plant near Long Beach is upwind from an area in which NO_X emissions are very high (wind blows from southwest). Decreasing NO_X in this VOC-limited area increases ozone concentration slightly near Long Beach. The power plant located in Huntington Beach is close to areas with less intense NO_X emissions than those in central Los Angeles. Therefore, a decrease in NO_X emissions in this area produces a decrease in ozone concentrations at locations downwind from the power plant. In addition, offshore wind circulation produces localized decreases in ozone concentration along the southern part of the coast. Although large changes in ozone concentration occur in localized areas, peak ozone concentration in scenario DGEED is equal to the baseline peak.

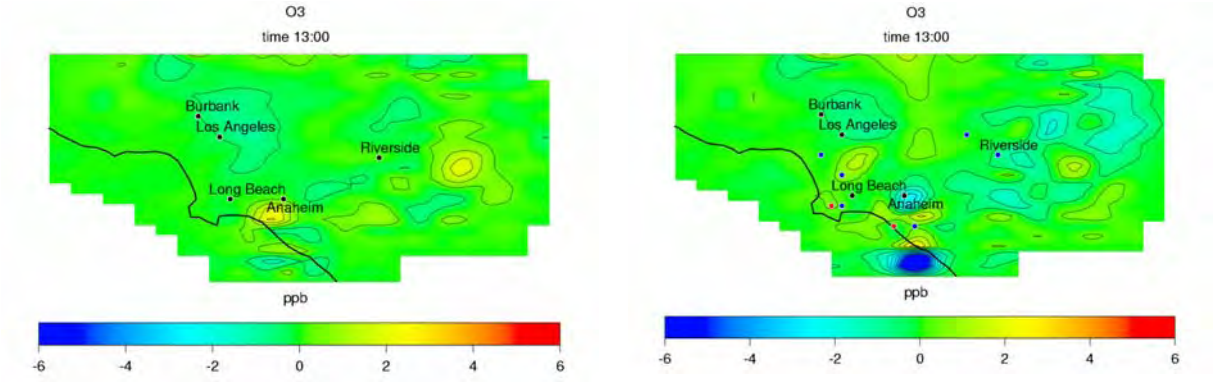

(a) (b)

Figure 56. Difference in O_3 concentration (in ppb) at hour 1300 between DG scenarios and baseline: (a) PW2010, (b) DGEED (red dots represent the two power plants; blue dots represent the large GT installed)

On the other hand, the maximum increase in ozone concentration in scenario DGEED is 34 ppb. These large increases occur at night and next to the power plant located in Huntington Beach. This is due to a highly localized decrease in NO_X emissions in this location. NO_X at night acts as an important sink for ozone. Thus, a localized decrease in NO_X emissions leads to localized increases in ozone concentration. However, such increases do not occur during the day, since baseline emissions are significantly larger.

3.4.2.9 Business-as-usual predictions

The specific mix of DG technologies that is likely to be installed in the SoCAB in 2010 is very difficult to forecast. This technology mix depends on the number and type of energy customers in the region, and a host of other economic and regulatory variables (e.g., electricity prices, gas prices, DG incentives, transmission constraints, emissions standards). Two scenarios have been developed to account for the current trends in DG technology adoption. Scenario BAU assumes a linear adoption of DG based on current data of DG penetration for each technology. Scenario BAU_par assumes a parabolic increase in the rate of adoption of DG technology. The emissions in scenario BAU end up being slightly lower than scenario PW2010; whereas, emissions in scenario BAU_par are approximately twice as large as the emissions in PW2010.

As in previous cases, the detailed simulation of these three scenarios as applied to the SoCAB in a state-of-the-art air quality model resulted in trends that are similar to those observed in most of the simulations. Figure 57 presents the difference in ozone concentrations between the DG scenarios (a) PW2010, (b) BAU, and (c) BAU_par, and the baseline case. Each of the three scenarios results in reduced ozone concentrations in the central areas and increased ozone concentrations over the eastern part of the basin. This trend has a larger and more widespread impact as emissions from DG increase (see Figure 57). Consistently observed trends such as these are perhaps the most certain results of the current effort, upon which the primary general conclusions of the study are based.

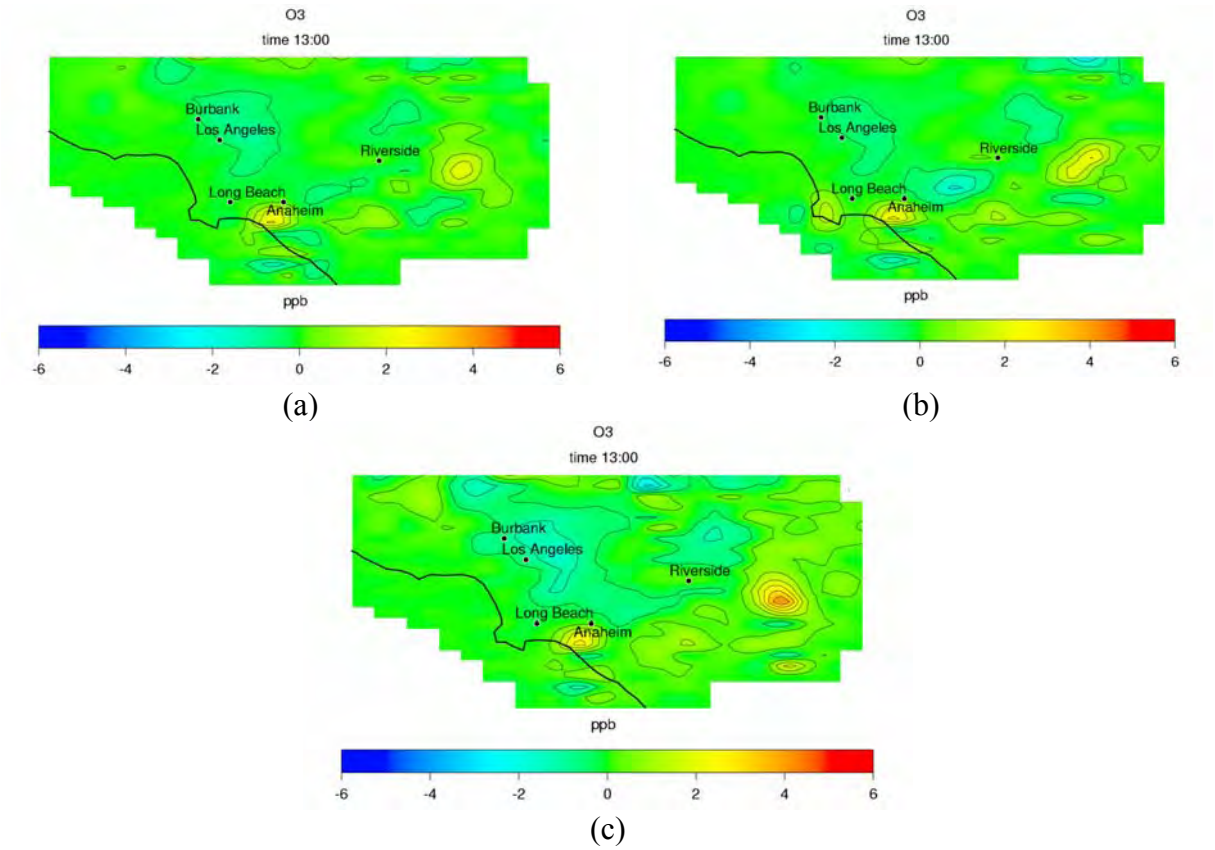

Figure 57. Difference in O_3 concentration (in ppb) at hour 1300 between DG scenarios and baseline: (a) PW2010, (b) BAU, and (c) BAU_par

3.4.2.10 DG penetration

Forecasts of DG market penetration by 2010 suggest that 20% of the increased power demand may be met by DG with high market penetration. However, socioeconomic factors might change the adoption of DG technologies in upcoming years. Scenario EHP assumes that 20% of the total energy demand will be supplied by DG, which is 5.5 times the DG power of scenario PW2010. EHP is the worst-case DG emissions scenario considered. Since scenario EHP uses the same DG technology mix as PW2010, emissions in EHP are 5.5 times larger than PW2010.

Figure 58 shows the difference in ozone concentrations at hour 1300 between (a) the PW2010, and (b) the EHP spanning scenarios and the baseline case. Results show the tendency to reduce O_3 in the central areas of the basin and to increase O_3 downwind. Since scenario EHP introduces the highest NO_X emissions, increases in ozone concentration at hour 1300 are the largest for this case. Also, the decrease in ozone over the central area is more pronounced in scenario EHP than for any scenario (except for PeakPW_2). Although total NO_X and VOC emissions of the EHP case are more than twice those of PeakPW_2, emissions of PeakPW_2 are concentrated in a six-hour time span. As a result, air quality impacts caused by scenarios EHP and PeakPW_2 are comparable, indicating the importance of both duty cycle and overall emissions levels. Certainly the high emissions of the EHP case (Figure 58b) lead to a more significant impact on ozone concentrations than the PW2010 case (Figure 58a).

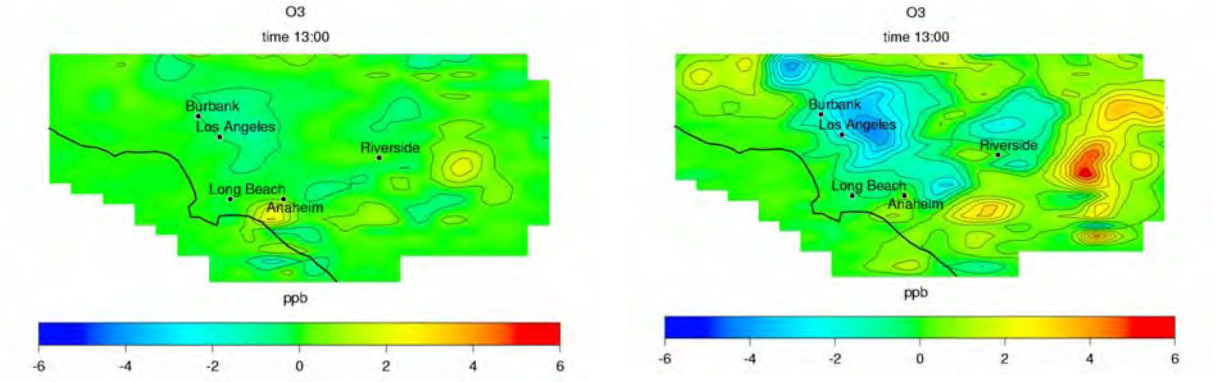

(a) (b)

Figure 58. Difference in O_3 concentration (in ppb) at hour 1300 between DG scenarios and baseline: (a) PW2010, and (b) EHP

Differences in 24-hour average $PM_{2.5}$ concentration between the baseline case and three different scenarios are shown in Figure 59. Scenario PeakPW_2 (Figure 59b) produces a larger impact on $PM_{2.5}$ concentration than the EHP scenario (Figure 59a), even though the EHP scenario has the highest emissions of all scenarios.

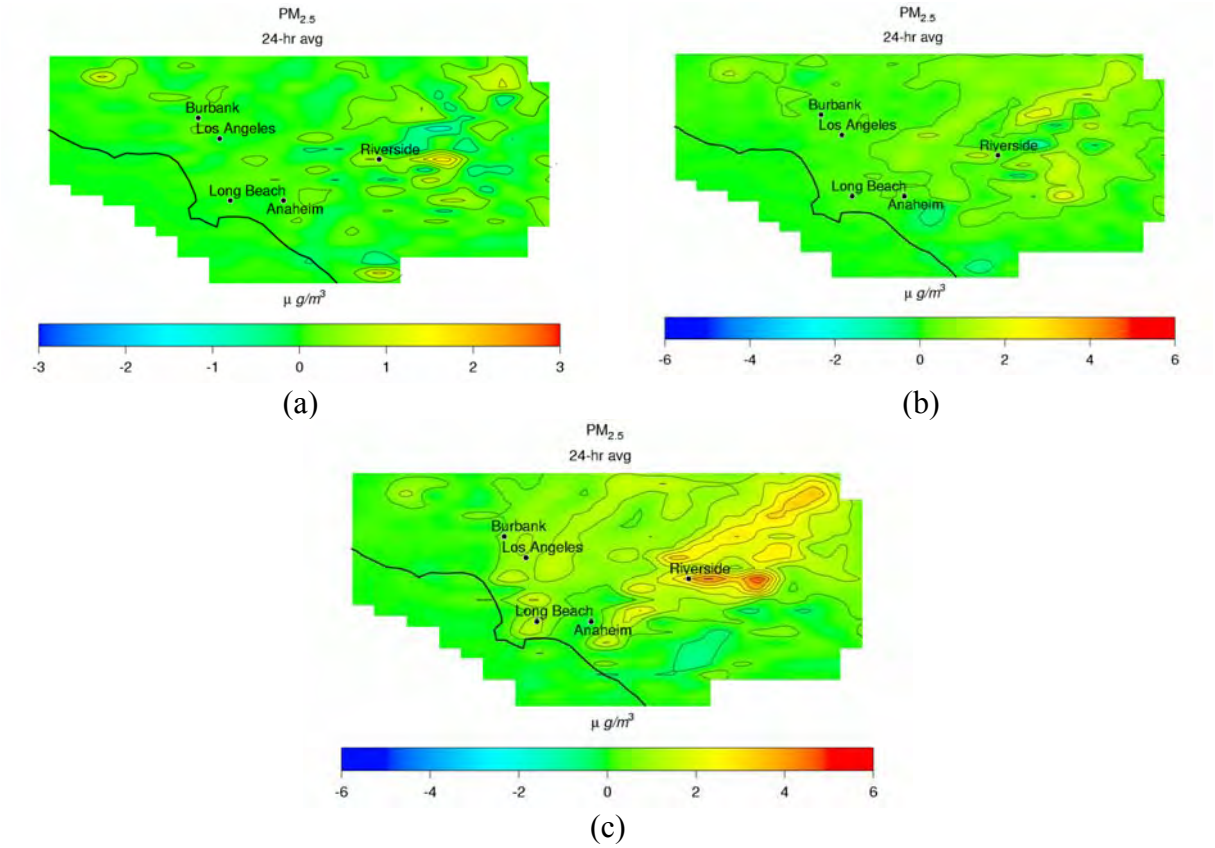

(a) (b)

(c)

Figure 59. Difference in $PM_{2.5}$ 24-hour average concentration (in $\mu g/m^3$) between DG scenarios and baseline: (a) PW2010, (b) EHP, and (c) PeakPW_2

In both scenarios (EHP and PeakPW_2) there is a net increase in $PM_{2.5}$ concentration over the eastern side of the basin, where nitric acid transported to this area from Los Angeles and ammonia emitted from cattle react to form secondary particulate matter. Scenario PeakPW_2 leads to a maximum increase in 24-hour average $PM_{2.5}$ concentration of 6 $\mu g/m^3$, being the largest increase among all the scenarios. Scenario EHP leads to a maximum increase in 24-hour average $PM_{2.5}$ concentration of 4 $\mu g/m^3$, the second largest increase among all the scenarios. As was the case for ozone concentration, operation of DG in a peaking duty cycle could impact secondary particulate matter formation much more significantly than if DG were operated constantly (base-loaded).

3.4.2.11 Performance degradation

Degradation of DG units with time produces an increase in emissions. Baseline degradation rate assumed for most of the scenarios is such that produces an annual 3% increase in emissions due to equipment degradation. Scenario HPD assumes a higher degradation rate, which causes an annual increase in emissions of 10%. The difference in the performance degradation implies that emissions introduced by scenario HPD are 13% higher than DG emissions assumed in scenario PW2010. Simulations show that small changes occur between scenarios regarding the impact on both ozone (Figure 60) and $PM_{2.5}$ concentration.

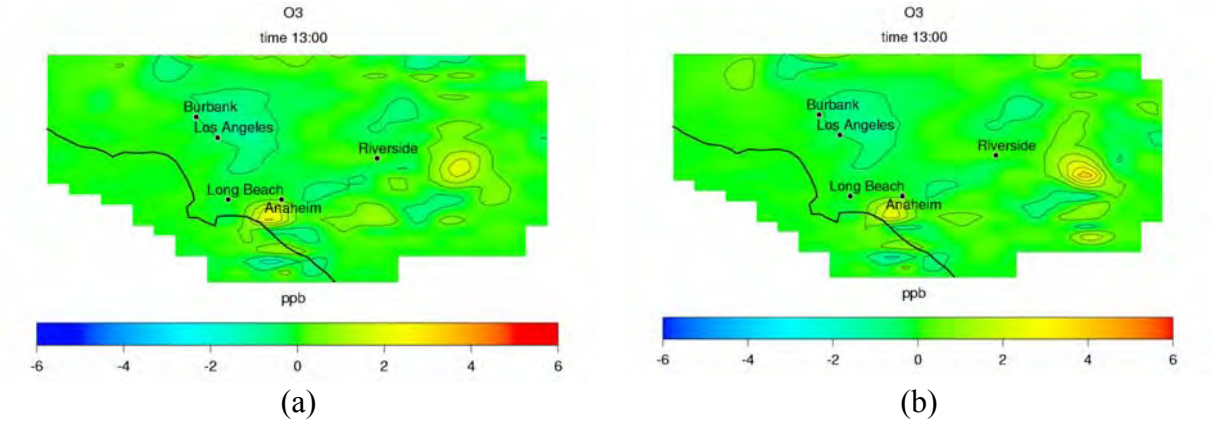

(a) (b)

Figure 60. Difference in O_3 concentration (in ppb) at hour 1300 between DG scenarios and baseline: (a) PW2010, and (b) HPD

3.4.3 Air Quality Impacts of DG with "Attainment" Inventory

The AQMD has been developing a baseline scenario for year 2010 in which ozone NAAQS is attained. This attainment emission inventory has been continuously modified to include all different emission controls considered in the 2003 Air Quality Management Plan, and it has not been available for this work until recently. Therefore, most of DG air quality impacts have been evaluated with the non-attainment emission inventory. Representative DG scenarios have been used with the attainment scenario to discuss the effect of baseline emissions on the overall air quality impacts of DG. Difference in emissions between attainment and non-attainment scenarios are presented in Table 53.

Table 53. Difference in emissions between attainment and non-attainment emission inventories

Species	Non-attainment ton/day	Attainment Ton/day	Change %
VOC	981	583	- 40.6
NO_X	407	296	- 27.3
CO	3,268	3,368	3.1
PM	580	580	0.0
SO_X	88	48	- 45.5
NH_3	168	168	0.0

In the attainment inventory, emissions of ozone precursors, VOC and NO_X, are reduced by 40% and 27%, respectively. These emission reductions lead to a decrease in peak ozone concentration of 20 ppb. In addition, the maximum 1-hour average concentration of NO_2 and the maximum 24-hour average concentration of $PM_{2.5}$ decrease by 48 ppb and 20 $\mu g/m^3$, respectively. Despite the emission reductions applied in the attainment inventory, ozone and $PM_{2.5}$ levels obtained in the simulations still exceed the NAAQS values (Table 54).

Table 54. Simulated concentration of some criteria pollutants: maximum hourly average concentration of O_3, NO_2 and CO and 24-hour average concentration of $PM_{2.5}$ (2010 attainment scenario)

Species	Maximum	Location	Average	Time
O_3	218 ppb	San Bernardino	1-hr average	1300
NO_2	110 ppb	Ontario	1-hr average	0100
CO	3.0 ppm	Los Angeles	1-hr average	0800
$PM_{2.5}$	95 $\mu g/m^3$	Riverside	24-hr average	N/A

With the use of the attainment inventory, one would expect the air quality impacts of DG to be more intense, because the net increase in emissions due to DG relative total emissions is higher. Table 55 shows the relative increase of emissions from DG with respect to the baseline and the attainment emission inventories, for selected DG scenarios. Even though the attainment emission inventory considers significantly lower emissions than the baseline inventory, emissions from DG are still a small fraction of the total emissions. In particular, increase of VOC and NO_X emissions due to DG represent 1.01%, or less, with respect to total emissions.

Table 55. Basin-wide increase of primary criteria pollutant emissions relative to baseline and attainment emission inventories, for selected DG scenarios

DG Scenario Name	DG Scenario #	CO %	NO_X %	VOC %	NH_3 %	SO_X %	PM %
With respect to baseline emission inventory							
PW2010	**1**	0.25	0.37	0.13	0.13	0.08	0.16
PeakPW_2	**21**	0.40	0.74	0.31	1.05	1.60	0.35
#R1	**22**	0.07	-0.01	0.03	0.11	0.02	0.07
With respect to attainment emission inventory							
PW2010	**1**	0.26	0.51	0.22	0.13	0.15	0.16
PeakPW_2	**21**	0.41	1.01	0.52	1.05	2.93	0.35
#R1	**22**	0.07	-0.01	0.05	0.11	0.04	0.07

Impacts of DG on O_3 obtained by using the two different inventories differ slightly, but increasingly, as the emissions from DG increase. As shown in Table 56 and Table 57, maximum increases in O_3 concentration due to DG are slightly larger if the attainment inventory is used. In increasing order of DG emissions, maximum increases in O_3 concentration from DG scenarios #R1, PW2010, and PeakPW-2 are 3, 6, and 11 ppb when the attainment inventory is used. The same values obtained with the baseline inventory are 3, 4, and 8 ppb, respectively. Similar trends are observed for maximum decreases in O_3 concentration. Nevertheless, maximum differences in ozone concentration occur in areas where the baseline O_3 concentration is below the O_3 NAAQS, regardless of which emission inventory is used.

Changes in the peak ozone concentration due to DG implementation are not affected significantly by the inventory used. As shown in table 56 and in Table 57, peak ozone concentration increases by less than 2 ppb due to DG implementation regardless the emission inventory used.

Table 56. Maximum O_3 concentration, and maximum decrease and increase in O_3 concentration in each scenario

Scenario	Max (ppb)	Time	Max Increase (ppb)	Baseline reference (ppb)	Time	Max Decrease (ppb)	Baseline reference (ppb)	Time
dg_24h_R1_att	219	13	3	41	6	-11	96	16
dg_PW2010_att	218	13	6	72	15	-11	93	15
DgPeakPW2_att	220	13	11	61	18	-28	32	1

Table 57. Maximum O_3 concentration, and maximum decrease and increase in O_3 concentration in each scenario

Scenario	Max (ppb)	Time	Max Increase (ppb)	Baseline reference (ppb)	Time	Max Decrease (ppb)	Baseline reference (ppb)	Time
dg_24h_R1	238	13	3	46	13	-2	60	12
dg_PW2010	238	13	4	46	13	-3	5	5
DgPeakPW2	239	13	8	10	2	-26	29	2

Impacts of DG scenarios on $PM_{2.5}$ using the attainment inventory are similar to the ones obtained when the baseline inventory is used. As shown in Table 58 and Table 59, maximum increases in 24-hour average $PM_{2.5}$ concentration due to DG scenarios using the attainment inventory are the same as the ones obtained by using the baseline inventory. On the other hand, increases in the maximum 24-hour average are slightly larger if the attainment inventory is used. In particular, maximum 24-hour average $PM_{2.5}$ concentration increases by 6 $\mu g/m^3$ (from 95 to 101 $\mu g/m^3$) in the DG scenario PeakPW-2, when the attainment inventory is used. In contrast, the same value only changes by 1 $\mu g/m^3$ (from 115 to 116 $\mu g/m^3$) if the baseline inventory is used. For the other two scenarios, differences due to the use of the two inventories are less important.

Table 58. Maximum 24-hour average $PM_{2.5}$ concentration, and maximun decrease and increase in 24-hour average $PM_{2.5}$ concentration in selected scenarios, using the attainment inventory

Scenario	Max ($\mu g/m^3$)	Max Increase ($\mu g/m^3$)	Baseline reference ($\mu g/m^3$)	Max Decrease ($\mu g/m^3$)	Baseline reference ($\mu g/m^3$)
#R1_att	95	3	72	-2	61
PW2010_att	96	3	53	-2	41
PeakPW-2_att	101	6	95	-3	41

Table 59. Maximum 24-hour average $PM_{2.5}$ concentration, and maximun decrease and increase in 24-hour average $PM_{2.5}$ concentration in selected scenarios, using the baseline inventory

Scenario	Max ($\mu g/m^3$)	Max Increase ($\mu g/m^3$)	Baseline reference ($\mu g/m^3$)	Max Decrease ($\mu g/m^3$)	Baseline reference ($\mu g/m^3$)
#R1	115	3	45	-2	44
PW2010	114	3	78	-1	90
PeakPW-2	116	6	75	-2	14

In general, DG scenarios add a relatively small mass of pollutants to the total emissions. Hence, even if baseline emissions are reduced significantly—as in the attainment scenario—emissions introduced by DG still add a small portion relative to total emissions. Therefore, air quality impacts of scenarios with low and moderate DG penetration do not vary significantly with

changes in the baseline emissions inventory. Conversely, air quality impacts of scenarios with high DG penetration are more sensitive to changes in the baseline emissions.

3.5 Uncertainty and Sensitivity Analysis

3.5.1 Chemical Mechanism

This section presents a portion of the overall sensitivity analysis methodology described above to the chemical mechanism itself. The results presented herein focus upon the examination of those chemical mechanism features that most significantly affect the prediction of ozone formation, destruction, and resulting atmospheric concentration.

Figure 61 presents mean ozone concentrations and their corresponding 1σ (standard deviation) uncertainty bounds as a function of time for each simulated case. The standard deviation provides a measure of how spread out the distribution of results is when perturbed in the manner described above. The standard deviation at each hour (σ_j) is defined as:

$$\sigma_j = \sqrt{\frac{\sum_{i=1}^{N}(X_{ij} - \mu_j)^2}{N-1}} \tag{26}$$

where X_{ij} is the value of the parameter for the i^{th} sample, μ_j is the mean at each simulated hour, and N is the number of samples. Final ozone concentrations range from 186±75 ppb at a VOC/NO_x ratio of 8:1 to 420±77 ppb at a VOC/NO_x ratio of 17:1. At VOC/NO_x ratios higher than 17:1, O_3 concentrations using nominal CACM parameters are closer to the mean values from the Monte Carlo simulations. A measure of the statistical deviation is the root mean square (*RMS*) deviation between nominal (c_n) and mean (μ) value concentrations defined as:

$$RMS = \sqrt{\frac{\sum_{i=1}^{N}(c_n - \mu)^2}{N}} \tag{27}$$

For the higher VOC/NO_X ratios, the *RMS* = 0.007 at a 17:1 ratio, and *RMS* = 0.006 at a 32:1 ratio. At the 8:1 ratio, the nominal parameters (parameters used in the baseline CACM model) lead to ozone concentrations that are consistently under-predicted compared to the best estimates (*RMS* = 0.01) of the sensitivity analyses. However, the predictions still lie within one standard deviation of the best estimates.

Figure 62 shows the time variation for ozone-relative uncertainties, presented as parts per million difference over the mean parts per million predicted. This figure illustrates that CACM exhibits the largest relative errors for ozone concentrations at a VOC/NO_x ratio of 8:1 where the maximum error is 44%; these uncertainties then decrease at the 17:1 ratio (28%), and are the smallest at 32:1 (down to 26%).

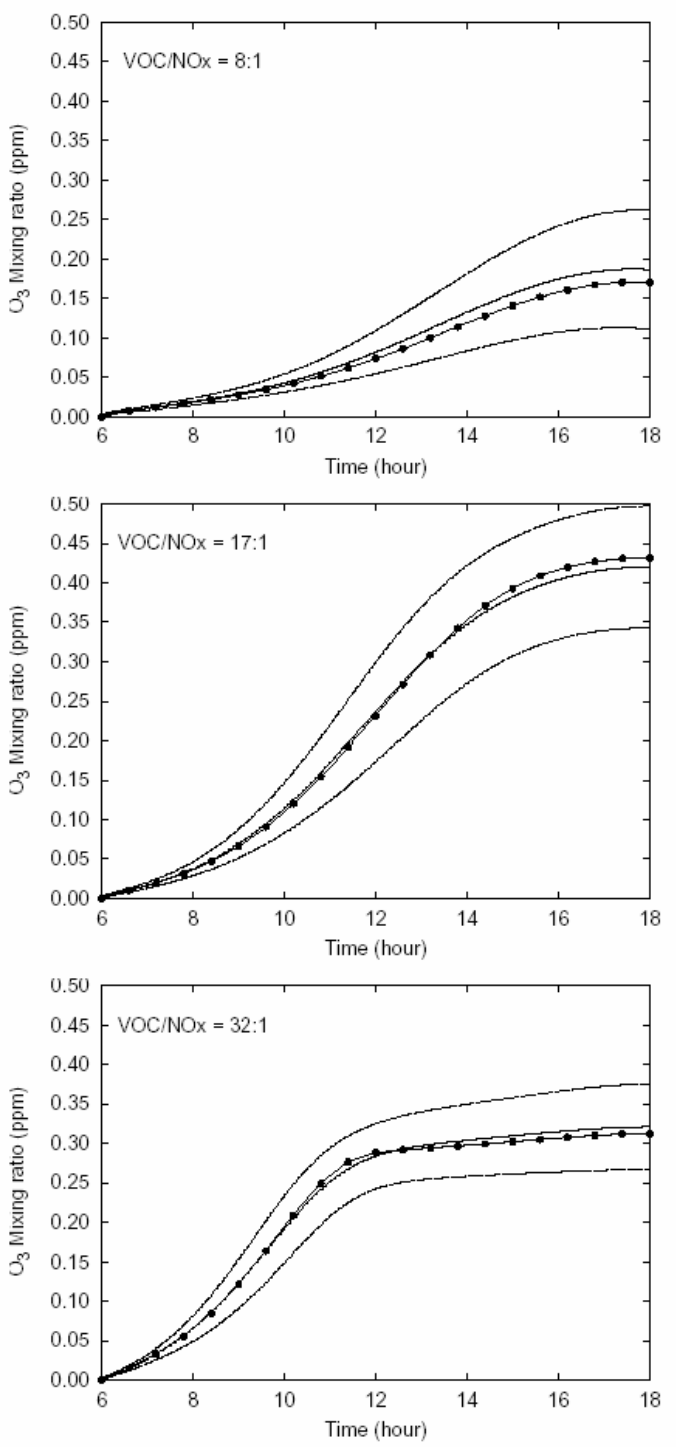

Figure 61. Mean concentrations and 1σ uncertainty ranges for ozone at different VOC/NO_X ratios. Solid line, mean from all results; line with circles, concentrations with nominal parameters; dashed curves, 1σ uncertainty bounds for result.

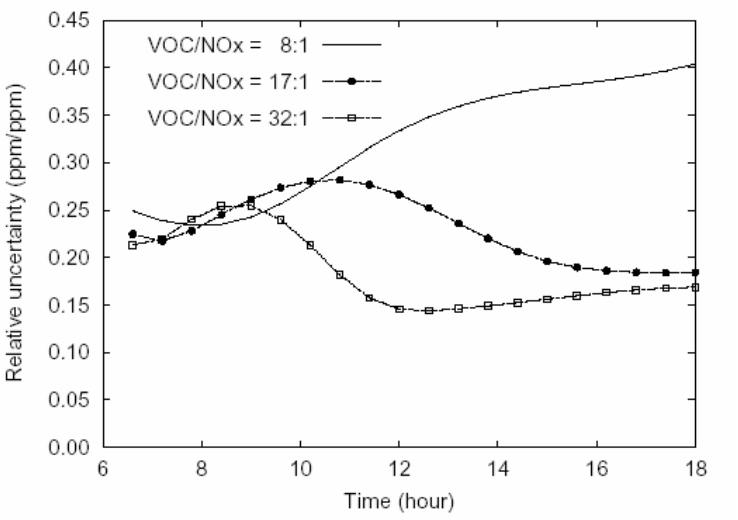

Figure 62. Relative uncertainty for ozone as a function of time for indicated VOC/NO_x ratios. Uncertainty is defined as the estimated σ divided by the mean from all results.

Table 60 shows the most important reactions ordered in terms of their contribution to ozone relative uncertainty, from most to least significant. The regression analysis shows that at VOC/NO_x ratios less than 17:1, the NO_2 photolysis rate and HCHO + $h\upsilon \rightarrow$ CO + 2 HO_2 are the reactions that most significantly contribute to ozone uncertainty. However, ozone itself is more sensitive to changes in the reaction rate of O_3 with NO to regenerate NO_2 and the reaction of OH with NO_2 to produce nitric acid. Reactions that also contribute to the total uncertainty of ozone are the photolysis reactions of methyl glyoxal (MGLY) and the lumped higher aldehydes. This is consistent with the original formulation of CACM, since MGLY is modeled to behave as an aldehyde.

Results at VOC/NO_x ratios of 32:1 differ from those at lower ratios. Although NO_2 photolysis remains the major contributor to ozone uncertainty, the second most uncertain rate parameter is that of the reaction of the acyl radical (RO_26) from aldehydic H abstraction of the lumped aldehydes with NO. However, in terms of sensitivity, ozone loss with NO is more important than that of RO_26. The fact that reactions that involve the acyl radical RO_26, the acyl peroxy radical RO_28, and peroxy alkyl nitrates (PAN1 and PAN2) become relevant at these ratios is a consequence of the low NO_x concentrations. As a result, peroxy radical reactions begin to become important at high VOC/NO_X ratios. At sufficiently low NO_x concentrations or high VOC/NO_x ratios, a further decrease in NO_x favors peroxy-peroxy reactions that in effect retard O_3 formation by removing free radicals from the system.

Table 60. Most Important Parameters Based on the Contributions to Uncertainty on the Time-Averaged O_3 Concentrations

Reaction : Product	Regression Coefficient	Uncertainty Contribution %
	***VOC/NO$_x$* = 8:1**	
HCHO + hυ → CO + 2 HO_2	0.413	25
NO_2 + hυ	0.470	19
ALD2 + hυ	0.240	8
NO_2 + OH + M	-0.699	5
MGLY + hυ	0.127	5
NO + O_3	-0.591	4
$RO_2$34 + NO	-0.088	3
ALKL + OH	0.181	3
$RO_2$34	0.080	2
HCHO + hυ	-0.125	2
	***VOC/NO$_x$* = 17:1**	
NO_2 + hυ	0.341	21
HCHO + hυ → CO + 2 HO_2	0.220	15
MGLY + hυ	0.142	12
$RO_2$6 + NO	0.085	6
$RO_2$6 + NO_2 + M	-0.106	3
$RO_2$34 + NO	-0.064	3
NO + O_3	-0.364	3
ALD2 + hυ	0.097	3
$RO_2$34	0.055	2
NO_2 + OH + M	-0.319	2
	***VOC/NO$_x$* = 32:1**	
NO_2 + hυ	0.342	35
$RO_2$6 + NO	0.091	11
MGLY + hυ	0.085	7
$RO_2$6 + NO_2 + M	-0.110	6
PAN1	0.094	4
$RO_2$8 + NO	0.057	4
HCHO + hυ → CO + 2 HO_2	0.088	4
NO + O_3	-0.306	4
PAN2	0.082	3
$RO_2$8 + NO_2 + M	-0.080	3

3.5.2 Air Quality Model

3.5.2.1 Model uncertainty

This section examines the uncertainty ranges exhibited by simulated ozone and particulate matter concentrations as the result of changes in selected input values. Both, spatial and temporal variations of model uncertainties are investigated for the SoCAB. Given the large amount of output data produced by the model evaluation, detailed study of the time variation of

uncertainties is performed only for six stations: Simi Valley, Burbank, Central Los Angeles, Long Beach, Riverside, and San Bernardino. However, modeling results for these sites represent the general aerosol dynamics and trends for ozone throughout the basin. For example, the location at Central Los Angeles experiences particularly intense emissions from automobiles as a hub of the region's freeway system and also exhibits great secondary photochemistry; whereas, Riverside represents those areas downwind of major emissions, where higher concentrations of both ozone and secondary species are typically present.

3.5.2.1.1 Time

In order to investigate the uncertainty of modeled species as time progresses, concentration time series are summarized as box plots. These box plots provide an alternative, more efficient display of the multiple distributions that result from the statistical analyses. Figure 63 shows ozone mixing ratios as a function of time at selected sites in the form of box plots, using the output of all Monte Carlo simulations. In this figure, the endpoints (hinges) of the gray boxes are formed by the lower and upper quartiles of the data, i.e., where the 25th and 75th percentiles lie. The horizontal line within the box represents the median. The bars above and below the box (whiskers) are drawn from each hinge to the most extreme measurement inside the inner fence. The inner fence is a distance equivalent to 1.5 times the difference between upper and lower quartiles (inter-quartile range, IQR). Box plots contain the same information as a distribution function, but in a reduced form, allowing the time dependence of the distributions to be presented in the regions of interest. The selection of a norm is necessary to investigate the error bounds of species considered. A value of interest is the 1-hr maximum concentration during the last day of simulation, since this norm is of most concern to those interested in complying with regional and national air quality standards (Gipson et al. 1981; Meyer 1986).

Figure 63 presents box plots for the six stations, each showing the photochemical nature of ozone formation. However, the particular hour at which the maximum ozone mixing ratio occurs differs in each site analyzed. It is apparent from Figure 63 that sites at Riverside and San Bernardino are located in areas with large domain-wide ozone mixing ratios. Ozone maxima occur at 1500 in Riverside (median = 96 ppb) and at 1600 in San Bernardino (median = 111 ppb). Model uncertainty at these peaks is similar as indicated by the IQR value of 15 ppb in both places.

Close examination of the box plots at the peaks shows that the length of the whiskers is approximately the same, an indication that the distribution is symmetrical. This observation suggests that a Gaussian distribution function fits the output data variation adequately and may better characterize the uncertainty of these predictions. Figure 64a compares the cumulative distribution function (CDF) as estimated by the model simulations and the best fit to a normal distribution curve. The comparison is made at Riverside and Central Los Angeles for a 12-hr average that comprises most of the daylight time, when ozone concentrations are significant, starting at 800 hours. Similar results (not shown) have been plotted also for the remaining stations. Two parameters are required to determine completely a normal CDF, namely the mean (μ) and the standard deviation (σ). Figure 64 shows that calculated normal distributions fit the data adequately. Furthermore, RMS of the difference between fitted and simulated values when the distributions are assumed normal is always smaller than when the distributions are assumed

log-normal. Therefore, a normal probability density distribution is adopted to describe the variance of predicted concentrations.

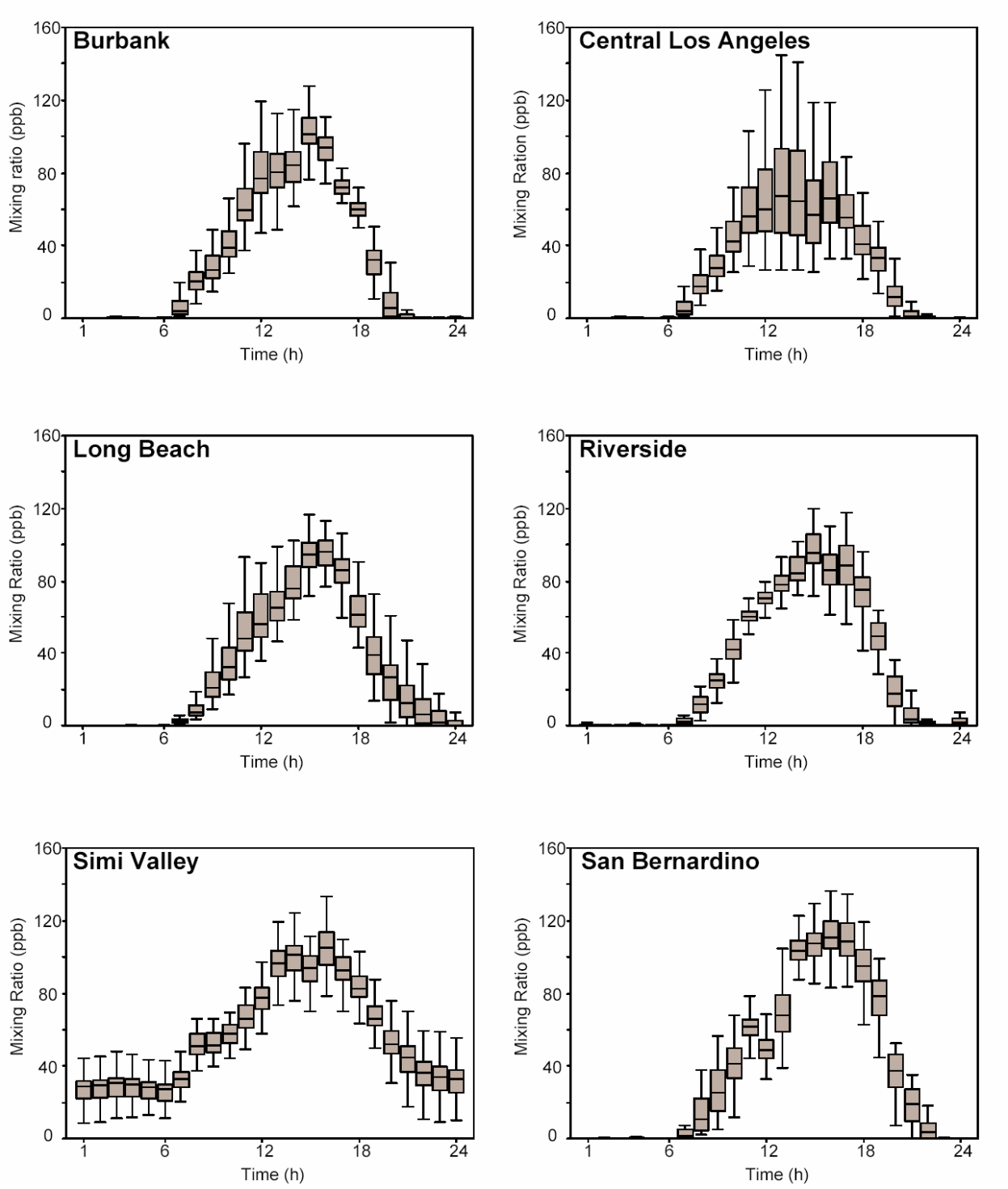

Figure 63. Box plots for simulated ozone mixing ratios from Monte Carlo runs at different sites in the SoCAB. Median, upper, and lower quartiles are shown inside the gray box.

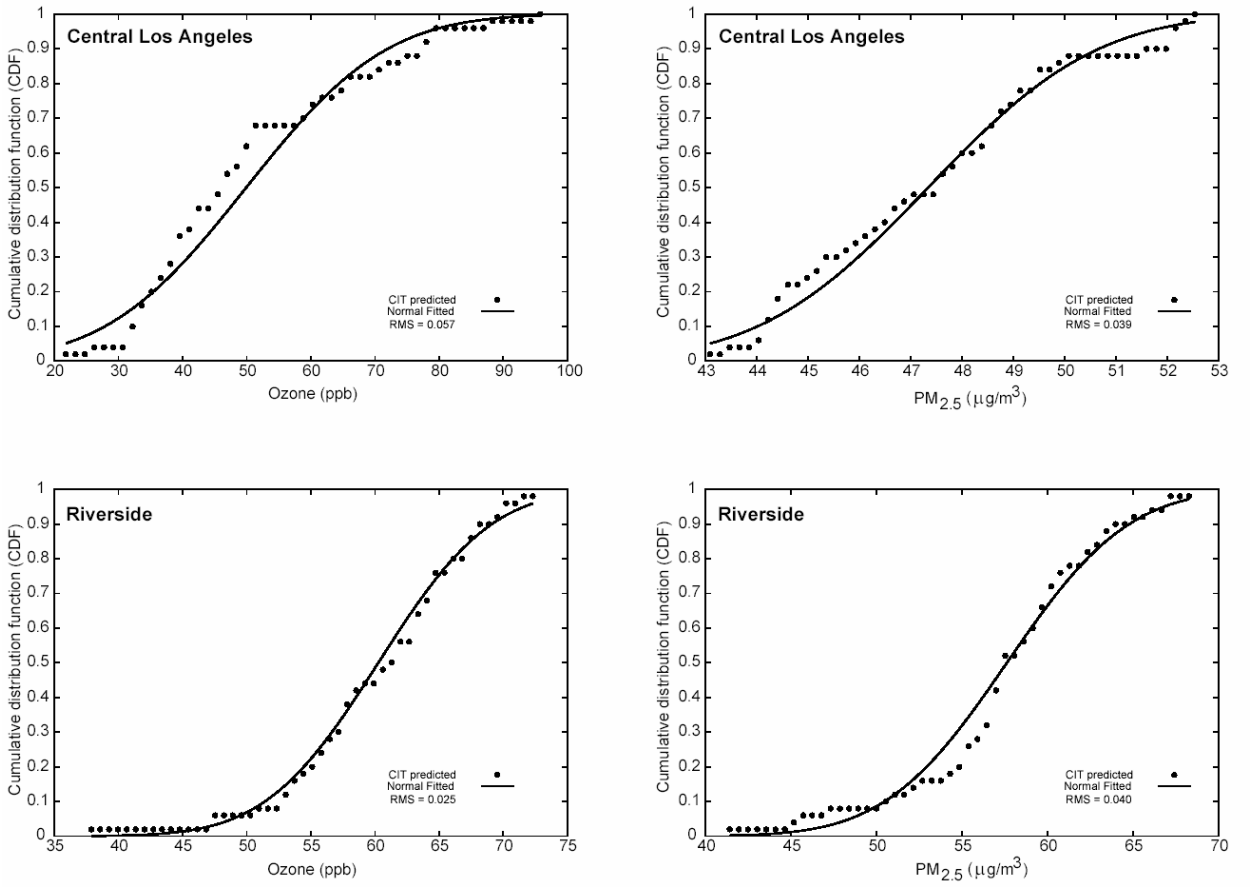

Figure 64. Comparison between the cumulative distribution function (CDF) estimated from 50 Monte Carlo runs (shown as bullets) and the best-fit normal distribution (solid line). Ozone and $PM_{2.5}$ concentrations shown for Riverside and Central Los Angeles.

Figure 65 shows the time evolution of $PM_{2.5}$ aerosol at selected sites in the form of box plots. Sites in Riverside and San Bernardino show the largest basin-wide aerosol concentrations, consistent with the formation of secondary particulate matter observed in measurements and previous studies (Meng et al. 1998; Nguyen and Dabdub 2002b). Predicted $PM_{2.5}$ maxima occur at 600 and 700 respectively in Riverside (mean = 114 $\mu g\ m^{-3}$) and San Bernardino (mean = 146 $\mu g\ m^{-3}$). Model uncertainty in these two locations is within the same order of magnitude given the IQR values of 10 and 21 $\mu g\ m^{-3}$ respectively. Figure 64b compares simulation results with the fit to a normal CDF. The comparison is made for 24-hr average $PM_{2.5}$ aerosol in Riverside and Central Los Angeles. As with ozone, variance of $PM_{2.5}$ data can also be characterized with a normal probability distribution. Calculated distributions show that the estimated variance is comparable in Riverside (σ = 11 $\mu g\ m^{-3}$) and San Bernardino (σ = 16 $\mu g\ m^{-3}$). As in the case of ozone, the hours in which the uncertainty of $PM_{2.5}$ predictions is the greatest do not coincide with the time when predicted concentrations reach their maximum.

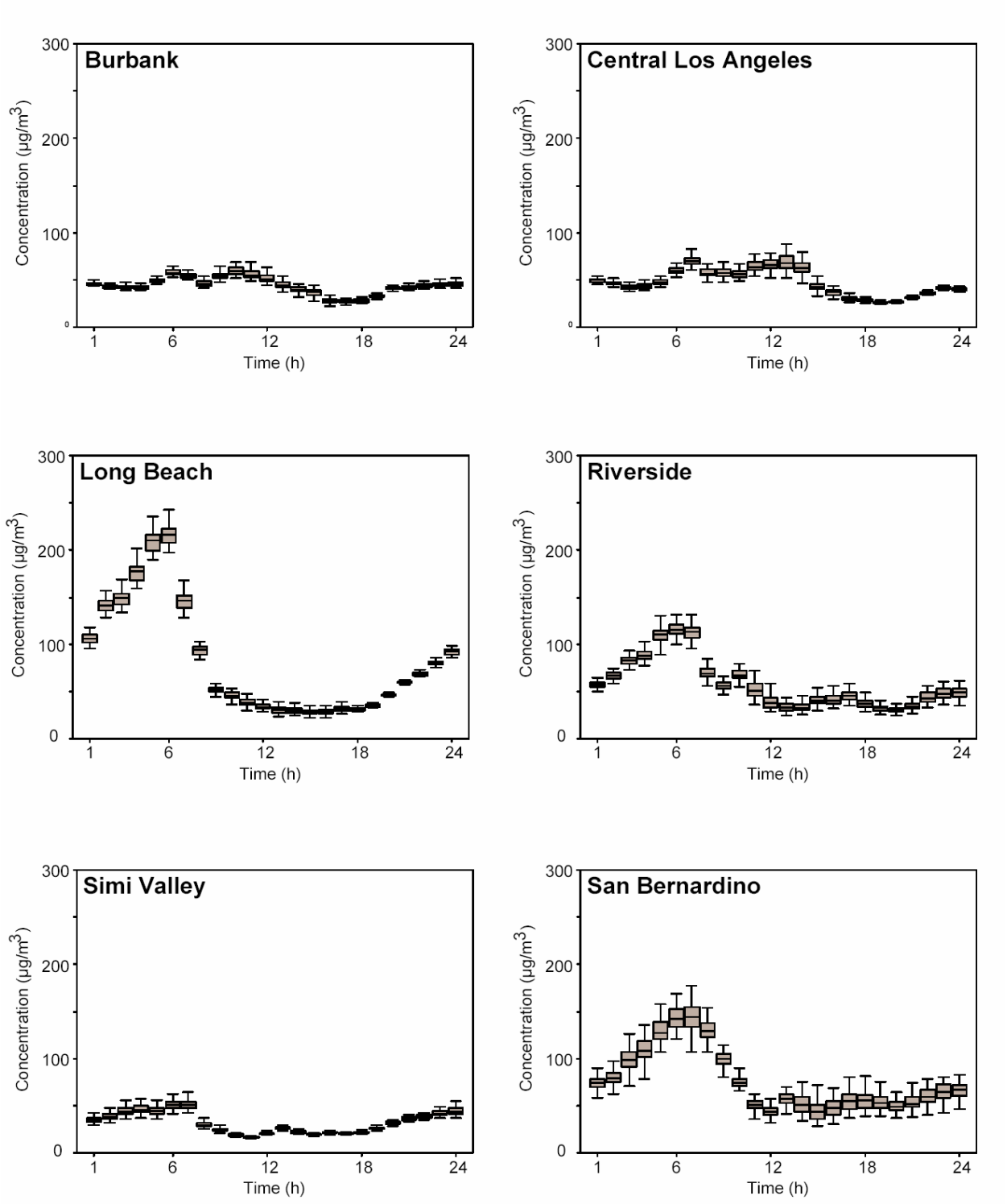

Figure 65. Box plots for simulated $PM_{2.5}$ concentrations from Monte Carlo runs at different sites in the SoCAB. Median, upper, and lower quartiles are shown inside the gray box.

3.5.2.1.2 Space

The spatial variation of model uncertainties is determined with probability density distributions that best describe the variance of predicted concentrations in the SoCAB. For ozone, 1-hr maximum concentrations are stored and subsequently plotted for each location in the basin during the 24 hours that correspond to the third day of simulation. This procedure offers a general portrait of maximum values everywhere in the domain, regardless of the specific hour in which they occurred. For $PM_{2.5}$, a similar process is followed, with the exception that concentrations stored represent 24-hr averages. Uncertainties associated with these concentrations are important, since compliance with air quality standards is required for domain-wide peak concentrations.

Figure 66 compares the basin-wide mean, estimated from Monte Carlo simulations, with the ozone base case throughout the SoCAB. The corresponding comparison for aerosol $PM_{2.5}$ is shown in Figure 67. Base case results in both figures characterize the concentrations calculated using nominal values for the input parameters. These figures show that the location and numerical values of maxima are equivalent for both the base case and the mean. Further comparison with calculated median concentrations (not shown) demonstrates that normal probability density distributions adequately describe the variance of predicted concentrations.

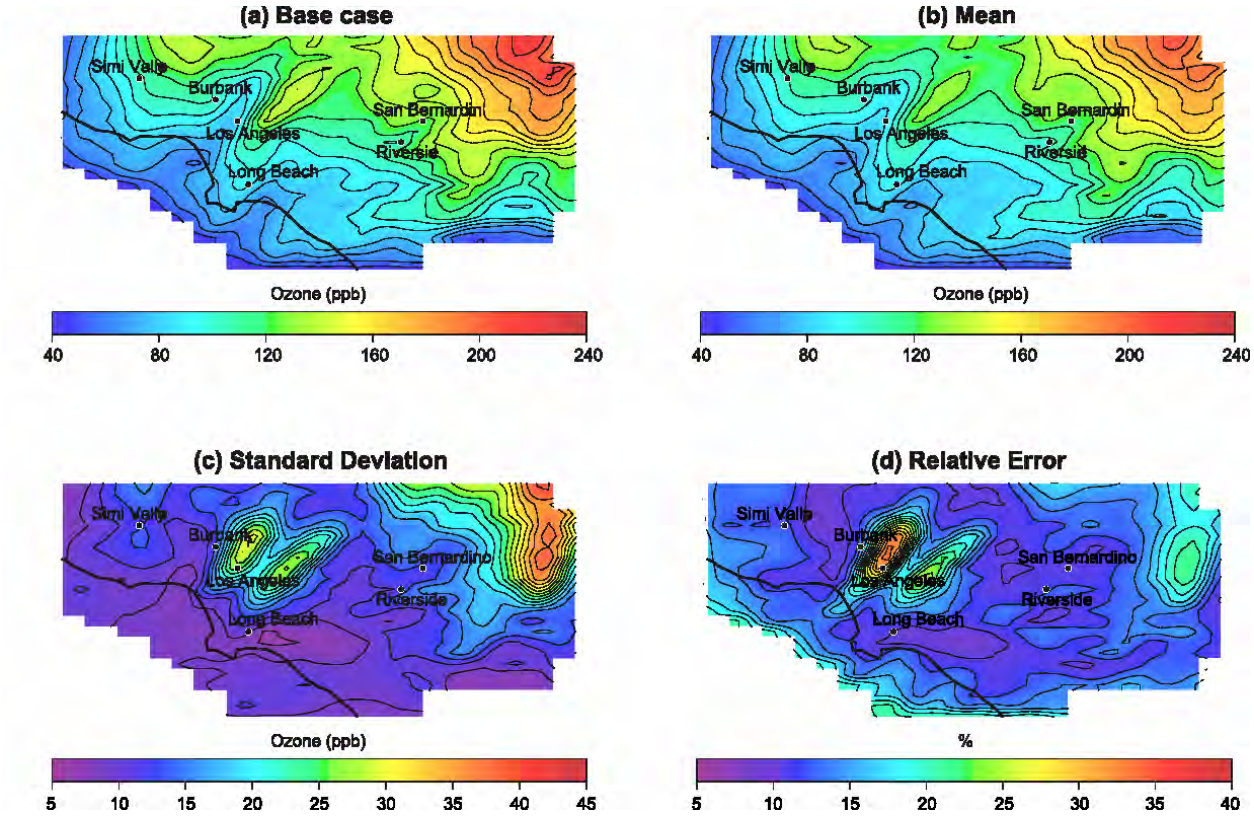

Figure 66. Plots of ozone (a) base case, (b) mean mixing ratios, (c) standard deviation, and (d) estimated relative error for the 1-hr maxima of the third day of simulation

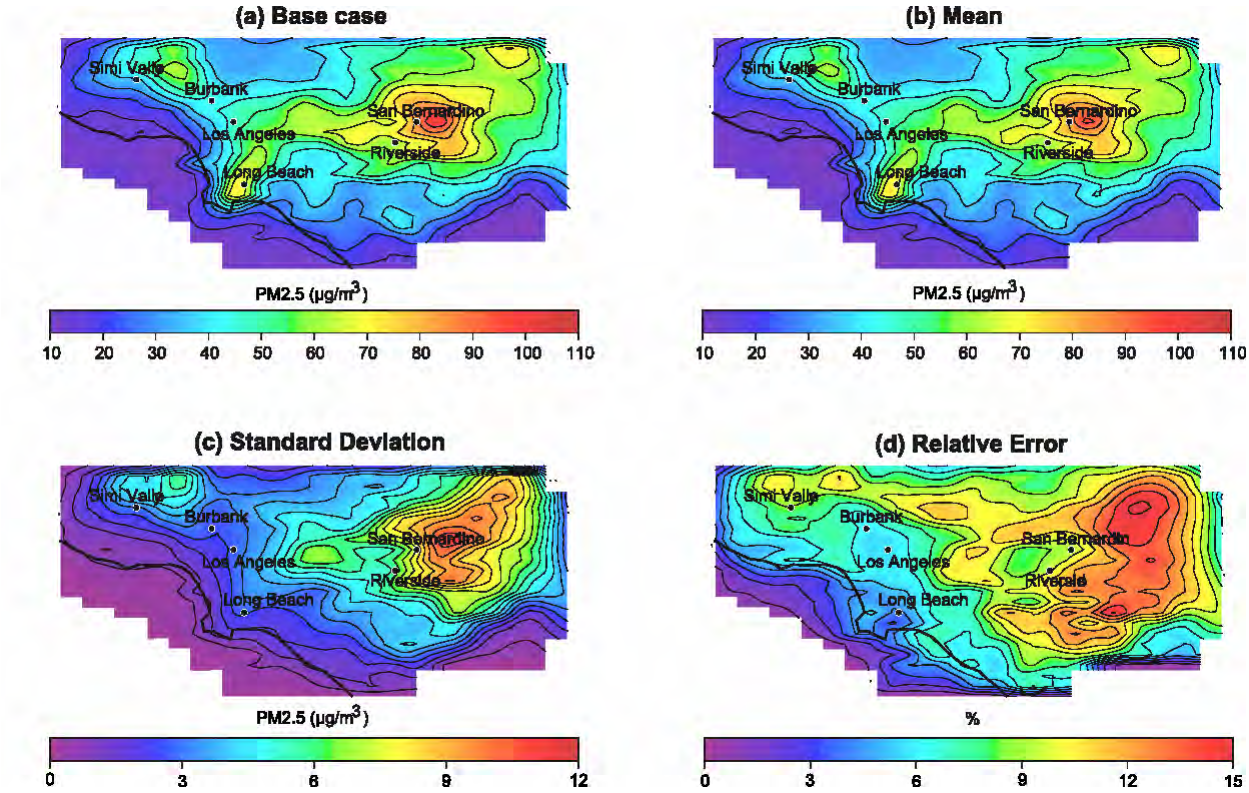

Figure 67. Plots of aerosol $PM_{2.5}$ (a) base case, (b) mean concentrations, (c) standard deviation, and (d) estimated relative error for the 1-hr maxima of the third day of simulation

Figures 66 and 67 present the estimated basin-wide standard deviation and mean for ozone and $PM_{2.5}$ concentrations, and not only the statistics of a limited number of sites. The largest ozone mixing ratios arise on the eastern side of the basin, consistent with previous studies (Meng et al. 1998; Nguyen and Dabdub 2002b) and observations (CARB 2002, 2003). Moreover, calculated σ reveals that the variation of modeled ozone mixing ratios is not the largest in this area of the basin. For instance, the location with the largest mixing ratio (221 ppb) shows a σ of 37 ppb, which is equivalent to a relative error of 17%. In contrast, a location with one of the largest basin-wide relative errors (42%) is Central Los Angeles, which exhibits concentrations in the range of 76 ± 32 ppb.

For $PM_{2.5}$ aerosol, Figure 67 illustrates that the highest concentrations are observed near Riverside and San Bernardino, consistent with previous predictions and observations. East of San Bernardino the largest domain-wide concentrations (108 ± 11 μg m^{-3}) present a relative error of 10%. However, the location with the largest relative error (17%) is found southeast of Riverside, with concentrations of 48 ± 8 μg m^{-3}. Although modeled output variations are not the smallest in the regions where $PM_{2.5}$ aerosol reaches its maximum, it is bounded to less than 15% relative error.

3.5.2.2 Sensitivity analysis

Sensitivity of ozone and $PM_{2.5}$ aerosol concentrations to selected input variables is explored following the methodology described in Section 2.3.3.1.2. Instead of using stepwise regression analysis at each time step, regression coefficients are calculated using 12-hr averaged concentrations for ozone and 24-hr averages are for $PM_{2.5}$ aerosol. This approach lessens the computational demands in the present analysis and also provides information of the sensitivity values that are of interest for compliance with air quality standards. Table 61 presents a list of the input variables with significant influence in the prediction of ozone mixing ratios at selected sites throughout the domain. Table 61 shows, for each parameter, the calculated standardized regression coefficients (SRC) and the corresponding contribution to the total uncertainty (UC) expressed as a percentage. The regression coefficients values are a measure of the sensitivity of ozone and $PM_{2.5}$ to changes in the input parameters.

Table 61. Most important parameters based on the contributions to uncertainty of ozone at selected cases

Riverside			San Bernardino			Los Angeles		
Parameter	SRC	UC	Parameter	SRC	UC	Parameter	SRC	UC
$R^2 = 0.69$			$R^2 = 0.93$			$R^2 = 0.98$		
NO_x emissions	-0.549	29.2	NO_x emissions	-0.755	56.2	NO_x emissions	-0.683	48.3
side VOC	0.478	23.7	side VOC	0.494	24.8	side VOC	0.531	32.9
NO + O_3	0.282	80.0	VOC emissions	0.250	6.4	side O_3	0.345	11.7
			NO + O_3	0.146	1.9	side NO_x	0.199	4.1
			alkenes + OH	0.120	1.4	VOC emissions	0.059	0.3

Burbank			Long Beach			Simi Valley		
Parameter	SRC	UC	Parameter	SRC	UC	Parameter	SRC	UC
$R^2 = 0.94$			$R^2 = 0.96$			$R^2 = 0.98$		
NO_x emissions	-0.767	60.7	NO_x emissions	-0.674	46.8	side O_3	0.702	45.1
side O_3	0.417	18.6	side O_3	0.518	29.4	side NO_x	0.572	28.2
side NO_x	0.259	7.7	side VOC	0.361	14.3	side VOC	-0.369	13.7
side VOC	0.234	5.4	side NO_x	0.217	4.6	NO_x emissions	0.305	9.4
						VOC emissions	0.062	0.4
						NH_3 emissions	-0.056	0.3

In general, the regression model explains 69% to 98% of the ozone uncertainty as reflected by the R^2 values, with the smallest value (69%) reported for Riverside. Variation in basin-wide NO_x emissions and side boundary conditions imposed on VOC are the most significant contributors to uncertainty and sensitivity of ozone predictions. Ozone boundary conditions have contributions to uncertainty that range from 18.6% to 45.1% in the west side of the SoCAB. The largest contribution (45.1%) is located in Simi Valley, a site close to the boundaries of the computational domain. The SRC sign indicates that increasing NO_x emissions leads to reductions in ozone mixing ratios. In contrast, increasing the values of ozone and VOC's side boundary conditions results in higher ozone mixing ratios.

Results in Table 61 suggest the regions analyzed are VOC-limited or have low VOC-to-NO_x ratios. This is typical of city centers and plumes immediately downwind of NO_x sources. The results are consistent with the basin residing in an overall NO_x-rich state, and with findings in previous studies (Meng et al. 1997). However, most sites also show that VOC and ozone boundary conditions have an important effect on ozone concentrations. Some of these results reflect the proximity to the computational boundaries, like Simi Valley, and the lesser amount of NO_x emissions in that region (higher VOC-to-NO_x ratios).

A similar analysis is applied to $PM_{2.5}$ for the selected sites in the SoCAB (Table 62). The regression model explains 90% to 95% of the variation that the computational model exhibits for $PM_{2.5}$ aerosol concentrations. In most selected sites, $PM_{2.5}$ aerosol concentrations are most sensitive to changes in NH_3 and NO_x emissions. The positive sign of the SRC values indicates that any increase in NO_x or NH_3 emissions results in higher $PM_{2.5}$ aerosol concentrations, consistent with the finding that a mayor component of this aerosol in the basin is ammonium nitrate (Nguyen and Dabdub 2002b).

Table 62. Most important input parameters based on the contributions to the uncertainty of $PM_{2.5}$ aerosol concentrations at selected cases

Riverside			**San Bernardino**			**Los Angeles**		
Parameter	SRC	UC	Parameter	SRC	UC	Parameter	SRC	UC
$R^2 = 0.90$			$R^2 = 0.93$			$R^2 = 0.93$		
NO_x emissions	0.792	61.1	NO_x emissions	0.773	56.6	NH_3 emissions	0.723	45.6
NH_3 emissions	0.436	18.9	NH_3 emissions	0.531	28.3	NO_x emissions	0.476	21.9
side VOC	-0.146	2.6	$NO + O_3$	0.174	3.1	side NO_x	0.316	10.8
$NO + O_3$	0.131	1.8	side O_3	-0.137	1.6	side O_3	0.258	7.2
side O_3	-0.131	1.5	VOC emissions	0.104	1.0	$NO + O_3$	0.157	2.5
side NO_x	-0.122	1.4	$NO_2 + h\nu$	0.096	0.9	$NO_2 + h\nu$	0.141	1.9
alkenes + OH	0.112	1.2				Side VOC	0.121	1.4

Burbank			**Long Beach**			**Simi Valley**		
Parameter	SRC	UC	Parameter	SRC	UC	Parameter	SRC	UC
$R^2 = 0.94$			$R^2 = 0.94$			$R^2 = 0.95$		
NO_x emissions	0.667	38.9	NH_3 emissions	0.685	39.1	NO_x emissions	0.701	43.7
NH_3 emissions	0.631	36.0	NO_x emissions	0.518	25.4	side NO_x	0.539	24.9
side NO_x	0.303	8.2	side NO_x	0.404	16.4	side VOC	-0.425	16.2
side VOC	-0.250	5.6	side O_3	0.300	9.1	NH_3 emissions	0.258	6.1
side O_3	0.126	1.6	$NO_2 + h\nu$	0.136	1.8	side O_3	0.128	1.7
$NO_2 + h\nu$	0.123	1.4	$NO + O_3$	0.098	0.9	$NO_2 + h\nu$	0.087	0.8
$NO + O_3$	0.111	1.3						

4. SUMMARY AND CONCLUSIONS

4.1 Summary

This study investigates the air quality impacts of DG in the SoCAB for the year 2010. The scenarios presented here were developed with a systematic process, which included the use of detailed data from GIS databases. The scenarios were simulated in a state-of-the-art air quality model to assess environmental impacts of potential DG installation throughout the SoCAB. The results of this work led APEP researchers to the following findings and conclusions:

- CHP emissions displacements associated with most of the realistic scenarios lead to significant reductions in some criteria pollutant emissions and CO_2 emissions. For NO_X, displaced boiler emissions are higher than NO_X emissions directly produced by DG, resulting in net negative values for realistic DG scenarios with CHP.
- Realistic DG implementation scenarios introduce small, basin-wide mass increments no larger than 0.43% with respect to baseline emissions. Mass increments for spanning DG scenarios are no larger than 1.35%.
- The DG spatial distribution based on GIS land-use data results in DG scenarios that concentrate large capacity DG technologies nearby industrial zones, because of the relatively high adoption rate intensity factor estimated for the industrial sector.
- The calculation of basin-wide DG power distribution among the various sectors estimated for the year 2010 that 60% of total DG power will be implemented in the industrial sector and nearly 32% will be implemented in the commercial-institutional sector.
- Results of basin-wide relative contribution of each type of DG technology estimated for the year 2010 showed that 49% of the DG market will be met by gas turbines; whereas ICEs, MTGs, PV, FC, and GT-FC hybrids will account for 17%, 15%, 5%, 10%, and 4% of the total 2010 DG power market, respectively.
- In general, increases in NO_X emissions produced by DG scenarios reduce ozone concentrations in the central area of Los Angeles—which is typically VOC-limited—and increase ozone concentrations at downwind locations—which are typically NO_X-limited. Increases in NO_X emissions also lead to an increase in 24-hour average $PM_{2.5}$ concentrations over downwind locations near Riverside. Scenarios in which there is a net reduction of NO_X due to emissions displacement by CHP produce small increments in ozone over the central area of Los Angeles and no significant changes elsewhere
- With representative characterizations of DG use in SoCAB for the year 2010, the air quality impacts of DG scenarios are:

  Realistic DG scenarios:
  - Maximum basin-wide ozone concentrations do not change. Changes in maximum 24-hour average $PM_{2.5}$ range from 0 to -3 $\mu g/m^3$.
  - Maximum changes in ozone concentrations at any point throughout the basin range from +5 ppb to -9 ppb. Increases of up to 3 ppb in ozone concentration occur in areas where baseline values already exceed air quality standards.

- Maximum changes in 24-hour average $PM_{2.5}$ concentrations range within ±3 $\mu g/m^3$.

Spanning DG scenarios:

- Changes in basin-wide maximum ozone concentration range within ±1 ppb. Maximum 24-hour average $PM_{2.5}$ changes from -2 $\mu g/m^3$ to +2 $\mu g/m^3$.
- Typically, maximum changes in ozone concentrations at any point throughout the basin are within ±10 ppb, although there are specific cases in which changes in ozone concentration range from -26 ppb to +34 ppb. Maximum changes in 24-hour average $PM_{2.5}$ concentrations range from -4 $\mu g/m^3$ to +6 $\mu g/m^3$.

- Various cases with different DG spatial distributions are explored. The level of emissions introduced by these spanning DG scenarios produces similar air quality impacts. However, additional scenarios that place a considerably higher concentration of DG show that air quality impacts due to DG are affected by the geographical location of DG units. In particular, results suggest that if DG is to be widely used in the basin, then it should not be concentrated in a small area.
- Different temporal distributions of DG emissions are explored. Results show that an amount of DG emissions concentrated during a 6-hour period (peak duty cycle) produce a larger impact in air quality than the same amount emitted during 24 hours (base load duty cycle).

Also, this study investigated the uncertainty and sensitivity of ozone and $PM_{2.5}$ aerosol to variations in selected input parameters using a Monte Carlo methodology. The selection of input parameters was based on their potential to affect the concentrations predicted by the model and also to reflect changes in emissions from DG implementation in the SoCAB. Numerical simulations were performed with the CIT three-dimensional air quality model. Multiple model evaluations were completed, and statistical methods applied to identify those parameters with the largest effect on both the predicted concentrations of selected species and the uncertainty associated with their prediction. This analysis led to the following findings:

- Comparison between basin-wide distributions of base case and calculated mean values demonstrate that normal probability density distributions are the most adequate to characterize the uncertainty of modeled spatial maxima throughout the basin. Therefore domain-wide error bounds for species considered here are reported in terms of standard deviation values, consistent with the normal distributions.
- The largest relative error for ozone is approximately 42% (76 ± 32 ppb); whereas, maximum concentrations show an error of approximately 17% (221 ± 37 ppb). For $PM_{2.5}$, the largest error is ~17% (48 ± 8 $\mu g\ m^{-3}$), but the largest domain-wide concentration (108 ± 11 $\mu g\ m^{-3}$) has a relative error of 10%.
- Results show that changes no greater than 70 to 80% in nominal values of input variables results in 18% to 40% variability of ozone mixing and $PM_{2.5}$ aerosol concentrations.
- Sensitivity analyses performed in this work demonstrate that the variation in side boundary conditions imposed on VOC and NO_X emissions are the major contributors to uncertainty and sensitivity of ozone predictions in most regions throughout the SoCAB.

- Ozone boundary conditions have a marginal contribution to uncertainty in most locations, except for sites located near the boundaries of the computational domain. An increase in NO_X emissions leads to reductions in ozone mixing ratios. In contrast, increasing the values of VOC's side boundary conditions results in higher ozone mixing ratios. This is due to ozone formation being VOC-limited over most of the SoCAB
- Sensitivity analyses also show that $PM_{2.5}$ aerosol is sensitive to changes in NH_3 and NO_X emissions. Furthermore, increasing these emissions results in higher $PM_{2.5}$ aerosol concentrations throughout the basin.

4.2 Conclusions

- Simulation of realistic* DG implementation scenarios for the year 2010 shows that peak basin-wide ozone concentration† does not increase as the result of DG installation.
- The CIT Airshed model is sensitive enough to predict trends in ozone and $PM_{2.5}$ concentrations in the basin from DG emissions.
- There are discernable increases and decreases in local concentrations of ozone and $PM_{2.5}$ that can be attributed to DG installation in SoCAB in 2010.
- Observed maximum local changes in air quality from the Realistic DG Scenarios are:
    - < 3 ppb O_3
    - < 2 $\mu g/m^3$ $PM_{2.5}$
- Observed maximum local changes in air quality from the Spanning DG Scenarios are:
    - < 10 ppb O_3
    - < 6 $\mu g/m^3$ for $PM_{2.5}$
- Simulation of DG scenarios shows consistently observable changes/trends in ambient concentrations of ozone and $PM_{2.5}$ as the result of DG installation
    - Maximum increases in pollutant concentrations occur in areas with typically poor air quality (San Bernardino, Riverside)
    - Maximum decreases occur in locations already in attainment
- Concentration of DG units in a small area leads to higher air quality impacts than spreading DG units over large areas.
- Operation of DG in a duty cycle with a high peak of electricity production leads to higher air quality impacts than DG operation in a base-loaded mode that introduces the same total daily emissions
- DG air quality impacts in years beyond 2010 or with higher DG penetration may have significant air quality impacts that affect both attainment and local air quality.

---

* Realistic DG implementation scenarios include consideration of the current regulatory framework (i.e., current CARB 2003 and 2007 standards and AQMD BACT requirements) and detailed DG market, DG use, and geographic information systems (GIS) data.

† Peak, basin-wide, 1-hour ozone concentration is the parameter upon which compliance with current federal standards is determined.

5. RECOMMENDATIONS AND FUTURE WORK

5.1 Recommendations

The current work has produced the following recommendations regarding the impacts of DG on air quality:

- The impact of DG installation on air quality should be studied through use of a detailed understanding and development of DG implementation scenarios.
- Air quality assessments should not be made without the application of DG emissions to a detailed atmospheric chemistry and transport model that includes all the major chemical and physical processes and geographic and meteorological features of the region of interest.
- Substantial DG emissions should not be released in concentrated spatial locations.
- Substantial DG emissions should not be released concentrated within a short period of time. In other words, in terms of air quality impacts, constant base-loaded DG operation is preferred over peak operation.
- If possible, DG should be installed and operated in as disperse a manner as possible in space and time, to reduce potential air quality impacts.
- Clean DG, such as fuel cells and photovoltaics, have the least air quality impact, and should be preferred to other DG that have higher emissions levels.

5.2 Future Work

Based on the conclusions of the present study listed above, the authors recommend that the Energy Commission investigate and consider several research and policy initiatives, as follows:

- This study is the first effort to design DG implementation scenarios at a urban level following a systematic procedure that ultimately generated gridded emissions to be used in a three-dimensional air quality model. The authors recommend using the capability for development of DG implementation scenarios advanced in the present study to develop DG implementation scenarios for other polluted local areas/regions in California.
- Air quality models and their input requirements are tools that are updated continuously. Hence, the authors recommend supporting advancement of air quality models and air quality models input data in other regions for consideration of DG implementation.
- DG has the potential of being implemented throughout the State of California. However, as in the Los Angeles area, there are other areas with air pollution problems. The authors recommend applying air quality modeling tools to study the impacts of DG on local air quality in other regions of interest such as:
    - San Joaquin Valley (California)
    - San Francisco Bay Area (California)
- This study is based on air quality impacts at 5 km x 5 km grid resolution. However, emissions from DG may impact exposure to contaminants at more local scale. Hence, it is recommended to support air quality studies for DG impacts at a localized scale, using high-resolution local models.

- DG use may reduce emissions of CO_2 and other greenhouse gases (GHGs) due to more efficient fuel utilization. The authors recommend that the Energy Commission support studies of DG impacts on emissions of green house gases on the California scale. These studies should be done using a life cycle analysis approach, which can address not only emissions during operation, but overall emissions associated with fuel production, technology manufacture, and technology disposal or recycle. In addition, the authors recommend analyses to consider and evaluate a carbon reduction policy that includes the benefits of fuel cells and other DG for GHG reductions.
- There is not sufficient data available on DG performance degradation to study increase of emissions caused by installation aging. For this study, performance degradation has been estimated, but authors recommend that the Energy Commission study performance degradation of DG and its effects on increase of DG emissions
- Speciation of DG emissions is limited to generic groups of contaminants. To better capture the air quality impacts of DG, the authors recommend the development of more comprehensive speciation profiles for DG emissions

6. REFERENCES

Allen, P. Personal communication (2002). SoCAB emissions inventory. The California Air Resources Board.

Allison, J. E., and Lents, J. 2002. "Encouraging distributed generation of power that improves air quality: Can we have our cake and eat it too?" *Energy Policy* 30 (9): 737–752.

Atkinson R. 2000. "Atmospheric chemistry of VOCs and NO_X." *Atmos. Environ.* 34:2063–2101.

Bärtsch-Ritter, N., J. Keller, J. Dommen, and S. H. Prévôt. 2003. "Effects of various meteorological conditions and spatial emission resolutions on the ozone concentration & ROG/Nox limitation in the Milan area (I)." *Atmos. Chem Phys. Discuss.* 3:733–768.

Baugues, K. 1986. *A review of NMOC, NO_x ratios measured in 1984 and 1985.* EPA/450/4-86-015, U.S. EPA, Research Triangle Park, N.C.

Benkovitz C. M., C. M. Berkowitz, R. C. Easter, S. Nemesure, R. Wagener, and S. E. Schwarz. 1994. "Sulfate over the North Atlantic and adjacent continental regions: Evaluation for October and November 1986 using a three-dimensional model driven by observation-derived meteorology." *J. Geophys. Res.* 99 (D10): 20,725–20,756.

Bergin, M. S., G. S. Noblet, K. Petrini, J. R. Dhieux, J. B. Milford, and R. A. Harley. 1999. "Formal uncertainty analysis of a Lagrangian photochemical air pollution model." *Environ. Sci. Technol.* 33: 1116–1126.

Boedecker, E., J. Cymbalsky, and S. Wade. 2000. Modeling Distributed Generation in the NEMS building models. Energy Information Administration.

CARB. 2000. Emission information for facilities: http://www.arb.ca.gov/app/emsinv/facinfo/facinfo.php.

CARB. 2002. *The 2002 California Almanac of Emissions and Air Quality of the California Air Resources Board.* www.arb.ca.gov/aqd/almanac/almanac.htm.

CARB. 2003. Monitoring Sites in the South Coast Air Basin. www.arb.ca.gov/adam/mapfiles/scozone.html.

Carmichael, G. R., A. Sandu, and F. A. Potra. 1997. "Sensitivity analysis for atmospheric chemistry models via automatic differentiation." *Atmos. Environ.* 31: 475–489.

Carreras M., M. Medrano, G. S. Samuelsen, J. Brouwer, M. A. Rodriguez, D. Dabdub. 2004. Urban air quality impacts of distributed generation. Proceedings of ASME Turbo Expo 2004, Power for Land, Sea, and Air. June 14–17, 2003. Vienna, Austria.

CEC (California Energy Commission). 1999. *Market Assessment of CHP in the State of California.* Onsite Sycom Energy Corporation, prepared for California Energy Commission.

CEC (California Energy Commission). 2001. California Power Plants Database. California Energy Commission. http://www.energy.ca.gov/database/index.html#powerplants.

CEC (California Energy Commission). 2003. Current, Expected and Approved Peaker Power Plants. California Energy Commission. http://www.energy.ca.gov/maps/PEAKER_MAP.PDF.

Chin, G., H. Dixon, J. Kato, and A. Komorniczack. 2001. Guidance for the Permitting of Electrical Generation Technologies. California Air Resources Board.

Chock D. P. 1991. "A comparison of numerical methods for solving the advection equation – III." *Atmos. Environ.* 19: 571–586.

Chock D. P., and S. L. Winkler. 1994. "A comparison of advective algorithms coupled with chemistry." *Atmos. Environ.* 28: 2659–2676.

CPUC. 2003. California Self-Generation Incentive Program. Second Year Impacts Evaluation Report. Tirón Inc., prepared for Southern California Edison.

Dabdub D., L. L. DeHaan, and J. H. Seinfeld. 1999. "Analysis of ozone in the San Joaquin Valley of California." *Atmos. Environ.* 33: 2501–2514.

Dabdub D., and Seinfeld J. H. 1994. "Numerical advective schemes used in air quality models—sequential and parallel implementation." *Atmos. Environ.* 28 (20): 3369–3385.

DeMore, W. B., S. P. Sander, D. M. Golden, M. J. Molina, R. F. Hampson, M. J. Kurlyo, C. J. Howard, and A. R. Ravishankara. 1990. Chemical Kinetics and Photochemical Data for Use in Stratospheric Modeling, Evaluation Number 9. JPL Publ., 90-1.

Derwent, R., and Ø. Hov. 1988. "Application of sensitivity and uncertainty analysis techniques to a photochemical ozone model." *J. Geophys. Res.* 93: 5185–5199.

Dunker, A. M., 1981. "Efficient calculation of sensitivity coefficients for complex atmospheric models." *Atmos. Environ.* 15: 1155–1161.

Dunker, A. M. 1984. "The decoupled direct method for calculating sensitivity coefficients in chemical kinetics." *J. Chem. Phy.* 81: 2385–2393.

Ehhalt, D. H., J. S. Chang, and D. M. Butler. 1979. "The probability distribution of the predicted CFM-induced ozone depletion." *J. Geophys. Res.* 84: 7889–7894.

EIA. 1999a. 1998 Manufacturing Energy Consumption Survey (MECS). Energy Information Administration.

EIA. 1999b. A Look at Residential Energy Consumption in 1997. Energy Information Administration.

EIA. 2000. A Look at Building Activities in the 1999 Commercial Buildings Energy Consumption Survey (CBECS). Energy Information Administration.

Gao, D., W. R. Stockwell, and J. B. Milford. 1995. "First-order sensitivity and uncertainty analysis for a regional-scale gas-phase chemical mechanism." *J. Geophys. Res.* 100: 23,153–23,166.

Gao, D., W. R. Stockwell, and J. B. Milford. 1996. "Global uncertainty analysis of a regional-scale gas-phase chemical mechanism." *J. Geophys. Res.* 101: 9107–9119.

Gipson, G. L., W. Freas, R. Kelly, E. Meyer. 1981. Guideline for use of city-specific EKMA in preparing ozone SIPs. EPA-450/4-80-027. U.S. Environmental Protection Agency. Research Triangle Park, N.C.

Grenfell, J. L., N. H. Savage, R. M. Harrison, S. A. Penkett, O. Forberich, F. J. Comes, K. C. Clemitshaw, R. A. Burgess, L. M. Cardenas, B. Davison, G. G. McFadyen. 1999. "Tropospheric box-modeling and analytical studies of the hydroxyl (OH) radical and related species: Comparison with observations." *J. Atmos. Chem.* 33: 183–214.

Griffin R. J., K. Nguyen, D. Dabdub, J. H. Seinfeld. 2003. "A coupled hydrophobic-hydrophilic model for predicting secondary organic aerosol formation." *Journal of Atmospheric Chemistry* 44: 171–190.

Griffin R. J., D. Dabdub, and J. H. Seinfeld. 2002a. "Secondary organic aerosol - 1. Atmospheric chemical mechanism for production of molecular constituents." *Journal of Geophysical Research-Atmospheres.* 107 (D17): 4332.

Griffin R. J., D. Dabdub, M. J. Kleeman, M. P. Fraser, G. R. Cass, J. H. Seinfeld. 2002b. "Secondary organic aerosol - 3. Urban/regional scale model of size- and composition-resolved aerosols." *Journal of Geophysical Research-Atmospheres.* 107 (D17): 4334.

Hakami, A., M. T. Odman, A. G. Russell. 2003. "High-order, direct sensitivity analysis of multidimensional air quality models." *Environmental Science and Technology* 37: 2442–2452.

Hanna, S. R, J. C. Chang, M. Fernau. 1998. "Monte Carlo estimates of uncertainties in predictions by a photochemical grid model (UAM-IV) due to uncertainties in input variables." *Atmospheric Environment* 32: 3619–3628.

Hanna, S. R, and J. M. Davis. 2002. "Evaluation of a photochemical grid model using estimates of concentration probability density functions." *Atmospheric Environment* 36 (11): 1793–1798.

Hanna, S. R, Z. G. Lu, H. C. Frey, N. Wheeler, J. Vukovich, S. Arunachalam, M. Fernau, and D. A. Hansen. 2001. "Uncertainties in predicted ozone concentrations due to input uncertainties

for the UAM-V photochemical grid model applied to the July 1995 OTAG domain." *Atmos. Environ.* 35: 891–903.

Harley R. A., A. G. Russell, G. J. McRae, G. R. Cass, and J. H. Seinfeld. 1993. "Photochemical Modeling of the Southern California Air Quality Study." *Environ. Sci. Technol.* 27: 378–388.

Helton, J. C. 1993. "Uncertainty and sensitivity analysis techniques for use in performance assessment for radioactive waste disposal." *Reliability Engineering and System Safety* 42: 327–367.

Ianucci, J., S. Horgan, J. Eyer, and L. Cibulka. 2000. *Air Pollution Emissions Impacts Associated with the Economic Market Potential of Distributed Generation in California.* Distributed Utility Associates, prepared for the California Air Resources Board.

Iman, R. L., and J.C. Helton. 1984. A comparison of uncertainty and sensitivity techniques for computer models. SAND83-2365. U.S. Dept. of Energy, Sandia Natl. Lab. Albuquerque, N.M.

Jenkin, M. E., S. M. Saunders, and M. J. Pilling. 1997. "The tropospheric degradation of volatile organic compounds: A protocol for mechanism development." *Atmospheric Environment* 31 (1): 81–104.

Jimenez P., J. M. Baldasano, D. Dabdub. 2003. "Comparison of photochemical mechanisms for air quality modeling." *Atmos. Environ.* 37: 4179–4194.

Kay, M. 2003. Personal communication. SCAQMD.

Knipping, E. M., and D. Dabdub. 2002. "Modeling surface-mediated 'renoxification' of the atmosphere via reaction of gaseous nitric oxide with deposited nitric acid." *Atmospheric Environment.* 36 (36-37): 5741–5748.

Knipping, E. M., and D. Dabdub. 2003. Impact of chlorine emissions from sea-salt aerosol on coastal urban ozone. *Environ. Sci. Technol*. 37 (2): 275–284.

Lenssen, N. 2001. "The California Power Crisis. The Role for Distributed Generation." *Cogeneration and On-Site Power Generation* 2 (3). May–June 20012.

Lents, J., and J. E. Allison. *Can We Have Our Cake and Eat It, Too? Creating Distributed Generation Technology to Improve Air Quality.* University of California Riverside, California, prepared for the Energy Foundation. 2000.

Li Y., R. L. Dennis, G. S. Tonnesen, and J. E. Pleim. 1998. Effects of uncertainty in meteorological inputs on O_3 concentration, O_3 production efficiency, and O_3 sensitivity to emissions reductions in the Regional Acid Deposition Modeling. In: *Preprints of the 10th Joint Conference on the Applications of Air Pollution Meteorology with Air and Waste Management Association.* January 11–16, 1998, Phoenix, Arizona. Paper no. 9A.14, American Meteorological Society. Boston, Mass. 529–533.

Little, A. 2000. *Opportunities for Micropower and Fuel Cell Gas Turbine Hybrid Systems in Industrial Applications.* Arthur D. Little, prepared for Lockheed Martin Energy Research Corporation and the DOE Office of Industrial Technologies.

Marnay, C., J. S. Chard, K. S. Hamachi, T. Lipman, M. M. Moezzi, et al. 2001. *Modeling of Customer Adoption of Distributed Energy Resources. Consortium for Electric Reliability Technology Solutions.* Ernest Orlando Lawrence Berkeley National Laboratory, prepared for California Energy Commission.

McCay, M. D., W. J. Conover, and R. J. Beckman. 1979. "A comparison of three methods for selecting values of input variables in the analysis of output from a computer code." *Technometrics* 221: 239–245.

Medrano M., J. Brouwer, G. S. Samuelsen, M. Carreras, and D. Dabdub. 2003. Urban air quality impacts of distributed generation. Proceedings of ASME Turbo Expo 2003, Power for Land, Sea, and Air. June 16–19, 2003. Atlanta, Georgia.

Meng, Z., D. Dabdub, and J. H. Seinfeld. 1998. "Size–resolved and chemically resolved model of atmospheric aerosol dynamics." *J. Geophys. Res.* 103: 3419–3435.

Meng, Z., D. Dabdub, J. H. Seinfeld. 1997. "Chemical coupling between atmospheric ozone and particulate matter." *Science* 277: 116–119.

Meng, Z., J. H. Seinfeld, P. Saxena, and Y. P. Kim. 1995. "Atmospheric gas-aerosol equilibrium, IV, Thermodynamics of carbonates." *Aerosol Sci. Technol.* 23: 131– 154.

Meyer, E. L. 1986. *Review of control strategies for ozone and their effects on other environmental issues.* EPA-450/4-85-0011. U.S. Environmental Protection Agency. Research Triangle Park, N.C.

Milford, J. D., D. Gao, A. G. Russell, and G. J. McRae. 1992. "Use of sensitivity analysis to compare chemical mechanisms for air-quality modeling." *Environ. Sci. Technol.* 26: 1179–1189.

Moore, G. E., and R. J. Londergan. 2001. "Sampled Monte Carlo uncertainty analysis for photochemical grid models." *Atmospheric Environment* 35: 4863–4876.

Moya, M., S. N. Pandis, and M. Z. Jacobson. 2002. "Is the size distribution of urban aerosols determined by thermodynamic equilibrium? An application to Southern California." *Atmospheric Environment.* 36 (14): 2349–2365. May.

Nexus. 2002. Performance and Cost Trajectories of Clean Distributed Generation Technologies. Energy Nexus Group, prepared for the Energy Foundation.

Nguyen K., and D. Dabdub. 2001. "Two-level time-marching scheme using splines for solving the advection equation." *Atmos. Environ.* 35: 1627–1637.

Nguyen, K., and D. Dabdub. 2002b. "NO_X and VOC control and its effects on the formation of aerosols." *Aerosol Science and Technology* 36: 560–572.

Nguyen, K., and D. Dabdub. 2002a. "Semi-Lagrangian flux scheme for the solution of the aerosol condensation/evaporation equation." *Aerosol Science and Technology* 36: 407–418.

NREL. 2003. Gas Fired Distributed Generation Technology Characterization: Microturbines. Energy and Environmental Analysis, Inc, prepared for National Renewable Energy Laboratory.

Phenix, B. D., J. L. Dinaro, M. A. Tatang, J. W. Tester, J. B. Howard, and G. J. McRae. 1998. "Incorporation of parametric uncertainty into complex kinetic mechanisms: Application to hydrogen oxidation in supercritical water." *Combust. Flame* 112: 132–146.

Pun, B. K., R. J. Griffin, C. Seigneur, and J. H. Seinfeld. 2002. "Secondary organic aerosol 2. Thermodynamic model for gas/particle partitioning of molecular constituents." *J. Geophys. Res.* 107 (D17): 4333. doi:10.1029/2001JD000542.

Qin, Y., G. S. Tonnesen, and Z. Wang. 2004a. "One-hour and eight-hour average ozone in the California South Coast air quality management district: Trends in peak values and sensitivity to precursors." *Atmospheric Environment* 38 (14): 2197–2207. May.

Qin, Y., G. S. Tonnesen, Z. Wang. 2004b. "Weekend/weekday differences of ozone, NO_X, CO, VOCs, PM_{10} and the light scatter during ozone season in southern California." *Atmospheric Environment* 38 (19): 3069–3087.

Rabitz, H., and J. Hales. 1995. An ACP Primer on Sensitivity Analysis, Monthly Update. DOE Atmospheric Chemistry Program. 6(11), K9-30, BPNL, POB 999, Richland, Washington, 1-7.

Rabitz, H., M. Kramer, and D. Docol. 1983. "Sensitivity analysis in chemical kinetics." *Ann. Rev. Phys. Chem.* 34: 419–461.

RAP. 2001. DG Emissions, National Renewable Energy Laboratory. Ongoing study for Regulatory Assistance Project. http://www.raponline.org/.

Rodriguez, M. A., and D. Dabdub. 2003. "Monte Carlo uncertainty and sensitivity analysis of the CACM chemical mechanism." *Journal of Geophysical Research* 108 (D15), 4443. (DOI:10.1029/2002JD003281).

Russell, A. G., and R. Dennis 2000. "NARSTO critical review of photochemical models and modeling." *Atmos. Environ.* 34: 2283–2324.

Samuelsen, G. S., J. Brouwer, and M. Medrano. 2003. *Air Quality Impacts of Distributed Generation.* Final DG Scenario Development Report. Prepared for the California Energy Commission. 500-00-033.

Sax, T., and V. Isakov. 2003. "A case study for assessing uncertainty in local-scale regulatory air quality modeling applications." *Atmospheric Environment* 37: 3481–3489.

SCAQMD. 2000. Best Available Control Technology Guidelines. SCAQMD.

SCAQMD 2003a. Addendum to the proposed modification to the draft 2003 air quality management plan and additional comments and responses, South Coast Air Quality Management District.

SCAQMD. 2003b. Air Quality Management Plan (AQMP). South Coast Air Quality Management District. Available at: www.aqmd.gov/aqmp/AQMD03AQMP.htm.

SCAQMD. 2003c. ATTACHMENT-7 - Technical Report: CALGRID Ozone Simulations. Attachment to the 2003 Air Quality Management Plan (AQMP). Attachment available at: www.aqmd.gov/aqmp/docs/2003aqmd_appv_calgrid.pdf.

Sillman, S., and P. J. Samson. 1995. "Impact of temperature on oxidant photochemistry in urban, polluted rural and remote environments." *J. Geophys. Res.* 100 (D6): 11,497–11,508.

Sistla G., N. Zhou, W. Hao, J.-Y. Ku, S. T. Rao, R. Bornstein, F. Freedman, and P. Thunis. 1996. "Effects of uncertainties in meteorological inputs on urban airshed model predictions and ozone control strategies." *Atmos. Environ.* 30: 2011–2055.

Stockwell, W. R., F. Kirchner, M. Kuhn, and S. Seefeld. 1997. "A new mechanism for regional atmospheric chemistry modeling." *J. Geophys. Res.* 102: 25,847–25,879.

Stolarski, R. S., D. M. Butler, and R. D. Rundel. 1978. "Uncertainty propagation in a stratospheric model, 2, Monte Carlo analysis of imprecisions due to reaction rates." *J. Geophys. Res.* 83: 3074–3078.

Thompson, A. M., and R. W. Stewart. 1991. "Effect of chemical kinetic uncertainties on calculated constituents in a tropospheric photochemical model." *J. Geophys. Res.* 96: 13,089–13,108.

Tomashefsky, S., and M. Marks. 2002. *Distributed Generation Strategic Plan.* California Energy Commission. P700-02-002.

Vardoulakis, S., B. E. A. Fisher, N. Gonzalez-Flesca, K. Pericleous. 2002. "Model sensitivity and uncertainty analysis using roadside air quality measurements." *Atmospheric Environment* 36: 2121–2134.

Vuilleumier, L., J. T. Bamer, R. A. Harley, and N. J. Brown. 2001a. "Evaluation of nitrogen dioxide photolysis rates in an urban area using data from the 1997 Southern California Ozone Study." *Atmos. Environ.* 35: 6525–6537.

Vuilleumier L., R. A. Harley, N. J. Brown, J. R. Slusser, D. Kolinski, and D. S. Bigelow. 2001b. "Variability in ultraviolet total optical depth during the Southern California Ozone Study (SCOS97)." *Atmos. Environ.* 35: 1111–1122.

Winner A. D., G. R. Cass, and R. A. Harley. 1995. "Effect of alternative boundary conditions on predicted ozone control strategy performance: A case study in the Los Angeles area." *Atmos. Environ.* 29: 3451–3464.

Yang, Y. J., J. G. Wilkinson, A. G. Russell. 1997. "Fast, direct sensitivity analysis of multidimensional models." *Environmental Science and Technology* 31: 2859–2868.

Yang, Y., W. R. Stockwell, and J. B.Milford. 1996. Effect of chemical product yield uncertainties on reactivities of VOCs and emissions from reformulated gasolines and methanol fuels. *Environ. Sci. Tech.* 30: 1392–1397.

Zeldin, M. D., L. D. Bregman, and Y. Horie. 1990. *A Meteorological and Air Quality Assessment of the Representativeness of the 1987 SCAQS Intensive Days.* Final report to the South Coast Air Quality Management District.

7. GLOSSARY

Nomenclature

C_i	Concentration of species *i*
K	Eddy diffusivity tensor
Q_i	Source term that accounts for the elevated point sources of species *i*
R_i	Rate of generation of species *i* by chemical reaction
u	Mean wind velocity
t	Time
$A_{i,k}$	Area of sector *i* in cell *k*
$S_{i,j}$	Relative area of sector *i* in size category *j*
$A_{i,j,k}$	Area of sector *i* in size category *j* in cell *k*
A_{SoCAB}	Total area in the SoCAB
$D_{i,h}$	Duty cycle factor in sector *i* and hour of the day *h*
$R_{i,j}$	Adoption rate relative intensity (in terms of DG power/square foot) for sector *i* in size category *j*
$F_{power,k}$	Factor accounting for the total DG power in each cell
$P_{Tot,k}$	Total DG power (in MW) assigned to each cell
$P_{Tot,SoCAB}$	Total DG power (in MW) estimated for the SoCAB in 2010
$P_{i,j,k}$	DG power (in MW) of specific sector *i* in size category *j* in cell *k*
$W_{l,i,j}$	Relative weight for DG type *l* in sector *i* and size category *j*
$T_{l,k}$	Relative contribution to DG power of DG type *l* in cell *k*
$T_{l,k,h}$	Relative contribution to DG power of DG type *l* in cell *k* at hour *h*
$P_{l,k}$	DG power (in MW) of DG type *l* in cell *k*
$P_{l,k,h}$	DG power (in MW) of DG type *l* in cell *k* at hour *h*
$e_{l,X}$	Emission factor for species *X* of DG type *l*
$[X]_{emiss,k}$	Total DG emissions of species *X* in cell *k*
f_{CHP}	Estimated fraction of DG with waste heat recovery
f_{HR}	Heat recovery utilization factor or heat recovery capacity factor
$f_{DG,i}$	Fraction of DG technology *i*, which can vary hourly
f_{old}	Fraction of old boilers
f_{new}	Fraction of new boilers
f_{boiler}	Avoidable boiler air emissions (lbs/Btu)
Q_{elec}	Electric energy produced by DG
Q_{HR}	Thermal heat recovered in each hour
Q_{fuel}	Offset fuel energy that would otherwise be burnt in the boilers
$\eta_{elec,i}$	Electrical efficiency of fuel driven DG technology *i*
$\eta_{total,i}$	Total efficiency of fuel driven DG technology *i*
ef_{old}	Old boilers efficiency
ef_{new}	New boilers efficiency
ef_{tot}	Total efficiency (mixed electricity and heat energy divided by fuel energy in)
ef_{elec}	Fuel-to-electricity conversion efficiency
ef_{boiler}	Fuel-to-heat conversion efficiency of boiler

$em_{old,i}$	Emission factors for pollutant species *i* for old boilers
$em_{new,i}$	Emission factors for pollutant species *i* for new boilers
$M_{CO,off}$	Displaced boiler CO emissions
$M_{CO,DG}$	DG CO emissions
$M_{CO,net}$	Net CO emissions from DG/CHP systems
DGHeatRate	Chemical energy of fuel divided by electrical output of DG [Btu/kWh]

Acronyms

AGT	Advanced Gas Turbine
AQMP	Air Quality Management Plan
CARB	California Air Resources Board
CACM	Caltech Atmospheric Chemistry Mechanism
CB-IV	Carbon Bond version IV chemical mechanism
CGT	Conventional Gas Turbine
CHP	Combined Cooling, Heating, and Power
CIT	California Institute of Technology
CO	Carbon Monoxide
CO_2	Carbon Dioxide
DER	Distributed Energy Resources
DG	Distributed Generation
FC	Fuel Cell(s)
GT	Gas Turbines(s)
HHV	Higher Heating Value
HT	High temperature
HTFC	High Temperature Fuel Cell
ICE	Internal Combustion Engine
LADWP	Los Angeles Department of Water and Power
LCC	Lurmann, Coyner, and Carter mechanism
LT	Low temperature
LTFC	Low Temperature Fuel Cell
MCFC	Molten Carbonate Fuel Cell(s)
MTG	Microturbine Generator(s)
MPMPO	Model to Predict the Multiphase Partitioning of Organics
NH_3	Ammonia
NO_X	Nitrogen Oxides
NG	Natural Gas
PEMFC	Proton Exchange Membrane Fuel Cell(s)
$PM_{2.5}$	Particulate Matter (less than 2.5 microns)
PM_{10}	Particulate Matter (less than 10 microns)
PV	Photovoltaics
SCAG	Southern California Association of Governments
SCAPE2	Simulating Composition of Atmospheric Particles at Equilibrium 2 model
SCAQMD	South Coast Air Quality Management District
SCAQS	Southern California Air Quality Study
SCE	Southern California Edison
SCR	Selective Catalytic Reduction
SoCAB	South Coast Air Basin
SOFC	Solid Oxide Fuel Cell(s)
SO_X	Sulfur Oxides
VOC	Volatile Organic Compounds

Appendix A

Results From the First Industry Stakeholder Workshop (September 19, 2002)

Appendix B

Results from the Second Industry Stakeholder's Workshop (May 21, 2003)

Appendix C

Plots of DG Emissions Factors from Different Sources

Appendix D

Conversion Tools

Appendix E

Location of Land-Use Parcels for the 13 Generic Land-Use Categories

Appendix F

Duty Cycle Approach

Appendix G

Tables of Estimated Contributions of DG Technology Types for Each Sector

Appendix H

Impacts of DG Scenarios at Specific Locations

Appendix I

Difference in 24-Hour Averaged $PM_{2.5}$ Concentration